University of Applied Sciences Biberach
Institute of Applied Biotechnology
Prof. Dr. Kerstin Otte

Identification, Characterization and Removal of Intracellular Secretion Bottlenecks in Industrial CHO Production Cell Lines

Cumulative dissertation submitted in partial fulfilment of the requirements for the degree of “Doctor rerum naturalium” (Dr.rer.nat.) of the Faculty of Natural Sciences of Ulm University

Sven Mathias
Hilden

2020

Dean of the Faculty:	Prof. Dr. Thomas Bernhardt
First supervisor:	Prof. Dr. Kerstin Otte
Second supervisor:	Prof. Dr. Bernhard Eikmanns
External reviewer:	Prof. Dr. Thomas Noll

Day doctorate awarded: 20.04.2021

The results described in this thesis are based on the three following peer-reviewed publications:

- **Mathias S**, Fischer S, Handrick R, Fieder J, Schulz P, Bradl H, Gorr I, Gamer M, Otte K (2018): Visualisation of intracellular production bottlenecks in suspension-adapted CHO cells producing complex biopharmaceuticals using fluorescence microscopy (*Journal of Biotechnology*) [appendix, page 84 ff.]
- **Mathias S**, Wippermann A, Raab N, Zeh N, Handrick R, Gorr I, Schulz P, Fischer S, Gamer M, Otte K (2019): Unravelling What Makes a Monoclonal Antibody Difficult-to-Express: From Intracellular Accumulation to Incomplete Folding and Degradation via ERAD (*Biotechnology and Bioengineering*) [appendix, page 97 ff.]
- Bauer J*, **Mathias S***, Kube S, Otte K, Garidel P, Gamer M, Blech M, Fischer S, Karow-Zwick, A (2020): Rational Optimization of a Monoclonal Antibody Improves the Aggregation Propensity and Enhances the CMC Properties Along the Entire Pharmaceutical Process Chain (*mAbs*; * shared first author) [appendix, page 129 ff.]

Further, significant contributions were made to the following peer-reviewed publications:

- Raab N, **Mathias S**, Alt K, Handrick R, Fischer S, Schmieder V, Jadhav V, Borth N, Otte K (2019): CRISPR/Cas9-Mediated Knockout of MicroRNA-744 Improves Antibody Titer of CHO Production Cell Lines (*Biotechnology Journal*)
- Zeh N, Schneider H, **Mathias S**, Raab N, Kleemann M, Schmidt-Hertel S, Weis B, Wissing S, Strempel N, Handrick R, Otte K (2019): Human CAP cells represent a novel source for functional, miRNA-loaded exosome production (*PLoS One*)

Detailed declaration of contribution to peer-reviewed original publications

The presented doctoral thesis is based on three original and peer-reviewed publications of which two are first-author papers by Mathias et al. and one is a shared first-author paper by Bauer and Mathias et al.

For the first publication entitled “Visualisation of intracellular production bottlenecks in suspension-adapted CHO cells producing complex biopharmaceuticals using fluorescence microscopy” and published in the *Journal of Biotechnology* in 2018, I established the presented high-throughput fluorescence microscopy methodology as well as designed, performed and analyzed all experiments and wrote the manuscript.

For the second publication “Unravelling What Makes a Monoclonal Antibody Difficult-to-Express: From Intracellular Accumulation to Incomplete Folding and Degradation via ERAD” published in *Biotechnology and Bioengineering* in 2019, I designed the study, did most of the experiments (except for gene expression analyses and mass spectrometric analyses), analyzed all data and wrote the manuscript.

In case of the third publication “Rational Optimization of a Monoclonal Antibody Improves the Aggregation Propensity and Enhances the CMC Properties Along the Entire Pharmaceutical Process Chain” published in *mAbs* in 2020, I contributed to experiments, analyzed all data regarding cell line development and wrote parts of the manuscript. Of note, this paper has a shared first authorship with Dr. Joschka Bauer.

The full versions of all mentioned publications are provided in the appendix of this doctoral thesis.

Table of Contents

1 SUMMARY 1

2 INTRODUCTION 2

2.1 Antibodies and more complex biopharmaceuticals 2

2.2 Production of biopharmaceuticals using biological systems 7

2.3 Industrial-scale manufacturing processes of biopharmaceuticals 11

2.4 Improving biopharmaceutical manufacturing processes 14

3 OBJECTIVE 16

4 RESULTS 17

4.1 Identification of intracellular bottlenecks 17

4.2 Characterization of intracellular bottlenecks 24

4.3 Removal of intracellular bottlenecks 33

5 DISCUSSION 43

6 CONCLUSIONS 55

7 REFERENCES 56

8 APPENDIX 83

List of abbreviations/symbols

Abbreviations/symbols used in this thesis are listed in alphabetical order.

Abbreviation/ symbol	**Name**
%	Percent
°C	Degree Celsius
AA	Amino acid
AC	Affinity chromatography
AEX	Anion exchange chromatography
ANOVA	Analysis of variance
API	Active pharmaceutical ingredient
APR	Aggregation prone region
ART-Ig	Asymmetric re-engineering technology-Ig
AT	Acidic treatment
ATF4	Activating transcription factor 4
ATF6	Activating transcription factor 6
ATF6f	ATF6 cytosolic fragment
BHK	Baby hamster kidney
BHQ	Benjamini-Hochberg false discovery rate
BIP	Binding immunoglobulin protein
BiTE®	Bispecific T cell engager
bsAb	Bispecific antibody
C domain	Constant domain
CD147	Cluster of differentiation 147
CDR	Complementarity determining region
cH	Common heavy

CHO	Chinese hamster ovary
CHOP	C/EBP homologous protein
cL	Common light
CODV	Crossover dual variable
COS	CV-1 in origin, carrying SV40 genetic material
CTFR	Cystic fibrosis transmembrane conductance regulator
Da	Dalton
DAPI	4′,6-diamidin-2´-phenylindol
DART	Dual-affinity re-targeting
DF	Depth filtration
DNA	Deoxyribonucleic acid
DP	Drug product
DTE	Difficult-to-express
DVD	Dual variable domain
EDEM	ER degradation-enhancing α-mannosidase-like protein
eIF2α	Eukaryotic translation initiation factor 2α
ER	Endoplasmic reticulum
ERAD	ER-associated degradation
ERGIC-53	ER-Golgi intermediate compartment 53 kDa protein
EU	European Union
Fab	Fragment antigen binding
Fc	Fragment crystallizable
FC	Fold change
FPKM	Fragments per kilobase million
Fv	Fragment variable
g	Gram
GADD34	Growth arrest and DNA damage-inducible protein GADD34

GM130	130 kDa cis-Golgi matrix protein
H	Heavy
HC	Heavy chain
HEK	Human embryonic kidney
HL	Heavy light
HMW	High-molecular weight
HPLC	High-performance liquid chromatography
HT	High-throughput
Ig	Immunoglobulin
IRE1	Inositol requiring enzyme 1
IVC	Integral of viable cells
L	Liter
LC	Light chain
LMW	Low-molecular weight
LVs	Lentivirus driven integration
m	Meter
M	Molar [mol/L]
mAb	Monoclonal antibody
MFI	Micro-flow imaging
mRNA	Messenger ribonucleic acid
MS	Mass spectrometry
mTOR	Mammalian target of rapamycin
NSF	N-ethylmaleimide-sensitive factor
PDI	Protein disulfide isomerase
PEG	Polyethylene glycol
PERK	Protein kinase RNA-like ER kinase
PPIB	Peptidyl-prolyl cis-trans isomerase B

qPCR	Quantitative polymerase chain reaction
RB	Russell body
RMCE	Recombinase-mediated cassette exchange
scFv	Single chain fragment variable
SDS-PAGE	Sodium dodecyl sulfate polyacrylamide gel electrophoresis
SEC	Size exclusion chromatography
Sel1L	Suppressor/enhancer of Lin-12-like
SNARE	Soluble NSF receptor
SPR	Surface plasmon resonance
T_{agg}	Onset aggregation temperature
TGE	Transient gene expression
T_m	Denaturation temperature
tPA	Tissue plasminogen activator
UF/DF	Ultrafiltration and diafiltration
UPR	Unfolded protein response
US	United States
V domain	Variable domain
VCD	Viable cell density
VHH	Variable heavy homodimer
WB	Western blot
XBP1	X-box binding protein 1
YY1	Yin and yang 1
ZFP-TFs	Zinc-finger protein transcription factors

All units were used according to the International System of Units with their metric prefixes.

1 SUMMARY

Monoclonal antibodies (mAbs) represent a class of therapeutic proteins which are highly potent to treat diverse diseases and address yet unmet medicinal needs. Their clinical as well as commercial success led to a continuous effort to generate innovative and artificial antibody-derived formats. At the discovery stage of drug candidates, the focus is primarily set on biological activity favoring the selection of highly potent drug candidates but sometimes showing poor expression, stability and/or solubility. In order to provide sufficient amounts to the market, there is an urgent need to identify, characterize and remove any rate-limiting processing step during cellular synthesis and transport (production bottleneck) which compromise the final amount of titer. To facilitate identification of production bottlenecks, we developed a streamlined high-throughput (HT) fluorescence microscopy-based methodology to identify unproductive or saturated organelle structures in production cell lines implementable in highly automated industrial work flows. Using this methodology, we identified a difficult-to-express (DTE) protein to be haltered within the secretory organelle endoplasmic reticulum (ER) finally leading to an affected morphologic appearance. Subsequently, a detailed characterization of the identified bottleneck revealed that the disulfide bridge formation within the antibody light chain (LC) was impaired probably due to less recognition by the disulfide bridge-catalyzing chaperone protein disulfide isomerase (PDI) concluded from co-immunoprecipitation studies. As a consequence, the DTE molecule was more heavily degraded intracellularly by the ubiquitin proteasome system via ER-associated degradation (ERAD) as revealed by gene expression analysis. Interestingly, the DTE antibody was already in a previous study identified to have liabilities and thus a sequence variant was generated, which displayed improved properties in a transient expression setup. We showed that the optimized properties of the variant established throughout a routine industrial manufacturing process from stable cell-based production, to downstream purification, formulation, and storage. Strikingly, the previously identified intracellular bottleneck was mitigated in the variant-producing cell line. Altogether, the presented studies describe a straightforward approach to identify and characterize intracellular production bottlenecks providing the starting points for cellular engineering and bioinformatic prediction tools to optimize the production processes of lead candidates.

2 INTRODUCTION

2.1 Antibodies and more complex biopharmaceuticals

Current medicinal treatments of serious diseases related to cancer, autoimmune disorders, diabetes, monogenic deficiencies as well as cardiovascular and infectious diseases are based on the application of state-of-the-art biopharmaceutical products (Ecker et al., 2015; Walsh, 2018). In contrast to the classical chemically synthesized small molecule-based pharmaceuticals the active ingredients of biopharmaceuticals represent a class of macromolecules such as peptides, proteins, vaccines, viral vectors or cells derived from biological sources.

Following the approval of the first biopharmaceutical product Humulin in 1982, a total number of 374 products have received license in the United States (US) and European Union (EU) market until mid-2018. Since 58 compounds were withdrawn from both the US and EU markets - almost always for commercial reasons - the number of now actively marketed biopharmaceuticals stands at 316 products, which are based on nearly 200 distinct active pharmaceutical ingredients (APIs) (Walsh, 2018). The following Fig. 1 illustrates the amount of marketed APIs summarized by category.

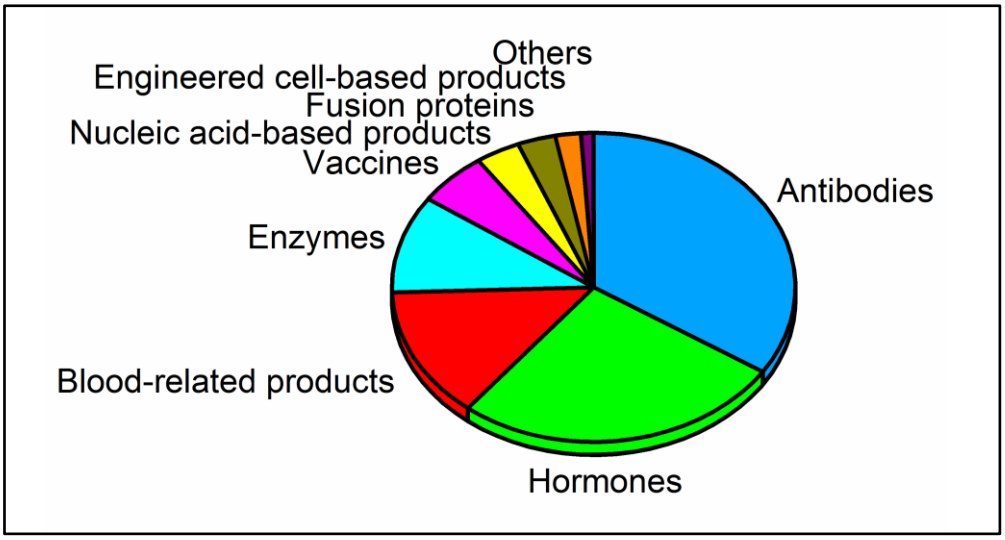

Fig. 1: Amount of currently marketed distinct active pharmaceutical ingredients (APIs) within the group of biopharmaceuticals by category (based on Walsh, 2018).

Notably, among all currently marketed APIs, mAbs represent the most prominent class of drugs with approx. 70 different entities actively marketed covering more than 65 % of the total annual revenue of all biopharmaceutical products ($ 188 billion) in 2017 (Grilo and Mantalaris, 2019; Walsh, 2018). The

increasing dominance of mAbs within the class of biopharmaceutical products is further demonstrated as more than 50 % of total approved biopharmaceuticals in the survey period from 2015 to July 2018 were mAb-based products (Walsh, 2018).

Antibodies, also called immunoglobulins (Igs), are generally well-tolerated as well as highly specific and therefore often provide the most rapid route to a clinical proof of concept for either activating, inhibiting or blocking newly identified molecular targets to modulate diseases (Ecker et al., 2015). Naturally, they are produced and secreted by specialized terminally differentiated b-cell lymphocytes - so called plasma cells - each producing only one specific antibody providing adaptive immunity to its host (Janeway et al., 2001; Nutt et al., 2015). The general structure of Igs is summarized in the following Fig. 2.

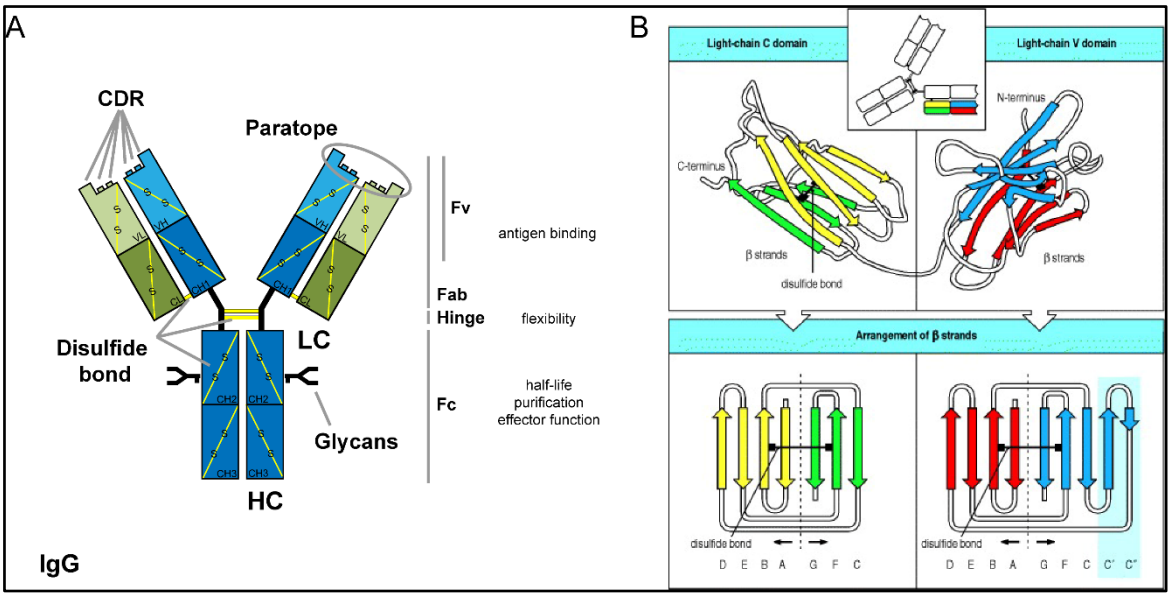

Fig. 2: General structure of human immunoglobulins (Igs). (A) Structure of a human IgG molecule with certain fragments and respective features annotated. (B) Exemplarily shown three-dimensional as well as schematic structure of the variable (V) and constant (C) Ig domains of the antibody light chain (LC), which is generally also applicable for heavy chain (HC). From IMMUNOBIOLOGY: THE IMMUNE SYSTEM IN HEALTH AND DISEASE by Daniel J. Siegel. Copyright 2001 by Garland Publishing. Used by permission of W. W. Norton & Company, Inc. (Janeway et al., 2001). Fab, fragment antigen binding; Fc, fragment crystallizable; Fv, fragment variable; CDR, complementarity determining region

The basic functional unit of human Igs is a Y-shaped glycosylated protein complex with two identical fragment antigen binding (Fab) regions each recognizing the same specific epitope on its antigen, and the fragment crystallizable (Fc) which facilitates interaction with the host immune system, confers long serum half-life and is targeted in industrial purification processes (Fig. 2A). The complex is composed of two

identical LC and two identical heavy chain (HC) polypeptides linked to each other via disulfide bridges. The individual chains are, in turn, composed of one variable and one (LC) or three to four (HC) constant independent structural subunits called Ig domains. These domains are usually built from two antiparallel beta-sheets connected to each other by one intra domain disulfide bridge (Fig. 2B). The variable domains of the HC and LC, together forming the fragment variable (Fv) with a binding site for a certain antigen (paratope), vary greatly between different antibodies and thus can confer the ability to bind specific targets. The paratopes are especially formed by three hypervariable binding loops per variable domain, so called complementarity determining regions (CDRs) which enable to bind a large variety of molecular targets with high affinity and specificity (Sormanni et al., 2018). In particular, an availability of at least 10^{11} antibody specificities in human individuals, which is facilitated by complex deoxyribonucleic acid (DNA) recombination and affinity maturation steps, enables the immune system to recognize nearly any foreign substance (Janeway et al., 2001).
There are several sequences for constant domains available in the human genome selected during a recombination-based process called class switch. According to the different constant HC sequences, human Igs have distinct effector functions and are therefore classified into isotypes (IgA, IgD, IgE, IgG, and IgM), of which each can be combined with the different constant LC sequences (kappa or lambda). However, thus far, IgG molecules represent the only pharmaceutically relevant isotype (Grilo and Mantalaris, 2019; Labrijn et al., 2019; Poiron et al., 2010).

After success in the initial studies antibodies can move rapidly towards commercialization and thus represent the most valuable and rapidly growing biopharmaceutical drug class (Ecker et al., 2015; Grilo and Mantalaris, 2019; Walsh, 2018). This clinical as well as commercial success of mAbs has been leading to a continuous effort to generate innovative and promising non-naturally existing antibody-derived biological formats with versatile but clearly distinguishable functions opening up a field of many new potential therapeutic applications.
As of August 2018, already 16 out of more than 70 approved and marketed antibody-related biopharmaceutical active ingredients on the US and/or EU market are non-classical full-length antibodies. The simplest Ig-derived molecules represent antibody fragments where the Fc part has been removed to generate highly specific

binders with short serum half-life and no interaction with the host immune system. By now, four Fab fragments (idarucizumab, certolizumab pegol, abciximab, ranibizumab) and one single-domain antibody (nanobody) derived from a variable heavy homodimer (VHH) antibody (Caplacizumab) are currently marketed. Inversely, the fusion of an unrelated enzyme, protein domain or peptide to the Fc part of an Ig might drastically increase its serum half-life, of which five are currently on the market (asfotase alfa, efmorogtocog alfa, eftrenonacog alfa, dulaglutide, romiblastim). Furthermore, instead of elaborately creating antibodies recognizing specific target proteins, the respective domain of its natural receptor/binder can be fused to an Ig Fc part to generate antibody-like protein traps, of which four are currently marketed (etanercept, aflibercept, belatacept, abatacept) (Poiron et al., 2010; Walsh, 2018).

The latest development in antibody-derived molecules are bispecific antibodies (bsAbs) which facilitate novel applications such as retargeting of effector T cells to kill tumor cells or to interact with different disease mediators such as cell surface receptors, soluble ligands and other proteins. BsAbs are a large class of molecules designed to recognize two different epitopes or antigens, which can be mono- or bivalent for each of their targets (Brinkmann et al., 2017; Spiess et al., 2015). When bsAbs were first developed the antibody had to be modified to recognize different antigens. By the simple approach of tacking two different HCs and two different LCs, it was challenging to obtain the desired functional bsAb from the mixture of ten possible HC_2LC_2 combinations, commonly referred to as the chain association problem (Labrijn et al., 2019). Therefore, over the past decades more than 20 different commercialized technology platforms have been developed and advanced to clinical studies whose structure diversity is summarized in the following Fig. 3.

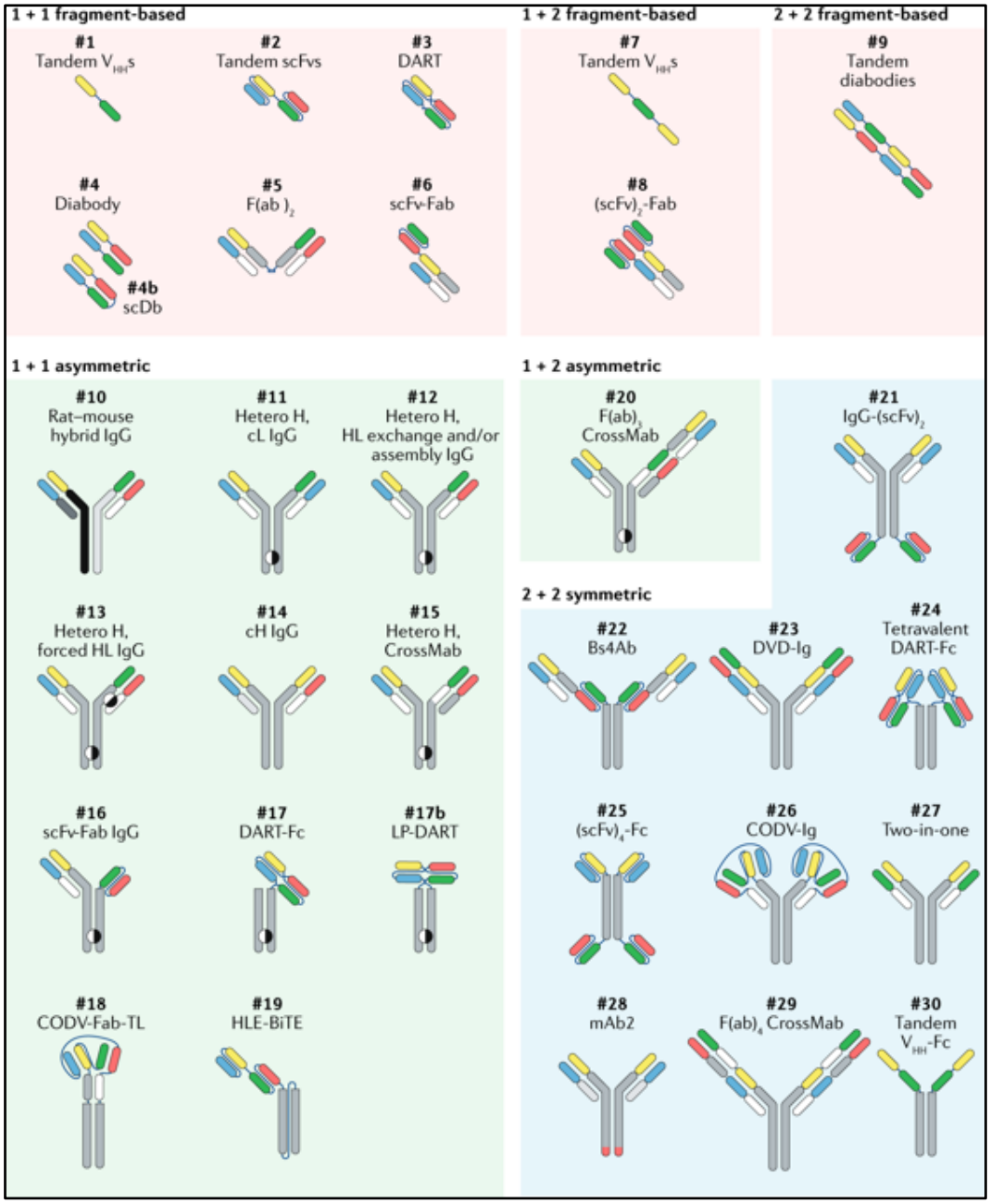

Fig. 3: A selection of bispecific antibody (bsAb) formats which advanced to clinical studies. The molecules are categorized according to their design features and functional properties (fragments, red background, #1 - #9; asymmetric, green background, #10 - 20; symmetric, blue background, #21 - #30). The molecules may contain mutations which affect chain pairing as well as biological activity. Reprinted by permission from Springer Nature Customer Service Centre GmbH: Springer Nature, Nature Reviews Drug Discovery, Bispecific antibodies: a mechanistic review of the pipeline, A. Labrijn et al, Copyright © 2019 (Labrijn et al., 2019). VHH, variable heavy homodimer; scFV, single chain fragment variable; DART, dual-affinity re-targeting; Fab, fragment antigen binding; IgG, immunoglobulin G, cL, common light, HL, heavy light; cH, common heavy, H heavy, Fc, fragment crystallizable; DVD, dual variable domain; CODV, crossover dual variable

BsAb formats can be categorized according to their design features and functional properties in three major groups. In particular, the simplest strategy to generate a bsAb is a combination of different antigen binding fragments linked to each other

without the use of a Fc part (Fig. 3, red background, #1 - #9). The highly modular nature of this approach enables to customize the valency of the generated molecule to fit the respective application. However, to retain the native architecture and properties of an antibody, asymmetric molecules, usually monovalent for each antigen, have been developed by forcing heterodimerization of different chains (Fig. 3, green background, #10 - #20). In contrast, the incorporation of both specificities in a single polypeptide chain or an individual HC-LC pair led to the development of symmetric molecules, which are usually bivalent for each antigen (Fig. 3, blue background, #21 - #30).

So far, two bsAbs are on the market: one is a bispecific T cell engager (BiTE®) composed of two linked single-chain fragment variable (scFV) molecules (blinatumomab, Fig. 3 #2) and one is a bispecific IgG_4 asymmetric re-engineering technology-Ig (ART-Ig) (emicizumab, Fig. 3 #11). The assembled bispecific rat-mouse hybrid antibody (Fig. 3 #10) catumaxomab was approved in 2009 but withdrawn from the EU market in 2017. Reviewing the development pipelines, more than 85 bispecific APIs are in clinical development illustrating the increasing significance of non-naturally existing antibody derived formats (Labrijn et al., 2019; Walsh, 2018).

2.2 Production of biopharmaceuticals using biological systems

Due to specific folding requirements and modifications (e.g. glycosylation), biological production systems are used as recombinant platforms for efficient biopharmaceutical manufacturing processes. During the last decades, a variety of different expression systems were established for the production of heterologous proteins including bacteria, fungi, insect, plant and mammalian cells as well as plants and even transgenic animals (Zhu, 2012). Early on, *Escherichia coli* represented the dominant work horse for recombinant protein production as it was extensively characterized, standardized methods were established and expenses for protein production were comparably low (Mahmound, 2007). However, with the development of more sophisticated therapeutic proteins, which consist of multiple subunits with complex modifications like disulfide bonds and glycosylations, bacterial expression systems rapidly reached their limits (Mahmound, 2007; Zhu, 2012). As a consequence, more than half of all currently marketed biopharmaceuticals are manufactured using mammalian cell-based expression

systems capable of secreting the final product into the culture medium (Walsh, 2018).

The generation, processing and final secretion of complex proteins by mammalian cells is a multi-step procedure which requires the secretory apparatus to work with high efficiency (Alberts et al., 2002; Lodish et al., 2000). A schematic overview of this machinery is shown in Fig. 4.

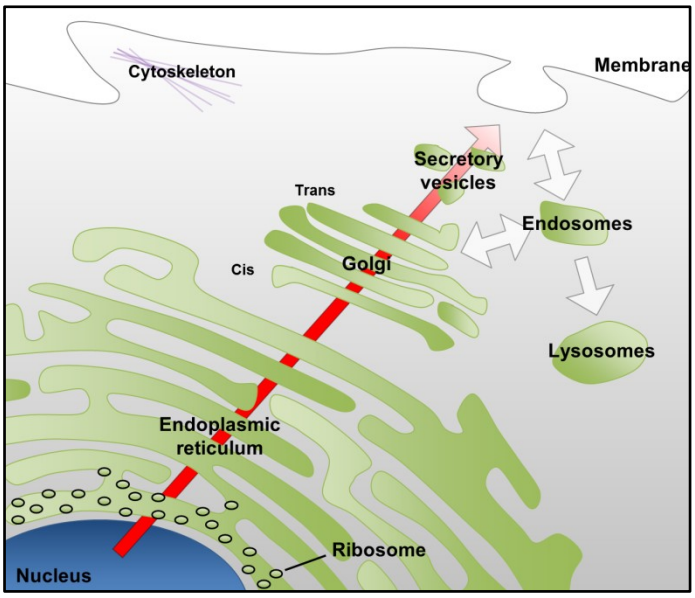

Fig. 4: Schematic overview of the biosynthetic-secretory and endocytic pathway. Proteins assigned for secretion are translocated into the lumen of the endoplasmic reticulum (ER) during translation. After folding and assembly, proteins are transported to the Golgi apparatus, where further post-translational modifications occur. Subsequently proteins are packed into secretion vesicles and finally expelled into the culture medium. Proteins from the outside are taken up by endocytosis, sorted and possibly degraded in lysosomes (based on Mathias et al., 2018).

Proteins assigned for final secretion into the culture medium are ribosomally synthesized and co-translationally translocated into the lumen of the ER, where resident chaperones assist in protein folding as well as assembly and first post-translational modifications including glycosylation and disulfide bridge formation occur (Braakman and Hebert, 2013; Ellgaard and Helenius, 2003). After having been processed in the ER, cargo vesicles transport secreted proteins to the Golgi apparatus, where they usually enter the *cis* face. During their passage through the Golgi apparatus, additional post-translational modifications such as further processing of the attached glycans occur before the proteins are sorted at the *trans* site of the Golgi and finally expelled into the culture medium via secretory vesicles (Alberts et al., 2002). However, the Golgi also represents an intersection

between endosomes which internalize molecules from the cellular exterior and lysosomes which execute the hydrolysis of biomolecules.

During the synthesis of secretory proteins, especially the ER has very central processing and signaling functions executed by numerous proteins summarized in the following Fig. 5.

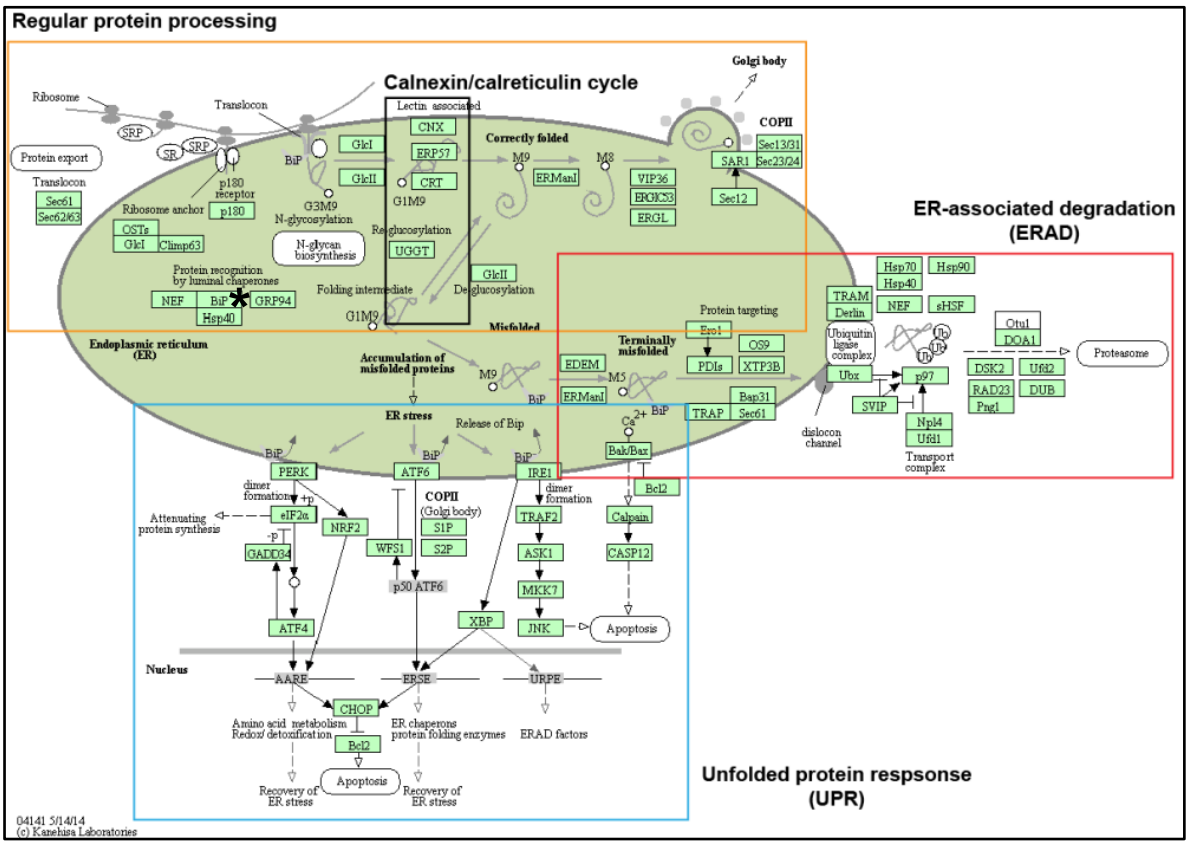

Fig. 5: Detailed pathway map of the canonical protein processing pathways within the organelle endoplasmic reticulum (ER) in the secretory apparatus of mammalian cells. The ER has three major canonical pathways: regular protein processing (orange), ER-associated degradation (ERAD) (red) and unfolded protein response (UPR) (blue). The calnexin/calreticulin cycle, representing an important folding machinery, is additionally marked in black. The central chaperon binding immunoglobulin protein (BIP) is highlighted with an asterisk (adapted from Kanehisa et al., 2017, 2019; Kanehisa and Goto, 2000).

After entry of newly synthesized proteins in the ER, binding immunoglobulin protein (BIP), one of the most central and versatile chaperones (Fig. 5, asterisk), recognizes and interacts with exposed hydrophobic sequences of proteins actively maintaining its clients in a folding competent state (Fig. 5, orange square) (Behnke et al., 2016; Pobre et al., 2019). Simultaneously, disulfide isomerases oxidize free cysteine residues to disulfide bridges stabilizing the native protein fold. Additionally, N-glycan structures are readily attached to the nascent protein chain, not only

having important roles in a matured protein´s functions but also in its folding procedure as many chaperons use glycans as sorting signals which are modified by the cell to reflect the current folding status of a certain protein (Apweiler et al., 1999; Helenius and Aebi, 2004). Especially during the initial folding, nascent protein chains may undergo several rounds of processing in the so called calnexin/calreticulin cycle (Fig. 5, black square). The iterative folding attempts are controlled and analyzed by one terminal glucose residue which is cleaved off after every folding attempt but re-added to the glycosylation tree when the folding was not successful (Aebi et al., 2010; Hebert et al., 2005; Helenius and Aebi, 2004). After folding and processing, only properly folded and assembled proteins are transported to the Golgi apparatus, where the premature Man5 N-glycans are further processed into the complex glycan type, sorted and finally expelled into the culture medium (Alberts et al., 2002; Lodish et al., 2000).

When a glycoprotein fails to fold, mannosidases and ER degradation-enhancing α-mannosidase-like proteins (EDEMs) trim terminal mannosidase residues of N-glycans paving the way for the protein to escape from the calnexin/calreticulin cycle to be cleared from the lumen of the ER by the ERAD pathway (Fig. 5, red square) (Helenius and Aebi, 2004; Olzmann et al., 2013). Here, specific lectins recognize the trimmed glycan structures and guide the respective proteins to a dislocation complex which performs the re-translocation and ubiquitination of substrate proteins. This complex, in turn, recruits ATP hydrolysis complexes necessary to drive substrate dislocation by providing energy and additionally represent a scaffold for further cytoplasmic effector proteins facilitating substrate modification and final degradation by the proteasome (Olzmann et al., 2013). Non-glycosylated proteins are most likely recognized by chaperones like BIP which extensively interact with exposed hydrophobic sequences and proteins with free cysteines are also actively recognized and finally degrade (Olzmann et al., 2013). However, an accumulation of unfolded or misfolded proteins in the lumen of the ER can impair ER functionality and will finally trigger the unfolded protein response (UPR) (Hetz, 2012; Xu et al., 2005).

The UPR is a complex feedback mechanism to ensure efficient adaptation to fluctuations in protein folding requirements by affecting and regulating the capacity of the organelles in the secretory pathway (Hetz, 2012). The reaction is enabled by the stress sensors inositol requiring enzyme 1 (IRE1), activating transcription

factor 6 (ATF6) and protein kinase RNA-like ER kinase (PERK) after the release of bound BIP, which interacts with nascent protein chains (Fig. 5, blue square) (Hetz, 2012; Hussain et al., 2014; Ma and Hendershot, 2002). The physiological reaction initially begins with a decreased overall protein translation via the phosphorylation of eukaryotic translation initiation factor 2α (eIF2a) and continuous with a massive gene expression response through the regulation of at least three distinct transcription factors. Activating transcription factor 4 (ATF4), X-box binding protein 1 (XBP1) and cleaved ATF6 (ATF6 cytosolic fragment, ATF6f) regulate the expression of a large range of genes which modulate adaptation to stress conditions. However, chronic ER stress and sustained activation of the UPR above a critical threshold results in the induction of programmed cell death and apoptosis via C/EBP homologous protein (CHOP) which is highly undesirable in large scale industrial production processes (Hetz, 2012).

2.3 Industrial-scale manufacturing processes of biopharmaceuticals

Mammalian expression systems are predominantly utilized for the industrial production of recombinant proteins and biopharmaceuticals (Walsh, 2018). Commonly used production cell lines are murine NS0 and Sp2/0, baby hamster kidney (BHK), human embryonic kidney (HEK)-derived HEK293 and Chinese hamster ovary (CHO) cells which are the most strongly represented producing more than half of all approved biopharmaceutical products (Walsh, 2018).

Originating from a clonal and likely to be spontaneously immortalized cell, a variety of different CHO cell lines have been established to date representing an entire CHO cell system (Puck et al., 1958; Wurm, 2013). Currently, three distinct CHO cell lines are commonly used for large scale industrial manufacturing processes: CHO-K1, CHO-DXB11 (also, CHO-DUKX) and CHO-DG44 (Wurm, 2013; Wurm and Hacker, 2011). The popularity of using CHO cell lines depends on their ability of attaining high production rates while simultaneously having the capability to grow to high cell densities in suspension. Furthermore, they can easily be adapted to grow in serum-free and chemically defined media, grow quickly and robustly and foreign DNA can easily be transferred into the genome of the cells (Lalonde and Durocher, 2017; Wurm and Hacker 2011). In addition, they are able to perform human-like glycosylations on produced proteins which are more likely to be compatible and bioactive within human hosts (Lalonde and Durocher, 2017). Its

biotechnological application and research efforts in cellular engineering are also sustainably accelerated by the continuously growing and public availability of comprehensive data on its genomic sequence (Kaas et al., 2015; Lewis et al., 2013; Xu et al., 2011), epigenome, transcriptome, miRnome, proteome as well as metabolome (as reviewed by Stolfa et al., 2017). Finally, sophisticated cell line development approaches and thorough process optimizations during the past decades resulted in markedly streamlined development process timelines.

Once a molecular target to modulate a disease has been identified in research studies the production process usually starts with the generation of highly specific and potent antibody candidates. Currently, there are two well-established procedures for the discovery of novel antibodies available. In the first approach the immune system is utilized, traditionally through animal (usually mice) immunization (Köhler and Milstein, 1975; Lindl, 1996; Sormanni et al., 2018). The second approach relies on the laboratory construction of large libraries of sequences reflecting the diversity achieved by the immune system which likely contain binding molecules for every antigen (Frenzel et al., 2017; Smith, 1985; Winter et al., 1994). In both cases extensive laboratory screenings and advanced analyses are necessary to identify relevant candidates.

After the identification of a potential drug candidate for biopharmaceutical manufacturing, the production process continues with the generation of recombinant production cell lines. First, the DNA coding sequence for the recombinant protein is obtained and cloned into a suitable expression vector using recombinant DNA technologies to transfer the respective information into the host cell (Kunert and Reinhart, 2016; Lalonde and Durocher, 2017; Wurm, 2004). As the generation of stable mammalian production cell lines requires a costly and lengthy cell line development process, expression of the respective genes is routinely performed in transient systems to test for the capability of efficient industrial-scale production (Baldi et al., 2007; Kim et al., 2012). Here, insufficient outcome in any regard including product titer and product quality represents an early indication of low manufacturability (Mason et al., 2012; Pybus et al., 2014). However, after capability studies, stable production cell lines are generated as depicted in the following Fig. 6.

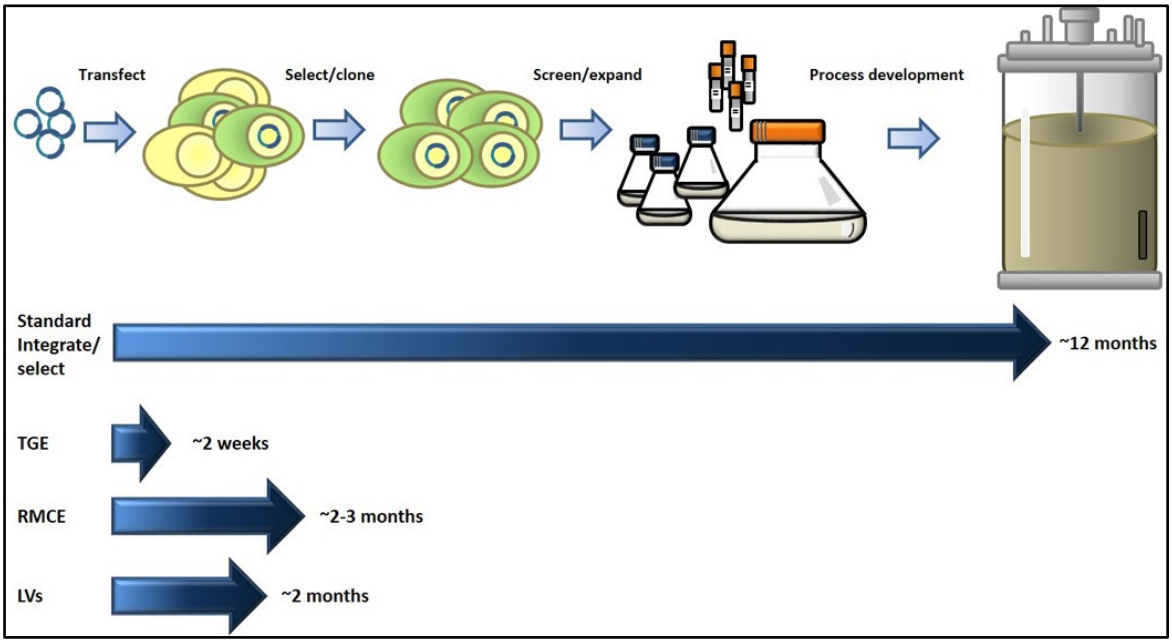

Fig. 6: Overview of the general cell line development process for the generation of stable production cell lines for biopharmaceutical manufacturing processes. Reprinted from FEBS Letters, Vol 588/edition number 2, A. Bandaranayake, S. Almo, Recent advances in mammalian protein production, pages 253-260, 2013, © 2015 Federation of European Biochemical Societies with permission from John Wiley & Sons, Inc (Bandaranayake and Almo, 2014). TGE, transient gene expression; RMCE, recombinase mediated cassette exchange; LVs, lentivirus driven integration

Host cell lines are transfected with an expression vector which, besides the information for the gene of interest, harbors a selection marker to enrich for cells that have received the respective construct (Wurm, 2004). Subsequently, clonal cell lines are derived from a single cell and screened to identify the best suited production cell line. This represents the most critical and time consuming process during cell line development, since it influences parameters as productivity, product quality as well as cost of goods (Ko et al., 2018). The chosen production cell line is then thoroughly characterized, the production process optimized and finally used in stirred tank bioreactor-based large scale manufacturing processes (Bandaranayake and Almo, 2014; Wurm, 2004). Besides standard integration/selection procedures several other methodologies have been established such as transient gene expression (TGE), recombinase mediated cassette exchange (RMCE) or lentivirus driven integration (LVs). However, besides the improvements in cultivation medium and appropriate feeding strategies, also the engineering of expression vectors, the host cell line itself and the amino acid (AA) sequences of the recombinant proteins contributed to the increased product yields from 0.1 g/L to more than 10 g/L (Huang et al., 2010; Kunert and Reinhart, 2016; Zhu, 2012).

2.4 Improving biopharmaceutical manufacturing processes

The production of biopharmaceuticals is highly expensive, therefore besides the continuous optimization of the cultivation medium, feeding strategy and process parameters also the respective host cell platforms have steadily been improved. Several genetic engineering approaches were established to generate CHO cells outperforming their parental cell lines. In particular, genetic engineering of CHO factories addressing cell growth and metabolism as well as apoptosis and autophagy resistance led to the establishment of derivatives with a prolonged cultivation and production phase and thus an overall enhanced process performance (Arden and Betenbaugh, 2004; Fischer et al., 2015a; Krampe and Al-Rubeai, 2010). Additionally, genes involved in cellular metabolism were targeted by genetic engineering in order to optimize nutrient consumption and decrease accumulation of toxic byproducts (Fischer et al., 2015a; Richelle and Lewis, 2017). Many efforts have also been aiming on the genetic engineering of the post-translational modification machinery of proteins (especially the N-glycosylation) yielding CHO cell lines which produce more biologically active and thus potent pharmaceuticals (Clausen et al., 2017; Hossler et al., 2009; Zhang et al., 2016). Further, the overall production and secretion capacity of CHO cells was improved by the stable co-expression of genes globally enhancing the cellular protein synthesis machinery or the secretory apparatus such as zinc-finger protein transcription factors (ZFP-TFs), ATF4, growth arrest and DNA damage-inducible protein (GADD34) and yin and yang 1 (YY1) or the mammalian target of rapamycin (mTOR) (Dreesen and Fussenegger, 2011; Fischer et al., 2015a; Kwon et al., 2006; Ohya et al., 2008; Omasa et al., 2008; Tastanova et al., 2016). Additionally, the ER folding and processing capacity has been addressed by the expression of several key chaperones including BIP, PDI and peptidyl-prolyl cis-trans isomerase B (PPIB) (Borth et al., 2005; Dorner et al., 1992; Hansen et al., 2017; Johari et al., 2015) as well as further proteins of the UPR (Becker et al., 2008; Cain et al., 2013; Rahimpour et al., 2013; Tigges and Fussenegger, 2006). Vesicular transport was improved by the overexpression of soluble N-ethylmaleimide-sensitive factor (NSF) receptor (SNARE) proteins (Peng et al., 2011, 2010; Peng and Fussenegger, 2009) and lipid transfer proteins (Florin et al., 2009). Alternative strategies relied on the application of microRNAs to modulate entire pathways associated with protein production (Barron et al., 2011;

Fischer et al., 2015a; Hackl et al., 2012; Jadhav et al., 2013). Culture medium additives like butyric and valproic acid as well as HDAC modulators have further been used to influence the overall transcription rate of genes (Backliwal et al., 2008; Fischer et al., 2015b; Wulhfard et al., 2010). However, beside the improvement of the production cell line itself also the expressed recombinant proteins can be engineered to better meet biopharmaceutical production requirements.

At the discovery stage of drug candidates the focus is primarily set on the biological activity leading to the selection of molecules with favorable potency but sometimes poor expression, stability and/or solubility which might later on result in the termination of the development affords (Kumar et al., 2018; Sormanni et al., 2018). However, biopharmaceutical informatics have long been aiming at the connection of sequence-structure attributes with their macroscopic behaviors (Kumar et al., 2018). Predictions regarding biological activity, pharmacology, thermodynamic stability, solubility and viscosity as well as accompanying challenges and hurdles encountered during manufacturing can then be used to select the overall most promising drug candidate very early in pipeline (Agrawal et al., 2016; Jain et al., 2017; Li et al., 2014; Sharma et al., 2015; Tomar et al., 2017). Even further understanding would enable to identify critical sequences and improve the macroscopic behavior of a given biological drug candidate via rational mutagenesis of the primary AA sequence (Geoghegan et al., 2016; Kumar et al., 2018; Nichols et al., 2015; Yadav et al., 2012). However, natural proteins are evolutionarily selected to be just as stable and soluble to optimally perform their function at physiological conditions (Tartaglia et al., 2007), which implies that there is the need to optimize the biophysical properties far beyond their natural levels to meet industrial manufacturing requirements e.g. to resist aggregation in highly concentrated formulations (Sormanni et al., 2018). This task is highly problematic as mutations that improve e.g. stability, solubility, affinity or selectivity usually tend to worsen the others (Ferreiro et al., 2014; Gianni et al., 2014), especially in case of antibodies which are evolutionarily already placed on the edge of a protein´s biophysical fitness (Sormanni et al., 2018). Nevertheless, in order to provide access to sufficient amounts of innovative drugs such as non-naturally existing more complex biologicals or DTE mAbs there is an urgent need to identify any cell or molecule-borne rate-limiting processing step during cellular synthesis and transport which might represent a secretion bottleneck.

3 OBJECTIVE

Therapeutic proteins, including mAbs, are nowadays increasingly developed to treat diverse diseases and address yet unmet medicinal needs. However, in contrast to the classical chemically synthesized small molecule-based pharmaceuticals, therapeutic proteins represent a class of macromolecules which are produced from biological sources requiring expensive and long-lasting development timelines. Additionally, the class of more complex biological formats is permanently increasing and mammalian expression systems more often show low performance. Therefore, in order to sustainably provide sufficient amounts to the market, it is mandatory to steadily improve the manufacturing efficiency.

The main objective of the present thesis was to develop and present a straight forward protocol to identify, characterize and remove production bottlenecks in industrial cell lines. Since the identification of post-translational secretion and transport bottlenecks was not routinely accessible in CHO production cell lines, we firstly aimed to develop a HT protocol to reveal intracellular production bottlenecks which should enable routine application in the highly-automated industrial work flow. In particular, we set out to develop a fluorescence microscopy-based methodology which is capable of identifying any rate-limiting processing step during cellular synthesis and transport indicated by saturated or unproductive organelle structures. After having identified molecular bottlenecks in several different production cell lines producing diverse therapeutic proteins, the underlying molecular mechanisms of a representative bottleneck should be characterized in great detail. Finally, the identified bottleneck should be addressed and removed using either classical recombinant DNA techniques and cell line engineering or bioinformatic tool-based mutant prediction to engineering the production cell line or the expressed recombinant protein, respectively, leading to superior mammalian cell-based production processes.

4 RESULTS

4.1 Identification of intracellular bottlenecks

The following chapter summarizes the establishment of an immunofluorescence microscopy-based methodology optimized for CHO cells to identify and visualize intracellular bottlenecks in industrial DTE protein-producing cell lines as published in the *Journal of Biotechnology* (Mathias et al., 2018; appendix, page 82 ff.).

Although mAbs belong to a class of recombinant therapeutic proteins that can routinely be produced in the multi-gram per liter range, some molecules turn out to be DTE. Additionally, mammalian expression systems often show low performance when producing more complex biological formats as fusion proteins or antibody derivatives. Since routine experimental methods to identify intracellular bottlenecks in CHO cell lines were not available, we developed a streamlined fluorescence microscopy-based methodology to identify unproductive or saturated organelles.

In this case study, a classical IgG1-producing CHO cell line was compared to a DTE symmetric, bsAb-producing cell line to establish a CHO-specific methodology capable of identifying secretion bottlenecks. As revealed by fed-batch cultivation, the cumulative titer was more than 2-fold lower in case of the bsAb-producing cell line but due to a superior growth and prolonged viabilities the respective calculated specific productivity was even less, reaching only one-third of the IgG-producing cell line. Classical biochemical analyses such as quantitative polymerase chain reaction (qPCR) and Western blot (WB) analyses revealed that the detected amount of transcripts and protein chains were generally sufficient to enable high protein secretion and thus did not sufficiently explain the particular low productivity of the bsAb-producing cell line (Mathias et al., 2018, Fig. 2; appendix, page 87). As the production process of secreted proteins after transcription in the nucleus and the beginning of translation in the cytoplasm is continued in different organelle structures of the cell, the distribution of the bsAb within these distinct compartments was analyzed facilitating the identification of repressive or saturated organelles hampering efficient recombinant protein production. The experimental setup comprised four fluorescent dyes having distinct excitation/emission properties which enabled to analyze four cellular compartments simultaneously. The nucleus and cytoskeleton were analyzed to obtain the fundamental cellular architecture of investigated cells. For analyzing the protein distribution, the LC or the HC of the

recombinant proteins, respectively, and one distinct organelle of the secretory pathway were concurrently visualized. However, no experimental setup was available to selectively detect the different organelles of the secretory pathway in CHO cell lines. Therefore, a variety of different antibodies established for human, rat and mouse cells were tested (full list of all tested antibodies can be found in Mathias et al., 2018, Table S1; appendix, page 95), in order to define the optimal set of antibodies specifically detecting the respective organelles in CHO cells, which is shown in the following Tab. 1.

Tab. 1: Selected primary antibodies to visualize organelles of the secretory and endocytic pathway in CHO cells using immunocytochemistry (based on Mathias et al., 2018). A full list of all tested antibodies can be found in Mathias et al., 2018, Table S1 or appendix, page 95. a: Cell Signaling Technology, Cambridge, UK; b: Abcam, Cambridge, UK; c: BD BioScience, San Jose, CA, USA; d: JacksonImmuno Research, West Grove, PA, USA

Organelle	Marker protein		Primary antibody
	Name	Abbreviation	
Ribosomes	40S ribosomal protein S6	RPS6	#5317[a]
Endoplasmic reticulum	Immunoglobulin heavy chain binding protein	BIP	#ab21685[b]
Golgi apparatus	Golgin subfamily A member 2/ 130 kDa cis-Golgi matrix protein	GM130	#610822[c]
Secretory vesicles	Ras-related protein Rab-8A	Rab8A	#ab188574[b]
Lysosomes	Lysosome-associated membrane glycoprotein 1	LAMP-1	#ab24170[b]
Endosomes	Early endosome antigen 1	EEA-1	#ab2900[b]

Investigated organelles included the ER and the Golgi apparatus as well as lysosomes, endosomes and secretory vesicles enabling the identification of unproductive or saturated organelles. Since ribosomes are sometimes also referred as organelles, the intracellular staining pattern for ribosomal proteins which represent the site of biological protein synthesis were also investigated (Mathias et al., 2018, Fig. 7; appendix, page 90).

First, the secretory organelles ER and Golgi apparatus were analyzed since important processing steps such as folding and post-translational modifications of the secreted proteins have previously been shown to represent rate-limiting steps and are performed in these compartments. The microscopic analyses of the distribution of the IgG and the bsAb within the ER are summarized in Fig. 7.

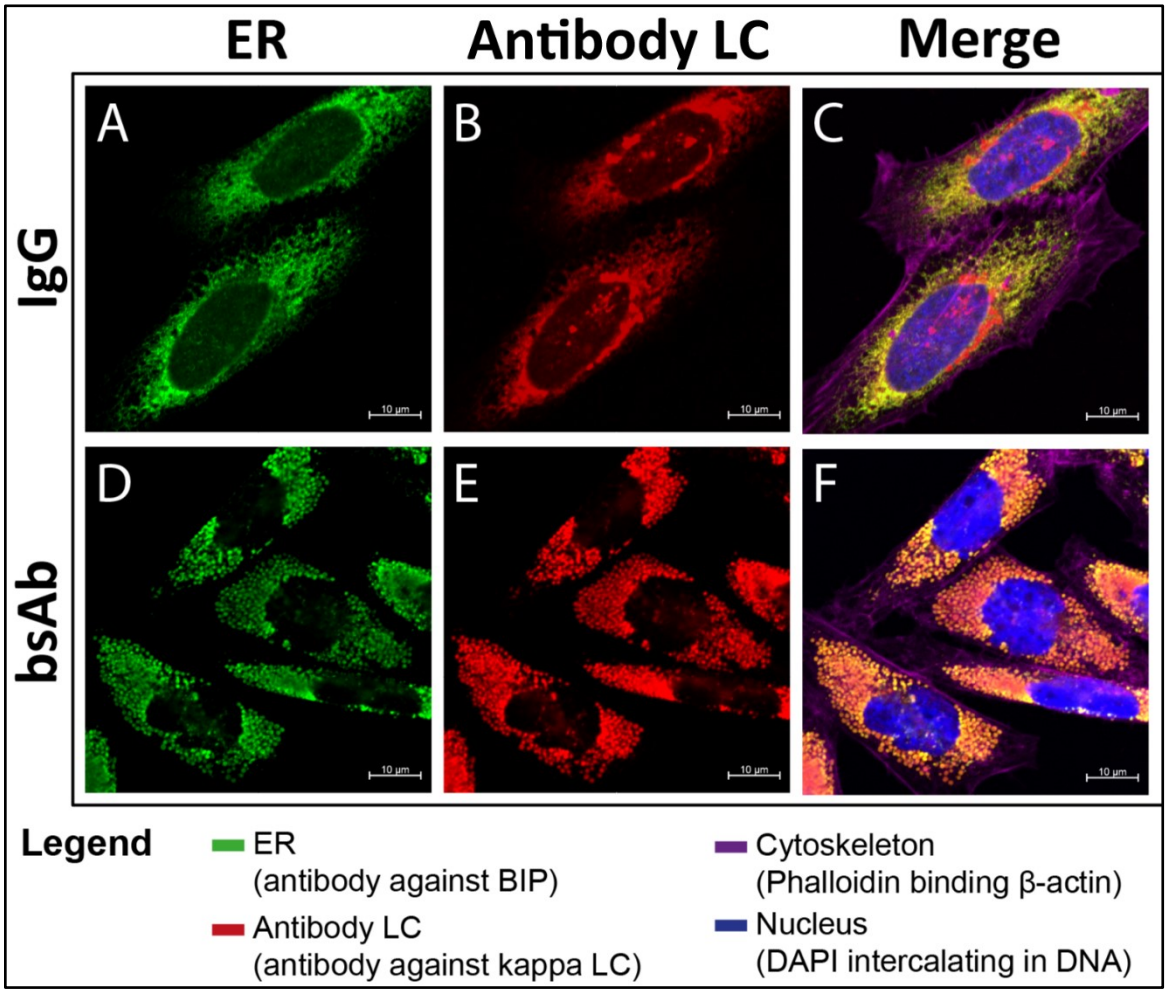

Fig. 7: Distribution of the recombinantly produced immunoglobulin G (IgG) and the bispecific antibody (bsAb) light chain (LC) (red) within the endoplasmic reticulum (ER) (green) of stable CHO production cell lines analyzed with a confocal microscope revealing aberrant ER morphology in the bsAb-producing cell line. The industrial suspension adapted CHO cell lines were cultured for the microscopic analyses adherently only. For immunocytochemistry, cells were fixed and permeabilized before staining with paraformaldehyde and TritonX-100. The ER was detected with an anti-binding immunoglobulin protein (BIP) antibody (A, D). The respective LCs were detected with a CaptureSelect™ Biotin Anti-LC-kappa (human) conjugate (B, E). Nucleus (blue) was stained with 4',6-diamidin-2´-phenylindol (DAPI) and cytoskeleton (magenta) with labeled phalloidin. Co-localization is indicated in yellow (C, F). Pictures were acquired at 63x primary magnification. The scale bars represent 10 µm (based on Mathias et al., 2018). DNA, deoxyribonucleic acid

In case of the IgG-producing cell line the ER represented a large filamentous network, which was very dense around the nucleus (Fig. 7A). In contrast, the bsAb-producing cell line showed an affected ER morphology with possibly inflated or overloaded larger irregular-shaped vesicles which were sometimes interconnected (Fig. 7D) pointing towards a secretion bottleneck. However, in both cases there was a strong co-localization of the recombinantly produced protein (Fig. 7B, E) and the respective organelle marker protein indicating that the entire ER was well-filled with recombinant protein in both cell lines (Fig. 7C, F).

After processing in the ER, secreted proteins are transported to the stacked membrane enclosed cisternae of the Golgi apparatus. Here, proteins receive further post-translational modifications before they are sorted and packed into secretory vesicles for final secretion (Alberts et al., 2002; Lodish et al., 2000). The microscopic analyses of the distribution of the IgG and the bsAb within the Golgi apparatus are summarized in the following Fig. 8.

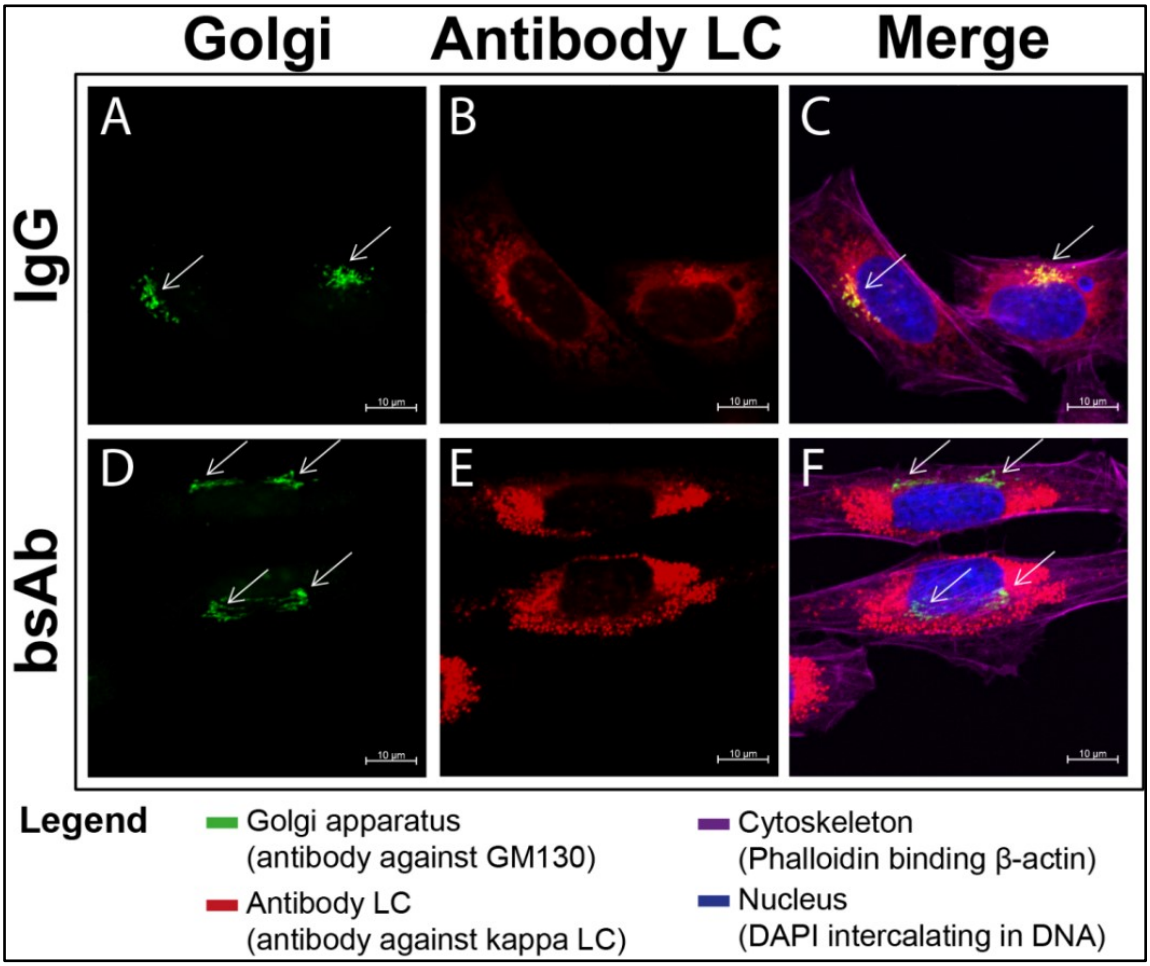

Fig. 8: Distribution of the recombinantly produced immunoglobulin G (IgG) and the bispecific antibody (bsAb) light chain (LC) (red) within the Golgi apparatus (green) of stable CHO production cell lines analyzed with a confocal microscope revealing the bsAb to be haltered in the ER. The industrial suspension adapted CHO cell lines were cultured for the microscopic analyses adherently only. For immunocytochemistry, cells were fixed and permeabilized before staining with paraformaldehyde and TritonX-100, respectively. The Golgi was detected with an anti-130 kDa cis-Golgi matrix protein (GM130) antibody (A, D). The respective LCs were detected with a CaptureSelect™ Biotin Anti-LC-kappa (human) conjugate (B, E). Nucleus (blue) was stained with 4′,6-diamidin-2´-phenylindol (DAPI) and cytoskeleton (magenta) with labeled phalloidin. Localization of the Golgi apparatus is highlighted with white arrows, co-localization is indicated in yellow (C, F). Pictures were acquired at 63x primary magnification. The scale bars represent 10 µm (based on Mathias et al., 2018). DNA, deoxyribonucleic acid

Compared to the ER, the Golgi was a small, compact and dense organelle which was found to be close to the nucleus (Fig. 8A, D), often described as perinuclear. Notably, a very strong signal for the produced recombinant protein (Fig. 8B, E) was observed within the Golgi apparatus of the IgG-producing cell line (Fig. 8C) whereas the bsAb-producing cell line showed no or only very weak co-localization of the recombinant protein and the Golgi marker (Fig. 8F). This retention of the recombinant protein within the ER of respective production cell lines additionally

pointed towards a cellular secretion bottleneck in the ER. The distribution of the HC of the recombinant proteins were generally comparable to the respective LC (Mathias et al., 2018, Fig. 4; appendix, page 86).

Since the Golgi apparatus represents an intersection between the lysosomal, secretory and endocytic pathways the distribution of the recombinantly produced protein within the lysosomes and endosomes was additionally investigated. Lysosomes and endosomes are membrane-enclosed vesicles used by the cell for hydrolysis of biomolecules and internalization of molecules from the plasma membrane. However, no co-localization was observed between the produced recombinant protein chains and lysosomes or endosomes and thus the recombinant proteins were neither detectably reinternalized nor degraded lysosomally (Mathias et al., 2018, Fig. S1; appendix, page 92). Additionally, it was not possible to detect any distribution of the produced recombinant protein chains within the secretory vesicles irrespective of whether the IgG or the bsAb-producing cell line was investigated.

As this confocal microscopy-based methodology is not compatible with industrial processes, it was investigated whether it could be transferred to an automated microscopic device facilitating the standardized identification of production bottlenecks very early in cell line development. The results of the intracellular distribution of the classical IgG and the bsAb within the secretory organelles of respective production cell lines analyzed with the HT fluorescence microscope Cellavista^{TM} are summarized in Fig. 9.

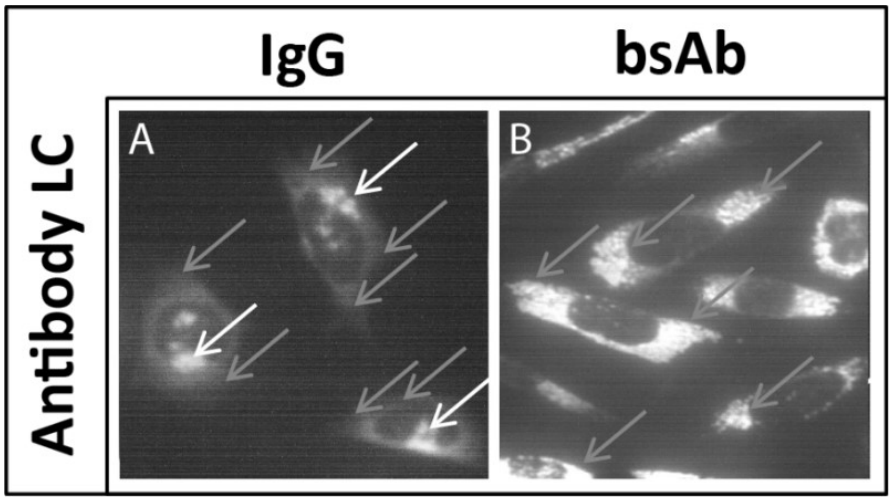

Fig. 9: Intracellular staining of (A) the recombinantly produced immunoglobulin G (IgG) and (B) the bispecific antibody (bsAb) within stable CHO production cell lines analyzed with an automated microscopic device revealing the bsAb to be haltered in the ER. The industrial suspension adapted CHO cell lines were cultured for the microscopic analyses adherently only. For immunocytochemistry, cells were fixed and permeabilized before staining with paraformaldehyde and TritonX-100, respectively. The respective light chains (LCs) were detected with a CaptureSelect™ Biotin Anti-LC-kappa (human) conjugate. Localization of the Golgi apparatus is highlighted with white arrows, the endoplasmic reticulum (ER) is highlighted with grey arrows. Pictures were acquired at 40x primary magnification (based on Mathias et al., 2018).

In the IgG-producing cell line two distinct organelle specific distribution patterns were identified, one slightly stained area spreading throughout the entire cell representing the ER (Fig. 9A, grey arrows), and a more intensely stained isolated entity close to the nucleus which represented the compact Golgi apparatus containing higher concentrations of the recombinant protein (Fig. 9A, white arrows). In case of the bsAb-producing cell line the distribution pattern of the ER was more intensely stained and the recombinant protein not detectable within the Golgi apparatus (Fig. 9B). Consequently, the bsAb appeared to be haltered within the ER leading to a more intensely stained ER. Since these results confirmed the findings obtained by confocal microscopy, the methodology is applicable to automated HT microscopy facilitating the use in industrial cell line development processes.

During this study it was shown that intracellular secretion bottlenecks can be identified by using a newly developed fluorescence microscopy-based experimental setup for CHO production cells which is transferable to industrial applications by using a HT microscopic device. This methodology represents a sophisticated starting point for further characterization of identified molecular secretion bottlenecks and subsequently facilitates organelle-tailored molecular approaches for cell line engineering to generate superior production cell lines.

4.2 Characterization of intracellular bottlenecks

This chapter summarizes the detailed characterization of a secretion bottleneck of the DTE antibody mAb2 which showed a significantly low manufacturability in a routine antibody manufacturing campaign using CHO production cells as published in *Biotechnology and Bioengineering* (Mathias et al., 2019; appendix, page 95 ff.).

All canonical steps in protein production including transcription, translation, protein folding and assembly, post-translational modification and intracellular protein transport are tightly regulated and define the specific productivity of production cell lines. Therefore, any rate-limiting step during this process might represent a bottleneck for final protein secretion into the culture medium. Especially during the production of DTE molecules, accumulation or haltering of proteins within the different cellular compartments may disturb transport or secretion (Le Fourn et al., 2014). Therefore, after having established a CHO specific methodology to identify hampering organelles in industrial production cell lines (chapter 4.1, page 17 ff.), underlying molecular mechanisms were characterized. Detailed knowledge about molecular mechanisms could finally enable molecular approaches for cell line engineering to abolish identified bottlenecks.

For detailed molecular characterization of an identified secretion bottleneck we choose a cell line expressing a classical IgG1 antibody (mAb2) with kappa LC which was identified to be DTE and compared it to a highly productive reference cell line (mAb1, IgG1 kappa) (a sequence comparison can be found in Mathias et al., 2019, Supplementary Fig. S1/S2 or appendix, page 110 f.). In particular, the comparison of the production capacity of the investigated cell lines unveiled a particular low productivity in case of the DTE antibody with > 80 % lower specific productivity compared to the mAb1-producing cell line. Subsequently, the intracellular fate of the DTE antibody mAb2 in respective stable CHO production cells was thoroughly investigated using our developed generic fluorescence microscopy-based methodology as depicted in Fig. 10.

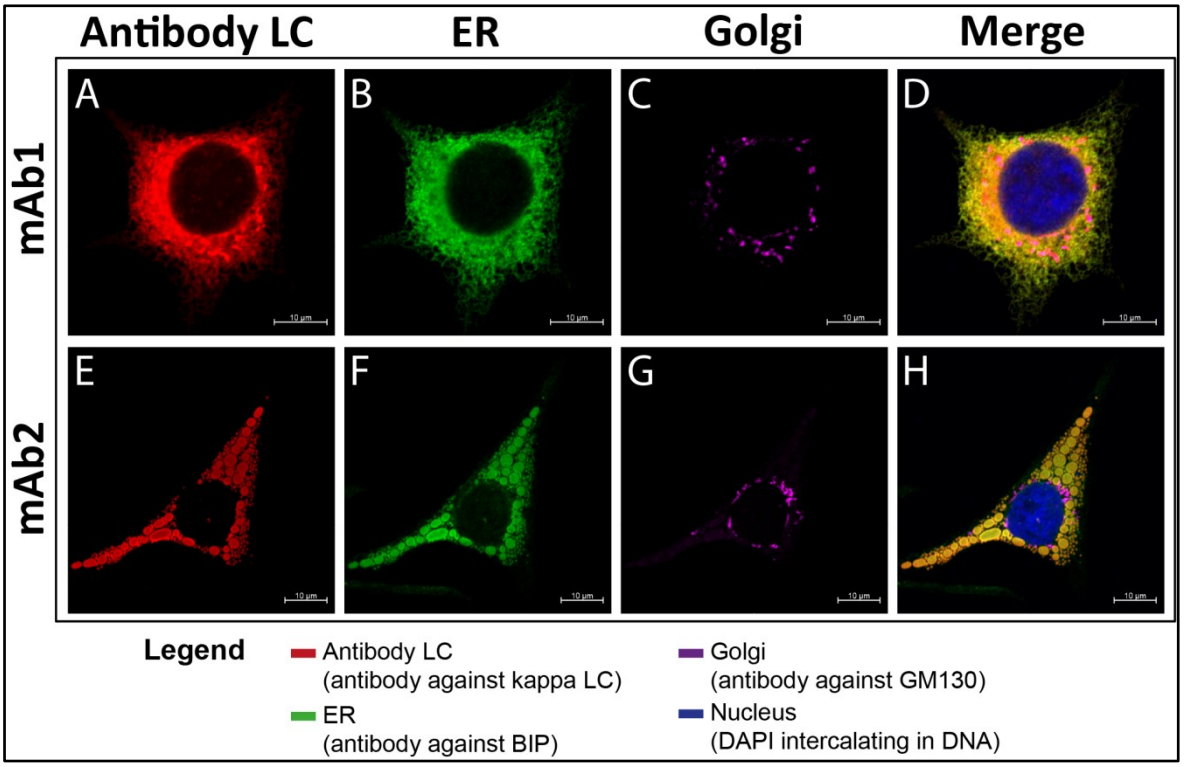

Fig. 10: Confocal microscopic images of the investigated cell lines visualizing the distribution of the produced recombinant proteins (red) within the secretory organelles endoplasmic reticulum (ER) (green) and Golgi apparatus (magenta) showing impaired ER structures in the DTE mAb2-producing cell line. The industrial suspension adapted CHO cell lines were cultured for the microscopic analyses adherently only. For immunocytochemistry, cells were fixed and permeabilized before staining with paraformaldehyde and TritonX-100, respectively. The light chains (LCs) were detected with a CaptureSelect™ Biotin Anti-LC-kappa (human) conjugate (A, E). The ER was detected with an anti-binding immunoglobulin protein (BIP) antibody (B, F). The Golgi was detected with an anti-130 kDa cis-Golgi matrix protein (GM130) antibody (C, G). Pictures were acquired at 63x primary magnification. Nucleus (blue) was stained with 4′,6-diamidin-2´-phenylindol (DAPI). The scale bars represent 10 µm. Individual signals were merged for co-localization analyses (D, H). The figure is licensed under Creative Commons Attribution - NonCommercial 4.0 International, https://creativecommons.org/licenses/by-nc/4.0/ (adapted from Mathias et al., 2019). DNA, deoxyribonucleic acid

In the highly productive mAb1-producing cell line the antibody LC (Fig. 10A) was distributed throughout the ER composed of very thin tubules (Fig. 10B) and the Golgi apparatus composed of isolated compact entities around the nucleus (Fig. 10C) as indicated by co-localization (Fig. 10D). In contrast, the mAb2-producing CHO cell line displayed a heavily altered ER morphology showing very large and possibly inflated but separated spherical structures (Fig. 10F) which co-localized with the mAb2 protein (Fig. 10E, H). In contrast to mAb1, the mAb2-producing cell line showed no or only very weak co-localization of the Golgi marker (Fig. 10G, H) and mAb2 fluorescence staining (Fig. 10E) indicating again an ER related production bottleneck.

In conclusion, microscopy-based distribution studies of the DTE protein mAb2 within the secretory organelles of respective CHO production cell lines revealed that the protein was not efficiently transported to the Golgi apparatus and thus retained in the ER. Additionally, the respective cells displayed a heavily altered ER morphology showing very large separated vesicular structures putatively including antibody deposits. In order to identify the molecular mechanisms for intracellular protein retention, electron microscopic and cell lysate fractionation experiments were performed. However, results did not point towards the formation of intracellular protein aggregates within the ER of mAb2-producing cells (Mathias et al., 2019, Fig. 3; appendix, page 102). Therefore, a certain protein processing step within the ER was likely to limit the overall secretion of mAb2, finally leading to an accumulation of proteins causative for the affected phenotype. This could include protein folding, post-translational modification and assembly. To identify the rate-limiting step hampering mAb2 from efficient transport to the Golgi apparatus and final secretion into the culture medium, a series of biochemical studies were performed. Antibody assembly was investigated using non-reducing sodium dodecyl sulfate polyacrylamide gel electrophoresis (SDS-PAGE) and subsequent WB analysis and the results are summarized in Fig. 11.

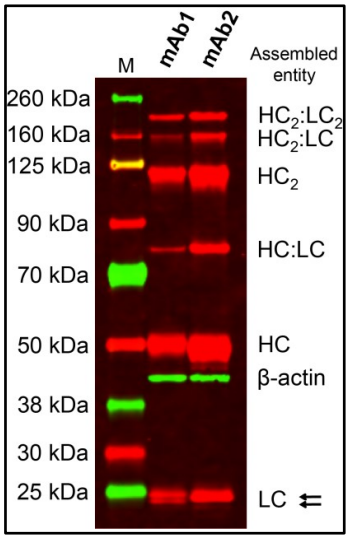

Fig. 11: Western blot (WB) analysis revealed that the difficult-to-express (DTE) mAb2 was assembled into a functional antibody unit within the respective production cells. The investigated antibody production cell lines were lysed and samples subjected to non-reducing sodium dodecyl sulfate polyacrylamide gel electrophoresis (SDS-PAGE) and subsequent WB analyses. The respective antibody light chain (LC) and heavy chain (HC) were detected with a specific anti-LC and a specific anti-HC antibody, respectively. An anti-β-actin antibody was used to confirm comparable sample loading. An identified double band for the free LC was highlighted with black arrows. The figure is licensed under Creative Commons Attribution - NonCommercial 4.0 International, https://creativecommons.org/licenses/by-nc/4.0/ (adapted from Mathias et al., 2019). kDa, kilo Dalton; M, marker

Surprisingly, both the highly productive mAb1-producing cell line as well as the DTE mAb2-producing cell line intracellularly displayed all possible assembling entities of an antibody and therefore the molecules assembled into functional antibodies within the respective production cells (Fig. 11). However, during this experiment it became apparent that the remaining free LC of the DTE protein mAb2 displayed two distinct bands with different intensities in comparison to mAb1 (Fig. 11, arrows).

As folding of LC domains is aided by intra domain disulfide bridges, non-formation of these bridges could lead to individual bands under non-reducing conditions, putatively representing different LC folding states due to slow or incomplete folding. To verify this hypothesis the amount of completely folded and thus entirely oxidized cysteines within the free antibody LC was assessed using a specific gel mobility shift assay. In brief, free LC molecules were coupled to Polyethylene glycol $(PEG)_{5000}$-maleimide, which specifically reacts with free cysteine residues, isolated from cell lysates by an immunoprecipitation protocol using a specific antibody against free kappa-LC (#MAB8461, Abnova, Taiwan) and subsequently subjected to SDS-PAGE and WB analyses. Thus, proteins with free cysteine residues will shift on a

SDS-Gel due to the addition of PEG_{5000}-maleimide. The respective results are shown in the following Fig. 12.

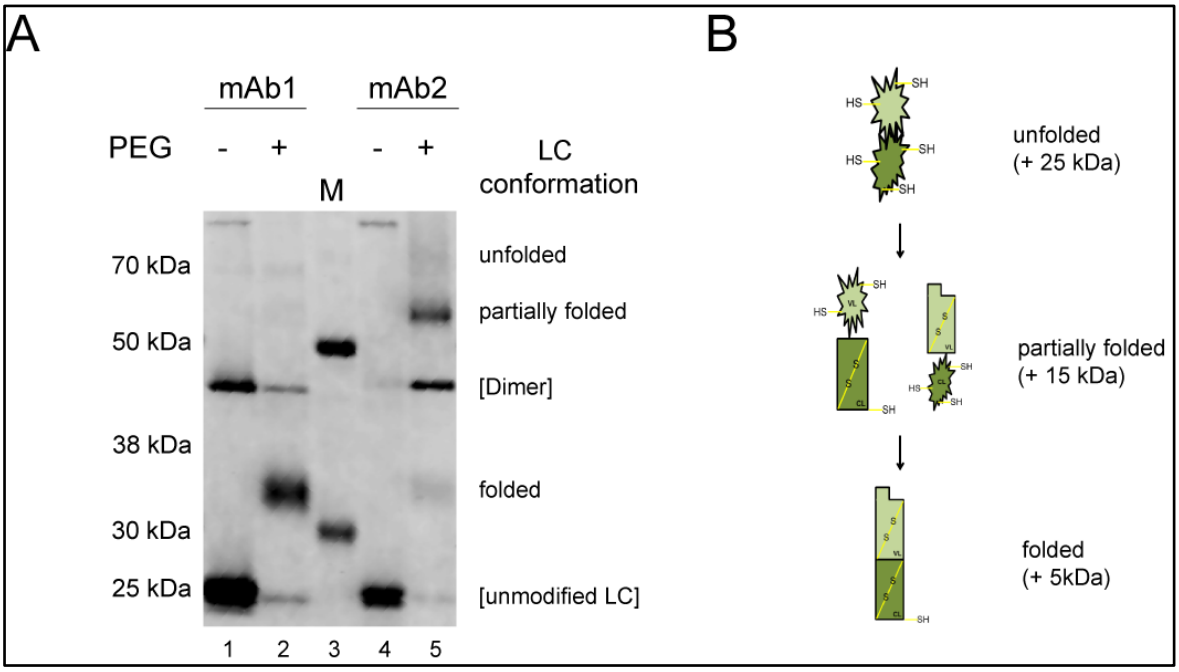

Fig. 12: A gel mobility shift assay and subsequent Western blot (WB) analysis revealed that a not formed disulfide bridge in the light chain (LC) hampered the difficult-to-express (DTE) mAb2 from efficient secretion. (A) The investigated antibody production cell lines were lysed and proteins coupled to PEG_{5000}-maleimide. Subsequently, free antibody LCs (not bound to heavy chain) were purified by an immunoprecipitation protocol using a specific antibody against free kappa-LC. Afterwards samples were subjected to sodium dodecyl sulfate polyacrylamide gel electrophoresis (SDS-PAGE) and WB experiments. Antibody LCs were detected with a specific antibody. The more unfolded a protein is the more it will shift in this assay due to the addition of respective PEG moieties. Since PEG does not interact well with SDS, PEGylated proteins appear to be heavier as they are in SDS-PAGE (White and Bode, 2018). (B) Schematic representation of folding intermediates of the antibody LC with cysteine residues highlighted. The figure is licensed under Creative Commons Attribution - NonCommercial 4.0 International, https://creativecommons.org/licenses/by-nc/4.0/ (adapted from Mathias et al., 2019). M, marker; PEG, polyethylene glycol; kDa, kilo Dalton

Confirmatively, the LC of the highly secreted antibody mAb1 was nearly entirely completely folded as indicated by a shift of the molecular weight to approx. 35 kDa corresponding to the addition of only one PEG_{5000}-maleimide residue probably to the free cysteine usually connecting LC and HC (Fig. 12A, lane 2). In contrast to this, the band of the free LC of the DTE mAb2 shifted to a molecular weight of approx. 60 kDa which corresponds to the addition of three PEG_{5000}-maleimide residues (Fig. 12A, lane 5). In consequence, the LC of the DTE mAb2 was mainly partially folded or misfolded caused by the missing formation of one disulfide bridge (Fig. 12B). Only marginal amounts of completely unfolded LC where detected

at approx. 75 kDa. PEG does not interact well with SDS, thus PEGylated proteins appear to be heavier as they are in SDS-PAGE (White and Bode, 2018).

Since cysteines are actively oxidized to disulfide bridges by chaperons of the PDI family, co-immunoprecipitation experiments were used to reveal an attenuated binding of PDIs to mAb2 LC as summarized in Fig. 13.

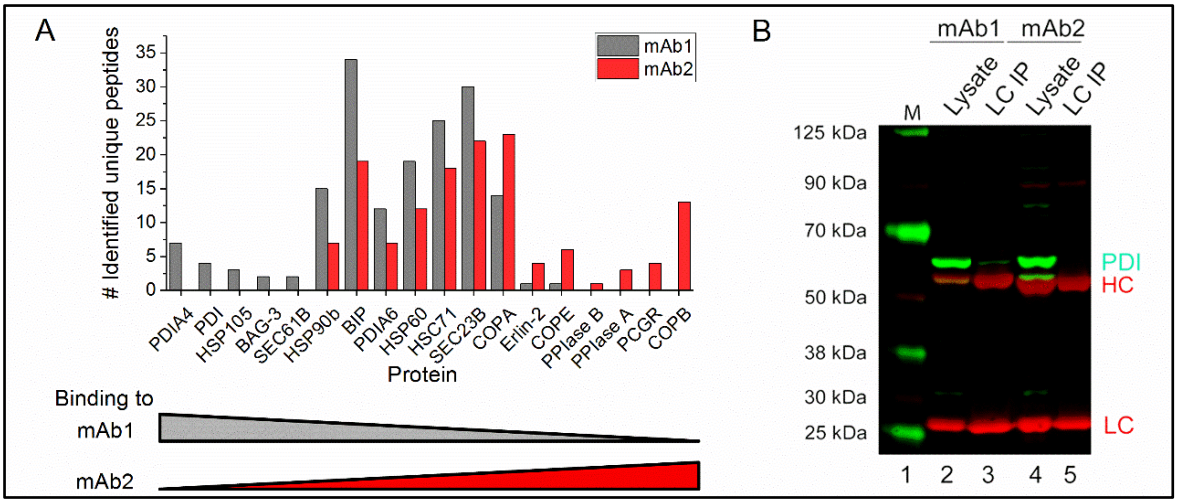

Fig. 13. Differential binding of chaperones to the investigated antibodies revealed less recognition of mAb2 by proteins of the protein disulfide isomerase (PDI) family. (A) Mass spectrometric identification of co-immunoprecipitated proteins bound to the investigated antibodies mAb1 and mAb2, respectively. The investigated antibodies were purified from respective cell lysates with a specific anti-human H+L antibody and co-immunoprecipitated proteins identified with a mass spectrometer (Thermo Fisher Scientific, Waltham, MA, USA). (B) Validation of less recognition of mAb2 by PDI using Western blot (WB) analyses. The investigated antibodies were immunoprecipitated from cell lysates as described above and subjected to reducing sodium dodecyl sulfate polyacrylamide gel electrophoresis (SDS-PAGE) and WB experiments detecting the antibody LC, HC and PDI with specific antibodies. The figure is licensed under Creative Commons Attribution - NonCommercial 4.0 International, https://creativecommons.org/licenses/by-nc/4.0/ (Mathias et al., 2019). kDa, kilo Dalton

Besides other protein classes, co-immunoprecipitation experiments with subsequent mass spectrometry (MS) analyses revealed that especially members of the PDI family (PDIA4, PDI[A1], PDIA6) were more heavily or exclusively bound to mAb1 molecules indicating a possible inaccessibility of mAb2 for oxidation of its cysteines to form intradomain disulfide bridges (Fig. 13A). Indeed, validation studies using WB analyses of co-immunoprecipitation experiments confirmed less binding of PDI to the mAb2 LC indicating that it is not recognized correctly by PDIs putatively due to improper folding (Fig. 13B, lane 3, 5). Therefore, the incomplete formation of disulfide bridges by disulfide isomerases might represent the reason for the retention of mAb2 in the ER hampering it from efficient secretion. As a consequence,

transient PDI expression experiments in the mAb2-producing CHO cell lines were performed (data not shown). Although mAb2 production cells showed high expression of PDI after transfection, no differences in mAb2 secretion were detected. However, the transfected cells showed low viability pointing towards the need of transfection optimization.

Since the DTE protein mAb2 accumulated intracellularly and caused a massive aberrant ER phenotype, it was of interest to analyze the adaptation process of the cell line to elucidate possible escape routes or survival mechanisms. Therefore, gene expression analyses were performed applying next generation sequencing of the transcriptome of both cell lines. Using functional clustering of differentially transcribed genes, several protein processing mechanisms in the ER were shown to be significantly affected by mAb2 production as summarized in Fig. 14.

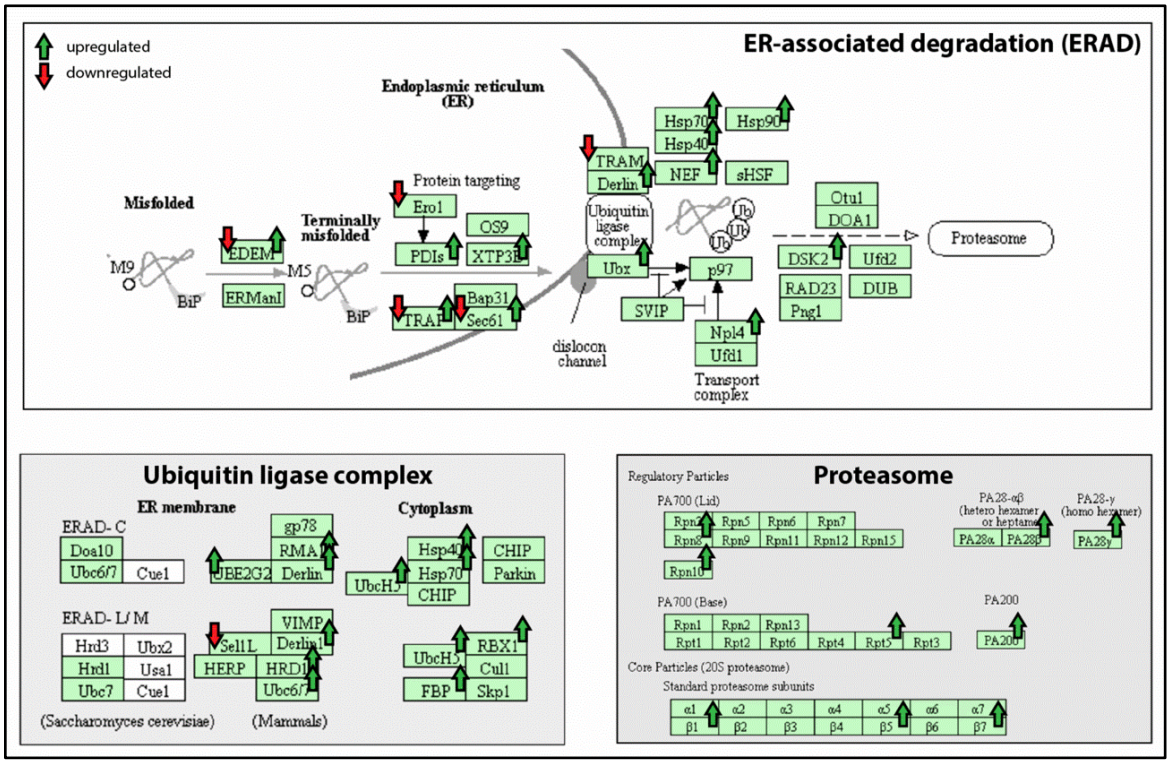

Fig. 14: Detailed pathway map of the endoplasmic reticulum-associated degradation (ERAD) process, the respective ubiquitin ligase complex and proteins constituting the proteasome with respective genes up- and downregulated during gene expression analysis indicated probably revealing an enhanced degradation of the DTE mAb2. Libraries from extracted total RNA were sequenced, processed, standardized on fragments per kilobase million (FPKM) values and statistically compared by contrast model (for details the reader is referred to Mathias et al., 2019, section 2.2 or appendix, page 98). Up- and downregulated genes are indicated by green and red arrows, respectively. A gene was considered to be regulated when Benjamini-Hochberg false discovery rate BHQ < 0.05 and fold change FC > 1.2 and FC < 1/1.2, respectively. The indication of both an upregulation and downregulation of a respective protein means that different proteins are available performing this function of which some were up- and downregulated, respectively. The figure is licensed under Creative Commons Attribution - NonCommercial 4.0 International, https://creativecommons.org/licenses/by-nc/4.0/ (adapted from Mathias et al., 2019).

The expression of the DTE mAb2 generally led to a downregulation of proteins performing regular processing steps, while proteins belonging to the ERAD pathway executing the removal of impaired polypeptides from the lumen of the ER were transcriptionally upregulated (Fig. 14). Especially transcripts of chaperons recruiting misfolded proteins for degradation via ERAD, effector proteins of the respective ubiquitin ligase complex as well as subunits of the proteasome were more abundant. Therefore, gene expression analyses indicated that the incomplete folding and accumulation of mAb2 in the lumen of the ER possibly led to an enhanced clearance of the secretory organelle from adverse protein chains via the ERAD pathway. Confirmatively, intracellular glycosylation analyses revealed an abundance of

trimmed high-mannose glycan structures like Man7, Man6 and Man5 in case of the DTE mAb2 which tag proteins in the ER for final proteasomal degradation (Mathias et al., 2019, Fig. 7; appendix, page 105).

In summary, using the established fluorescence microscopy-based methodology the DTE protein mAb2 was shown to accumulate in the lumen of the ER leading to an aberrant ER phenotype. Analysis of underlying cellular mechanisms revealed that neither aggregation nor antibody assembly, but folding represented the reason for hampered secretion. In more detail, disulfide bridge formation in the antibody LC was impaired due to less recognition by PDI. As a consequence, the DTE molecule was degraded intracellularly by the ubiquitin proteasome system via ERAD pathway. This revealed that especially with the advent of artificially designed and DTE therapeutic protein candidates more attention needs to be drawn to molecule optimization processes to ensure manufacturability.

4.3 Removal of intracellular bottlenecks

The following chapter summarizes a proof of concept study of a mAb variant that was optimized with *in silico* tools to remove a previously identified secretion bottleneck in the ER and to investigate its improved manufacturability throughout the entire production process, which was published in the journal *mAbs* (Bauer and Mathias et al., 2020; appendix page 129 ff.).

Recent advances in biopharmaceutical informatics provided efficient computational tools for the optimization of protein sequences and structures. Particular attention was payed to the Solubis method capable of identifying aggregation prone regions (APRs) which do not significantly contribute to the thermodynamic stability of a given protein and thus might promote particle formation/aggregation under native conditions (Van Der Kant et al., 2017; Van Durme et al., 2016). Since the CDRs of mAbs are primarily selected for target binding rather than for protein scaffold structure and folding, APRs herein may result in low intracellular folding kinetics and colloidal stability, the property to resist particle or precipitate formation, and thus aggregation of a molecule in concentrated solutions (Van Der Kant et al., 2017). Interestingly, by using the Solubis method, the investigated DTE antibody mAb2 which showed intracellular accumulations leading to an aberrant ER morphology during expression in CHO cells (chapter 4.2, page 23 ff.) was identified to have a critical APR in the variable domain of the LC as revealed in a previous study (Van Der Kant et al., 2017). Further, a sequence variant of mAb2 (variant) inheriting a single AA exchange in the LC (S52R) was shown to have reduced aggregation properties in transient expression experiments (Van Der Kant et al., 2017). In the here presented study (Bauer and Mathias et al., 2020), mAb2 and its *in silico* optimized variant were developed in accordance with a bioprocess widely established in the pharmaceutical industry to investigate the transfer of properties of rationally optimized antibody sequences throughout the entire industrial process chain.

The computationally optimized sequence variant and its parental counterpart were investigated during a routine drug product (DP) manufacturing campaign starting with the recombinant production of the proteinous API using stable and single clone-derived CHO production cell lines. The best eight production cell lines were first investigated in a micro-bioreactor fed-batch cultivation process to identify the overall most suitable production clones which were further investigated in a

representative 3 L benchtop bioreactor system to produce starting material for later DP comparison. The results of the upstream cultivation processes are summarized in the following Fig. 15.

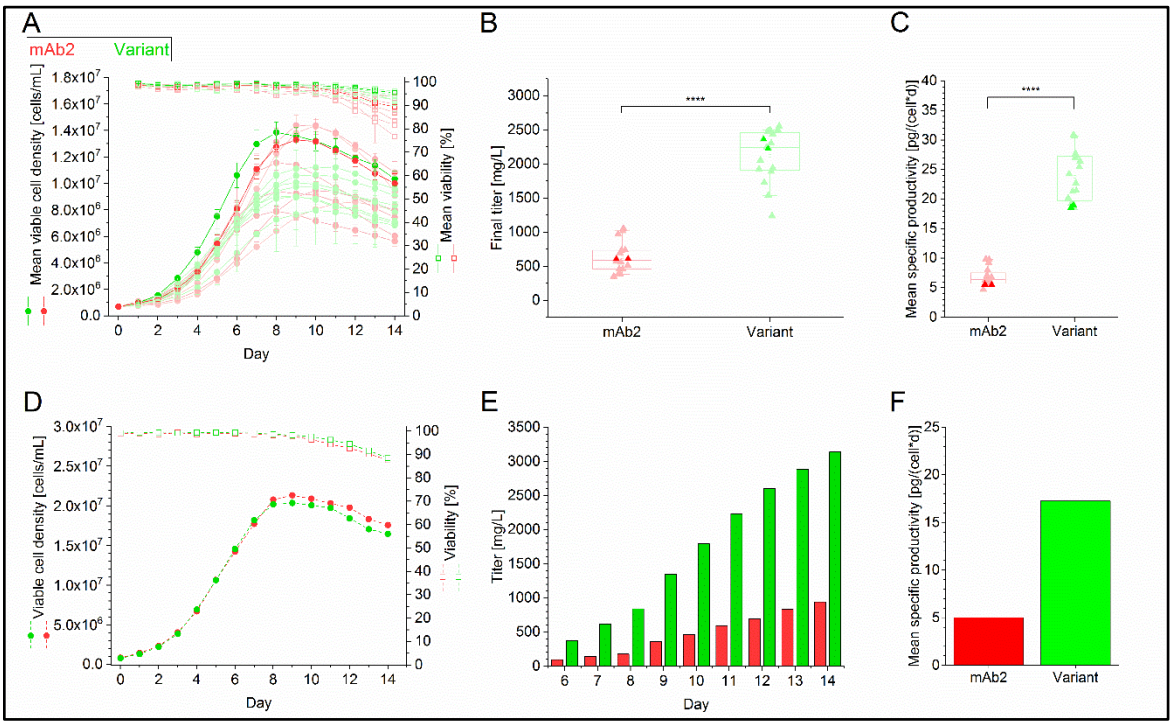

Fig. 15: Controlled fed-batch production process performance of clonal cell lines producing either the antibody mAb2 or its *in silico* optimized variant (variant) revealing an enhanced manufacturability of the variant. (A) Viable cell density (VCD) and viability, (B) final antibody titer as well as (C) specific productivity of the best eight clonal cell lines are shown for a controlled 14-day micro-bioreactor fed-batch cultivation process (ambr® 15, Sartorius, Göttingen). In case of VCD and viability the mean and standard deviation of biological duplicates (n = 2) are displayed. For boxplot generation, each replicate was used as single data point, shown whiskers represent the 10th and the 90th percentile. The highlighted clones (bold line and more intense color) were further investigated in 3 L benchtop bioreactors and further characterized this study. An unpaired Students t-test was used to determine statistical significance (**: p < 0.0001). (D) VCD and viability, (E) cumulative antibody titer as well as (F) specific productivity of the investigated clonal cell lines are shown for a controlled 14-day fed-batch cultivation process performed in a 3 L bioreactor (Bauer and Mathias et al., 2020).**

The observed high variability in peak viable cell density (VCD) ranging from approx. 8 x 10^6 to 14 x 10^6 cells/mL were comparable between all analyzed cell lines regardless of the identity of the mAb and are likely due to clonal variances (Fig. 15A). The cell viability (Fig. 15A) and as a consequence the integral of viable cells (IVC, data not shown) of the investigated cell lines was slightly higher in case of the cell lines producing the *in silico* optimized variant. However, the cell lines that expressed the variant showed a nearly four times higher average antibody titer on day 14 and mean specific productivity (Fig. 15B, C). These results,

illustrating enhanced properties of the *in silico* optimized variant regarding manufacturability, were confirmed by a more representative 3L benchtop bioreactor cultivation showing very comparable growth behavior (Fig. 15D) and in addition a significantly elevated antibody production capacity in case of the variant-producing cell line (Fig. 15E, F). More specifically, final titer of the mAb2-producing cell line was approx. 1.0 g/L with a mean specific productivity of approx. 5 pg/(cell·day), while the variant-expressing cell line achieved a final antibody titer of approx. 3.3 g/L with a mean specific productivity of approx. 17 pg/(cell·day).

As it was shown that the DTE antibody mAb2 accumulated in the lumen of the ER finally leading to an aberrant ER morphology (Fig. 10, page 24), the five best-performing production cell lines of both antibody candidates were analyzed for the formation of intracellular antibody accumulations using immunofluorescence microscopy. A non-related and highly productive reference cell line producing mAb1 was investigated for comparable reasons. The results are summarized in Fig. 16.

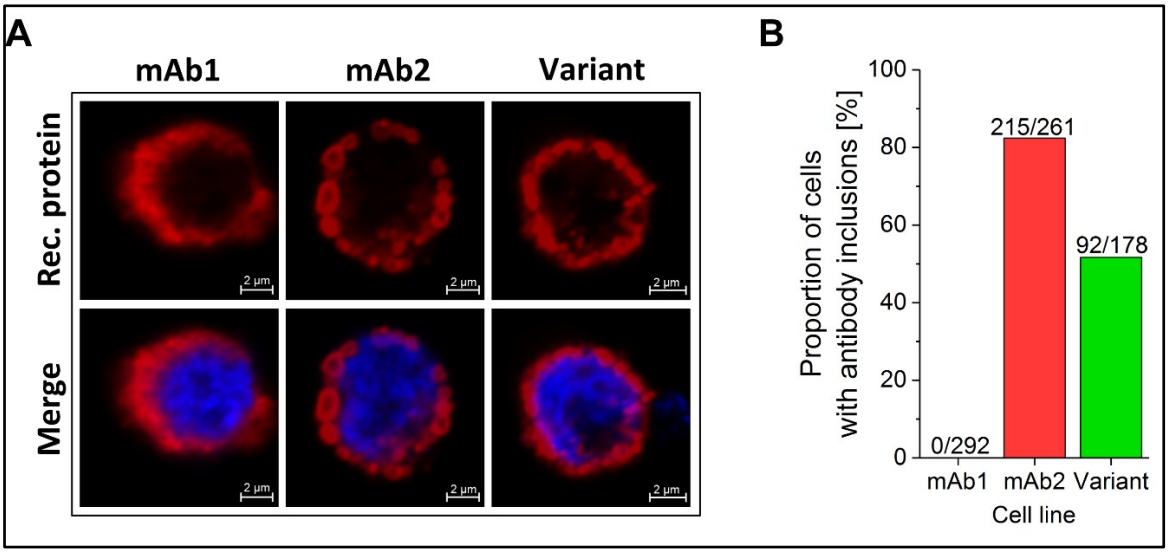

Fig. 16: Analyzed distribution of the investigated antibody mAb2 and its *in silico* optimized variant (variant) within the respective CHO production cell lines revealed a relieved phenotype in the variant-producing cell line. (A) Confocal images of the investigated cell lines. For immunocytochemistry, cells were fixed and permeabilized before staining. Recombinant protein (red) was detected with an anti-FC antibody. Nucleus (blue) was stained with 4′,6-diamidin-2´-phenylindol (DAPI). Pictures were acquired at 63x primary magnification. For comparative reasons an easy-to-express antibody (mAb1) was additionally investigated. The scale bars represent 2 µm. Overview pictures can be found in Bauer and Mathias et al., 2020, Supplementary Fig. S3 or appendix, page 145. (B) Amount of single cells with intracellular antibody inclusions. For this analysis cells have been cultured adherently only. Overview pictures can be found in Bauer and Mathias et al., 2020, Supplementary Fig. S4 or appendix, page 146 (based on Bauer and Mathias et al., 2020).

The recombinant protein within the non-related mAb1-producing reference cell line (same cell line as described in chapter 4.2, page 24 ff) showed a very fine filamentous distribution which was dispensed throughout the entire cytoplasm (Fig. 16A, left column). However, all five investigated (independently generated and single-clone derived) mAb2-producing cell lines consistently displayed large distinct round-shaped vesicles up to approx. 2 µm in size as exemplarily shown in Fig. 16A (center column) (further images can be found in Bauer and Mathias et al., 2020, Supplementary Fig. S3 or appendix, page 145). As previously described, these vesicles represent non-aggregated intracellular antibody accumulations in aberrant ER structures (chapter 4.2, page 23 ff.). Remarkably, the five best-performing CHO cell lines producing the *in silico* optimized variant still displayed an affected morphology albeit consistently in an attenuated form, where significantly less filamentous structures were inflated still forming a dense network (Fig. 16A, right column). Since some cells of the *in silico* optimized variant-producing cell lines did not show a compromized structure at all, a representative number of individual cells

(n > 150) was microscopically inspected and categorized regarding their morphologic appearance (Fig. 16B). Cells with compromized structures were completely absent from the reference cell line population and nearly all cells produced the recombinant protein. In case of mAb2 more than 80 % of the investigated individual cells within five independently generated distinct populations showed an affected cell morphology. Interestingly, the remaining 20 % showed normal morphology but seemed to be rescued by escaping from mAb2 production (data not shown). Contrary to this, only 50 % of individual cells within the five *in silico* optimized populations exhibited a compromised morphology with nearly all cells producing the recombinant protein. These analyses indicated that the production of mAb2 inevitably led to an affected morphology in all productive cells, whereas some cells were able to produce the generated *in silico* optimized variant without restrictions. As a consequence, the *in silico* optimized variant cell populations not only showed less cells with compromised structures of the ER, but most affected cells also showed a relieved phenotype indicating a beneficial effect on the upstream development of the *in silico* optimized antibody.

Since it was previously shown that a non-established disulfide bridge in the LC affected retention and intracellular accumulation of mAb2 (chapter 4.2, page 23 ff.), the developed gel mobility shift assay was used to estimate and compare intracellular folding of mAb2 and its *in silico* optimized variant. The results are summarized in the following Fig. 17

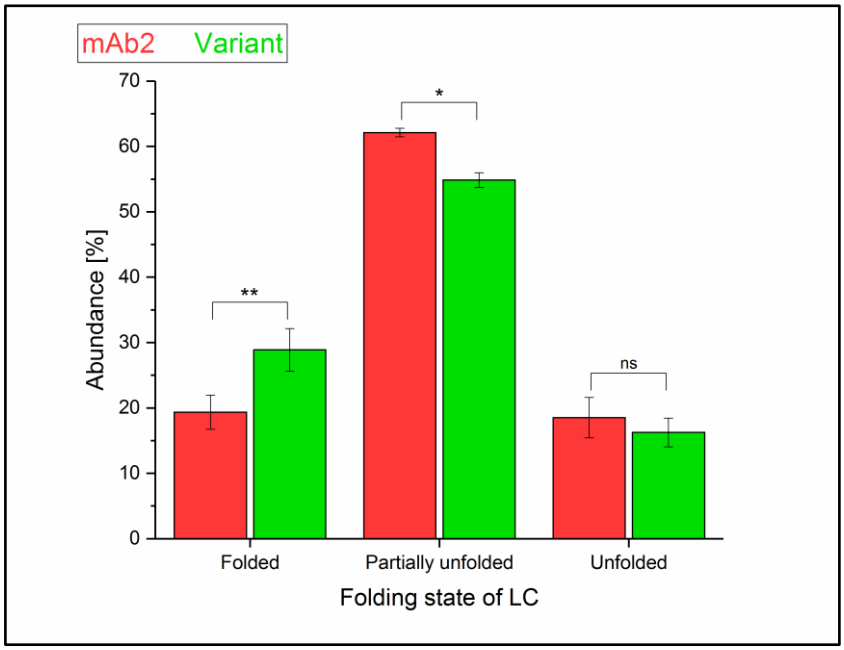

Fig. 17: The *in silico* optimized variant (variant) showed enhanced intracellular folding of the light chain (LC) in comparison to its parental counterpart mAb2. The described gel mobility shift assay (compare Fig. 12, page 28) was used to investigate intracellular folding intermediate abundance. In brief, free cysteine residues of proteins were coupled to PEG_{5000}-maleimide in cell lysates. Subsequently free antibody light chains (LCs) not bound to heavy chain (HC) were purified by an immunoprecipitation protocol using a specific antibody against free kappa-LC. Afterwards the samples were subjected to sodium dodecyl sulfate polyacrylamide gel electrophoresis (SDS-PAGE) and Western blot (WB) experiments. Antibody LCs were detected with a specific antibody. Densitometric analyses of three independent WBs (n = 3, mean and standard deviation is displayed) were performed using Image Studio Software Version 5.2.5 (LI-COR, Lincoln, NE, USA). An analysis of variance (ANOVA) was used to determine statistical significance (*: $p < 0.05$; **: $p < 0.01$). A figure of a representative WB can be found in Bauer and Mathias et al., 2020, Supplementary Fig. S5 or appendix, page 147 (adapted from Bauer and Mathias et al., 2020 distributed under the Attribution-NonCommercial 4.0 International License (CC BY-NC 4.0), https://creativecommons.org/licenses/by-nc/4.0/). ns, not significant

The gel mobility shift assay in which different antibody folding states are identified by remaining free cysteine residues (compare Fig. 12, page 28), revealed that the intracellular steady-state concentration of completely folded antibody LC was increased in case of the *in silico* optimized variant (Fig. 17). Further, less incompletely folded LC molecules were identified to accumulate intracellularly in case of variant-producing cells probably leading to a relieved phenotype due to enhanced folding of the *in silico* optimized variant. As a consequence, the identified bottleneck in the investigated DTE mAb2-producing cell line, in which proteins are trapped in the lumen of the ER due to insufficient folding, could at least partially be rescued by one single AA substitution in the variable domain of the LC.

To further evaluate the effect of the computationally predicted sequence variant of mAb2 on the entire biopharmaceutical manufacturing process, the investigated antibodies were purified from cell culture supernatant using a routine downstream purification strategy. After each step of purification comprising antibody capture with Protein A affinity chromatography (AC) and acidic treatment (AT), depth filtration (DF), anion exchange chromatography (AEX), ultrafiltration and diafiltration (UF/DF) as well as formulation (Initial DP), samples were taken and investigated regarding critical quality attributes including protein aggregation and glycosylation. The results are summarized in Fig. 18.

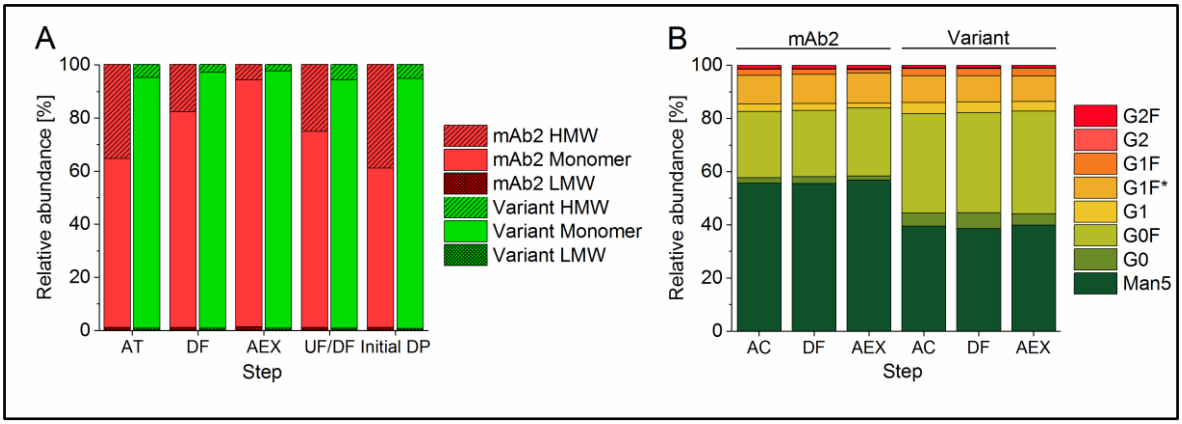

Fig. 18: Characterization of the product quality at different steps of a routine antibody downstream purification process revealed lower aggregation propensities in case of the *in silico* engineered variant (variant) in comparison to its parental counterpart mAb2. (A) Proportion of high-molecular weight (HMW), low-molecular weight (LMW) species and monomer and (B) N-glycosylation profile of mAb2 and its variant after Protein A affinity chromatography (AC), acidic treatment (AT), depth filtration (DF), anion exchange chromatography (AEX), ultrafiltration and diafiltration (UF/DF) and achievement of the initial drug product (Initial DP). HMW/LMW species represent aggregates/fragments monitored during a size exclusion chromatography (SEC) on a high-performance liquid chromatography (HPLC) system. N-glycosylation pattern was determined by capillary electrophoresis (based on Bauer and Mathias et al., 2020). Man5, mannose-5, G, galactose, F, fucose

As identified by size exclusion chromatography (SEC), the *in silico* optimized variant of the DTE antibody mAb2 showed a significant reduction in aggregates, monitored during SEC experiments as high-molecular weight (HMW) species, throughout the entire purification process (Fig. 18A). The wild type antibody mAb2 showed very high levels of HMW species, especially after initial purification, AT and after concentration of the drug (UF/DF, Initial DP). The amount of fragmented antibodies, which were detected during SEC experiments as low-molecular weight (LMW) species, were very comparable between both antibodies (< 2 %). As a consequence, the amount of monomeric antibody, which with HMW and LMW

species sum up to 100 %, was significantly advanced in the *in silico* optimized variant throughout the entire purification process. More specifically, after all purification steps mab2 showed a monomer content of approx. 60 %, while the *in silico* optimized variant had a monomer content of nearly 90 %. Further, the N-glycosylation pattern of the *in silico* optimized variant showed slightly improved glycosylation with less abundance of premature Man5 glycan structures, however, both antibodies still showed high levels of immature glycan species which was not altered during the purification process (Fig. 18B). In summary, the *in silico* optimized variant showed enhanced properties during antibody purification processes and a slightly more mature N-glycosylation pattern.

After routine purification of the investigated antibody and its *in silico* optimized variant, both APIs were prepared in a formulation buffer (25 mM sodium citrate, pH = 6.0, 125 nm NaCl) and biophysically characterized. While the thermodynamic stability (T_m) was maintained (Bauer and Mathias et al., 2020, Fig. 4; appendix, page 134), the onset aggregation temperature (T_{agg}), where molecules start to aggregate, was significantly increased in the *in silico* optimized variant pointing towards a higher resistance towards aggregation in case of the *in silico* optimized variant (Bauer and Mathias et al., 2020, Fig. 5; appendix, page 134). Another often encountered challenge in drug development is high viscosity of the concentrated DP hampering processing, filling and also administration. The viscosity of the formulation was reduced in the *in silico* optimized variant, but was also not critical in mAb2 containing formulations (Bauer and Mathias et al., 2020, Supplementary Fig. S8; appendix, page 149). However, viscosity measurements could only be performed up to a protein concentration of 10 mg/mL due to precipitation of mAb2 upon further concentration in UF/DF, an effect that was not observed in case of the *in silico* optimized variant (Bauer and Mathias et al., 2020). The predicted strong self-association/-aggregation tendency of mAb2 was confirmed by an exponentially increasing diameter, while that of the *in silico* optimized variant increased linearly with increasing concentration (Bauer and Mathias et al., 2020, Fig. 5; appendix, page 134).

Finally, the product was filled in glass vials and investigated regarding its stability during a six-month stability study under intended storage conditions (2 - 8 °C) and additionally under accelerated conditions (25 °C and 40 °C) to estimate stability

under unintended storage or for longer periods. Samples were taken at defined analytical time points and investigated as summarized in Fig. 19.

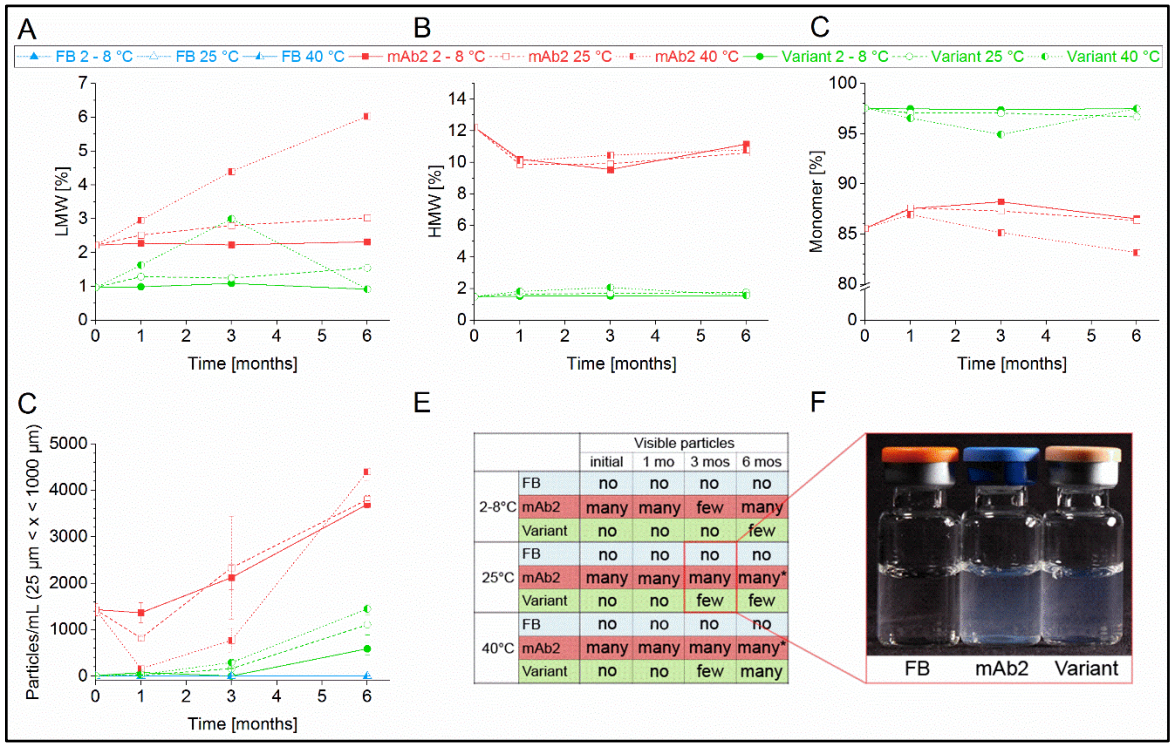

Fig. 19: Product quality and colloidal stability (property to resist aggregation) of the formulated drug products (DPs) containing mAb2 and its *in silico* optimized variant (variant) were evaluated in a stability study indicating enhanced storage stability in case of the variant. Proportion of (A) low-molecular weight (LMW) species, (B) high-molecular weight (HMW) species and (C) monomer of the respective antibody at different analytical time points of the storage study. HMW/LMW species represent aggregates/fragments monitored during a size exclusion chromatography (SEC) on a high-performance liquid chromatography (HPLC) system. (D) Concentration of particles with a size between 25 µm and 1000 µm measured with a micro-flow imaging (MFI) system characterizing each sub-visible particle in a micro-fluidic channel with a fixed camera. (E) By visual inspection identified turbidity of formulation in glass vials due to the formation of visible particles. * Filamentous particles. (F) Example image of DPs in filled glass vials stored for three month at 25 °C (based on Bauer and Mathias et al., 2020). FB, formulation buffer; mo, month

Beside no obvious alterations in biophysical properties such as pH, osmolality and viscosity of the formulated drugs after a storage period of six month at 2 - 8 °C, 25 °C, or 40 °C (Bauer and Mathias et al., 2020), the formulated DPs were also investigated for changes in levels of fragments and aggregates of the respective antibody, monitored during SEC experiments as LMW and HMW species, respectively. The relative abundance of LMW species was comparable between both antibodies and did not further increase under normal storage conditions (Fig. 19A). However, under intensified storage conditions mAb2 was found to fragment over time as indicated by an elevated amount of LMW species.

Further, the *in silico* optimized variant showed significantly reduced initial levels of aggregates directly after filling which did not further increase in case of both molecules during the storage for six month at described conditions (Fig. 19B). Since LMW species, HMW species and monomeric antibody represent all entities during SEC experiments, the consistently increased levels of HMW species (aggregates) and the increasing levels of LMW species (fragments) over time under exacerbated conditions resulted in a significant loss of active antibody monomer in case of mAb2 (Fig. 19C). Interestingly, a subvisual particle formation was observed in all antibody containing formulations and under all storage conditions, however, was significantly more prominent in mAb2 containing formulations (Fig. 19D). Not only the initial particle concentration after filling but also the increase over time was significantly elevated in case of mAb2. Additionally, by visual inspection of the liquid formulations in glass vials it became apparent that not only subvisual but also visible particle formation was substantially triggered in mAb2 containing formulations but also in the variant containing formulations during storage at 25 °C and 40 °C finally leading to a visible turbidity of the respective solutions (Fig. 19E, F). Additionally, formulations of the *in silico* optimized variant showed reduced color intensity and opalescence in comparison to mAb2 formulations (Bauer and Mathias et al., 2020, Fig. 6; appendix, page 135). Finally, storage of both DPs for up to six month under intended and intensified storage conditions did not alter the antigen binding activity as revealed by surface plasmon resonance (SPR) binding experiments (Bauer and Mathias et al., 2020, Fig. 7 and Tab. 1; appendix, page 136 and 136, respectively). In conclusion, our data suggest that *in silico* analysis and optimization of mAb sequences can enhance its manufacturability throughout the entire production process from antibody production during cell culture, downstream purification, final formulation and storage, without negatively affecting product quality and antigen binding capacity. This was exemplarily shown with a mAb which was identified to be DTE and its *in silico* optimized variant with significantly enhanced manufacturability enabled by one predicted AA substitution in the LC. Confirmatively, the previously identified intracellular secretion bottleneck hampering the DTE antibody mAb2 from efficient secretion and finally leading to an aberrant ER morphology was relieved in the *in silico* optimized variant-producing cells.

.

5 DISCUSSION

Using modern fed-batch cultivation processes, mAbs can routinely be produced in the multi-gram per liter range (Bandaranayake and Almo, 2014; Kunert and Reinhart, 2016). However, some drug candidates turn out to be DTE and with the additional advance of artificial molecule formats mammalian expression systems more often show low performance during cellular production processes (Lee et al., 2007). Therefore, there is an urgent need to identify any rate-limiting step and de-bottleneck current expression systems to provide highly innovative but affordable biologics to the market (Pybus et al., 2014).

To identify the most suitable production cell line and access drug candidate manufacturability, small-scale production processes with biochemical analyses such as qPCR and WB are routinely performed already during cell line development to investigate transcription and translation rates. However, it was previously shown that the routine application of these classical biochemical methods are usually not sufficient to reveal limiting intracellular protein processing steps as many bottlenecks were identified to occur late in the process of cell-based protein production process beyond protein translation (Johari et al., 2015; Lee et al., 2007; Le Fourn et al., 2014). Especially, transcription of the recombinant genes was shown not to be a major limiting step probably due to the usage of highly efficient gene transfer methodologies, optimized gene expression cassettes and gene amplification strategies (Browne and Al-Rubeai, 2007; Wurm, 2004). In addition, the identification of a non-linear relationship between transcript level and secretion of certain recombinant proteins revealed that indeed a post-transcriptional processing step might be the rate-limiting step (Johari et al., 2015; Ku et al., 2008). Regarding the molecular process in protein production after transcription namely translation, it was shown that recombinant messenger ribonucleic acids (mRNAs) are as efficiently processed as endogenous mRNAs and therefore translation also seems not to represent a major bottleneck (Kallehauge et al., 2017). Insufficient correlation between intracellular and secreted recombinant protein amount further pointed towards the presence of post-translational secretion bottlenecks (Fann et al., 1999; Schröder and Friedl, 1997). Indeed, during the last decades several post-translational processing steps within the ER and Golgi apparatus have been identified to be rate-limiting for the overall production and secretion of recombinant proteins in CHO cells (Lattenmayer et al., 2007; Le Fourn et al., 2014; O'Callaghan

et al., 2010; Reinhart et al., 2014). Particularly, assembly and secretion were detected to represent a major rate-limiting step in case of some antibody molecules (Bibila and Flickinger, 1992; Mohan et al., 2008; O'Callaghan et al., 2010). However, when comparing different cell lines and products, at best similar pathways but not the same genes were identified to be rate-limiting and thus bottlenecks may be very specific to a certain molecule or production cell line emphasizing the need for a standardized methodology capable of identifying post-translational bottlenecks in industrial work flows. Therefore, we have established a streamlined CHO specific fluorescence microscopy-based methodology to routinely identify and visualize post-translational bottlenecks during cellular production processes (chapter 4.1, page 17 ff.). In particular, saturated or unproductive cellular compartments of CHO production cell lines were identified by tracing the recombinant protein being processed, transported and finally secreted by the organelles of the secretory pathway. Further, the established confocal microscopy-based methodology was optimized and transferred to a HT compatible automated microscopic device to enable successful implementation in highly automated industrial cell line development processes (Fig. 9, page 22). Especially in combination with automated picture analysis tools and TGE attempts, the integration of automated microscopic analyses might lead to the rapid identification of suitable drug candidates and production cell lines.

A cell line expressing a symmetric bsAb was used for the establishment of the microscopy-based methodology and investigated for the presence of a post-translational intracellular secretion bottleneck. Although it became apparent that transcript levels of both HC and LC were reduced in comparison to the highly productive reference cell line (Mathias et al., 2018, Fig. 3; appendix, page 86), varying transcript levels can only in part explain differences in a protein´s abundance, which is further complemented by mechanisms as translation and protein degradation rates (de Sousa Abreua et al., 2009; Vogel and Marcotte, 2012). Confirmatively, it has also been described by others that slightly reduced transcript levels did not sufficiently explain a dramatically reduced protein production capacity pointing towards another rate-limiting step (Chromikova et al., 2015; Mathias et al., 2019, 2018; Reisinger et al., 2008). In addition, the mRNAs of the expressed bsAb were efficiently translated into protein sequences as revealed by WB experiments (Mathias et al., 2018, Fig. 3; appendix, page86). However, by using the

established microscopic methodology, an aberrant ER morphology could be identified in the DTE bsAb-producing cell line pointing towards the presence of saturated organelle structures. Here, the normally observed interconnected network of sacs and tubules collapsed to become large and distinct round-shaped structures resembling previously described Russell bodies (RBs) (Kopito and Sitia, 2000; Stoops et al., 2012). RBs host insoluble Ig aggregates within the dilated cisternae of the ER or derived vesicles thereof containing ER resident proteins like BIP and calnexin (Hasegawa et al., 2017, 2011; Stoops et al., 2012). These structures can also be found in plasma cells undergoing excessive synthesis of Igs especially as a manifestation of physiological abnormalities (Decourt et al., 2004; Jiang et al., 1997; Maldonado et al., 1966). In addition, RBs have also been described when mutant antibody molecules with shortened HC, as seen in various lymphoid malignancies, were expressed in mammalian cells (Giannone et al., 2017; Mattioli et al., 2006; Mossuto et al., 2015; Valetti et al., 1991). Interestingly, several reports described that even full length antibodies can induce RB formation in recombinant protein-producing cell lines such as CHO and HEK293 (Hasegawa et al., 2017, 2014; Reinhart et al., 2014; Stoops et al., 2012). Especially, the LC was identified to play an important role as a mutant HC protein accumulating in the ER could be rescued by co-expression of LC proteins (Corcos et al., 2010). Further, by the expression of several non-cognate antibody HC/LC pairs, Stoops and co-workers showed that a LC´s low secretion competence was sufficient to promote RB formation which resulted in low manufacturability of the respective antibodies. Contrarily, a LC´s high secretion competence alone was not sufficient to ensure high secretion levels (Stoops et al., 2012). But also other proteins and especially mutants thereof such as in case of α-1-antitrypsin and antithrombin can induce RB formation (Carlson et al., 1989; Kimura et al., 2015; Manetto et al., 1989). All these studies indicate that the primary AA sequence and the resulting structure of the expressed antibodies might represent a major reason for a cell´s productivity and the formation of RBs.

Despite intracellular recombinant protein aggregation, the aberrant ER morphology has also been described as a consequence of several other conditions. Hendershot and co-workers showed that the recombinant expression of mutant BIP, one of the most important chaperones in the ER, deficient in any ATPase activity in CV-1 in origin, carrying SV40 genetic material (COS) cells led to a vesicularization of the ER

membrane resembling a RB-like phenotype (Hendershot et al., 1995). Later it was found that the ATPase activity of BIP is regulated by sensing the level of oxidative stress turning BIP from a “foldase” into a “holdase” under oxidative conditions to prevent the aggregation of proteins under stress conditions (Wang et al., 2014; Wang and Sevier, 2016; Wei et al., 2012). This indicates that oxidative stress might reduce the inherent folding activity of the important ER chaperone BIP which in turn results in an affected ER morphology due to overwhelming protein folding requirements. Confirmatively, the artificial knockdown of BIP using siRNAs in HEK293 cells also led to a massive ER expansion and disorganization indicating that a downregulation or depletion of BIP might result in the aberrant ER morphology probably induced by spontaneous UPR activation (Li et al., 2008). Interestingly, simultaneous knockdown of BIP and XBP-1 recovered normal physiological conditions (Li et al., 2008). Further, also the inducible knockout of the ERAD machinery component suppressor/enhancer of Lin-12-like (Sel1L) resulted in dilated ER vesicles (Sun et al., 2014). Possibly all of these conditions have in common that proteins (soluble or insoluble) accumulate within the lumen of the ER which cannot be purged finally leading to the aberrant ER morphology.

Interestingly, the in this study investigated bsAb-producing cells displayed normal growth behavior and did not undergo extended cell death, although they accumulated massive amounts of proteins in the lumen of the ER. This phenomenon has also been described in previous reports by Valetti and co-workers (Valetti et al., 1991). It was further shown that essential proteins for growth and cell division are translated at free ribosomes within the cytoplasm (Kronja and Orr-weaver, 2011; Pyronnet and Sonenberg, 2001; Stumpf et al., 2013). As a consequence, the accumulation of recombinant proteins in the ER might not have affected proteins relevant for cell division or growth. However, Hasegawa and co-workers showed a compromised cell growth in RB-producing HEK293 cells due to UPR activation (Hasegawa et al., 2017). Contrary to these reports we showed unaltered growth, the affected cells were also still able to secrete appreciable amounts of recombinant proteins indicating that the basic cellular functions of the secretory pathway appeared not to be disrupted completely. In fact, due to much lower secretion rates of recombinant proteins in the affected cells more free energy might have been available finally leading to the observed better growth.

The establishment of the microscopy-based bottleneck screening methodology was performed with a non-naturally existing bsAb-producing cell line as this format likely has specific requirements and thus is to some extent limited in its secretion (Lee et al., 2007). For detailed molecular characterization of an identified secretion bottleneck a classical IgG1 kappa-producing cell line (mAb2) was used not to focus on bottlenecks which are induced by and/or specific for the respective artificial protein design. Interestingly, both cell lines showed the same outcome with an accumulation of recombinant proteins within the ER, no detectable amounts within the Golgi apparatus and a heavily affected ER morphology putatively pointing towards a common molecular bottleneck (chapter 4.1, page 17 ff.; chapter 4.2, page 23 ff.). Particularly, since this aberrant morphology was found in all investigated cell lines producing either the bsAb or mAb2 even under different culture conditions as well as different time points in cultivation it did neither represent a clone-specific phenomenon nor was it exclusively induced by exogenous stress conditions. By electron microscopy and cell lysate fractionation the recombinant protein mAb2 was found not to form intracellular aggregates within the secretory organelles of the respective production cell lines (Mathias et al., 2019, Fig. 3; appendix, page 100). This is contrary to the previously described RB structures which host insoluble Ig aggregates (Hasegawa et al., 2017, 2011; Stoops et al., 2012). We did also not observe evidences for other aforementioned reasons resulting in an affected ER morphology such as oxidative stress or downregulation of essential chaperones in the mAb2-producing cell lines (Mathias et al., 2019, Fig. S7 and Table S2; appendix, page 113 and 121 ff., respectively). Interestingly, the antibody mAb2 was found to be as efficiently assembled as the highly secreted reference molecule (Fig. 11, page 26). However, when folding of the intracellularly accumulated antibody mAb2 was investigated it became apparent that one of the two intra domain disulfide bridges within the LC was not established (Fig. 12, page 28). We speculated that it might be the variable domain which was devoid of the respective disulfide bridge and thereby hampered efficient secretion as mAb2 and the highly expressed reference antibody mAb1 comprised the same constant kappa LC sequence (Mathias et al., 2019, Fig. S1; appendix, page 108). Interestingly, in literature several other Ig LC molecules have been described to be secretion incompetent (Dul and Argon, 1990; Köhler et al., 1976). It was found that they accumulate in the lumen of the ER until degradation also devoid of the

intradomain disulfide bridge in the variable domain (Knittler et al., 2006; Leitzgen et al., 2002; Skowronek et al., 2002). All of these molecules possibly have in common that they were not readily recognized by ER resident chaperones. One of the key players in oxidative protein folding catalyzing the oxidation of cysteine residues to form disulfide bridges is PDI (Appenzeller-Herzog, 2011). Indeed, we were able to show that the incompletely folded mAb2 LC investigated in this study was less bound by the chaperone PDI which might have led to an inefficient catalysis of the respective disulfide bridge. Another very important protein for folding in the ER is BIP which interacts with unfolded or partially folded proteins by the recognition of exposed hydrophobic core patches and assists in folding (Behnke et al., 2017; Feige et al., 2016). During our study (chapter 4.2, page 24 ff.), we were not able to detect a stronger interaction between the central ER chaperon BIP and the partially unfolded mAb2 LC (in comparison to the reference antibody mAb1) (Mathias et al., 2019, Fig. S8; appendix, page 116). This is contrary to previous reports, which reported a strong interaction between BIP and the expressed recombinant proteins (Knittler et al., 2006; Skowronek et al., 2002; Vincenz-donnelly et al., 2018). However, it was shown that some antibodies can escape cellular quality control mechanisms as shown by a study of Stoyle and co-workers, where the investigated antibody did escape interaction with the chaperon BIP (Stoyle et al., 2017). Since it was shown that the association with BIP is not only determined by sequences but also the folding state of client proteins (Hellman et al., 1999), we further speculate that the variable LC domain of mAb2 is not unfolded per se but spontaneously adopts an atypical stable folding state which might in turn impair chaperone recognition and terminal native folding. As a consequence, mAb2 is likely to be intracellularly retained and thus not efficiently secreted due to protein quality control mechanisms taking place in the ER. Especially, free cysteine residues of only partially folded proteins have been shown to lead to active retention (Alberini et al., 1990; Sitia et al., 1990). Also fully assembled mAb2 antibody might have been actively retained and accumulated due to the assembly of HCs with only partially folded LCs.

To finally elucidate possible escape routes or survival mechanisms of cells suffering from aberrant ER morphology gene expression analyses were performed. In particular, canonical pathways including normal protein processing in the ER, degradation of proteins via ERAD and the UPR were closely investigated (compare

Fig. 5, page 9). The observed cellular reaction of the examined DTE mAb2-producing cell line included a general downregulation of genes involved in regular protein synthesis (ribosomal proteins), translocation (Sec61/62/63) and protein processing in the ER (chaperones like endoplasmin, PDIA3 and calnexin as well as ER-Golgi intermediate compartment 53 kDa protein (ERGIC-53)) (Mathias et al., 2019, Tabel S2; appendix, page 121 ff.). An upregulation of genes was observed for pathways involved in protein degradation, especially the ERAD pathway and subunits of the proteasome (Fig. 14, page 31). Confirmatively, the expressed recombinant protein mAb2 was tagged for proteasomal degradation via ERAD which is indicated by increased amounts of trimmed high-mannose N-type glycan species (Aebi et al., 2010; Ferris et al., 2014; Hebert et al., 2005). We concluded that mAb2 was marked for more heavy degradation via ERAD which possibly overloaded the respective degradation machinery. The resulting massive accumulation of proteins might have represented the reason for the observed aberrant ER morphology. Also in other reports, a direct and detrimental degradation of recombinant proteins was identified including Vergara et al., who illustrated that a significant fraction of recombinant human tissue plasminogen activator (tPA) was directly degraded after translation in CHO cells (Vergara et al., 2015). It was further shown that in case of several proteins a large proportion of the newly synthesized proteins can directly be degraded by the proteasome via ERAD mechanisms even under physiological conditions (Schubert et al., 2000), e.g. cystic fibrosis transmembrane conductance regulator (CTFR) (Kopito, 1999; Ward and Kopito, 1994) and cluster of differentiation 147 (CD147) (Tyler et al., 2012). Some mutant variants of certain proteins such as the aforementioned α-1-antitrypsin can also disturb apparently efficient protein synthesis rates tremendously (Merulla et al., 2013; Teckman and Perlmutter, 2000). As described above, mutant α-1-antitrypsin also showed an intracellular accumulation leading to an aberrant ER morphology (Teckman and Perlmutter, 2000). This again points towards some protein sequences due to inherent properties being more prone to (intracellular) aggregation as well as degradation and as a consequence more DTE than others.

The accumulation of (unfolded) proteins in the ER usually initiates the UPRs, a complex feedback mechanism ensuring efficient adaptation to fluctuations in protein folding requirements triggered by the release of BIP from its stress sensors ATF6, PERK and IRE1α (Bertolotti et al., 2000; Hetz, 2012; Hussain et al., 2014; Ma and

Hendershot, 2002). The UPR is a cascade not only regulated via gene expression but especially through post-translational modifications. In particular, the activation of PERK leads to the upregulation of ATF4 which in turn results in the phosphorylation of eIF2α globally downregulating translation processes (Harding et al., 1999). Further ATF6 is proteolytically spliced into ATF6f which is transported into the nucleus to act as a transcription factor upregulating the transcription of genes encoding ERAD components (Hetz, 2012). However, for the DTE mAb2-producing cell line the UPR was not explicitly triggered as revealed by gene expression analyses, although high amounts of only partially folded proteins accumulated in the lumen of the ER and the morphology was heavily affected. This is contrary to a report of Hasegawa and co-workers who showed that the formation of RBs triggered UPR leading to a phosphorylation of eIF2α and a subsequent downregulation of global translation processes (Hasegawa et al., 2017). In our case, the respective UPR cascade was probably not triggered as BIP did not more heavily (in comparison to the mAb1-producing cell line) interact with the only partially folded LC of mAb2 and thus was not released from its stress sensors. Confirmatively, Rivera and co-workers showed that some proteins might accumulate in the lumen of the ER without triggering the UPR (Rivera et al., 2012). However, in these reports intracellular aggregation was the underlying principle of RB formation which is contrary to our findings. Here, the UPR was probably still enabled in mAb2-producing cells without more interaction of BIP with the partially folded LC as a downregulation of global translation processes and an upregulation of ERAD associated genes were observed on transcript level. However, this is still unlikely as the cells show no compromise or reduction in growth behavior.

Over the past decades, plenty of strategies have been developed to remove those proposed post-transcriptional rate-limiting steps and secretion bottlenecks in CHO production cell lines (Delic et al., 2014; Xiao et al., 2014; Zhou et al., 2018). For example, the efficiency of protein translocation into the ER was improved by using appropriate signal peptides and co-expression of parts of the signal recognition particle complex (Gibson et al., 2017; Le Fourn et al., 2014). Further, ER processing capacity was enhanced by overexpression of chaperons like BIP and calnexin, however with varying outcome (Delic et al., 2014; Nishimiya, 2014). Intracellular vesicular trafficking and secretion was improved by overexpression of SNARE proteins (Peng et al., 2011, 2010; Peng and Fussenegger, 2009) and lipid transfer

proteins (Florin et al., 2009). An alternative way, targeting entire pathways, is the overexpression of miRNAs which have been associated with production bottlenecks (Fischer et al., 2017; Pieper et al., 2017a, 2017b). However, the formation of disulfide bridges in the ER, with PDI being one of the key players, is one of the major bottlenecks during oxidative protein folding (Delic et al., 2014). Therefore, other studies investigated the co-expression of members of the PDI family to enable superior expression of non- or partially folded recombinant proteins, unfortunately with inconsistent outcome (Borth et al., 2005; Davis et al., 2000; Hansen et al., 2017; Mohan and Lee, 2010). In the present study (chapter 4.2, page 23 ff.), the transient co-expression of PDI in the investigated mAb2-producing cell line did also not increase secretion of the DTE molecule (data not shown). After transfection, mAb2-producing cells showed high expression of PDI but also low viability pointing towards the need of transfection optimization. Further, there are nearly 20 different disulfide isomerases available in the human species with overlapping functions which might influence mAb2 LC folding efficiency to different extent (Appenzeller-Herzog and Ellgaard, 2008; Ellgaard and Ruddock, 2005). Also, more related disulfide isomerases e.g. from mouse should be tested in CHO production cell lines to improve mAb2 production. In summary, the presented study represents a straight forward strategy which can be used as an instruction to characterize the molecular mechanism of secretion bottlenecks in great detail and may in some cases even provide targets for molecular engineering. Especially the intracellular folding analysis of the recombinantly produced protein, for which a method was presented in this work (chapter 4.2, page 23 ff.), might substantially enable the identification of folding deficiencies aiding the selection of favorable drug candidates. The analyzes of further cell lines might finally elucidate whether different molecules show the same secretion bottleneck hampering efficient secretion which might subsequently be overcome by further cell line engineering attempts leading to the generation of superior production cell lines in general. However, the aim of in-detail characterization of the mAb2 secretion bottleneck was the subsequent removal, achievable with either cell line engineering or engineering of the recombinant protein sequence.

Individual mAbs can differ greatly in their biophysical properties, although they share high protein sequence identity with differences largely in their variable domains (Kumar et al., 2018; Nichols et al., 2015; Tomar et al., 2016). During the

past decade computational prediction tools correlating biophysical characteristics to sequence-structural attributes have become feasible enabling to identify adverse sequences and interesting mutants with improved properties (Kumar et al., 2018; Sormanni et al., 2018). Interestingly, the investigated DTE mAb2 antibody was identified to have a critical APR in its variable LC domain already in a previous study (van der Kant et al., 2017). Confirmatively, the in-detail characterization of mAb2-expressing CHO cells revealed folding deficiencies of the LC to be the molecular reason for low secretion (Fig. 12, page 27) which might have been provoked by the predicted APR. Therefore mAb2 was rationally optimized *in silico* by using the TANGO algorithm (Fernandez-Escamilla et al., 2004) estimating the intrinsic aggregation propensity under consideration of the thermodynamic stability of native structures using the FoldX force field algorithm (Schymkowitz et al., 2005) to diminish the identified APR which was already previously investigated in a transient expression setup (Van Der Kant et al., 2017). In the here presented work (chapter 4.3, page 33 ff.), the *in silico* optimized variant of the DTE antibody mAb2 was shown to effectively have sustained beneficial properties throughout the entire antibody manufacturing process and DP lifetime. Starting from mammalian cell-based production, the CHO cell line stably producing the *in silico* optimized variant showed a threefold increase in antibody titer while maintaining appreciated cell growth characteristics. Interestingly, enhanced performance of mammalian cell lines producing antibody variants with improved biophysical properties was already described in several earlier studies (Kumar et al., 2018; Pybus et al., 2014; Van Der Kant et al., 2017). All of these studies might further indicate that superior biophysical properties of an antibody candidate might not only be beneficial in defined aqueous formulations but also during intracellular production and processing. This might also explain the great differences obtained when individual antibodies are compared in its expression (Bentley et al., 1998). Strikingly, also the identified intracellular bottleneck leading to an affected ER morphology in mAb2 production cells was shown to be mitigated in case of the *in silico* optimized variant. The *in silico* optimized variant was more efficiently folded and finally secreted possibly preventing intracellular accumulation due to enhanced folding of the antibody LC. Confirmatively, Hasegawa and co-workers showed that one single AA substitution in the variable domain of an antibody LC can determine on the formation of intracellular antibody aggregates within the ER in HEK293 cells (Hasegawa et

al., 2017). However, the single mutant was not rationally designed but found during routine antibody selection processes. Interestingly, we showed that an extensive recovery of ER morphology of variant-expressing cells also correlated with an improved N-linked glycosylation pattern including elevated levels of processed glycans (Fig. 18, page 39). However, both antibodies still showed very high levels of immature glycan structures of the high-mannose type indicating that the affected organelle structure might not be the reason for inefficient catalysis rather the protein sequence or structure itself. As the glycosylation is known to affect mAbs' biological activity, protein conformation, stability, solubility, secretion, pharmacokinetics, and antigenicity (Dwek, 1998) further improvements are needed. Especially high-mannose structures were shown to have undesirable elevated clearance from blood (Goetze et al., 2011; Reusch and Tejada, 2015; Yu et al., 2012).

To further unravel the benefits of a computationally optimized therapeutic antibody on the distinct bioprocess development stages the investigated antibodies were developed in accordance with an entire manufacturing process used in the pharmaceutical industry. Often observed challenges in antibody manufacture are aggregation and fragmentation, high viscosity, solubility issues, opalescence and immunogenicity (Kumar et al., 2018; Tomar et al., 2016; Wang, 1999). The *in silico* optimized variant consistently showed less aggregates throughout the individual steps of the entire downstream purification process which even further increased the absolute amount of obtained active monomeric product. Interestingly, it was described earlier that optimized antibody candidates, where APRs were rationally disrupted showed improved monomer content during purification procedures (Kumar et al., 2018; Nichols et al., 2015). Contrarily, in these studies the focus was primarily set on using *in silico* prediction tools to reduce the viscosity of respective DP formulations, which is especially important in case of highly concentrated liquid drug formulations for subcutaneous and intravitreal administration via thin needles. In case of mAb2, which precipitated at concentrations above 15 mg/mL, viscosity at higher concentrations could not be investigated. However, it can reasonably be assumed that if the viscosity of mAb2 and variant DPs had been compared at higher concentrations the differences identified would have been even more pronounced. Further, the *in silico* optimized variant of mAb2 also showed elevated T_{agg} indicating significantly improved non-native aggregation properties of the variant (Bauer and Mathias et al., 2020, Fig. 4;

appendix, page 134). However, a six-month stability study revealed that also formulations of the *in silico* optimized variant showed particle formation after storage. A simple aqueous formulation buffer without any additive agents was used in this study which are usually necessary to optimally stabilize liquid protein formulations (Wang, 1999). By using a more sophisticated formulation buffer, also moderately aggregation-prone antibodies might meet safety and efficacy requirements (Van Der Kant et al., 2017). Since the structural diversity of the antibody drug candidates and therewith associated greatly different biophysical properties prevents the use of an universal stabilization strategy, finding the right additives to stabilize the protein solution as best as possible is a time consuming, resource-intensive, trial and error process (Wang, 1999). However, with the prediction and selection of molecules with favorable biophysical properties e.g. the use of platform buffers in development of the formulation might be achievable further reducing costs and time to market. Strikingly, selection of candidates with favorable properties was shown to be beneficial not only for downstream purification and development of formulation of the final DPs, but also for cell culture-based production during upstream development as illustrated by a rescued ER phenotype and increase in titer and product quality without negatively affecting antigen binding (chapter 4.3, page 33 ff.). As a consequence, routine implementation of appropriate sequence-structure-based selection of candidates would render the current procedure in engineering the manufacturing process to control the quality of the product, to defining a better product suitable for the established process to maximize manufacturing and clinical success (Zhong et al., 2011; Zurdo et al., 2011).

6 CONCLUSIONS

In order to provide sufficient amounts of biotherapeutics to the market, we developed a streamlined HT fluorescence microscopy-based methodology to identify any rate-limiting processing step which might represent a bottleneck in currently used industrial CHO production cell lines. In case of an exemplarily investigated DTE antibody we characterized the identified intracellular production bottleneck and identified intracellular folding of the LC to be the molecular reason for its unexpectedly low secretion. To remove the identified bottleneck, an *in silico* optimized variant thereof was shown to have significantly enhanced secretion properties and an improved manufacturability throughout the entire production process. Finally, the strategy and analytical toolbox established during this study can be used as guideline to straightforwardly identify, characterize and remove intracellular bottlenecks in industrial CHO production cell lines.

The presented studies emphasized that the identification and characterization of intracellular bottlenecks might be useful to identify superior mammalian cell factories producing therapeutic proteins very efficiently. The developed HT microscopy-based methodology and used analytical tools (e.g. intracellular protein folding assay) might enable rapid identification of suitable drug candidates early in the development pipeline and in addition may reveal starting points for cell line engineering. As further demonstrated, modulation of the antibody sequence represents a complementary strategy to improve the production of recombinant proteins leading to highly efficient production processes. In the future, classical cell line engineering attempts might be complemented by already available bioinformatic-based selection of drug candidates and prediction of superior protein sequence variants. Besides protein therapeutics, alternative biopharmaceutical formats such as viral vectors for gene therapy or oncolytic viral therapy will also gain more importance in the next decades. Since these biopharmaceuticals are also manufactured using mammalian production cell systems, the identification, characterization and removal of production bottleneck will gain more importance especially with regard to meeting challenges encountered during the production of new medicinal therapies.

7 REFERENCES

Aebi, M., Bernasconi, R., Clerc, S., Molinari, M., 2010. N-glycan structures: recognition and processing in the ER. Trends Biochem. Sci. 35, 74–82. https://doi.org/10.1016/j.tibs.2009.10.001

Agrawal, N.J., Helk, B., Kumar, S., Mody, N., Sathish, H.A., Samra, H.S., Buck, P.M., Li, L., Trout, B.L., 2016. Computational tool for the early screening of monoclonal antibodies for their viscosities. MAbs 8, 43–48. https://doi.org/10.1080/19420862.2015.1099773

Alberini, C.M., Bet, P., Milstein, C., Sitia, R., 1990. Secretion of immunoglobulin M assembly intermediates in the presence of reducing agents. Nature 374, 485–487. https://doi.org/10.1016/0021-9797(80)90501-9

Alberts, B., Johnson, A., Lewis, J., Raff, M., Roberts, K., Walter, P., 2002. The Molecular Biology of the Cell.

Appenzeller-Herzog, C., 2011. Glutathione- and non-glutathione-based oxidant control in the endoplasmic reticulum. J. Cell Sci. 124, 847–855. https://doi.org/10.1242/jcs.080895

Appenzeller-Herzog, C., Ellgaard, L., 2008. The human PDI family: Versatility packed into a single fold. Biochem. Biophys. Acta - Mol. Cell Res. 1783, 535–548. https://doi.org/10.1016/j.bbamcr.2007.11.010

Apweiler, R., Hermjakob, H., Sharon, N., 1999. On the frequency of protein glycosylation, as deduced from analysis of the SWISS-Prot database. Biochim. Biophys. Acta 1473, 4–8.

Arden, N., Betenbaugh, M.J., 2004. Life and death in mammalian cell culture: Strategies for apoptosis inhibition. Trends Biotechnol. 22, 174–180. https://doi.org/10.1016/j.tibtech.2004.02.004

Backliwal, G., Hildinger, M., Kuettel, I., Delegrange, F., Hacker, D.L., Wurm, F.M., 2008. Valproic acid: A viable alternative to sodium butyrate for enhancing protein expression in mammalian cell cultures. Biotechnol. Bioeng. 101, 182–189. https://doi.org/10.1002/bit.21882

Baldi, L., Hacker, D.L., Adam, M., Wurm, F.M., 2007. Recombinant protein production by large-scale transient gene expression in mammalian cells : state of the art and future perspectives. Biotechnol. Lett. 29, 677–684. https://doi.org/10.1007/s10529-006-9297-y

Bandaranayake, A.D., Almo, S.C., 2014. Recent advances in mammalian protein production. FEBS Lett. 588, 253–260. DOI: 10.1016/j.febslet.2013.11.035

Barron, N., Sanchez, N., Kelly, P., Clynes, M., 2011. MicroRNAs: Tiny targets for engineering CHO cell phenotypes? Biotechnol. Lett. 33, 11–21. https://doi.org/10.1007/s10529-010-0415-5

Bauer, J., Mathias, S., Kube, S., Otte, K., Garidel, P., Gamer, M., Blech, M., Fischer, S., Karow-Zwick, A., 2020. Rational Optimization of a Monoclonal Antibody Improves the Aggregation Propensity and Enhances the CMC Properties Along the Entire Pharmaceutical Process Chain .

Becker, E., Florin, L., Pfizenmaier, K., Kaufmann, H., 2008. An XBP-1 dependent bottle-neck in production of IgG subtype antibodies in chemically defined serum-free Chinese hamster ovary (CHO) fed-batch processes. J. Biotechnol. 135, 217–223. https://doi.org/10.1016/j.jbiotec.2008.03.008

Behnke, J., Mann, M.J., Scruggs, F., Feige, M.J., Hendershot, L.M., 2017. sequences to execute ER quality control 63, 739–752. https://doi.org/10.1016/j.molcel.2016.07.012.Members

Behnke, J., Mann, M.J., Scruggs, F., Feige, M.J., Hendershot, M., 2016. Members

of the Hsp70 family recognize distinct types of sequences to execute ER quality control. Mol. Cell 63, 739–752. https://doi.org/10.1016/j.molcel.2016.07.012.Members

Bentley, K.J., Gewert, R., Harris, W.J., 1998. Differential efficiency of expression of humanized antibodies in transient transfected mammalian cells. Hybridoma 17, 559–567. https://doi.org/10.1089/hyb.1998.17.559

Bertolotti, A., Zhang, Y., Hendershot, L.M., Harding, H.P., Ron, D., 2000. Dynamic interaction of BiP and ER stress transducers in the unfolded- protein response. Nat. Cell Biol. 2, 326–332.

Bibila, T.A., Flickinger, M.C., 1992. Use of a Structured Kinetic Model of Antibody Synthesis and Secretion for Optimization of Antibody Production. Biotechnol. Adv. 39, 251–261.

Borth, N., Mattanovich, D., Kunert, R., Katinger, H., 2005. Effect of Increased Expression of Protein Disulfide Isomerase and Heavy Chain Binding Protein on Antibody Secretion in a Recombinant CHO Cell Line. Biotechnol. Prog. 21, 106–111.

Braakman, I., Hebert, D., 2013. Protein Folding in the Endoplasmic Reticulum. Cold Spring Harb. Prespectives Biol. 5. https://doi.org/10.1016/B978-0-08-088504-9.00029-5

Brinkmann, U., Kontermann, R.E., Group, F., Brinkmann, L.L.C.U., Roland, E., Brinkmann, U., 2017. The making of bispecific antibodies The making of bispeci fi c antibodies. MAbs 9, 182–212. https://doi.org/10.1080/19420862.2016.1268307

Browne, S.M., Al-Rubeai, M., 2007. Selection methods for high-producing mammalian cell lines. Trends Biotechnol. 25, 425–432.

https://doi.org/10.1016/j.tibtech.2007.07.002

Cain, K., Peters, S., Hailu, H., Sweeney, B., Stephens, P., Heads, J., Sarkar, K., Ventom, A., Page, C., Dickson, A., 2013. A CHO cell line engineered to express XBP1 and ERO1-Lα has increased levels of transient protein expression. Biotechnol. Prog. 29, 697–706. https://doi.org/10.1002/btpr.1693

Carlson, J.A., Rogers, B.B., Sifers, R.N., Finegold, M.J., Cliff, S.M., Demayo, F.J., Bullock, D.W., Woo, S.L.C., 1989. Accumulation of PiZ a1-Antitrypsin Causes Liver Damage in Transgenic Mice. J. Clin. Invest. 83, 1183–1190.

Chromikova, V., Mader, A., Steinfellner, W., Kunert, R., 2015. Evaluating the bottlenecks of recombinant IgM production in mammalian cells. Cytotechnology 67, 343–356. https://doi.org/10.1007/s10616-014-9693-4

Clausen, H., Wandall, H.H., Steentoft, C., Stanley, P., Schnaar, R.L., 2017. Glycosylation Engineering, in: Varki A, Cummings RD, Esko JD, et Al., Editors. Essentials of Glycobiology, 2015-2017, Chapter 56.

Corcos, D., Osborn, M.J., Matheson, L.S., Santos, F., Zou, X., Smith, J.A., Morgan, G., Hutchings, A., Hamon, M., Oxley, D., Brüggemann, M., 2010. Immunoglobulin aggregation leading to Russell body formation is prevented by the antibody light chain. Blood 115, 282–288. https://doi.org/10.1182/blood-2009-07-234864.The

Davis, R., Schooley, K., Rasmussen, B., Thomas, J., Reddy, P., 2000. Effect of PDI Overexpression on Recombinant Protein Secretion in CHO cells. Biotechnol. Prog. 16, 736–743.

de Sousa Abreua, R., Penalvaa, L.O., Marcotte, E.M., Vogel, C., 2009. Global signatures of protein and mRNA expression levels. Mol. Biosyst. 5, 1512–1526. https://doi.org/10.1039/b908315d.Global

Decourt, C., Galea, H.R., Sirac, C., Cogné, M., 2004. Immunologic basis for the rare occurrence of true nonsecretory plasma cell dyscrasias. J. Leukoc. Biol. 76, 528–536. https://doi.org/10.1189/jlb.0803382

Delic, M., Gongrich, R., Mattanovich, D., Gasser, B., 2014. Engineering of Protein Folding and Secretion — Strategies to Overcome Bottlenecks for Efficient Production of Recombinant Proteins. Antioxid. Redox Signal. 21, 414–437. https://doi.org/10.1089/ars.2014.5844

Dorner, A.J., Wasley, L.C., Kaufman, R.J., 1992. Overexpression of GRP78 mitigates stress induction of glucose regulated proteins and blocks secretion of selective proteins in Chinese hamster ovary cells. EMBO J. 11, 1563–1571.

Dreesen, I.A.J., Fussenegger, M., 2011. Ectopic expression of human mTOR increases viability, robustness, cell size, proliferation, and antibody production of chinese hamster ovary cells. Biotechnol. Bioeng. 108, 853–866. https://doi.org/10.1002/bit.22990

Dul, J.L., Argon, Y., 1990. A single amino acid substitution in the variable region of the light chain specifically blocks immunoglobulin secretion. Proc. Natl. Acad. Sci. 87, 8135–8139. https://doi.org/10.1073/pnas.87.20.8135

Dwek, R.A., 1998. Biological importance of glycosylation. Dev. Biol. Stand. 96, 34–7.

Ecker, D.M., Jones, S.D., Levine, H.L., 2015. The therapeutic monoclonal antibody market. MAbs 7, 9–14. https://doi.org/10.4161/19420862.2015.989042

Ellgaard, L., Helenius, A., 2003. Quality control in the endoplasmic reticulum. Nat. Rev. Mol. Cell Biol. 4, 181–191. https://doi.org/10.1038/nrm1052

Ellgaard, L., Ruddock, L.W., 2005. The human protein disulphide isomerase family: Substrate interactions and functional properties. EMBO Rep. 6, 28–32.

https://doi.org/10.1038/sj.embor.7400311

Fann, C., Guarna, M., DG, K., Piret, J., 1999. Relationship between recombinant activated protein C secretion rates and mRNA levels in baby hamster kidney cells. Biotechnol. Bioeng. 63, 464–72.

Feige, M.J., Hendershot, L.M., Buchner, J., 2016. How antibodies fold 35, 189–198. https://doi.org/10.1016/j.tibs.2009.11.005.How

Fernandez-Escamilla, A.M., Rousseau, F., Schymkowitz, J., Serrano, L., 2004. Prediction of sequence-dependent and mutational effects on the aggregation of peptides and proteins. Nat. Biotechnol. 22, 1302–1306. https://doi.org/10.1038/nbt1012

Ferreiro, D.U., Komives, E.A., Wolynes, P.G., 2014. Frustration in Biomolecules. Q. Rev. Biophys. 47, 285–363. https://doi.org/10.1038/jid.2014.371

Ferris, S.P., Kodali, V.K., Kaufman, R.J., 2014. Glycoprotein folding and quality-control mechanisms in protein-folding diseases. Dis. Model. Mech. 7, 331–341. https://doi.org/10.1242/dmm.014589

Fischer, S., Handrick, R., Otte, K., 2015a. The art of CHO cell engineering: A comprehensive retrospect and future perspectives, Biotechnology Advances. Elsevier B.V. https://doi.org/10.1016/j.biotechadv.2015.10.015

Fischer, S., Marquart, K.F., Pieper, L.A., Fieder, J., Gamer, M., Gorr, I., Schulz, P., Bradl, H., 2017. miRNA engineering of CHO cells facilitates production of difficult-to-express proteins and increases success in cell line development. Biotechnol. Bioeng. 114, 1495–1510. https://doi.org/10.1002/bit.26280

Fischer, S., Paul, A.J., Wagner, A., Mathias, S., Geiss, M., Schandock, F., Domnowski, M., Zimmermann, J., Handrick, R., Hesse, F., Otte, K., 2015b. miR-2861 as novel HDAC5 inhibitor in CHO cells enhances productivity while

maintaining product quality. Biotechnol. Bioeng. 112, 2142–2153. https://doi.org/10.1002/bit.25626

Florin, L., Pegel, A., Becker, E., Hausser, A., Olayioye, M.A., Kaufmann, H., 2009. Heterologous expression of the lipid transfer protein CERT increases therapeutic protein productivity of mammalian cells. J. Biotechnol. 141, 84–90. https://doi.org/10.1016/j.jbiotec.2009.02.014

Frenzel, A., Kügler, J., Helmsing, S., Meier, D., Schirrmann, T., Hust, M., Dübel, S., 2017. Designing Human Antibodies by Phage Display. Transfus. Med. Hemotherapy 44, 312–318. https://doi.org/10.1159/000479633

Geoghegan, J.C., Fleming, R., Damschroder, M., Bishop, S.M., Sathish, H.A., Esfandiary, R., 2016. Mitigation of reversible self-association and viscosity in a human IgG1 monoclonal antibody by rational, structure-guided Fv engineering. MAbs 8, 941–950. https://doi.org/10.1080/19420862.2016.1171444

Gianni, S., Camilloni, C., Giri, R., Toto, A., Bonetti, D., Morrone, A., Sormanni, P., Brunori, M., Vendruscolo, M., 2014. Understanding the frustration arising from the competition between function, misfolding, and aggregation in a globular protein. Proc. Natl. Acad. Sci. U. S. A. 111, 14141–14146. https://doi.org/10.1073/pnas.1405233111

Giannone, C., Fagioli, C., Valetti, C., Sitia, R., Anelli, T., 2017. Roles of N-glycans in the aggregation of mutant Ig- μ chains in the early secretory pathway. Sci. Rep. 7, 1–10. https://doi.org/10.1038/srep41815

Gibson, S.J., Bond, N.J., Milne, S., Lewis, A., Sheriff, A., Pettman, G., Pradhan, R., Higazi, D.R., Hatton, D., 2017. N-terminal or signal peptide sequence engineering prevents truncation of human monoclonal antibody light chains. Biotechnol. Bioeng. 114, 1970–1977. https://doi.org/10.1002/bit.26301

Goetze, A.M., Liu, Y.D., Zhang, Z., Shah, B., Lee, E., Bondarenko, P. V., Flynn, G.C., 2011. High-mannose glycans on the Fc region of therapeutic IgG antibodies increase serum clearance in humans. Glycobiology 21, 949–959. https://doi.org/10.1093/glycob/cwr027

Grilo, A.L., Mantalaris, A., 2019. The Increasingly Human and Profitable Monoclonal Antibody Market. Trends Biotechnol. 37, 9–16. https://doi.org/10.1016/j.tibtech.2018.05.014

Hackl, M., Borth, N., Grillari, J., 2012. MiRNAs - pathway engineering of CHO cell factories that avoids translational burdening. Trends Biotechnol. 30, 405–406. https://doi.org/10.1016/j.tibtech.2012.05.002

Hansen, H.G., Pristovšek, N., Kildegaard, H.F., Lee, G.M., 2017. Improving the secretory capacity of Chinese hamster ovary cells by ectopic expression of effector genes : Lessons learned and future directions. Biotechnol. Adv. 35, 64–76. https://doi.org/10.1016/j.biotechadv.2016.11.008

Harding, H.P., Zhang, Y., Ron, D., Harding, H.P., Zhang, Y., Ron, D., 1999. Protein translation and folding are coupled by an endoplasmic- reticulum-resident kinase 397, 271–274.

Hasegawa, H., Hsu, A., Tinberg, C.E., Siegler, K.E., Aaron, A., Tsai, M., 2017. Single amino acid substitution in LC-CDR1 induces Russell body phenotype that attenuates cellular protein synthesis through eIF2 α phosphorylation and thereby downregulates IgG secretion despite operational secretory pathway traffic. MAbs 9, 854–873. https://doi.org/10.1080/19420862.2017.1314875

Hasegawa, H., Wendling, J., He, F., Trilisky, E., Stevenson, R., Franey, H., Kinderman, F., Li, G., Piedmonte, D.M., Osslund, T., Shen, M., Ketchem, R.R., 2011. In vivo crystallization of human IgG in the endoplasmic reticulum of

engineered chinese hamster ovary (CHO) cells. J. Biol. Chem. 286, 19917–19931. https://doi.org/10.1074/jbc.M110.204362

Hasegawa, H., Woods, C.E., Kinderman, F., He, F., Lim, A.C., 2014. Russell body phenotype is preferentially induced by IgG mAb clones with high intrinsic condensation propensity: Relations between the biosynthetic events in the ER and solution behaviors in vitro. MAbs 6, 1518–1532. https://doi.org/10.4161/mabs.36242

Hebert, D.N., Garman, S.C., Molinari, M., 2005. The glycan code of the endoplasmic reticulum: Asparagine-linked carbohydrates as protein maturation and quality-control tags. Trends Cell Biol. 15, 364–370. https://doi.org/10.1016/j.tcb.2005.05.007

Helenius, A., Aebi, M., 2004. Roles of N-Linked Glycans in the Endoplasmic Reticulum. Annu. Rev. Biochem. 73, 1019–1049. https://doi.org/10.1146/annurev.biochem.73.011303.073752

Hellman, R., Vanhove, M., Lejeune, A., Stevens, F.J., Hendershot, L.M., 1999. The In Vivo Association of BiP with Newly Synthesized Proteins Is Dependent on the Rate and Stability of Folding and Not Simply on the Presence of Sequences That Can Bind to BiP — JCB. J. Cell Biol. 144, 21–30.

Hendershot, L.M., Wei, J.Y., Gaut, J.R., Lawson, B., Freiden, P.J., Murti, K.G., 1995. In vivo expression of mammalian BiP ATPase mutants causes disruption of the endoplasmic reticulum. Mol. Biol. Cell 6, 283–296. https://doi.org/10.1091/mbc.6.3.283

Hetz, C., 2012. The unfolded protein response: Controlling cell fate decisions under ER stress and beyond. Nat. Rev. Mol. Cell Biol. 13, 89–102. https://doi.org/10.1038/nrm3270

Hossler, P., Khattak, S.F., Li, Z.J., 2009. Optimal and consistent protein glycosylation in mammalian cell culture. Glycobiology 19, 936–949. https://doi.org/10.1093/glycob/cwp079

Huang, Y.M., Hu, W.W., Rustandi, E., Chang, K., Yusuf-Makagiansar, H., Ryll, T., 2010. Maximizing productivity of CHO cell-based fed-batch culture using chemically defined media conditions and typical manufacturing equipment. Biotechnol. Prog. 26, 1400–1410. https://doi.org/10.1002/btpr.436

Hussain, H., Maldonado-Agurto, R., Dickson, A.J., 2014. The endoplasmic reticulum and unfolded protein response in the control of mammalian recombinant protein production. Biotechnol. Lett. 36, 1581–1593. https://doi.org/10.1007/s10529-014-1537-y

Jadhav, V., Hackl, M., Druz, A., Shridhar, S., Chung, C.Y., Heffner, K.M., Kreil, D.P., Betenbaugh, M., Shiloach, J., Barron, N., Grillari, J., Borth, N., 2013. CHO microRNA engineering is growing up: Recent successes and future challenges. Biotechnol. Adv. 31, 1501–1513. https://doi.org/10.1016/j.biotechadv.2013.07.007

Jain, T., Sun, T., Durand, S., Hall, A., Houston, N.R., Nett, J.H., Sharkey, B., Bobrowicz, B., Caffry, I., Yu, Y., Cao, Y., Lynaugh, H., Brown, M., Baruah, H., Gray, L.T., Krauland, E.M., Xu, Y., Vásquez, M., Wittrup, K.D., 2017. Biophysical properties of the clinical-stage antibody landscape. Proc. Natl. Acad. Sci. U. S. A. 114, 944–949. https://doi.org/10.1073/pnas.1616408114

Janeway, C.A., Travers, P., Walport, M., Shlomchik, M.J., Jr, J.C. a, York, N., Science, G., Charles A Janeway, J., Travers, P., Walport, M., Shlomchik, M.J., 2001. Immunobiology: The immune System in Health and Disease, 5th edition.

Jiang, Y., Hirose, S., Hamano, Y., Kodera, S., Tsurui, H., Abe, M., Terashima, K.,

Ishikawa, S., Shirai, T., 1997. Mapping of a gene for the increased susceptibility of B1 cells to Mott cell formation in murine autoimmune disease. J Immunol 158, 992–997.

Johari, Y.B., Estes, S.D., Alves, C.S., Sinacore, M.S., James, D.C., 2015. Integrated cell and process engineering for improved transient production of a “difficult-to-express” fusion protein by CHO cells. Biotechnol. Bioeng. 112, 2527–2542. https://doi.org/10.1002/bit.25687

Kaas, C.S., Kristensen, C., Betenbaugh, M.J., Andersen, M.R., 2015. Sequencing the CHO DXB11 genome reveals regional variations in genomic stability and haploidy. BMC Genomics 16. https://doi.org/10.1186/s12864-015-1391-x

Kallehauge, T.B., Li, S., Pedersen, L.E., Ha, T.K., Ley, D., Andersen, M.R., Kildegaard, H.F., Lee, G.M., Lewis, N.E., 2017. Ribosome profiling-guided depletion of an mRNA increases cell growth rate and protein secretion. Nat. Publ. Gr. 7, 1–12. https://doi.org/10.1038/srep40388

Kanehisa, M., Furumichi, M., Tanabe, M., Sato, Y., Morishima, K., 2017. KEGG: New perspectives on genomes, pathways, diseases and drugs. Nucleic Acids Res. 45, D353–D361. https://doi.org/10.1093/nar/gkw1092

Kanehisa, M., Goto, S., 2000. KEGG : Kyoto Encyclopedia of Genes and Genomes. Nucleic Acid Res. 28, 27–30.

Kanehisa, M., Sato, Y., Furumichi, M., Morishima, K., Tanabe, M., 2019. New approach for understanding genome variations in KEGG. Nucleic Acids Res. 47, D590–D595. https://doi.org/10.1093/nar/gky962

Kim, J.Y., Kim, Y., Lee, G.M., 2012. CHO cells in biotechnology for production of recombinant proteins : current state and further potential. Appl. Microbiol. Biotechnol. 93, 917–930. https://doi.org/10.1007/s00253-011-3758-5

Kimura, K., Kawaguchi, K., Ueda, Y., Arai, S., Morita, M., Imanaka, T., Wada, I., 2015. Characterization of Russell Bodies Accumulating Mutant Antithrombin Derived from the Endoplasmic Reticulum. Biol. Pharm. Bull. 38, 852–861.

Knittler, M.R., Dirks, S., Haas, I.G., 2006. Molecular chaperones involved in protein degradation in the endoplasmic reticulum: quantitative interaction of the heat shock cognate protein BiP with partially folded immunoglobulin light chains that are degraded in the endoplasmic reticulum. Proc. Natl. Acad. Sci. 92, 1764–1768. https://doi.org/10.1073/pnas.92.5.1764

Ko, P., Misaghi, S., Hu, Z., Zhan, D., Tsukuda, J., Yim, M., Sanford, M., Shaw, D., Shiratori, M., Snedecor, B., Laird, M., Shen, A., 2018. Probing the importance of clonality: Single cell subcloning of clonally derived CHO cell lines yields widely diverse clones differing in growth, productivity, and product quality. Biotechnol. Prog. 34, 624–634. https://doi.org/10.1002/btpr.2594

Köhler, G., Howe, S.C., Milstein, C., 1976. Fusion between immunoglobulin-secreting and nonsecreting myeloma cell lines. Eur. J. Immunol. 6, 292–295.

Köhler, G., Milstein, C., 1975. Continuous cultures of fused cells secreting antibody of predefined specificity. Nature 256, 495–497.

Kopito, R.R., 1999. Biosynthesis and Degradation of CFTR. Physiol. Rev. 79, 167–173.

Kopito, R.R., Sitia, R., 2000. Aggresomes and Russell bodies. EMBO Rep. 1, 225–231. https://doi.org/10.1093/embo-reports/kvd052

Krampe, B., Al-Rubeai, M., 2010. Cell death in mammalian cell culture: Molecular mechanisms and cell line engineering strategies. Cytotechnology 62, 175–188. https://doi.org/10.1007/s10616-010-9274-0

Kronja, I., Orr-weaver, T.L., 2011. Translational regulation of the cell cycle : when ,

where , how and why ? Philos. transctions R. Soc. London. Deries B, Biol. Sci. 366, 3638–3652. https://doi.org/10.1098/rstb.2011.0084

Ku, S.C.Y., Ng, D.T.W., Yap, M.G.S., Chao, S., 2008. Effects of Overexpression of X-Box Binding Protein 1 on Recombinant Protein Production in Chinese Hamster Ovary and NS0 Myeloma Cells. Biotechnol. Bioeng. 99, 155–164. https://doi.org/10.1002/bit

Kumar, S., Roffi, K., Tomar, D.S., Cirelli, D., Luksha, N., Meyer, D., Mitchell, J., Allen, M.J., Li, L., 2018. Rational optimization of a monoclonal antibody for simultaneous improvements in its solution properties and biological activity. Protein Eng. Des. Sel. 1–13. https://doi.org/10.1093/protein/gzy020

Kunert, R., Reinhart, D., 2016. Advances in recombinant antibody manufacturing. Appl. Microbiol. Biotechnol. 100, 3451–3461. https://doi.org/10.1007/s00253-016-7388-9

Kwon, R.J., Kim, S.K., Lee, S. Il, Hwang, S.J., Lee, G.M., Kim, J.S., Seol, W., 2006. Artificial transcription factors increase production of recombinant antibodies in Chinese hamster ovary cells. Biotechnol. Lett. 28, 9–15. https://doi.org/10.1007/s10529-005-4680-7

Labrijn, A.F., Janmaat, M.L., Reichert, J.M., Parren, P.W.H.I., 2019. Bispecific antibodies: a mechanistic review of the pipeline. Nat. Rev. Drug Discov. https://doi.org/10.1038/s41573-019-0028-1

Lalonde, M.E., Durocher, Y., 2017. Therapeutic glycoprotein production in mammalian cells. J. Biotechnol. 251, 128–140. https://doi.org/10.1016/j.jbiotec.2017.04.028

Lattenmayer, C., Trummer, E., Schriebl, K., Vorauer-uhl, K., Mueller, D., Katinger, H., Kunert, R., 2007. Characterisation of recombinant CHO cell lines by

investigation of protein productivities and genetic parameters. J. Biotechnol. 128, 716–725. https://doi.org/10.1016/j.jbiotec.2006.12.016

Le Fourn, V., Girod, P.A., Buceta, M., Regamey, A., Mermod, N., 2014. CHO cell engineering to prevent polypeptide aggregation and improve therapeutic protein secretion. Metab. Eng. 21, 91–102. https://doi.org/10.1016/j.ymben.2012.12.003

Lee, G.W., Fecko, J.K., Yen, A., Donaldson, D., Wood, C., Tobler, S., Vunuum, S., Luo, Y., Leonard, M., 2007. Improving the Expression of a Soluble Receptor:Fc fusion Protein in CHO Cells by Coexpression with the Receptor Ligand. Cell Technol. Cell Prod. 29–39. https://doi.org/10.1007/978-1-4020-5476-1_4

Leitzgen, K., Knittler, M.R., Haas, I.G., 2002. Assembly of Immunoglobulin Light Chains as a Prerequisite for Secretion. J. Biol. Chem. 272, 3117–3123. https://doi.org/10.1074/jbc.272.5.3117

Lewis, N.E., Liu, X., Li, Y., Nagarajan, H., Yerganian, G., O'Brien, E., Bordbar, A., Roth, A.M., Rosenbloom, J., Bian, C., Xie, M., Chen, W., Li, N., Baycin-Hizal, D., Latif, H., Forster, J., Betenbaugh, M.J., Famili, I., Xu, X., Wang, J., Palsson, B.O., 2013. Genomic landscapes of Chinese hamster ovary cell lines as revealed by the Cricetulus griseus draft genome. Nat. Biotechnol. 31, 759–765. https://doi.org/10.1038/nbt.2624

Li, J., Ni, M., Lee, B., Barron, E., Hinto, D.R., Lee, A.S., 2008. The unfolded protein response regulator GRP78/BiP is required for endoplasmic reticulum integrity and stress-induced autophagy in mammalian cells. Cell Death Differ. 15, 1460–1471. https://doi.org/10.1016/j.cgh.2008.07.016.Cytokeratin

Li, L., Kumar, S., Buck, P.M., Burns, C., Lavoie, J., Singh, S.K., Warne, N.W., Nichols, P., Luksha, N., Boardman, D., 2014. Concentration dependent

viscosity of monoclonal antibody solutions: Explaining experimental behavior in terms of molecular properties. Pharm. Res. 31, 3161–3178. https://doi.org/10.1007/s11095-014-1409-0

Lindl, T., 1996. Development of human monoclonal antibodies: A review. Cytotechnology 21, 183–193. https://doi.org/10.1007/BF00365341

Lodish, H., Berk, A., Zipursky, S.L., Matsudaira, P., Baltimore, D., Darnell, J., 2000. Molecular Cell Biology. https://doi.org/10.1002/bmb.8

Ma, Y., Hendershot, L.M., 2002. The mammalian endoplasmic reticulum as a sensor for cellular stress. Cell Stress Chaperones 7, 222–229.

Mahmound, K., 2007. Recombinant Protein Production: Strategic Technology and a Vital Research Tool. Res. J. Cell Mol. Biol. 1, 9–22.

Maldonado, J., Brown, A.J., Bayrd, E., Pease, G., 1966. Cytoplasmic and intranuclear electron-dense bodies in the myeloma cell. Rchieves Pathol. 81, 484–500.

Manetto, V., Abdul-karim, F.W., Perry, G., Tabaton, M., Autilio-Gambetti, L., Gambetti, P., 1989. Selective Presence of Ubiquitin in Intracellular Inclusions. Am. J. Pathol. 134, 505–513.

Mason, M., Sweeney, B., Cain, K., Stephens, P., Susan, T., 2012. Identifying bottlenecks in transient and stable production of recombinant monoclonal-antibody sequence variants in Chinese hamster ovary cells. Biotechnol. Prog. 28, 846–855. https://doi.org/10.1002/btpr.1542.Identifying

Mathias, S., Fischer, S., Handrick, R., Fieder, J., Schulz, P., Bradl, H., Gorr, I., Gamer, M., Otte, K., 2018. Visualisation of intracellular production bottlenecks in suspension-adapted CHO cells producing complex biopharmaceuticals using fluorescence microscopy. J. Biotechnol. 271, 47–55.

https://doi.org/10.1016/j.jbiotec.2018.02.009

Mathias, S., Wippermann, A., Najda, R., Zeh, N., Handrick, R., Gorr, I., Schulz, P., Fischer, S., Gamer, M., Otte, K., 2019. Unravelling What Makes a Monoclonal Antibody Difficult-to-Express: From Intracellular Accumulation to Incomplete Folding and Degradation via ERAD. Biotechnol. Bioeng. 117, 5–16. Licensed under Creative Commons Attribution – NonCommercial 4.0 International, https://creativecommons.org/licenses/by-nc/4.0/.

Mattioli, L., Anelli, T., Fagioli, C., Tacchetti, C., Sitia, R., Valetti, C., 2006. ER storage diseases : a role for ERGIC-53 in controlling the formation and shape of Russell bodies. J. Cell Sci. 19, 2532–2541. https://doi.org/10.1242/jcs.02977

Merulla, J., Fasana, E., Sold, T., Molinari, M., 2013. Specificity and Regulation of the Endoplasmic Reticulum-Associated Degradation Machinery. Traffic 14, 767–777. https://doi.org/10.1111/tra.12068

Mohan, C., Kim, Y., Koo, J., Lee, G.M., 2008. Assessment of cell engineering strategies for improved therapeutic protein production in CHO cells. Biotechnol. J. 3, 624–630. https://doi.org/10.1002/biot.200700249

Mohan, C., Lee, G.M., 2010. Effect of Inducible Co-Overexpression of Protein Disulfide Isomerase and Endoplasmic Reticulum Oxidoreductase on the Specific Antibody Productivity of Recombinant Chinese Hamster Ovary Cells. Biotechnol. Bioeng. 107, 337–346. https://doi.org/10.1002/bit.22781

Mossuto, M.F., Ami, D., Anelli, T., Fagioli, C., Doglia, S.M., Sitia, R., 2015. Biochemical nature of Russell Bodies. Sci. Rep. 5, 12585. https://doi.org/10.1038/srep12585

Nichols, P., Li, L., Kumar, S., Buck, P.M., Singh, S.K., Goswami, S., Balthazor, B., Conley, T.R., Sek, D., Allen, M.J., 2015. Rational design of viscosity reducing

mutants of a monoclonal antibody: Hydrophobic versus electrostatic inter-molecular interactions. MAbs 7, 212–230. https://doi.org/10.4161/19420862.2014.985504

Nishimiya, D., 2014. Proteins improving recombinant antibody production in mammalian cells. Appl. Microbiol. Biotechnol. 98, 1031–1042. https://doi.org/10.1007/s00253-013-5427-3

Nutt, S.L., Hodgkin, P.D., Tarlinton, D.M., Corcoran, L.M., 2015. The generation of antibody-secreting plasma cells. Nat. Rev. Immunol. 15, 160–171. https://doi.org/10.1038/nri3795

O'Callaghan, P.M., McLeod, J., Pybus, L.P., Lovelady, C.S., Wilkinson, S.J., Racher, A.J., Porter, A., James, D.C., 2010. Cell line-specific control of recombinant monoclonal antibody production by CHO cells. Biotechnol. Bioeng. 106, 938–951. https://doi.org/10.1002/bit.22769

Ohya, T., Hayashi, T., Kiyama, E., Nishii, H., Miki, H., Kobayashi, K., Honda, K., Omasa, T., Ohtake, H., 2008. Improved production of recombinant human antithrombin III in Chinese hamster ovary cells by ATF4 overexpression. Biotechnol. Bioeng. 100, 317–324. https://doi.org/10.1002/bit.21758

Olzmann, J.A., Kopito, R.R., Christianson, J.C., 2013. The mammalian endoplasmic reticulum-associated degradation system. Cold Spring Harb. Perspect. Biol. 5, 1–16. https://doi.org/10.1101/cshperspect.a013185

Omasa, T., Takami, T., Ohya, T., Kiyama, E., Hayashi, T., Nishii, H., Miki, H., Kobayashi, K., Honda, K., Ohtake, H., 2008. Overexpression of GADD34 Enhances Production of Recombinant Human Antithrombin III in Chinese Hamster Ovary Cells. J. Biosci. Bioeng. 106, 568–573. https://doi.org/10.1263/jbb.106.568

Peng, R.W., Abellan, E., Fussenegger, M., 2011. Differential effect of exocytic SNAREs on the production of recombinant proteins in mammalian cells. Biotechnol. Bioeng. 108, 611–620. https://doi.org/10.1002/bit.22986

Peng, R.W., Fussenegger, M., 2009. Molecular engineering of exocytic vesicle traffic enhances the productivity of chinese hamster ovary cells. Biotechnol. Bioeng. 102, 1170–1181. https://doi.org/10.1002/bit.22141

Peng, R.W., Guetg, C., Tigges, M., Fussenegger, M., 2010. The vesicle-trafficking protein munc18b increases the secretory capacity of mammalian cells. Metab. Eng. 12, 18–25. https://doi.org/10.1016/j.ymben.2009.08.007

Pieper, L.A., Strotbek, M., Wenger, T., Gamer, M., Olayioye, M.A., Hausser, A., 2017a. Secretory pathway optimization of CHO producer cells by co-engineering of the mitosRNA-1978 target genes CerS2 and Tbc1D20. Metab. Eng. 40, 69–79. https://doi.org/10.1016/j.ymben.2017.01.003

Pieper, L.A., Strotbek, M., Wenger, T., Olayioye, M.A., Hausser, A., 2017b. ATF6β-based fine-tuning of the unfolded protein response enhances therapeutic antibody productivity of Chinese hamster ovary cells. Biotechnol. Bioeng. 114, 1310–1318. https://doi.org/10.1002/bit.26263

Pobre, K.F.R., Poet, G.J., Hendershot, L.M., 2019. The endoplasmic reticulum (ER) chaperone BiP is a master regulator of ER functions: Getting by with a little help from ERdj friends. J. Biol. Chem. 294, 2098–2108. https://doi.org/10.1074/jbc.REV118.002804

Poiron, C., Wu, Y., Ginestoux, C., Ehrenmann, F., Duroux, P., Lefranc, M.-P., 2010. IMGT/mAb-DB: the IMGT® database for therapeutic monoclonal antibodies. Jobim.

Puck, T.T., Cieciura, S.J., Robinson, A., 1958. Genetics of Somatic Mammalian

Cells. J. Exp. Med. 108, 945–956.

Pybus, L.P., James, D.C., Dean, G., Slidel, T., Hardman, C., Smith, A., Daramola, O., Field, R., 2014. Predicting the Expression of Recombinant Monoclonal Antibodies in Chinese Hamster Ovary Cells Based on Sequence Features of the CDR3 Domain. Biotechnol. Prog. 30, 188–97. https://doi.org/10.1002/btpr.1839

Pyronnet, S., Sonenberg, N., 2001. Cell-cycle-dependent translational control. Curr. Opin. Genet. Dev. 11, 13–18.

Rahimpour, A., Vaziri, B., Moazzami, R., Nematollahi, L., Barkhordari, F., Kokabee, L., Adeli, A., Mahboudi, F., 2013. Engineering the Cellular Protein Secretory Pathway for Enhancement of Recombinant Tissue Plasminogen Activator Expression in Chinese Hamster Ovary Cells: Effects of CERT and XBP1s Genes. J. Microbiol. Biotechnol. 23, 1116–1122.

Reinhart, D., Sommeregger, W., Reinhart, D., Debreczeny, M., Gludovacz, E., Kunert, R., 2014. In search of expression bottlenecks in recombinant CHO cell lines - A case study. Appl. Microbiol. Biotechnol. 98, 5959–5965. https://doi.org/10.1007/s00253-014-5584-z

Reisinger, H., Steinfellner, W., Stern, B., Katinger, H., Kunert, R., 2008. The absence of effect of gene copy number and mRNA level on the amount of mAb secretion from mammalian cells. Appl. Microbiol. Biotechnol. 81, 701–710. https://doi.org/10.1007/s00253-008-1701-1

Reusch, D., Tejada, M.L., 2015. Fc glycans of therapeutic antibodies as critical quality attributes. Glycobiology 25, 1325–1334. https://doi.org/10.1093/glycob/cwv065

Richelle, A., Lewis, N.E., 2017. Improvements in protein production in mammalian

cells from targeted metabolic engineering. Curr. Opin. Syst. Biol. 6, 1–6. https://doi.org/10.1016/j.coisb.2017.05.019

Rivera, V.M., Wang, X., Wardwell, S., Courage, N.L., Volchuk, A., Keenan, T., Holt, D.A., Gilman, M., Orci, L., Cerasoli Jr, F., Rothman, J.E., Clackson, T., 2012. Regulation of Protein Secretion Through Controlled Aggregation in the Endoplasmic Reticulum. Science (80-.). 287, 826–830. https://doi.org/10.1126/science.287.5454.826

Schröder, M., Friedl, P., 1997. Overexpression of Recombinant Human Antithrombin III in Chinese Hamster Ovary Cells Results in Malformation and Decreased Secretion of Recombinant Protein. Biotechnol. Bioeng. 53, 547–559.

Schubert, U., Antón, L.C., Norbury, C.C., Yewdell, J.W., Bennink, J.R., 2000. Rapid degradation of a large fraction of newly synthesized proteins by proteasomes. Nature 404, 770–774.

Schymkowitz, J., Borg, J., Stricher, F., Nys, R., Rousseau, F., Serrano, L., 2005. The FoldX web server: An online force field. Nucleic Acids Res. 33, 382–388. https://doi.org/10.1093/nar/gki387

Sharma, V.K., Patapoff, T.W., Kabakoff, B., Pai, S., Hilario, E., Zhang, B., Li, C., Borisov, O., Kelley, R.F., Chorny, I., Zhou, J.Z., Dill, K.A., Swartz, T.E., 2015. In silico selection of therapeutic antibodies for development: Viscosity, clearance, and chemical stability. Proc. Natl. Acad. Sci. U. S. A. 111, 18601–18606. https://doi.org/10.1073/pnas.1519997112

Sitia, R., Neuberger, M., Alberini, C., Bet, F., Fra, A., Valetti, C., Williams, G., Milstein, C., 1990. Developmental regulation of IgM secretion: the role of the carboxy-terminal cysteine. Cell 60, 781–90.

Skowronek, M.H., Hendershot, L.M., Haas, I.G., 2002. The variable domain of nonassembled Ig light chains determines both their half-life and binding to the chaperone BiP. Proc. Natl. Acad. Sci. 95, 1574–1578. https://doi.org/10.1073/pnas.95.4.1574

Smith, G.P., 1985. Filamentous fusion phage: Novel expression vectors that display cloned antigens on the virion surface. Science (80-.). 228, 1315–1317. https://doi.org/10.1126/science.4001944

Sormanni, P., Aprile, F.A., Vendruscolo, M., 2018. Third generation antibody discovery methods : in silico rational design. Chem. Soc. Rev. 47, 9137–9157. https://doi.org/10.1039/C8CS00523K

Spiess, C., Zhai, Q., Carter, P.J., 2015. Alternative molecular formats and therapeutic applications for bispecific antibodies. Mol. Immunol. 67, 95–106. https://doi.org/10.1016/j.molimm.2015.01.003

Stolfa, G., Smonskey, M.T., Boniface, R., Hachmann, A.-B., Gulde, P., Joshi, A.D., Pierce, A.P., Jacobia, S.J., Campbell, A., 2017. CHO-omics Review: The impact of Current and Emerging Technologies on Chinese Hmaster Ovary Based Bioproduction. Biotechnol. J.

Stoops, J., Byrd, S., Hasegawa, H., 2012. Russell body inducing threshold depends on the variable domain sequences of individual human IgG clones and the cellular protein homeostasis. Biochim. Biophys. Acta - Mol. Cell Res. 1823, 1643–1657. https://doi.org/10.1016/j.bbamcr.2012.06.015

Stoyle, C.L., Stephens, P.E., Humphreys, D.P., Heywood, S., Cain, K., Bulleid, N.J., 2017. IgG light chain-independent secretion of heavy chain dimers: consequence for therapeutic antibody production and design. Biochem. J. 474, 3179–3188. https://doi.org/10.1042/BCJ20170342

Stumpf, C.R., Moreno, M. V, Olshen, A.B., Taylor, B.S., Ruggero, D., 2013. The Translational Landscape of the Mammalian Cell Cycle. Mol. Cell 52, 574–582. https://doi.org/10.1016/j.molcel.2013.09.018

Sun, S., Shi, G., Han, X., Francisco, A.B., Ji, Y., Mendonça, N., Liu, X., Locasale, J.W., Simpson, K.W., Duhamel, G.E., Kersten, S., Yates, J.R., Long, Q., Qi, L., 2014. Sel1L is indispensable for mammalian endoplasmic reticulum-associated degradation, endoplasmic reticulum homeostasis, and survival. Proc. Natl. Acad. Sci. 111, E582–E591. https://doi.org/10.1073/pnas.1318114111

Tartaglia, G.G., Pechmann, S., Dobson, C.M., Vendruscolo, M., 2007. Life on the edge: a link between gene expression levels and aggregation rates of human proteins. Trends Biochem. Sci. 32, 204–206. https://doi.org/10.1016/j.tibs.2007.03.008

Tastanova, A., Schulz, A., Folcher, M., Tolstrup, A., Puklowski, A., Kaufmann, H., Fussenegger, M., 2016. Overexpression of YY1 increases the protein production in mammalian cells. J. Biotechnol. 219, 72–85. https://doi.org/10.1016/j.jbiotec.2015.12.005

Teckman, J.H., Perlmutter, D.H., 2000. Retention of mutant ␣ 1 -antitrypsin Z in endoplasmic reticulum is associated with an autophagic response. Am. J. Physiol. Gastrointest. liver Physiol. 279, G961-974.

Tigges, M., Fussenegger, M., 2006. Xbp1-based engineering of secretory capacity enhances the productivity of Chinese hamster ovary cells. Metab. Eng. 8, 264–272. https://doi.org/10.1016/j.ymben.2006.01.006

Tomar, D.S., Kumar, S., Singh, S.K., Goswami, S., Li, L., 2016. Molecular basis of high viscosity in concentrated antibody solutions: Strategies for high concentration drug product development. MAbs 8, 216–228.

https://doi.org/10.1080/19420862.2015.1128606

Tomar, D.S., Li, L., Broulidakis, M.P., Luksha, N.G., Burns, C.T., Singh, S.K., Kumar, S., 2017. In-silico prediction of concentration-dependent viscosity curves for monoclonal antibody solutions. MAbs 9, 476–489. https://doi.org/10.1080/19420862.2017.1285479

Tyler, R.E., Pearce, M.M.P., Shaler, T.A., Olzmann, J.A., Greenblatt, E.J., Kopito, R.R., 2012. Unassembled CD147 is an endogenous endoplasmic reticulum – associated degradation substrate. Mol. Biol. Cell 23, 4668–4678. https://doi.org/10.1091/mbc.E12-06-0428

Valetti, C., Grossi, C.E., Milstein, U., Sitia, R., 1991. Russell Bodies : A General Response of Secretory Cells to Synthesis of a Mutant Immunoglobulin Which Can Neither Exit from , Nor Be Degraded in , the Endoplasmic Reticulum. J. Cell Biol. 115, 983–994.

Van Der Kant, R., Karow-zwick, A.R., Durme, J. Van, Blech, M., Gallardo, R., Seeliger, D., Aßfalg, K., Baatsen, P., Compernolle, G., Gils, A., Studts, J.M., Schulz, P., Garidel, P., Schymkowitz, J., Rousseau, F., 2017. Prediction and Reduction of the Aggregation of Monoclonal Antibodies. J. Mol. Biol. 429, 1244–1261. https://doi.org/10.1016/j.jmb.2017.03.014

Van Durme, J., De Baets, G., Van Der Kant, R., Ramakers, M., Ganesan, A., Wilkinson, H., Gallardo, R., Rousseau, F., Schymkowitz, J., 2016. Solubis: A webserver to reduce protein aggregation through mutation. Protein Eng. Des. Sel. 29, 285–289. https://doi.org/10.1093/protein/gzw019

Vergara, M., Berrios, J., Martínez, I., Díaz-Barrera, A., Acevedo, C., Reyes, J.G., Gonzalez, R., Altamirano, C., 2015. Endoplasmic Reticulum-Associated rht-PA Processing in CHO Cells : Influence of Mild Hypothermia and Specific Growth

Rates in Batch and Chemostat Cultures. PLoS One 1–12. https://doi.org/10.1371/journal.pone.0144224

Vincenz-donnelly, L., Holthusen, H., Körner, R., Hansen, E.C., Presto, J., Johansson, J., Sawarkar, R., Hartl, F.U., Hipp, M.S., 2018. High capacity of the endoplasmic reticulum to prevent secretion and aggregation of amyloidogenic proteins. EMBO J. 37, 337–350. https://doi.org/10.15252/embj.201695841

Vogel, C., Marcotte, E.M., 2012. Insights into the regulation of protein abundance from proteomics and transcriptomis analyses. Nat. Rev. Genet. 13, 227–232. https://doi.org/10.1038/nrg3185.Insights

Walsh, G., 2018. Biopharmaceutical benchmarks 2018. Nat. Biotechnol. 36, 1136–1145. https://doi.org/10.1038/nbt0706-769

Wang, J., Pareja, K.A., Kaiser, C.A., Sevier, C.S., 2014. Redox signaling via the molecular chaperone BiP protects cells against endoplasmic reticulum-derived oxidative stress. Elife 3, e03496. https://doi.org/10.7554/eLife.03496

Wang, J., Sevier, C.S., 2016. Formation and Reversibility of BiP Protein Cysteine Oxidation Facilitate Cell Survival during and post Oxidative Stress. J. Biol. Chemest 291, 7541–7557. https://doi.org/10.1074/jbc.M115.694810

Wang, W., 1999. Instability, stabilization, and formulation of liquid protein pharmaceuticals, International Journal of Pharmaceutics.

Ward, C.L., Kopito, R.R., 1994. Intracellular Turnover of Cystic Fibrosis Transmembrane C . onductance Regulator. J. Biol. Chem. 269, 25710–25718.

Wei, P.-C., Hsieh, Y.-H., Su, M.-I., Jiang, X.-J., Hsu, P.-H., Lo, W.-T., Jeng, Y.-M., Wang, J.-M., Chen, P., Chang, Y.-C., Lee, K.-F., Tsai, M.-D., Shew, J.-Y., Lee, W.-H., 2012. Loss of the oxidative stress sensor NPGPx compromises GRP78 chaperone activity and induces systemic disease 48, 747–759.

https://doi.org/10.1016/j.molcel.2008.04.008.Comprehensive

White, C.J., Bode, J.W., 2018. PEGylation and Dimerization of Expressed Proteins under Near Equimolar Conditions with Potassium 2-Pyridyl Acyltrifluoroborates. ACS Cent. Sci. 4, 197–206. https://doi.org/10.1021/acscentsci.7b00432

Winter, G., Griffiths, A.D., Hawkins, R.E., Hoogenboom, H.R., 1994. Making Antibodies by Phage Display Technology. Annu. Rev. Immunol. 12, 433–455. https://doi.org/10.1146/annurev.iy.12.040194.002245

Wulhfard, S., Baldi, L., Hacker, D.L., Wurm, F., 2010. Valproic acid enhances recombinant mRNA and protein levels in transiently transfected Chinese hamster ovary cells. J. Biotechnol. 148, 128–132. https://doi.org/10.1016/j.jbiotec.2010.05.003

Wurm, F., 2013. CHO Quasispecies—Implications for Manufacturing Processes. Processes 1, 296–311. https://doi.org/10.3390/pr1030296

Wurm, F., 2004. Production of recombinant protein therapeutics in cultivated mammalian cells. Nat. Biotechnol. 22, 1393–1398. https://doi.org/10.1038/nbt1026

Wurm, F., Hacker, D., 2011. First CHO genome. Nat. Biotechnol. 29, 718–720. https://doi.org/10.1038/nbt.1943

Xiao, S., Shiloach, J., Betenbaugh, M.J., 2014. Engineering cells to improve protein expression. Curr. Opin. Struct. Biol. 26, 32–38. https://doi.org/10.1016/j.sbi.2014.03.005.Engineering

Xu, C., Bailly-Maitre, B., Reed, J.C., 2005. Endoplasmic reticulum stress: cell life and death decisions. J Clin Invest 115, 2656–2664. https://doi.org/10.1172/JCI26373.2656

Xu, X., Nagarajan, H., Lewis, N.E., Pan, S., Cai, Z., Chen, W., Xie, M., Wang, W.,

Hammond, S., Mikael, R., Neff, N., Passarelli, B., Koh, W., Fan, H., Gui, Y., Lee, K., Betenbaugh, M., Quake, S., Famili, I., Palsson, B., Wang, J., 2011. The Genomic Sequence of the Chinese Hamster Ovary (CHO) K1 cell line 29, 735–741. https://doi.org/10.1038/nbt.1932.The

Yadav, S., Laue, T.M., Kalonia, D.S., Singh, S.N., Shire, S.J., 2012. The influence of charge distribution on self-association and viscosity behavior of monoclonal antibody solutions. Mol. Pharm. 9, 791–802. https://doi.org/10.1021/mp200566k

Yu, M., Brown, D., Reed, C., Chung, S., Lutman, J., Stefanich, E., Wong, A., Stephan, J.-P., Bayer, R., 2012. Production, characterization and pharmacokinetic properties of antibodies with N-linked Mannose-5 glycans. MAbs 4, 475–487.

Zhang, P., Woen, S., Wang, T., Liau, B., Zhao, S., Chen, C., Yang, Y., Song, Z., Wormald, M.R., Yu, C., Rudd, P.M., 2016. Challenges of glycosylation analysis and control: An integrated approach to producing optimal and consistent therapeutic drugs. Drug Discov. Today 21, 740–765. https://doi.org/10.1016/j.drudis.2016.01.006

Zhong, X., Neumann, P., Corbo, M., Loh, E., 2011. Recent Advances in Biotherapeutics Drug Discovery and Development. Drug Discov. Dev. https://doi.org/10.5772/28094

Zhou, Y., Raju, R., Alves, C., Gilbert, A., 2018. Debottlenecking protein secretion and reducing protein aggregation in the cellular host. Curr. Opin. biotechnolo 53, 151–157.

Zhu, J., 2012. Mammalian cell protein expression for biopharmaceutical production. Biotechnol. Adv. 30, 1158–1170.

https://doi.org/10.1016/j.biotechadv.2011.08.022

Zurdo, J., Michael, R., Stallwood, Y., Hedman, K., Aastrup, T., 2011. Improving the Developability of Biopharmaceuticals. Innov. Pharm. Technol. 34–39.

8 APPENDIX

Mathias et al. 2018, Journal of Biotechnology

J Biotechnol. 2018 Apr 10;271:47-55

doi: 10.1016/j.jbiotec.2018.02.009

Epub 2018 Mar 2

Reprinted with permission from Elsevier B.V.

Journal of Biotechnology 271 (2018) 47–55

Contents lists available at ScienceDirect

Journal of Biotechnology

journal homepage: www.elsevier.com/locate/jbiotec

Visualisation of intracellular production bottlenecks in suspension-adapted CHO cells producing complex biopharmaceuticals using fluorescence microscopy

Sven Mathias[a,*], Simon Fischer[b], René Handrick[a], Jürgen Fieder[c], Patrick Schulz[b], Harald Bradl[b], Ingo Gorr[c], Martin Gamer[c], Kerstin Otte[a]

[a] University of Applied Sciences Biberach, Institute of Applied Biotechnology, Hubertus-Liebrecht-Straße 35, 88400 Biberach, Germany
[b] Boehringer Ingelheim Pharma GmbH & Co KG, Cell Culture Development CMB, Birkendorfer Straße 65, 88397 Biberach, Germany
[c] Boehringer Ingelheim Pharma GmbH & Co KG, Early Stage Bioprocess Development, Birkendorfer Straße 65, 88397 Biberach, Germany

ARTICLE INFO

Keywords:
Production bottleneck
CHO cell line engineering
Difficult-to-express proteins
Secretory pathway
Bispecific antibody production
Confocal microscopy

ABSTRACT

With the advance of complex biological formats such as bispecific antibodies or fusion proteins, mammalian expression systems often show low performance. Described determining factors may be accumulation or haltering of heterologous proteins within the different cellular compartments disturbing transport or secretion. In case of the investigated bispecific antibody (bsAb)-producing Chinese hamster ovary (CHO) cell line neither impaired transcription nor decreased translation processes were identified and thus satisfactorily explained its low production capacity. Hence, we established a streamlined confocal microscopy-based methodology for CHO production cells investigating the distribution of the recombinant protein within the respective organelles of the secretory pathway and visualised the structure of the endoplasmic reticulum (ER) to be affected pinpointing towards an intra-ER bottleneck putatively hampering or limiting efficient secretion. The ER displayed not only a heavily altered morphology in comparison to a high immunoglobulin G (IgG)-producing cell line with a possibly inflated or overloaded structure, but the recombinant protein was also completely absent in the Golgi apparatus. Notably, the results obtained using an automated microscopy approach suggest the possible application of this methodology in cell line development and engineering.

1. Introduction

Monoclonal antibodies are generally well-tolerated biopharmaceuticals highly specific in activating, inhibiting or blocking molecular targets to modulate diseases. Even though the optimisation of production processes for therapeutic antibodies is a continuing challenge, cell line development approaches establishing high-yielding production cell systems have been thoroughly optimised during the past decades, resulting in markedly streamlined developmental process timelines (Kunert and Reinhart, 2016). The clinical and commercial success of monoclonal antibodies led to a continuous effort to generate innovative and promising non-naturally existing antibody-derived biological formats. Many molecules are designed to be bispecific or multivalent for example to retarget T cells to kill tumour cells or to interact with different disease mediators (Spiess et al., 2015). At least 30 different antibody-derived biological formats are currently in clinical development and even more intriguing formats are under investigations (Spiess et al., 2015). As the generation of stable mammalian production cells requires a considerable investment of time and resources, the respective antibody encoding genes are first transiently expressed to test its efficacy and manufacturability, especially in case of artificial antibody-derived biological formats (Kim et al., 2012). However, in case of these more complex biological formats, mammalian expression systems often show low performance with cell lines displaying inferior product titers, low specific productivity or insufficient product quality as they may have artificial domain-specific folding, processing and/or secretion requirements (Lee et al., 2007).

All canonical steps in protein production such as transcription, translation, post-translational modification and intracellular protein transport are tightly regulated in the wild-type host cell line and will

Abbreviations: bsAb, bispecific antibody; CHO, chinese hamster ovary; ER, endoplasmic reticulum; IgG, Immunoglobulin G; DTE, difficult-to-express; DHFR, dihydrofolate reductase; MTX, Methotrexate; VCD, viable cell density; qRT-PCR, quantitative real-time polymerase chain reaction; HC, heavy chain; LC, light chain; DAPI, 4′,6-Diamidin-2′-phenylindol; SD, standard deviation

* Corresponding author.
E-mail address: mathias@hochschule-bc.de (S. Mathias).

https://doi.org/10.1016/j.jbiotec.2018.02.009
Received 2 November 2017; Received in revised form 17 February 2018; Accepted 19 February 2018
0168-1656/ © 2018 Elsevier B.V. All rights reserved.

impact the specific productivity of any producer cell line derived from this host. Any rate limiting step during production might represent a bottleneck for the final secretion of proteins into the culture medium. Especially, during production of difficult-to-express (DTE) molecules, which may accumulate or be haltered within the different cellular compartments and transport or secretion may be disturbed (Le Fourn et al., 2014). Furthermore, non-optimised heterologous proteins might be degraded intracellularly by the ubiquitin proteasome system or the unfolded protein response machinery (Johari et al., 2015). Over the past decades, several cellular pathways and processes have been identified as putative rate-limiting steps in mammalian production cell lines resulting in low product quantities or quality. Investigated pathways and mechanisms include translation (Kallehauge et al., 2017), folding and assembly (Pybus et al., 2014, O'Callaghan et al., 2010), intracellular transport and secretion (Florin et al., 2009, Peng and Fussenegger, 2009; Peng et al., 2010, 2011) as well as aggregation (Hasegawa et al., 2011, 2017; Stoops et al., 2012) and degradation (Johari et al., 2015) of the produced recombinant proteins. Generation of energy as well as precursor molecules can also represent a bottleneck (Dickson, 2014; Sellick et al., 2011). However, when comparing different cell lines and products, at best similar pathways but not the same genes were identified to represent rate-limiting steps and thus bottlenecks may be very specific to a certain molecule or production cell line.

Consequently, there is an urgent need to identify rate-limiting steps and de-bottleneck current expression systems especially in the context of novel emerging protein formats and engineer superior cell factories with improved properties as a basis for efficient and high yielding manufacturing processes. Therefore we here provide a streamlined fluorescence microscopy based methodology optimised for CHO production cells tracing the recombinantly produced protein traveling through the distinct cellular compartments of the secretory pathway. Visualised possibly molecule or production cell specific rate-limiting steps in recombinant protein production can be used as a starting point for cell engineering. Investigated organelles include the nucleus, the ER and the Cis-Golgi as well as lysosomes and endosomes facilitating the identification of repressive or saturated organelle structures hampering efficient protein production. We further demonstrate that using an automated high-throughput fluorescence microscope enables screening of production rate limiting steps in CHO production cell lines.

2. Materials and methods

2.1. Cell line generation

For generation of the investigated bsAb-producing and IgG-producing cell lines Boehringer Ingelheim proprietary suspension-adapted CHO DG44 dihydrofolate reductase (DHFR)-deficient host cells were transfected with two different expression plasmids. Beside DHFR and aminoglycoside phosphotransferase expression cassettes, respectively, the expression plasmids code for a classical IgG1 antibody and the individual chains of a symmetric, bispecific antibody molecule using similar regulatory elements, respectively. Afterwards IgG1- and bsAb-positive cells were selected in hypoxanthine and thymidine-deficient medium supplemented with 200 mg/L Geneticin as well as 200 nM Methotrexate (MTX) and 100 nM MTX, respectively.

2.2. Cell culture maintenance

Suspension-adapted CHO DG44 cells were cultured in Boehringer Ingelheim proprietary serum-free, chemically-defined and animal component free media (Boehringer Ingelheim, Biberach, Germany). The cultivation was performed in shake flasks (Corning, Oneonta, NY, USA) with 120 rpm (50 mm orbit) in an orbital shaker incubator (Infors, Bottmingen, Switzerland) at 37 °C and a relative CO_2 concentration of 5 %. Cell cultures were seeded with a viable cell density (VCD) of 3×10^5 cells/ml and passaged every 2–3 days. Cell concentration was measured using the Cedex device (Roche Diagnostics, Indianapolis, IN, USA) by means of trypan blue exclusion.

2.3. Fed-batch cultivation

Cells were seeded with a VCD of 3×10^5 cells/ml in an initial volume of 250 ml in a 1000 ml shake flask (Corning) and incubated as mentioned before. For each liter of total culture volume 30 ml feed medium (Boehringer Ingelheim) were added daily. 72 h post-seeding the relative CO_2 concentration was shifted to 2 %. Product concentration was determined using the Octet® device by FortéBio® (Menlo Park, CA, USA). The Biosen S-line analyser (EKF Diagnostics, Cardiff, UK) was used for measurement of glucose and lactate concentrations. Glucose bolus was added (Boehringer Ingelheim) when the concentration fell below a pre-defined critical value of 3.0 g/l.

2.4. Quantitative real-time polymerase chain reaction (qRT-PCR)

The isolation of total RNA from cell cultures was robotically processed using the automated QIAsymphony® platform (Qiagen, Hilden, Germany). Afterwards, concentrations were determined with a NanoDrop™ spectrophotometer (Thermo Fisher Scientific, Waltham, MA, USA). For reverse transcription, a final concentration of 2.5 ng/µl total RNA was used for each reaction performed with the High Capacity cDNA Reverse Transcription Kit (Applied Biosystems, Foster City, CA, USA). Final qRT-PCR was done with the TaqMan® Gene Expression Master Mix (Applied Biosystems) processed on a Rotor-Gene® Q (Qiagen). TaqMan® Ribosomal RNA Control Reagents (Applied Biosystems) were used to detect 18S ribosomal RNA as an endogenous control.

2.5. Western blotting

For protein analyses cells were lysed by incubation for 25 min at 23 °C in Passive Lysis Buffer (Promega, Madison, WI, USA) agitated at 600 rpm in an orbital shaker (Eppendorf, Hamburg, Germany). After centrifugation lysates were separated within NuPAGE® 4–12 % Bis-Tris Gels (Invitrogen, Carlsbad, California, USA) under reducing conditions and transferred to a nitrocellulose membrane using the iBlot® 2 dry blotting system (Invitrogen). Afterwards, iBind™ Flex FD Solution (Invitrogen) was used for blocking as well as antibody incubation applied via the iBind™ Western System (Invitrogen). The antibodies used for heavy chain (HC, #ab98616, abcam, Cambridge, UK) as well as light chain (LC, #K4377, Sigma Aldrich, St. Louis, MO, USA) detection were diluted 1:4000 and 1:8000, respectively. The loading control antibody against β-actin (#ab8227, abcam) was diluted 1:2000. Secondary IRDye® 800CW-labeled goat anti-mouse (#926-32210) as well as the IRDye® 680RD-labeled goat anti-rabbit (#926-68071) antibodies were diluted 1:4000 and the IRDye®800CW-labeled donkey anti-goat antibody (#926-32214) was diluted 1:2000 (LI-COR, Lincoln, NE, USA). Membranes were analysed using the Odyssey Infrared Scanning System (LI-COR).

2.6. Immunocytochemistry for confocal microscopic analysis

For microscopic analyses 1.7×10^4 cells/cm^2 were seeded into Nunc™ Lab-Tek™ II Chamber Slides™ (Nunc, Roskilde, Denmark) in 420 µl/cm^2 Ham´s F-12 Nutrient Mixture supplemented with 1 % fetal calf serum (Sigma Aldrich). Adherent growth of the suspension-adapted CHO cells was achieved after a cultivation for 72 h at 37 °C in a humidified HERAcell® incubator chamber (Heraeus, Hanau, Germany). After cultivation cells were fixed with 4 % paraformaldehyde (Alfa Aesar, Haverhill, MA, USA) and permeabilised with 0.1 % Triton X-100 (Carl-Roth, Karlsruhe, Germany). Subsequently, samples were blocked and incubated with an appropriate dilution of primary as well as secondary antibodies for 1.5 h and 1 h, respectively. Table 1 summarises

Table 1
Selected primary and secondary antibodies to stain organelles of the secretory and endocytic pathway in CHO cells using immunocytochemistry.

Organelle	Marker protein		Primary antibody	Secondary antibody
	Name	Abbreviation		
Ribosomes	40S ribosomal protein S6	RPS6	#5317S[a]	(Primary antibody directly Alexa Fluor® 488-labeled)
Endoplasmic reticulum	78 kDa glucose-regulated protein/Immunoglobulin heavy chain binding protein	GRP78/BIP	#ab21685[b]	#711-545-152[d], Alexa Fluor® 488-labeled
Cis-Golgi	Golgin subfamily A member 2/ 130 kDa cis-Golgi matrix protein	GM130	#610822[c]	#715-545-150[d], Alexa Fluor® 488-labeled
Secretory vesicles	Ras-related protein Rab-8A	Rab8A	#ab188574[b]	#711-545-152[d], Alexa Fluor® 488-labeled
Lysosomes	Lysosome-associated membrane glycoprotein 1	LAMP-1	#ab24170[b]	
Endosomes	Early endosome antigene 1	EEA-1	#ab2900[b]	

[a] Cell Signaling Technology, Cambridge, UK.
[b] Abcam, Cambridge, UK.
[c] BD BioScience, San Jose, CA, USA.
[d] JacksonImmuno Research, West Grove, PA, USA.

the selected primary and secondary antibodies to stain organelles of the secretory and endocytic pathway in CHO cells, all the antibodies tested during this study are available in the Supplementary Table S1. The antibodies against GRP78/BIP (#ab21685), Rab8 (#ab188574), LAMP-1 (#ab24170) and EEA1 (#ab2900) from abcam as well as against GM130 (#610822) from BD Bioscience (San Jose, CA, USA) were diluted 1:200 in blocking buffer. The directly Alexa Fluor® 488-labeled antibody against the S6RP (#5317S, Cell Signaling Technology, Cambridge, UK) was also diluted 1:200. The secondary Alexa Fluor® 488-labeled donkey anti-mouse (#715-545-150) and donkey anti-rabbit (#711-545-152) antibodies were diluted 1:500 (JacksonImmuno Research, West Grove, PA, USA). The directly Dylight® 550-labeled antibody (#ab98620, abcam) used for HC detection of the recombinantly produced proteins was diluted 1:50. CaptureSelect™ Biotin Anti-LC-kappa (human) conjugate (#7103272100, Thermo Fisher Scientific) used for LC detection of the recombinantly produced proteins was diluted 1:500. Alexa Fluor® 568-labeled Streptavidin (Thermo Fisher Scientific) was diluted 1:10000. Isotype controls were diluted accordingly. Actin cytoskeleton was labeled with Alexa Fluor® 647-labeled Phalloidin (#8940S, Cell Signaling Technology) and the nuclei counterstained with 4′,6-Diamidin-2´-phenylindol (DAPI, Sigma-Aldrich). After staining, samples were mounted with Prolong® Diamond Antifade Mountant medium (Invitrogen) and analysed. Pictures were acquired with a Zeiss LSM 710 confocal microscope equipped with a 405 nm, 488 nm, 561 nm, 633 nm laser (Carl Zeiss, Oberkochen, Germany).

2.7. Immunocytochemistry for automated fluorescence microscopy

For automated microscopic analyses 1.7×10^4 cells/cm^2 were seeded into 96-Well plates (Greiner Bio-One, Frickenhausen, Germany) in 440 µl/cm^2 Ham´s F-12 Nutrient Mixture supplemented with 1 % fetal calf serum (Sigma Aldrich). Adherent growth of the suspension-adapted CHO cells was achieved after a cultivation for 72 h at 37 °C in a humidified HERAcell® incubator chamber (Heraeus, Hanau, Germany). Afterwards cells were fixed, permeabilised and blocked as described in method section 2.6. For detection of the HC as well as the LC of the recombinant proteins the directly Dylight® 550-labeled antibody (#ab98620, abcam) and the CaptureSelect™ Biotin Anti-LC-Kappa (human) conjugate (#7103272100, Thermo Fisher Scientific) which again was detected with Alexa Fluor® 568-labeled Streptavidin (Thermo Fisher Scientific) were used. Isotype controls were diluted accordingly. Pictures were acquired with the automated microscopic device Cellavista™ (SynenTec, Elmshorn, Germany).

2.8. Statistical analysis

In general, data were displayed as mean ± standard deviation (SD) of two biological samples. Technical triplicates of each biological sample have only been performed in case of qRT-PCR as well as titer measurements. Here, mean and SD were calculated from the mean of the triplicate of each individual biological sample. For Western blot analysis the two biological samples were pooled. Origin 2016G SR1 (OriginLab, Northampton, MA, USA) was used for *t*-test calculations ($^{**}p < 0.01$, $^{***}p < 0.001$).

3. Results

3.1. Fed-batch cultivation revealed production bottleneck in a bsAb-producing cell line

A 12-day fed-batch cultivation process was used to compare the production capacity of a CHO cell line that stably produced a bsAb with a high IgG-producing cell line. Both investigated cell lines showed comparable viabilities until day 6 from which day on the viability of the IgG-producing cell line constantly decreased. The viability of the bsAb-producing cell line started to drop at day 10. Final viabilities at day 12 were approximately 85% in both cell lines. VCD was also comparable until day 6. From day 7 the bsAb-expressing cell line showed a constantly higher VCD (Fig. 1A). As a consequence, the integral of viable cells were $1.615 \times 10^{10} \pm 3 \times 10^7$ cells*d and $1.966 \times 10^{10} \pm 2.4 \times 10^8$ cells*d for the IgG-producing cell line and bsAb producing cell line, respectively (Fig. 1B).

However, contrary to the observed better growth characteristics of the bsAb-producing cell line the measured relative cumulative titer (IgG-producing cell line was set to a reference value of 1) at day 12 of culture was more then 2-fold lower when compared to the IgG-producing cell line (Fig. 2A). In consequence, the calculated mean specific productivity of each individual bsAb-producing cell was even less due to the superior cell growth and prolonged high viabilities (Fig. 2B). In fact, the relative mean specific productivity of the bsAb-producing cell line was approximately one-third of the IgG-producing cell line.

3.2. Classical cell line analyses were not sufficient to characterise production bottlenecks

For comparison of the recombinant protein production capability of the IgG- and bsAb-producing cell lines transcription and translation levels of the produced proteins were analysed. Transcripts of both HC and LC were analysed using qRT-PCR and detected at high levels in both cell lines as indicated by Ct values of 14.83 ± 0.07 and 13.90 ± 0.23 (HC) as well as 12.10 ± 0.05 and 11.21 ± 0.11 (LC) for the bsAb- and IgG-producing cell line, respectively. When compared to the highly expressed housekeeping gene 18S rRNA with Ct values of 10.00 ± 0.04 and 10.41 ± 0.45 (Fig. 3A) for the bsAb- and IgG-producing cell line, respectively, it is highly likely that the detected amounts of transcript were more than sufficient to produce high

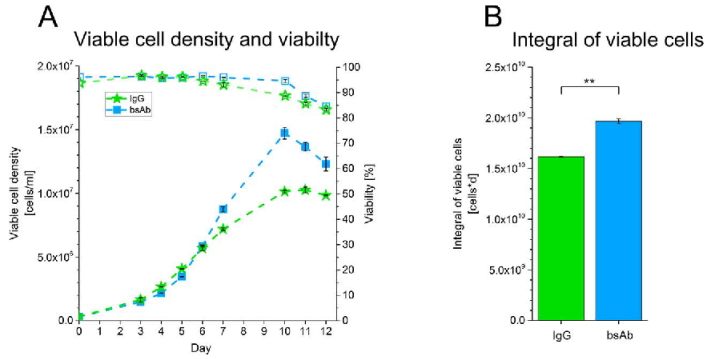

Fig. 1. Results of a fed-batch cultivation process of the IgG- and bispecific antibody (bsAb)-producing cell lines. (A) Measured viable cell density and viability. (B) Calculated cumulative integral of viable cells. The data are shown as mean ± SD of two biological replicates (n = 2). An unpaired two-tailed *t*-test was used to determine statistical significance ($^{**}p < 0.01$).

amounts of recombinant protein. Further, Western blot analysis was used to analyse the intracellular amount of HC and LC of the respective recombinant proteins (Fig. 3B). For both cell lines comparable amounts of LC as well as corresponding HC fragments were detected.

Summarising, neither transcription nor translation processes satisfactorily explained the low production capacity of the bsAb-producing cell line. As the production process of secreted proteins after transcription in the nucleus and translation start in the cytoplasm is continued in different organelle structures of the cell, we decided to analyse the distribution of the bsAb within these distinct compartments to identify unproductive or saturated organelles which might represent production bottlenecks.

3.3. Confocal microscopy identified intracellular transport and production bottlenecks

Since classical analyses for cell line characterisation were not able to sufficiently explain the low titer and even lower specific productivity of the bsAb-producing cell line a streamlined methodology optimised for CHO cells was developed to visualise the distribution of the recombinant proteins within the respective organelles of the secretory pathway. An experimental setup comprising four fluorescent dyes having distinct excitation/emission properties enabled us to analyse four cellular compartments simultaneously. Nucleus and cytoskeleton were stained for obtaining the fundamental cellular architecture. For analysing the protein distribution, the LC or the HC of the recombinant proteins, respectively, and one distinct organelle of the secretory pathway were concurrently visualised. In order to define the optimal set of antibodies specifically staining the respective organelles in CHO cells (Table 1) a variety of different antibodies established for human, rat and mouse cells were tested (see Supplementary Table S1).

First, we investigated the ER and the Golgi apparatus since folding and post-translational modification of the secreted proteins have previously been shown to represent rate-limiting steps in the production and final secretion of the recombinant protein. The ER is composed of an interconnected network of membrane-enclosed tubules or vesicles which is very dense around the nucleus and becomes looser the closer it gets to the plasma membrane (Schwarz and Blower, 2016) as observed with the IgG-producing cell line (Fig. 4). In case of the bsAb-producing cell line the ER showed an affected morphology with possibly inflated or overloaded larger irregular-shaped and sometimes interconnected circular structures, however, in both cases there was a strong colocalisation of recombinant protein and ER staining indicating that the entire ER was well-filled with both chains of the respective recombinant proteins.

After having been processed in the ER secreted proteins are transported to the Golgi apparatus which consists of stacks of membrane-enclosed cisternae. Here, proteins are further modified and packed into secretory vesicles for final secretion. Each individual stack can further be subdivided into the Cis-Golgi facing the nucleus and receiving vesicles from the ER and the Trans-Golgi network releasing secretory vesicles to its final destination. Compared to the ER the Cis-Golgi is a very small and compact but dense organelle usually located near the nucleus (Fig. 5). Notably, the bsAb-producing cell line showed no or only very weak colocalisation of staining for the Cis-Golgi and the recombinant protein whereas a very strong signal for the produced

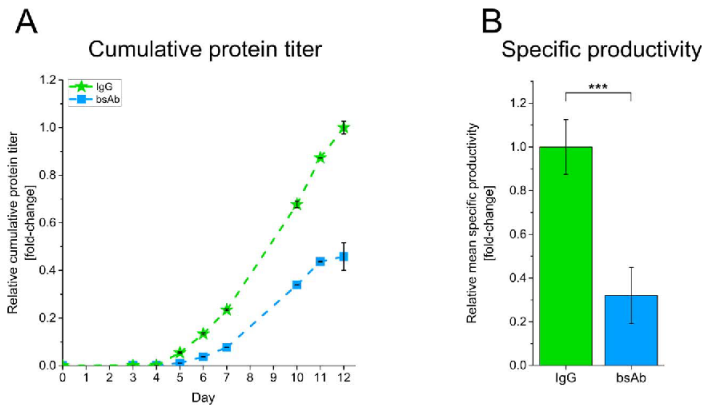

Fig. 2. Relative titer and specific productivity of the IgG- and bispecific antibody (bsAb)-producing cell lines during a fed-batch cultivation process. (A) Measured cumulative titer of the respective recombinant proteins. The data are shown as mean ± SD of two biological replicates (n = 2) whereas each biological sample was analysed in technical triplicates (n = 3). (B) Calculated relative mean specific productivity of the individual biological replicates from day 5 to 12. The data are shown as mean ± SD (n = 2). An unpaired two-tailed *t*-test was used to determine statistical significance ($^{***}p < 0.001$).

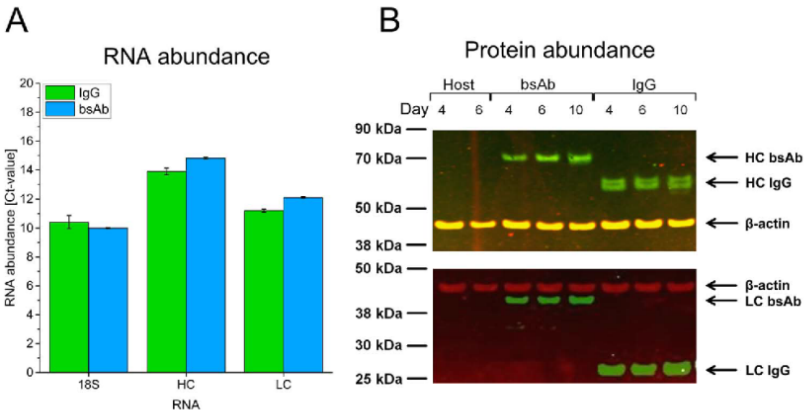

Fig. 3. Classical molecular biological analysis of the investigated IgG- and bispecific antibody (bsAb)-producing cell lines. (A) mRNA abundance of both chains of the respective recombinant proteins. 18S ribosomal RNA was used as internal control. The data are displayed as mean ± SD of two individual cultivations (n = 2) whereas mean and SD were calculated from the mean of three technical replicates of each individual cultivation (n = 3). (B) Intracellular amount of both chains of the recombinant proteins. Different samples were taken from the fed-batch cultivation process at day 4, 6 and 10. The two individual cultivations were pooled for Western blot analysis under reducing and denaturing conditions. β-actin was used as internal loading control.

recombinant IgG was observed within the Cis-Golgi apparatus of the respective cell line. This aberrant distribution of the bsAb additionally points towards a bottleneck within the ER of the respective cell line.

Finally, we analysed the distribution of the recombinant proteins within secretory vesicles designated for final release into the culture medium. They appeared as many very small vesicular structures distributed throughout the entire cell excepting the nucleus. Here again, it was not possible to detect any colocalisation of the produced recombinant protein chains within these vesicles irrespective weather the IgG or the bsAb was produced (Fig. 6).

Since the Golgi apparatus represents an intersection between the lysosomal, the secretory and the endocytic pathway we additionally analysed co-localisation of the respective produced recombinant proteins within the lysosomes and endosomes. Lysosomes and endosomes are membrane-enclosed vesicles used by the cell for hydrolysis of biomolecules and internalisation of molecules from the plasma membrane, respectively. However, no co-localisation was observed between the produced recombinant protein chains and lysosomes or endosomes (Supplementary Fig. S1). As a consequence, the recombinant proteins are neither detectably reinternalised nor degraded lysosomally.

Since ribosomes are sometimes referred as organelles we furthermore investigated the intracellular staining pattern for ribosomal proteins which represent the site of biological protein synthesis. In case of the bsAb-producing cell line the ribosomes showed a very diffuse staining pattern which did not co-localise with the recombinant protein at all. However, in case of the IgG-producing cell line the ribosomes quite well co-localised with the signal of the recombinant protein mainly reflecting the shape of the ER (Fig. 7). Notably, hotspots where a large number of ribosomes are available were appearently located on or even in the nucleus of both cell lines addressing the controversly discussed topic of nuclear translation (Reid and Nicchitta, 2012).

3.4. Automated microscopy enables high-throughput detection of transport bottlenecks

As the analysis of cellular protein distribution using confocal microscopy enabled us to visualise heavily altered ER structures in the bsAb-producing cell line, we investigated whether this methodology

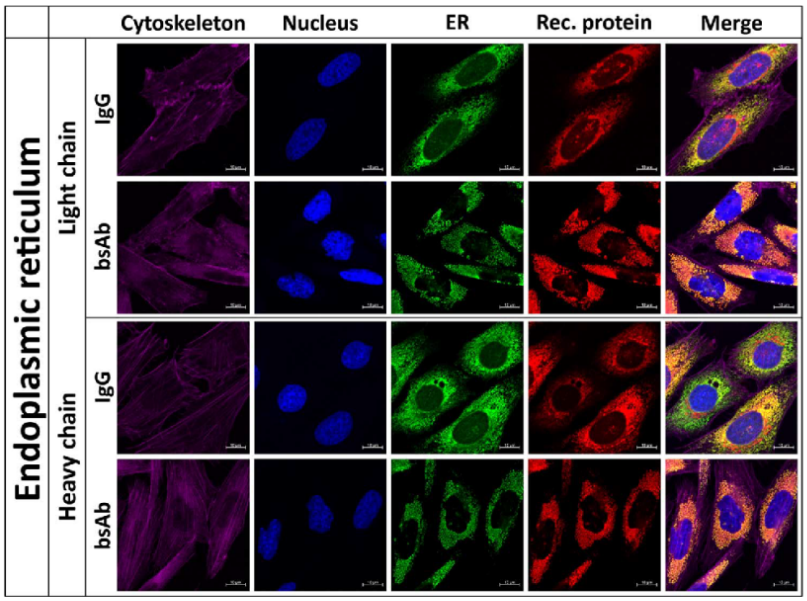

Fig. 4. Distribution of both chains of the recombinantly produced IgG and of the bispecific antibody (bsAb) (red) within the secretory organelle endoplasmic reticulum (ER) (green) of stable CHO production cell lines was analysed with a confocal microscope. Nucleus (blue) and cytoskeleton (magenta) were stained for obtaining the fundamental cellular architecture. Colocalisation is indicated in yellow. Cells were fixed and permeabilised before staining. Pictures were acquired at 63× primary magnification. The scale bars represent 10 µm. The respective light chains were detected with a CaptureSelect™ Biotin Anti-LC-kappa (human) conjugate and visualised with Alexa Fluor® 568-labeled Streptavidin. The respective heavy chains were detected with a directly Dylight® 550-labeled antibody. The ER was detected with an anti-GRP78 antibody and visualised with an Alexa Fluor® 488-labeled secondary antibody. (For interpretation of the references to colour in this figure legend, the reader is referred to the web version of this article.)

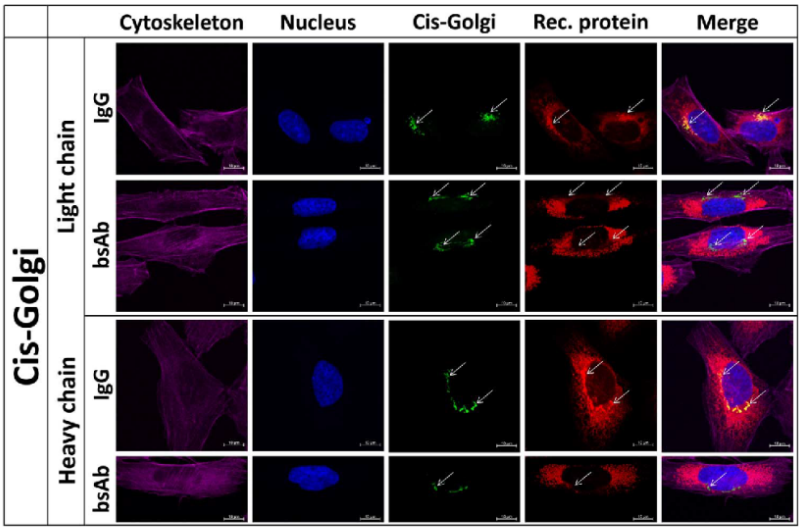

Fig. 5. Distribution of both chains of the recombinantly produced IgG and of the bispecific antibody (bsAb) (red) within the secretory organelle Cis-Golgi (B) (green) of stable CHO production cell lines was analysed with a confocal microscope. Nucleus (blue) and cytoskeleton (magenta) were stained for obtaining the fundamental cellular architecture. The localisation of the Cis-Golgi is highlighted with white arrows, colocalisation is indicated in yellow. Cells were fixed and permeabilised before staining. Pictures were acquired at 63× primary magnification. The scale bars represent 10 µm. The respective light chains were detected with a CaptureSelect™ Biotin Anti-LC-kappa (human) conjugate and visualised with Alexa Fluor® 568-labeled Streptavidin. The respective heavy chains were detected with a directly Dylight® 550-labeled antibody. The Cis-Golgi was detected with an anti-GM130 antibody and visualised with an Alexa Fluor® 488-labeled secondary antibody. (For interpretation of the references to colour in this figure legend, the reader is referred to the web version of this article.)

could be transferred to high-throughput applications using an automated microscopic device.

Evaluation of the intracellular distribution of the synthesised IgG using a high-throughput fluorescence microscope (Cellavista™) showed that two distinct organelle specific distribution patterns could be identified for LC and HC of the recombinant antibody. The less filled ER spread throughout the whole cell and the more compact Cis-Golgi apparatus containing higher concentrations of the recombinant protein which was indicated by a higher fluorescence intensity (Fig. 8). In case of the bsAb-producing cell line both LC and HC chains of the recombinant bispecific antibody were heavily concentrated within the ER and not detectable within the Cis-Golgi at all. These results confirmed distribution of the IgG throughout the ER as well as the Cis-Golgi whereas the bsAb appeared to be haltered within the ER.

4. Discussion

The generation of stable mammalian production cell lines requires a costly and lengthy cell line development process utilising stably transfection, time-consuming selection processes and extensive cell line screening procedures. Therefore expression of the respective genes is routinely first performed in transient systems to test for its capability to be efficiently produced (Baldi et al., 2007; Kim et al., 2012). This is especially important in case of artificial molecules where mammalian expression systems often show low performance during cellular production processes, most likely due to artificial domain-folding, processing or secretion requirements (Lee et al., 2007). Very low transient production titer and insufficient product quality are an early indication of low stable manufacturability (Mason et al., 2013; Pybus et al., 2014). As a consequence there is an urgent need to identify rate-limiting steps and de-bottleneck current expression systems, especially in the context of novel emerging protein formats. In the current work, comparative analysis of cellular production processes for a classical IgG antibody and a novel bsAb format indicated that classical methods used for cell line characterisation are not sufficient to reveal limiting intracellular transport or secretion processes responsible for the low productivity of cell lines producing DTE molecules. In particular, transcript levels revealed mRNA synthesis not to be a major limiting step probably due to previous establishment of highly efficient gene transfer methodologies, optimised gene expression cassettes and amplification steps (Wurm,

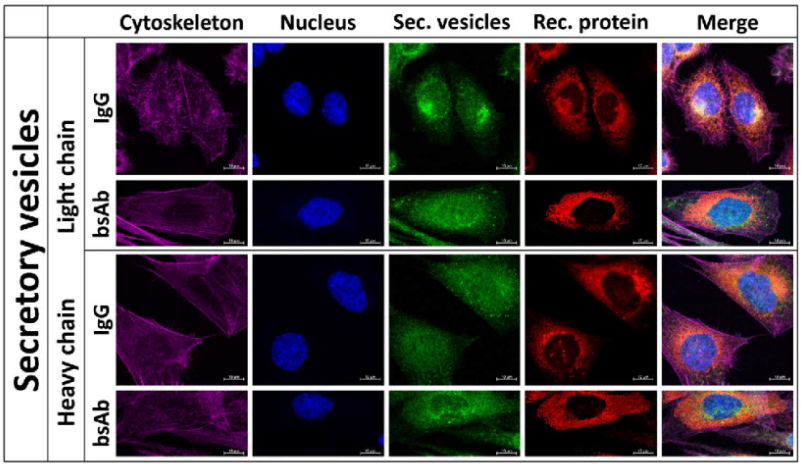

Fig. 6. Distribution of both chains of the recombinantly produced IgG and of the bispecific antibody (bsAb) (red) within the secretory vesicles (green) of stable CHO production cell lines was analysed with a confocal microscope. Nucleus (blue) and cytoskeleton (magenta) were costained for obtaining the fundamental cellular architecture. Cells were fixed and permeabilised before staining. Pictures were acquired at 63× primary magnification. The scale bars represent 10 µm. The respective light chains were detected with a CaptureSelect™ Biotin Anti-LC-kappa (human) conjugate and visualised with Alexa Fluor® 568-labeled Streptavidin. The respective heavy chains were detected with a directly Dylight® 550-labeled antibody. The secretory vesicles were detected with an anti-Rab8A antibody and visualised with an Alexa Fluor® 488-labeled secondary antibody. (For interpretation of the references to colour in this figure legend, the reader is referred to the web version of this article.)

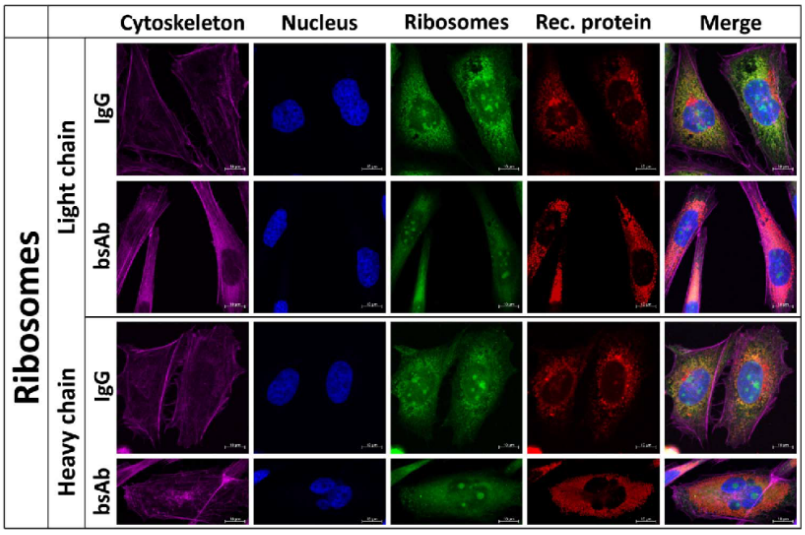

Fig. 7. Colocalisation of both chains of the recombinantly produced IgG and of the bispecific antibody (bsAb) (red) with ribosomes (green) in stable CHO production cell lines was analysed with a confocal microscope. Nucleus (blue) and cytoskeleton (magenta) were stained to visualise the fundamental architecture of the cell. Cells were fixed and permeabilised before staining. Pictures were acquired at 63× primary magnification. The scale bars represent 10 µm. The respective light chains were detected with a CaptureSelect™ Biotin Anti-LC-kappa (human) conjugate and visualised with Alexa Fluor® 568-labeled Streptavidin. The respective heavy chains were detected with a directly Dylight® 550-labeled antibody. The ribosomes were visualised with a directly Alexa Fluor® 488-labeled anti S6RP antibody. (For interpretation of the references to colour in this figure legend, the reader is referred to the web version of this article.)

2004). Since also comparable amounts of LC and HC proteins were detected within both cell lines in this study, it was concluded that neither transcription nor translation processes satisfactorily explained the low production capacity of the cell line producing the bsAb.

Over the past decades, plenty of strategies have been developed to improve protein production in mammalian expression systems, and since it has previously been shown that the ER and Golgi apparatus can in some cases represent a secretion bottleneck (Pybus et al., 2014, O'Callaghan et al., 2010) we have established a streamlined fluorescence microscopy-based methodology for CHO production cell lines to visualise bottlenecks during cellular production processes by tracing the recombinant protein being transported through the organelles of the secretory pathway. Strikingly, with this method we were able to reveal a production bottleneck within the examined CHO cell line producing a bsAb where the DTE protein was highly concentrated within the ER. Moreover we were not able to detect the bsAb within the Cis-Golgi although substantial amounts of the DTE molecule have been found in the supernatant during fed-batch cultivation. In practice, the comparatively high amount of detected recombinant protein within the ER might hamper the detection of the essential amounts within the Cis-Golgi. However, since considerable amounts of IgG have been found in the Cis-Golgi of the high-producing reference cells we revealed that transport to the Golgi apparatus seemed to be haltered in the bsAb-producing cell line. Additionally, the ER showed an affected morphology displaying distended or overloaded larger irregular-shaped structures which resemble previously described Russell bodies (Stoops et al., 2012), where insoluble and slowly degraded aggregates containing immunoglobulins are hosted within the dilated cisternae of the ER or the cytoplasm (Kopito and Sitia, 2000). In fact, Russell bodies are defined through ER-resident proteins like GRP78/BIP and Calnexin which co-localise within the described spherical structures (Hasegawa et al., 2011, 2017; Stoops et al., 2012) as shown in the recent study. However, other specific cellular processes may be responsible for the obtained phenotype e.g. impaired ER translocation during translation (Le Fourn et al., 2014) or a misregulated export as speculated by Hasegawa (Hasegawa et al., 2011). The emergence of the described structures within the dilated cisternae of the ER was observed under different culture conditions as well as different time points in cultivation. So, we assumed that the affected ER morphology is not a phenomenon exclusively induced by exogenous stress conditions. To clarify the molecular mechanisms behind the appearance of Russell bodies and the affected ER morphology, further investigations are needed. Possible reasons for accumulation of the bsAb in the ER might be that the different chains do not assemble efficiently, the molecule is prone to missfolding or is highly lipophilic and thus associates with membranous structures within the ER. The current study focused on the establishment of a generic methodology that enables the identification of production bottlenecks which will subsequently allow for in depth studies to reveal the mechanisms underlying secretion bottlenecks.

Interestingly, not only the morphology of the ER but also the staining pattern for the ribosomes was affected in the cells producing the bsAb, where the ribosomes seemed not to accumulate on the membrane of the ER, but being more heavily distributed throughout the cytoplasm. However, even though the ER/ribosomes showed a heavily affected phenotype the basic cellular functions appeared not to be disrupted completely since the respective cells stayed viable throughout the whole cultivation period, did not undergo cell death more heavily and have even grown to higher cell densities in comparison to the IgG-expressing cell line which was not expected. Effectively, in previous studies it has been shown that cells producing easy-to-express mAbs maintained higher cell viability in comparison to cells producing DTE mAbs throughout the cultivation (Hasegawa et al., 2017; Stoops et al., 2012). Additionally, Stoops and co-workers showed that the ER stress marker CHOP was induced regardless of whether the cells expressed easy-to-express or DTE IgG molecules, however, the kinetics and the magnitude of induction appeared to be different (Stoops et al., 2012). Only a certain percentage of intracellular proteins are glycoproteins and cytosolic proteins are translated at free ribosomes within the cytoplasm. Hence, essential proteins required for growth and cell division might have not been affected by the accumulating bsAb in the ER leading to normal growth behaviour which was finally even better than that of the IgG-producing cell line. In addition, since secretion rates of the bsAb producing cell line were obviously much lower compared to the cell line producing the IgG more free energy might have been available in the bsAb producing cell line resulting in a growth advantage. In order to further understand the physiological conditions in the investigated CHO cell line producing a novel antibody format, future experiments will be necessary to analyse the expression profile of proteins indicating ER stress conditions such as CHOP, belonging to the unfolding protein response or ER associated degradation (Hussain et al., 2014).

When estimating the detected recombinant protein of the high IgG-producing cell line, we showed that by far the largest part of the

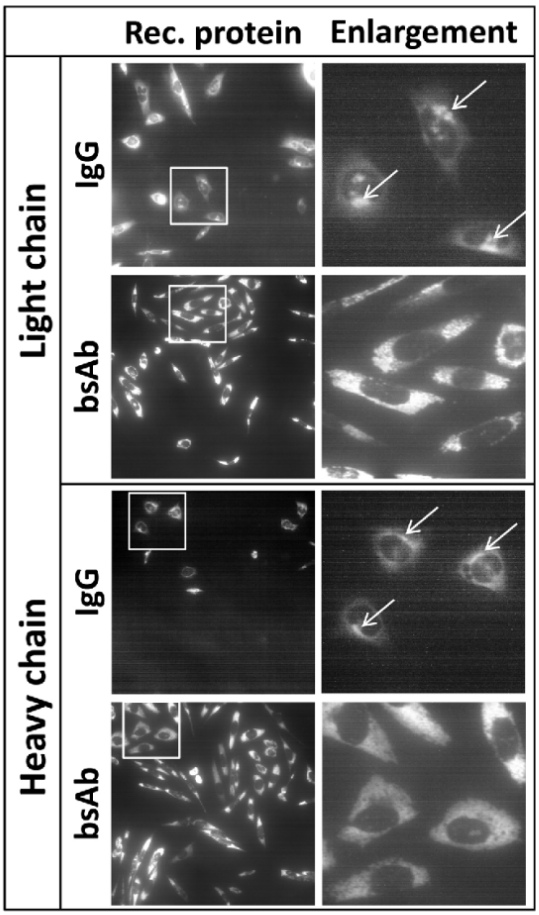

Fig. 8. Intracellular staining of the recombinantly produced IgG and of the bispecific antibody (bsAb) within stable CHO production cell lines analysed with an automated microscopic device. The enlarged area is depicted with white lines. Localisation of the Cis-Golgi is highlighted with white arrows. Cells were fixed and permeabilised before staining. Pictures were acquired at 40× primary magnification. The respective light chains were detected with a CaptureSelect™ Biotin Anti-LC-kappa (human) conjugate and visualised with Alexa Fluor® 568-labeled Streptavidin. The respective heavy chains were detected with a directly Dylight® 550-labeled antibody.

intracellularly detectable recombinant protein chains were located within the organelles ER and Cis-Golgi. We were not able to detect the low amount of potentially remaining IgG in secretory vesicles. It has previously been shown that ER to Cis-Golgi trafficking is known to be a major bottleneck in the secretory pathway (Pybus et al., 2014, O'Callaghan et al., 2010). Cellular processes following the Cis-Golgi compartment may possibly be very fast resulting in a rapid turnover and a low steady-state-concentration of the recombinant protein within the respective organelles which may argue for a possible detection limit for microscopic analyses (O'Callaghan et al., 2010). Alternatively, since secretory vesicles are known to be highly specific for their cargo (Bonifacino and Glick, 2004), the marker protein for staining secretory vesicles, Rab8, which is a GTPase globally involved in vesicular transport between the Trans-Golgi network and the basolateral plasma membrane (Huber et al., 1993), may not stain the vesicles involved in antibody transport. However, we also tested other vesicular markers like VAMP2/Synaptobrevin 2 which as well did not show colocalisation of the IgG and the secretory vesicles (data not shown).

The current study showed that specific intracellular production bottlenecks can be identified by using a globally applicable fluorescence microscopy-based experimental setup which in consequence facilitates organelle-tailored molecular approaches for target identification and molecular engineering leading to the generation of cell lines with superior properties. This method, however, is based on confocal microscopy which is incompatible with industrial processes. Hence, we transferred this procedure to an automated microscopic device which might facilitate its industrial application. In combination with picture analysis tools high-throughput microscopic analysis might enable automatic processing of the generated images leading to rapid identification of suitable clonal production cell lines. Furthermore, this method might enable investigations of diverse mutants or sequence variants of candidate molecules especially in combination with transient gene expression. Conclusively, the described streamlined methodology enables the visualisation and identification of unproductive or saturated organelles in CHO production cell lines pointing towards cell line engineering approaches.

Contributors

Sven Mathias performed laboratory work, data analysis and wrote the manuscript. Simon Fischer, Martin Gamer and Kerstin Otte designed the study, contributed to experimental design and co-authored the manuscript. René Handrick, Jürgen Fieder, Patrick Schulz, Harald Bradl and Ingo Gorr helped with study design and reviewed the manuscript.

All authors declare that they approved the final article.

Disclosure of potential conflicts of interest

The authors declare no conflict of interest. S. Fischer, J. Fieder, P. Schulz, H. Bradl, I. Gorr and M. Gamer are employees of Boehringer Ingelheim Pharma which develops and sells pharmaceuticals.

Grant support

Boehringer Ingelheim funded all of this research.

Acknowledgements

The authors are especially grateful to Tobias Kiechle, Jennifer Schütt and Kathrin Höhne for excellent technical assistance on confocal microscopy and qRT-PCR experiments, respectively. Further, we thank Karin Rechtsteiner for supporting cell culture experiments, Anja Ebe for assisting with automated high-throughput fluorescence microscopy and Melanie Luz for recombinant protein concentration measurements. We also thank Ursula Bauknecht for technical support on Western blot analyses.

Appendix A. Supplementary data

Supplementary material related to this article can be found, in the online version, at doi: https://doi.org/10.1016/j.jbiotec.2018.02.009.

References

Baldi, L., Hacker, Æ.D.L., Adam, Æ.M., Wurm, F.M., 2007. Recombinant protein production by large-scale transient gene expression in mammalian cells : state of the art and future perspectives. Biotechnol. Lett. 29, 677–684. http://dx.doi.org/10.1007/s10529-006-9297-y.

Bonifacino, J.S., Glick, B.S., 2004. The mechanisms of vesicle budding and fusion. Cell 116, 153–166. http://dx.doi.org/10.1016/S0092-8674(03)01079-1.

Dickson, A.J., 2014. Enhancement of production of protein biopharmaceuticals by mammalian cell cultures : the metabolomics perspective. Curr. Opin. Biotechnol. 30, 73–79. http://dx.doi.org/10.1016/j.copbio.2014.06.004.

Florin, L., Pegel, A., Becker, E., Hausser, A., Olayioye, M.A., Kaufmann, H., 2009. Heterologous expression of the lipid transfer protein CERT increases therapeutic protein productivity of mammalian cells. J. Biotechnol. 141, 84–90. http://dx.doi.

org/10.1016/j.jbiotec.2009.02.014.
Hasegawa, H., Hsu, A., Tinberg, C.E., Siegler, K.E., Aaron, A., Tsai, M., 2017. Single amino acid substitution in LC-CDR1 induces Russell body phenotype that attenuates cellular protein synthesis through eIF2 α phosphorylation and thereby downregulates IgG secretion despite operational secretory pathway traffic. MAbs 9, 854–873. http://dx.doi.org/10.1080/19420862.2017.1314875.
Hasegawa, H., Wendling, J., He, F., Trilisky, E., Stevenson, R., Franey, H., Kinderman, F., Li, G., Piedmonte, D.M., Osslund, T., Shen, M., Ketchem, R.R., 2011. In vivo crystallization of human IgG in the endoplasmic reticulum of engineered chinese hamster ovary (CHO) cells. J. Biol. Chem. 286, 19917–19931. http://dx.doi.org/10.1074/jbc.M110.204362.
Huber, L.A., Pimplikar, S., Parton, R.G., Virta, H., Zerial, M., Simons, K., 1993. Rab8, a small GTPase involved in vesicular traffic between the TGN and the basolateral plasma membrane. J. Cell Biol. 123, 35–45. http://dx.doi.org/10.1083/jcb.123.1.35.
Hussain, H., Maldonado-Agurto, R., Dickson, A.J., 2014. The endoplasmic reticulum and unfolded protein response in the control of mammalian recombinant protein production. Biotechnol. Lett. 36, 1581–1593. http://dx.doi.org/10.1007/s10529-014-1537-y.
Johari, Y.B., Estes, S.D., Alves, C.S., Sinacore, M.S., James, D.C., 2015. Integrated cell and process engineering for improved transient production of a "difficult-to-express" fusion protein by CHO cells. Biotechnol. Bioeng. 112, 2527–2542. http://dx.doi.org/10.1002/bit.25687.
Kallehauge, T.B., Li, S., Pedersen, L.E., Ha, T.K., Ley, D., Andersen, M.R., Kildegaard, H.F., Lee, G.M., Lewis, N.E., 2017. Ribosome profiling-guided depletion of an mRNA increases cell growth rate and protein secretion. Nat. Publ. Gr. 7, 1–12. http://dx.doi.org/10.1038/srep40388.
Kim, J.Y., Kim, Y., Lee, G.M., 2012. CHO cells in biotechnology for production of recombinant proteins : current state and further potential. Appl. Microbiol. Biotechnol. 93, 917–930. http://dx.doi.org/10.1007/s00253-011-3758-5.
Kopito, R.R., Sitia, R., 2000. Aggresomes and Russell bodies. EMBO Rep. 1, 225–231. http://dx.doi.org/10.1093/embo-reports/kvd052.
Kunert, R., Reinhart, D., 2016. Advances in recombinant antibody manufacturing. Appl. Microbiol. Biotechnol. 100, 3451–3461. http://dx.doi.org/10.1007/s00253-016-7388-9.
Le Fourn, V., Girod, P.A., Buceta, M., Regamey, A., Mermod, N., 2014. CHO cell engineering to prevent polypeptide aggregation and improve therapeutic protein secretion. Metab. Eng. 21, 91–102. http://dx.doi.org/10.1016/j.ymben.2012.12.003.
Lee, G.W., Fecko, J.K., Yen, A., Donaldson, D., Wood, C., Tobler, S., Vunuum, S., Luo, Y., Leonard, M., 2007. Improving the expression of a soluble receptor: Fc fusion protein in CHO cells by coexpression with the receptor ligand. Cell Technol. Cell Prod. 29–39. http://dx.doi.org/10.1007/978-1-4020-5476-1_4.
Mason, M., Sweeney, B., Cain, K., Stephens, P., Susan, T., 2013. Identifying bottlenecks in transient and stable production of recombinant monoclonal-antibody sequence variants in Chinese hamster ovary cells. Biotechnol. Prog. 28, 846–855. http://dx.doi.org/10.1002/btpr.1542.Identifying.
O'Callaghan, P.M., McLeod, J., Pybus, L.P., Lovelady, C.S., Wilkinson, S.J., Racher, A.J., Porter, A., James, D.C., 2010. Cell line-specific control of recombinant monoclonal antibody production by CHO cells. Biotechnol. Bioeng. 106, 938–951. http://dx.doi.org/10.1002/bit.22769.
Peng, R.W., Abellan, E., Fussenegger, M., 2011. Differential effect of exocytic snares on the production of recombinant proteins in mammalian cells. Biotechnol. Bioeng. 108, 611–620. http://dx.doi.org/10.1002/bit.22986.
Peng, R.W., Fussenegger, M., 2009. Molecular engineering of exocytic vesicle traffic enhances the productivity of Chinese hamster ovary cells. Biotechnol. Bioeng. 102, 1170–1181. http://dx.doi.org/10.1002/bit.22141.
Peng, R.W., Guetg, C., Tigges, M., Fussenegger, M., 2010. The vesicle-trafficking protein munc18b increases the secretory capacity of mammalian cells. Metab. Eng. 12, 18–25. http://dx.doi.org/10.1016/j.ymben.2009.08.007.
Pybus, L.P., Dean, G., West, N.R., Smith, A., Daramola, O., Field, R., Wilkinson, S.J., James, D.C., 2014. Model-directed engineering of "'difficult-to-express'" monoclonal antibody production by Chinese hamster ovary cells. Biotechnol. Bioeng. 111, 372–385. http://dx.doi.org/10.1002/bit.25116.
Reid, D.W., Nicchitta, C.V., 2012. The enduring enigma of nuclear translation. J. Cell Biol. 197, 7–9. http://dx.doi.org/10.1083/jcb.201202140.
Schwarz, D.S., Blower, M.D., 2016. The endoplasmic reticulum: structure, function and response to cellular signaling. Cell. Mol. Life Sci. 73, 79–94. http://dx.doi.org/10.1007/s00018-015-2052-6.
Sellick, C.A., Croxford, A.S., Maqsood, A.R., Stephens, G., Westerhoff, H.V., Goodacre, R., Dickson, A.J., 2011. Metabolite profiling of recombinant CHO cells : designing tailored feeding regimes that enhance recombinant antibody production. Biotechnol. Bioeng. 108, 3025–3031. http://dx.doi.org/10.1002/bit.23269.
Spiess, C., Zhai, Q., Carter, P.J., 2015. Alternative molecular formats and therapeutic applications for bispecific antibodies. Mol. Immunol. 67, 95–106. http://dx.doi.org/10.1016/j.molimm.2015.01.003.
Stoops, J., Byrd, S., Hasegawa, H., 2012. Russell body inducing threshold depends on the variable domain sequences of individual human IgG clones and the cellular protein homeostasis. Biochim. Biophys. Acta Mol. Cell Res. 1823, 1643–1657. http://dx.doi.org/10.1016/j.bbamcr.2012.06.015.
Wurm, F.M., 2004. Production of recombinant protein therapeutics in cultivated mammalian cells. Nat. Biotechnol. 22, 1393–1398. http://dx.doi.org/10.1038/nbt1026.

Mathias et al. 2018, Journal of Biotechnology Supplementary Material

J Biotechnol. 2018 Apr 10;271:47-55

doi: 10.1016/j.jbiotec.2018.02.009

Epub 2018 Mar 2

Reprinted with permission from Elsevier B.V.

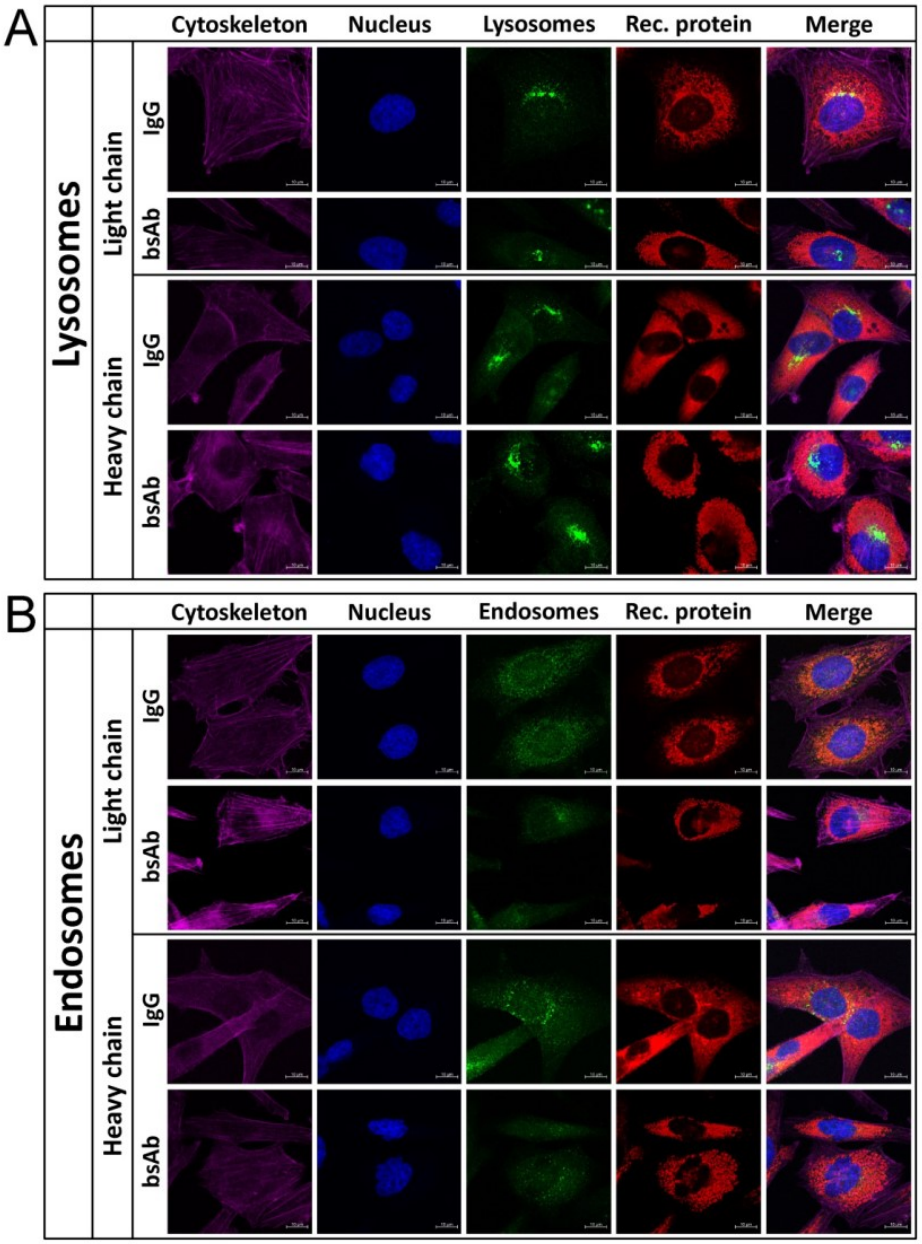

Fig. S1. Intracellular staining of the recombinantly produced IgG and of the bispecific antibody (bsAb) (red) within the endocytic and biosynthetic-secretory organelles lysosomes (A) and endosomes (B) (green) of stable CHO production cell lines analysed with an automated microscopic device. Nucleus (blue) and cytoskeleton (magenta) were stained to visualise the fundamental cellular architecture. Cells were fixed and permeabilised before staining. Pictures were acquired at 63x primary magnification. The scale bars represent 10 µm. The respective light chains were detected with a CaptureSelect™ Biotin Anti-LC-kappa (human) conjugate and visualised with Alexa Fluor® 568-labeled Streptavidin. The respective heavy chains were detected with a directly Dylight® 550-labeled antibody. The lysosomes and endosomes were detected with an anti-LAMP1 and anti-EEA1 antibodiy, respectively, and visualised with a Alexa Fluor® 488-labeled secondary antibody.

Table S1: Antibodies tested during this study to stain organelles of the secretory and endocytic pathway in CHO cells using immunocytochemistry.

Organelle	Marker protein		Primary antibody	Results obtained using described approaches
	Name	Abbreviation		
Ribosomes	40S ribosomal protein S6	RPS6	#5317S[a]	reasonable
Endoplasmic Reticulum (ER)	Calnexin	-	#sc-23954[e]	inconclusive
	78 kDa glucose-regulated protein/Immunoglobulin heavy chain binding protein	GRP78/BIP	#ab21685[b]	Reasonable (were also already used in other studies)
	Protein disulfide-isomerase	PDI	#ab3672[b]	inconclusive
			#ab2792[b]	inconclusive
ER-Golgi intermediate compartment (ERGIC)	ER-Golgi intermediate compartment 53 kDa protein	ERGIC-53	#sc-398777[e]	inconclusive
Cis-Golgi	Golgin subfamily A member 2/ 130 kDa cis-Golgi matrix protein	GM130	#610822[c]	reasonable
			#G7295[d]	inconclusive
	58K Golgi protein	-	#201999[b]	inconclusive
	Golgin-97	-	#53-9767[g]	inconclusive
Secretory vesicles	Ras-related protein Rab-8A	Rab8A	#ab188574[b]	reasonable
	Vesicle-associated membrane protein 2	VAMP2	#MAB5136[f]	reasonable
			#104211[h]	reasonable
	Syntaxin-4	Stx4	#ab184545[b]	reasonable
	Clathrin heavy chain	Clathrin HC	#sc-12734[e]	inconclusive
Lysosomes	Lysosome-associated membrane glycoprotein 1	LAMP-1	#sc-20011[e]	inconclusive
			#ab24170[b]	Reasonable (were also already used in other studies)
Endosomes	Early endosome antigene 1	EEA-1	#ab2900[b]	Reasonable (were also already used in other studies)

a: Cell Signaling Technology, Cambridge, UK; b: Abcam, Cambridge, UK; c: BD BioScience, San Jose, CA, USA; d: JacksonImmuno Research, West Grove, PA, USA; e: Santa Cruz Biotechnology, Dallas, TX, USA; f: R&D Systems, Minneapolis, MN, USA; g: Affymetrix, Santa Clara, CA, USA; h: Synaptic Systems, Goettingen, Germany

Mathias et al. 2019, Biotechnology and Bioengineering

Biotechnol Bioeng. 2020 Jan;117(1):5-16

doi: 10.1002/bit.27196

Epub 2019 Nov 15

Licensed under Creative Commons Attribution - NonCommercial 4.0 International,
https://creativecommons.org/licenses/by-nc/4.0/

Received: 8 June 2019 | Revised: 13 August 2019 | Accepted: 15 October 2019

DOI: 10.1002/bit.27196

BIOTECHNOLOGY & BIOENGINEERING WILEY

ARTICLE

Unraveling what makes a monoclonal antibody difficult-to-express: From intracellular accumulation to incomplete folding and degradation via ERAD

Sven Mathias[1] | Anna Wippermann[2] | Nadja Raab[1] | Nikolas Zeh[1] | René Handrick[1] | Ingo Gorr[3] | Patrick Schulz[2] | Simon Fischer[4] | Martin Gamer[2] | Kerstin Otte[1]

[1]Institute of Applied Biotechnology, University of Applied Sciences Biberach, Biberach, Germany

[2]Cell Line Development, Bioprocess Development Biologicals, Boehringer Ingelheim Pharma GmbH & Co. KG, Biberach, Germany

[3]Early Stage Bioprocess Development, Bioprocess Development Biologicals, Boehringer Ingelheim Pharma GmbH & Co. KG, Biberach, Germany

[4]Cell Line Development CMB, Bioprocess & Analytical Development, Boehringer Ingelheim Pharma GmbH & Co. KG, Biberach, Germany

Correspondence
Sven Mathias, Institute of Applied Biotechnology, University of Applied Sciences, Biberach Hubertus-Liebrecht-Str. 35, 88400 Biberach, Germany.
Email: mathias@hochschule-bc.de

Funding information
Boehringer Ingelheim Pharma GmbH & Co. KG

Abstract

Although most therapeutic monoclonal antibodies (mAbs) can routinely be produced in the multigram per litre range, some mAb candidates turn out to be difficult-to-express (DTE). In addition, the class of more complex biological formats is permanently increasing and mammalian expression systems like Chinese hamster ovary (CHO) cell lines can show low performance. Hence, there is an urgent need to identify any rate limiting processing step during cellular synthesis. Therefore, we assessed the intracellular location of the DTE antibody mAb2 by fluorescence and electron microscopy (EM) and revealed an accumulation of the antibody, which led to an aberrant morphology of the endoplasmic reticulum (ER). Analysis of underlying cellular mechanisms revealed that neither aggregation nor antibody assembly, but folding represented the reason for hampered secretion. We identified that the disulfide bridge formation within the antibody light chain (LC) was impaired due to less recognition by protein disulfide isomerase (PDI). As a consequence, the DTE molecule was degraded intracellularly by the ubiquitin proteasome system via ER-associated degradation (ERAD). This study revealed that with the continuous emergence of DTE therapeutic protein candidates, special attention needs to be drawn to optimization processes to ensure manufacturability.

KEYWORDS
CHO cell line engineering, difficult-to-express mAbs, ER-associated degradation, incomplete domain folding, production bottleneck, protein disulfide isomerase

1 | INTRODUCTION

Monoclonal antibodies (mAbs) represent a class of therapeutic proteins, which are highly specific in activating, inhibiting, or blocking molecular targets to modulate diseases and can routinely be produced in the multigram per litre range using modern fed-batch cultivation processes (Kunert & Reinhart, 2016). However, the number of innovative and nonnaturally existing more complex biologicals such as multispecific formats has been increasing dramatically during the past years (Jost & Plückthun, 2014; Spiess, Zhai, & Carter, 2015). Since these artificially generated molecules have never undergone an evolutionary optimization, mammalian cellular expression systems often show low performance with cell lines displaying inferior product titer, low specific productivity, or insufficient product quality (Johari, Estes, Alves, Sinacore, & James, 2015; Lee et al., 2007). In addition, even some classical mAb candidates can be difficult-to-express (DTE), which might result in the termination of the

This is an open access article under the terms of the Creative Commons Attribution-NonCommercial License, which permits use, distribution and reproduction in any medium, provided the original work is properly cited and is not used for commercial purposes.
© 2019 The Authors. *Biotechnology and Bioengineering* Published by Wiley Periodicals, Inc.

product development (Pybus et al., 2014). To provide access to sufficient amounts of innovative drugs, there is an urgent need to identify any rate limiting processing step during cellular synthesis and transport, which might represent a secretion bottleneck.

The biosynthesis, processing, and subsequent secretion of extracellular proteins is a complex and multistep procedure, which requires several different compartments within the respective cell to function highly efficiently. Each organelle thereby represents a tightly regulated and balanced network to provide the basis for performing specific tasks (Alberts et al., 2002; Lodish et al., 2000). Any disturbances in this equilibrium will impair the functionality as well as morphological appearance of the respective compartment. Therapeutic proteins which are assigned for secretion are ribosomally synthesized and cotranslationally translocated into the lumen of the endoplasmic reticulum (ER). Here, proper folding is facilitated by various resident chaperones such as members of the 70-kDa heat shock protein family like binding immunoglobulin (IgG) protein (BIP), lectins including calnexin and calreticulin as well as peptidyl–prolyl isomerases (Braakman & Hebert, 2013; Ellgaard & Helenius, 2003). After folding, the native protein structure is stabilized by disulfide bridges, which are simultaneously established via protein disulfide isomerases (PDIs) oxidizing free cysteine residues (Appenzeller-Herzog, 2011). Subsequently, evolutionarily conserved mechanisms ensure that only correctly folded proteins are transported to the Golgi apparatus where further posttranslational modifications occur before the packaging into secretory vesicles for final secretion. Unfolded or terminally misfolded proteins are cleared by the ER-associated degradation (ERAD) pathway, which retranslocates respective proteins into the cytoplasm for proteasomal degradation (Olzmann, Kopito, & Christianson, 2013; Ruggiano, Foresti, & Carvalho, 2014; Wu & Rapoport, 2018). However, an accumulation of unfolded or misfolded proteins in the lumen of the ER (due to an overloading of the processing capacity or the ERAD machinery) can impair ER functionality and will finally trigger the unfolded protein response (UPR; Hetz, 2012; Xu, Bailly-Maitre, & Reed, 2005).

Since DTE proteins will gain in importance during the next years current industrial Chinese hamster ovary (CHO) host cell lines need to be improved to ensure reliable manufacturing processes (Spiess et al., 2015; Walsh, 2018). Therefore, we investigated and characterized the intracellular fate of the DTE antibody mAb2 in CHO production cells in molecular detail.

2 | MATERIALS AND METHODS

2.1 | Fed-batch cultivation

Cells were seeded with a viable cell density (VCD) of $7 \cdot 10^5$ cells/ml in an initial volume of 60 ml Boehringer Ingelheim (BI, Biberach, Germany) proprietary production medium in a 250-ml shake flask (Corning, Oneonta, NY) and incubated at 34.5 °C in an orbital shaker incubator (Infors, Bottmingen, Switzerland) with 120 rpm (50 mm) and a CO_2 concentration of 10 % (v/v). The cultures were fed daily with 30 ml/L of culture start volume starting from Day 1 using BI proprietary feed medium. Since cultures were not fed on weekends, they received 60 ml/L of start volume feed on Fridays. Glucose levels were adjusted to 5 g/L via glucose bolus addition, if determined < 3 g/L. Relevant cellular and metabolic output parameters were determined daily: Cell concentration as well as viability was determined using the Cedex device (Roche Diagnostics, Mannheim, Germany) by means of trypan blue exclusion. A Biosen S-line analyser (EKF Diagnostics, Barleben, Germany) was used to determine glucose and lactate concentrations, pH and pO_2 were analyzed using a RAPIDLab®248 system (Siemens Healthcare, Erlangen, Germany). mAb concentration was determined by biolayer interferometry on an Octet® HTX system (Pall Life Science, Dreireich, Germany).

2.2 | Gene expression analysis

Total RNA was extracted from investigated CHO cells in triplicates using the RNA isolation Kit on the automated QIAsymphony® platform (Qiagen, Hilden, Germany). For library generation, 250 ng total RNA was processed with the TruSeq Stranded mRNA Library Prep Kit (Illumina, San Diego, CA) according to the manufacturer's instructions while using a total of 12 different unique indexes for multiplexing during analyses. Quality of isolated RNA and generated libraries was assessed using the High Sensitivity RNA analysis Kit (DNF-472, 15 nt) and Standard Sensitivity NGS Fragment Analysis Kit (DNF-473) on an Advanced Analytical Fragment Analyzer™ (Advanced Analytical Technologies, Heidelberg, Germany), respectively. The quantification of generated sequencing libraries was performed with the Quant-iT™ ProGreen® dsDNA Kit (Invitrogen) analyzed with a Tecan Infinite® 200 Pro Reader (Tecan Group, Männedorf, Switzerland). By using the unique multiplexing indexes, each of the 12 libraries was pooled for sequencing on a HiSeq4000 instrument (Illumina) in single-end mode and 85 cycles. After demultiplexing, acquired data were quality trimmed using trimmomatic (Bolger, Lohse, & Usadel, 2014) and mapped to the BI proprietary CHO K1 genome using STAR (Dobin et al., 2013). For quantification of mAb heavy chain (HC) and antibody light chain (LC) transcripts, data were mapped to the respective plasmids. Gene expression was quantified based on algorithms of the Cufflinks Suite (Trapnell et al., 2010) and standardized on fragments per kilobase million (FPKM) values. For statistical analysis of differentially expressed genes, the contrast model within the Profiler Genome software (Genedata, Basel, Switzerland) was used. Genes were considered to be significantly different when the Benjamini–Hochberg false discovery rate BHQ < 0.05 and a fold change (FC) > 1.2 and FC < 1/1.2, respectively. Functional annotation of significantly regulated genes was performed using David Bioinformatics Resources (Huang, Sherman, & Lempicki, 2009a; 2009b).

2.3 | Western blot (WB) analysis

For routine protein analyses, cells were lysed for 30 min on ice using Western blot lysis buffer (1 % Triton X-100 [v/v], 50 mM Tris (hydroxymethyl)-aminomethan (TRIS), 150 mM NaCl, pH = 7.5) and

vortexed approximately every 10 min. After centrifugation, lysates were separated within NuPAGE® 4–12 % or 10 % Bis-Tris Gels (Invitrogen, Carlsbad, CA) and transferred to a nitrocellulose membrane using the iBlot® 2 dry blotting system (Invitrogen). The antibodies used for HC (#ab98616; Abcam, Cambridge, UK) as well as LC (#K3502, Sigma Aldrich, St. Louis, MO) detection were diluted 1:20,000 and 1:5,000, respectively. Secondary IRDye® 800CW-labeled donkey anti-mouse (#925–32212), IRDye® 680RD-labeled donkey anti-goat (#925–68074) and IRDye® 800CW-labeled donkey anti-rabbit (#926–32213) antibodies were diluted 1:5,000 (LI-COR, Lincoln, NE). An antibody against β-actin (#4970; Cell Signaling Technologies, Cambridge, UK) was used as loading control in a dilution of 1:2,000. The anti-PDI antibody (#ab 3672; Abcam) was diluted 1:1,000. Membranes were afterward analyzed using the Odyssey Infrared Scanning System (LI-COR).

2.4 | Immunocytochemistry for confocal microscopic analysis

The procedure for immunocytochemistry was described elsewhere (Mathias et al., 2018).

2.5 | Transmission electron microscopy

CHO cells were fixed using prewarmed fixing solution (4 % paraformaldehyde [v/v], 2 % Glutaraldehyde [v/v, Sigma Aldrich], phosphate buffered saline [PBS]) for 30 min at 37 °C. Depleted fixing solution was replaced by ice-cold fixing solution and incubation continued for 1.5 hr on ice. The samples were washed three times with ice-cold PBS for 10 min each and stained with 1 % osmium tetroxide (v/v) for 1 hr on ice. Subsequently, specimens were dehydrated through a graded ethanol series (30 % [v/v], 50 % [v/v], 70 % [v/v], 90 % [v/v], 100 % [v/v]) and embedded into Glycid ether/Methylnadic/Dodecylsuccinic acid/Tris(dimethyl-aminomethyl)phenol epoxy resin (Serva, Heidelberg, Germany) overnight at 70 °C in an oven (Binder, Tuttlingen, Germany). On the next day, ultrathin sections were prepared with the ultramicrotome Ultracut UCT (Leica Microsystems, Wetzlar, Germany) and investigated on the transmission electron microscope LEO 912 AB (Zeiss, Oberkochen, Germany).

2.6 | Cell lysate separation using ultracentrifugation

Investigated CHO cells were lysed with UZ lysis buffer (1 % Triton X-100 [v/v], 20 mM 4-(2-hydroxyethyl)-1-piperazineethanesulfonic acid (HEPES), 150 mM KCl, pH = 7.8) for 30 min on ice and subsequently separated into soluble and insoluble fractions by centrifugation at 100,000 *g* and 4 °C for 1 hr using the ultracentrifuge Optima XE-90 (Beckmann Coulter, Bera, CA). The insoluble components were resuspended in the original sample volume with UZ lysis buffer and solubilized using sonication (Bandelin, Berlin, Germany). Equal volumes of insoluble and soluble fraction were used for WB analyses.

2.7 | Gel mobility shift assay

CHO cells were lysed with WB lysis buffer supplemented with either 20 mM PEG_{5000}-maleimide (Sigma Aldrich) or *N*-ethylmaleimide (Alfa Aesar) for 30 min on ice to modify free thiols. After centrifugation, an immunoprecipitation of the free mAb LC was performed using a mouse anti-human κ free LC antibody (MAB8461; Abnova, Taiwan), which was desthiobiotinylated with the DSB-X Biotin Protein Labeling Kit (D20655; Thermo Fisher Scientific) according to the manufacturer's instructions. In brief, after addition of the desthiobiotinylated mouse anti-human κ free LC antibody to the centrifuged cell lysates, the samples were incubated overnight at 4 °C on a rotary shaker. Afterward, equilibrated Pierce™ Streptavidin Plus Ultralink™ Resin (Thermo Fisher Scientific) was added and the samples were further incubated for 1 hr at 4 °C. The beads were washed several times with ice-cold WB lysis buffer and subsequently subjected to WB analyses.

2.8 | Coimmunoprecipitation experiments

For coimmunoprecipitation experiments, CHO cells were harvested and lysed with UZ lysis buffer. After centrifugation, a biotinylated anti-human IgG (HC+LC) antibody fragment (#709-066-149; Jackson ImmunoResearch) was added and samples subsequently incubated overnight at 4 °C on a rotary shaker. The immunocomplexes were purified as described earlier and washed several times with 50 mM ammonium bicarbonate pH = 8.5. Isolated proteins were directly digested on the beads using Trypsin (Roche, Penzberg, Germany). The resulting peptides were desalted using C18 stage tips (Supelco; Sigma Aldrich), separated using a 2 hr high-performance liquid chromatography (HPLC) gradient and identified by an Q-Exactive Plus mass spectrometer (Thermo Fisher Scientific). Obtained data were evaluated using Scaffold software version 4.8.6. (Proteome Software, Portland, OR).

2.9 | Glycan profile analysis

Purification of secreted mAbs was performed using a XK 16/20 column (GE Healthcare, Munich, Germany) run with MabSelect™ SuRe™ resin (GE Healthcare) on an ÄKTApurifier. Elution was performed with sodium citrate buffer pH = 2.8 and adjusted to pH = 6.0.

Intracellular antibody was purified using an anti-human IgG fragment crystallisable (Fc) antibody fragment, which was desthiobiotinylated with the DSB-X Biotin Protein Labeling Kit (D20655; Thermo Fisher Scientific) according to the manufacturer's instructions. Purification of the immunocomplexes was performed as described earlier. The beads were washed several times with ice-cold sodium citrate pH = 6.0 and purified antibody eluted with 50 mM biotin, 25 mM TRIS, pH = 10. The buffer was afterwards exchanged to sodium citrate pH = 6.0 using 10 kDa MWCO PES Vivaspin 500 filter units (GE Healthcare).

For *N*-linked glycosylation analysis, samples were diluted in 0.1 % formic acid, reduced with 5 mM Tris(2-carboxyethyl) phosphin (TCEP), and separated on a LaChrom Ultra HPLC system (VWR, Radnor, PA) using a reverse-Phase MAbPac RP column (Thermo Fisher Scientific). Proteins were eluted with 0.1 % formic acid and 0.1 % formic acid in acetonitrile. Mass spectrometric analysis was performed with a micrOTOF-Q II (Bruger Daltonik, Billerica, MA). Spectra were summed, deconvoluted, and smoothed using DataAnalysis (Bruker Daltonik).

3 | RESULTS

3.1 | Identification of an intracellular processing bottleneck in an immunoglobulin producing cell line during fed-batch cultivation

Although mAbs belong to a class of recombinant therapeutic proteins that can routinely be produced in the multigram per litre range, some molecules turn out to be DTE. A low productivity of stable cell lines represents a severe disadvantage of a biological drug candidate and can lead to termination of product development. To explore the intracellular fate of a DTE mAb, we assessed its location in a stable CHO production cell line.

The production capacity of a highly productive reference CHO cell line (mAb1) was compared with a DTE mAb2 producing CHO cell line. Both recombinant proteins were monoclonal IgG1 antibodies with κ LCs (Figures S1 and S2). However, in a 12-day fed-batch cultivation process, both investigated cell lines showed comparable growth behavior with a peak VCD of approximately 1.0×10^7 cells/ml and 1.4×10^7 cells/ml, respectively, as well as high viability (Figure 1a). The VCD and viability of both cell lines started to decline from Day 11 onward. Final mAb concentrations in the supernatant of 4.75 g/L ± 0.29 g/L and 0.86 g/L ± 0.06 g/L were determined for the mAb1 and mAb2 producing cell line on Day 12, respectively (Figure 1b). Consequently, the calculated cell-specific productivity (q_P) of the mAb2 producing cell line was > 80 % lower compared to the mAb1 producing cell line. To exclude that inefficient transcription and translation processes were the reason for inferior protein secretion in case of mAb2, classical biochemical analyses were performed. Even though the mAb2 producing cell line showed significantly reduced mRNA levels of both LC and HC in comparison to the mAb1 producing cell line (Figure 1c), WB analyses confirmed that the respective messenger RNAs (mRNAs) were sufficiently translated in both cell lines (Figure 1d). Interestingly, intracellular HC and LC protein concentrations were determined to be higher in the mAb2 producing CHO cell line. In addition, the *N*-glycosylation pattern of the secreted and subsequently Protein A purified mAbs revealed that mAb2 antibodies exhibited much less maturated glycans as indicated by a lower degree of galactosylation and increased amounts of high-mannose type glycans, which pointed toward an intracellular processing issue of mAb2 (Figure 1e,f). These data suggested that neither transcription nor translation processes sufficiently explained the particular low secretion of the DTE protein. However, increased intracellular levels of mAb2 protein and an impaired glycosylation pointed towards an intracellular processing bottleneck.

3.2 | Immunofluorescence based cellular analyses revealed impaired endoplasmic reticulum structures in the mAb2 producing CHO cell line

After translocation into the ER, secreted proteins are processed in different organelle structures, therefore we decided to analyze the distribution of the investigated mAbs within these distinct compartments to identify unproductive or saturated organelles in respect to recombinant protein processing. Fluorescence microscopy of the LC (Figure 2) and HC (Figure S3) of the recombinant proteins and concurrent visualization of the distinct secretory organelles, ER and Golgi apparatus was performed. Interestingly, the ER of the highly productive mAb1 producing CHO cell line was composed of very thin tubules, which were distributed throughout the entire cytoplasm (Figure 2). In contrast, the mAb2 producing CHO cell line displayed a heavily altered ER morphology showing very large and possibly inflated but separated spherical structures, which colocalized with the staining pattern of the mAb2 protein and thus putatively included antibody deposits. This aberrant morphology was found in five individually analyzed clonal cell lines stably producing mAb2 (Figure S4).

After folding and assembly in the lumen of the ER, secreted proteins are transported to the Golgi apparatus consisting of stacks of membrane-enclosed cisternae. Here, proteins are further modified and packed into secretory vesicles for final secretion. Notably, the mAb2 producing cell line showed no or only weak colocalization of the Golgi marker and mAb fluorescence staining, whereas a very strong signal for the produced recombinant mAb was observed in the Golgi apparatus of mAb1 producing cells (Figure 2 and Figure S5). In conclusion, immunofluorescence based microscopic analyses revealed putative antibody deposits in the lumen of the ER possibly pointing toward intracellular aggregation of mAb2.

3.3 | Intracellular aggregation of mAb2 and oxidative stress is not the causative for inefficient mAb2 secretion

Since immunofluorescence based microscopic analyses revealed putative antibody deposits and thus an aberrant ER morphology, we investigated the degree of intracellular protein aggregation of mAb2. In contrast to the control cell line, EM pictures confirmed a distinct ER morphology within the mAb2 producing cell line showing aberrant and possibly inflated or overloaded larger round-shaped structures (Figure 3a,b). However, no electron dense and thus aggregation indicative structures were identified inside the vesicular ER structures (Figure 3c). Furthermore, separation of cell lysates into soluble as well as insoluble

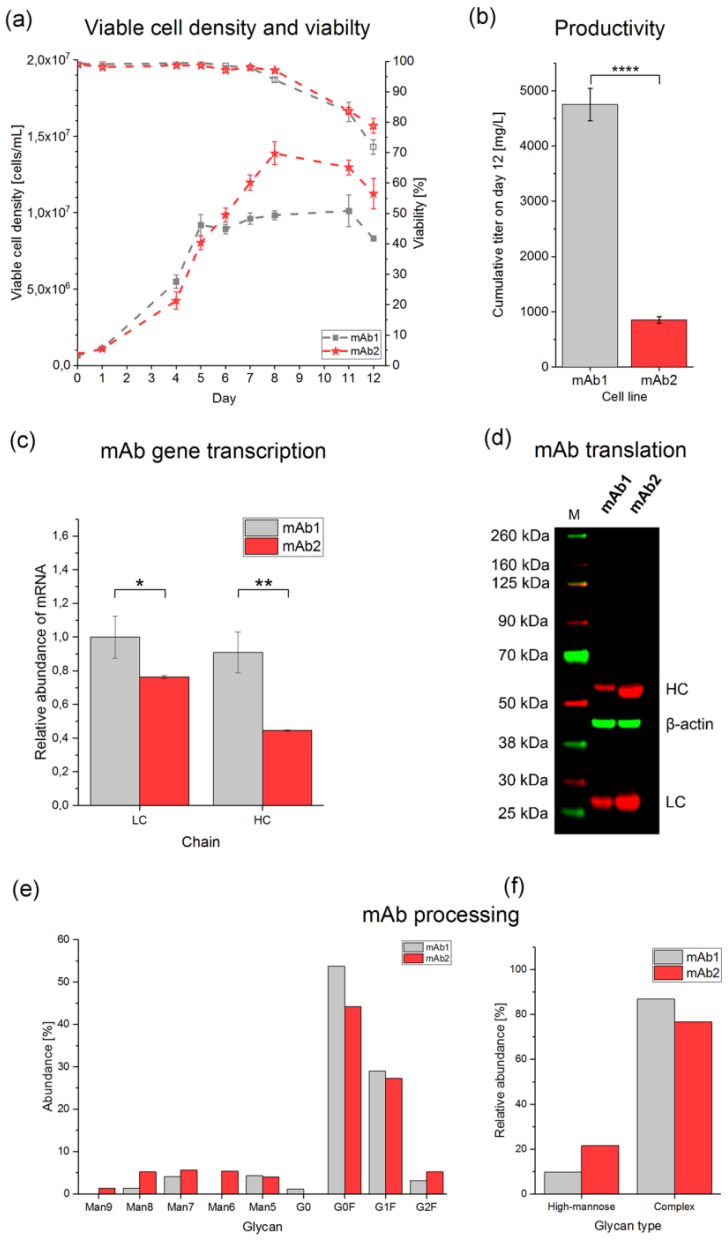

FIGURE 1 The fed-batch cultivation process of the monoclonal antibody 1 (mAb1) and mAb2 producing cell lines revealed an intracellular processing bottleneck in the mAb2 producing cell line. (a) Measured viable cell density (VCD) and viability of a 12-day fed-batch cultivation process. The data are shown as mean ± *SD* ($n = 3$). (b) Absolute mean cumulative antibody titer of the individual biological replicates measured on Day 12. The data are shown as mean ± *SD* ($n = 3$). An unpaired two-tailed *t*-test was used to determine statistical significance (****$p < .0001$). (c) Messenger RNA (mRNA) abundance of both chains of the respective recombinant proteins as determined by next generation sequencing. The data are displayed as mean ± *SD* of three individual cultivations ($n = 3$). (d) Intracellular amount of both chains of the recombinant proteins. Sample was taken from the fed-batch cultivation process on Day 4. One of three independent replicates was used for Western blot (WB) analysis under reducing and denaturing conditions. β-Actin was used as loading control. (e) Abundance of different glycan forms were analyzed using mass spectrometry (MS). (f) Glycan structures from Figure 1e were grouped according to high-mannose or complex glycan species. One sample of the three independent replicates was taken on Day 4, the antibody purified as described and subsequently subjected to MS under reducing conditions. M, marker; HC, heavy chain; LC, light chain [Color figure can be viewed at wileyonlinelibrary.com]

fractions using ultracentrifugation and WB analyses (Figure 3d) confirmed for both mAb producing cell lines that only marginal amounts of the HC could be found in the insoluble fraction of the cell lysate. In addition, it was shown that purified inflated vesicles can be dissolved completely using Triton X-100 (Figure S6) indicating that mAb2 did not form intracellular detergent resistant protein aggregates. Subsequent investigation of oxidative stress levels revealed no differences between both cell lines demonstrating that vesicularization of the ER is not a consequence of oxidative stress (Figure S7).

These data demonstrated that oxidative stress or intracellular protein aggregation of mAb2 within the lumen of the ER is not the reason for the reduced protein secretion.

3.4 | Incomplete folding of the LC hampers mAb2 from efficient intracellular transport and secretion

In the ER, proteins assigned for final secretion are cotranslationally folded and assembled into multifunctional complexes. A fully assembled antibody of subtype γ is composed of two identical LCs and two identical

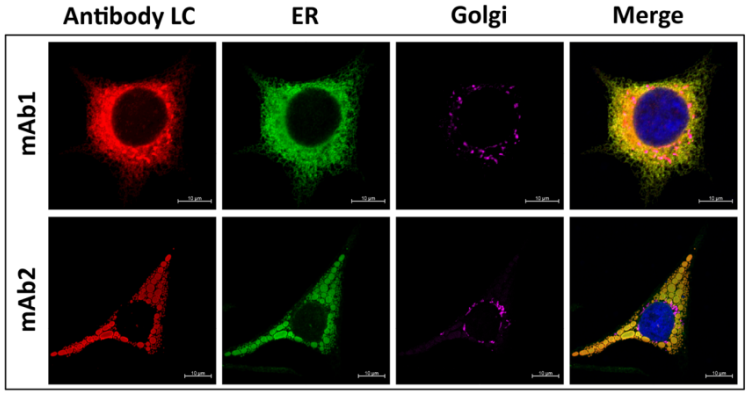

FIGURE 2 Immunofluorescence based cellular distribution analyses of the produced monoclonal antibodies showed impaired endoplasmic reticulum (ER) structures in the mAb2 producing cell line. Confocal images of the investigated cell line visualizing the distribution of the produced recombinant protein (LC) within the secretory organelles ER and Golgi apparatus. For superior visualization of the distinct organelles, cells have been cultured adherently for this analysis only. Investigated cell lines were fixed and the produced recombinant proteins, the ER as well as the Golgi apparatus were visualized with immunofluorescent antibodies and are shown in red, green, and magenta, respectively. Nuclei were counterstained with 4′,6-diamidino-2-phenylindole (DAPI; blue). Pictures were acquired at ×63 primary magnification. The scale bar represents 10 µm [Color figure can be viewed at wileyonlinelibrary.com]

HCs, which are interconnected via disulfide bridges. To access antibody assembly, production cell samples were subjected to nonreducing sodium dodecyl sulfate polyacrylamide gel electrophoresis (SDS-PAGE) and subsequent WB analysis. LC and HC displayed all possible antibody assembling entities, however, the total intracellular amount was increased for all entities in the mAb2 producing CHO cell line (Figure 4a), indicating that the DTE antibody mAb2 was as efficiently assembled as the highly secreted mAb1. However, in contrast to mAb1, free LC of the mAb2 antibody displayed two distinct bands with different intensities (Figure 4a). These two bands putatively indicated different folding states of the LC where individual intradomain disulfide bridges have not been formed due to incomplete or slow folding. As a consequence, the amount of completely folded and thus entirely oxidized cysteines was assessed using a gel mobility shift assay (Figure 4b). Free LC molecules were isolated from cell lysates, coupled to PEG_{5000}-maleimide (reacts specifically with cysteine residues) and subsequently subjected to SDS-PAGE and WB

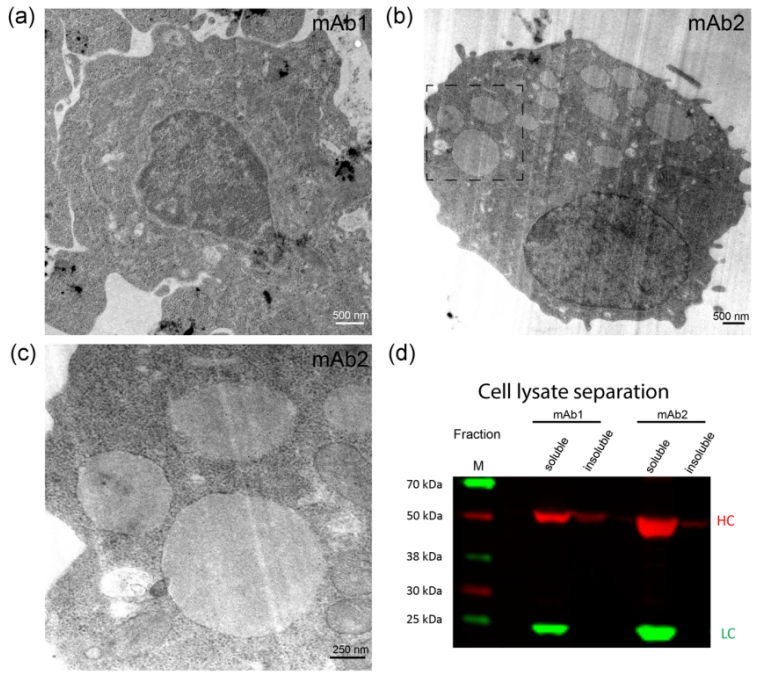

FIGURE 3 Examination of the intracellular aggregation of the investigated monoclonal antibodies within the respective production cell lines indicated no antibody deposits. (a) Transmission electron microscopic image of the mAb1 producing cell line using a magnification of × 4,000. (b) Transmission electron microscopic image of the mAb2 producing cell line using a magnification of × 3,150. The dotted square is enlarged in (c) using a magnification of × 10,000. (d) Recombinant protein heavy chain (HC) and light chain (LC) detection using Western blot (WB) analyses of cell lysate samples which were separated in soluble and insoluble fraction by ultracentrifugation. M, marker [Color figure can be viewed at wileyonlinelibrary.com]

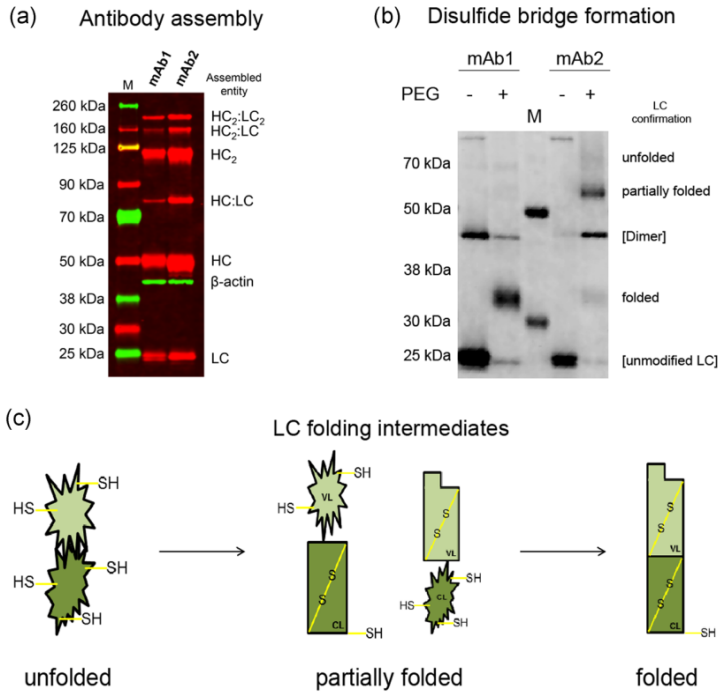

FIGURE 4 Intracellular antibody assembly and light chain (LC) folding indicated that incomplete folding of the LC hampered mAb2 from efficient secretion. (a) Western blot (WB) analyses of antibody assembling entities by detection of heavy chain (HC) and LC under nonreducing but denaturing conditions, respectively. β-actin was used as loading control. (b) Gel mobility shift assay detecting not formed intradomain disulfide bridged in the antibody LC. In brief, available cysteines of the free LC were coupled to PEG_{5000}-maleimide and the respective molecule subsequently purified and subjected to WB analyses. Representative result of three independent WBs. (c) Intermediate folding entities during intracellular LC folding. M, Marker; PEG, polyethylene glycol [Color figure can be viewed at wileyonlinelibrary.com]

detection of the LC. The three different potential folding intermediates are completely unfolded LC, partially folded, and entirely folded free LC molecules displaying five, three, and one free cysteine for efficient coupling, respectively (Figure 4c). Confirmatively, the highly secreted antibody mAb1 only showed marginal amounts of incompletely or partially folded free LC molecules, whereas the free LC of the DTE mAb2 was mainly partially folded or misfolded indicated by one disulfide bridge which has not been formed.

3.5 | The LC of the DTE antibody mAb2 is less recognized by cellular disulfide bridge forming chaperones of the protein disulfide isomerase family

In eukaryotes, protein resident cysteines are oxidized by chaperons of the PDI family in the lumen of the ER. Therefore, coimmunoprecipitation experiments of both antibodies with subsequent mass spectrometry (MS) analyses were used to identify differentially bound proteins and chaperones (Figure 5a).

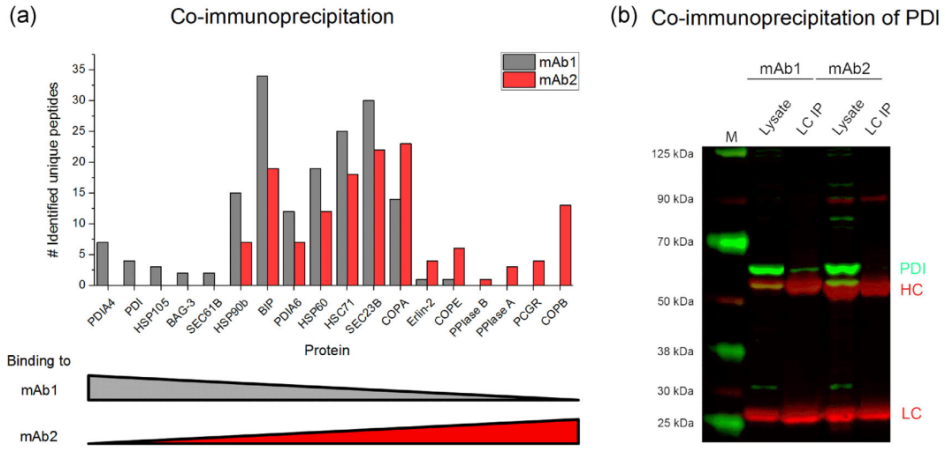

FIGURE 5 Differential binding of chaperones revealed less recognition of mAb2 light chain (LC) by disulfide bridge forming proteins of the protein disulfide isomerase (PDI) family. (a) Mass spectrometric identification of coimmunoprecipitated proteins bound to the investigated antibodies mAb1 and mAb2, respectively. (b) Validation of less recognition of mAb2 by PDIA1 by Western blot (WB) analyses. A full list of the abbreviations of identified proteins is available in Table S1. HC, heavy chain; IP, immunoprecipitation [Color figure can be viewed at wileyonlinelibrary.com]

Interestingly, PDIs (PDIA4, PDI[A1], PDIA6) were found to bind more heavily or exclusively to mAb1 molecules indicating a possible inaccessibility of mAb2 for oxidation of its cysteines to form intradomain disulfide bridges. To validate these results, WB analyses of coimmunoprecipitation experiments were carried out and showed comparable binding of the molecular chaperone BIP (Figure S8) but less binding of PDI to the mAb2 LC indicating that it is not recognized correctly by PDIs putatively due to improper folding (Figure 5b). In addition, other protein classes were found to bind differentially to mAb1 and mAb2 molecules including members of the heat shock protein family (e.g. HSP90β1, HSPA8) binding more intensively to mAb1 but prolyl-peptidyl isomerases (PPIA, PPIB) binding exclusively to mAb2. In summary, incomplete formation of disulfide bridges may lead to incomplete folding hampering mAb2 from efficient secretion.

3.6 | mAb2 is partially degraded via the ERAD pathway

Since the DTE antibody mAb2 accumulated in the lumen of the ER probably due to incomplete folding of the LC, it was of interest to examine the adaptation process of the cell line. Using transcriptome analysis of both mAb2 and mAb1 cell lines and subsequent functional clustering of differentially transcribed genes, protein processing mechanisms in the ER were shown to be significantly affected by mAb2 production (Figure 6a). While regular protein processing pathways were downregulated in the mAb2 producing CHO cell line, proteins belonging to the ERAD pathway were predominantly enriched indicating enhanced protein degradation (Figure 6b). Especially chaperones recruiting misfolded proteins for degradation via ERAD and effector proteins of the respective ubiquitin ligase complex (Figure 6c) were transcriptionally upregulated. Finally, subunits of the proteasome for final protein degradation were also upregulated indicating that the incomplete folding and accumulation of mAb2 in the lumen of the ER possibly led to an enhanced clearance of the secretory organelle from adverse protein chains. Interestingly, the UPR was not explicitly triggered (Figure S9). To further investigate the intracellular fate of the antibody and access possible degradation of mAb2 via ERAD, the intracellular glycosylation of purified mAb2 was investigated (Figure 7a). Glycosylation was found to be mainly of the premature high-mannose type (Figure 7b, Man9-Man6) usually found in the early secretory pathway (Aebi, Bernasconi, Clerc, & Molinari, 2010; Hebert, Garman, & Molinari, 2005; Helenius & Aebi, 2004). In addition, intracellular trimmed glycan branches like Man7, Man6, and Man5 indicated degradation of the respective chains via ERAD (Aebi et al., 2010; Ferris, Kodali, & Kaufman, 2014; Hebert et al., 2005). Grouping of the individual glycan forms clearly highlighted that nearly half of the molecules of mAb2 are marked for proteasomal degradation via ERAD (Figure 7c).

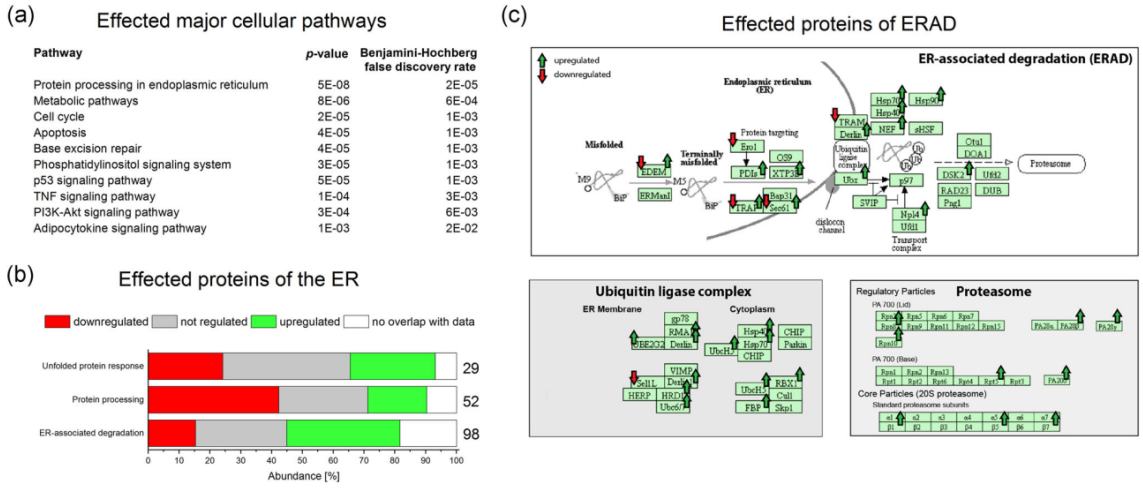

FIGURE 6 Gene expression analyses putatively indicated degradation of mAb2 via ER-associated degradation (ERAD). (a) Canonical pathways which are affected by the production of the difficult-to-express antibody mAb2 in comparison to mAb1. (b) Transcriptionally upregulated and downregulated proteins in respect to mAb2 production belonging to major biochemical pathways within the ER: unfolded protein response (UPR), general protein processing, and ERAD. (c) Detailed pathway map of the ERAD process and components of the respective ubiquitin ligase complex and proteasome where upregulated and downregulated genes are indicated by green and red arrows, respectively. The indication of an upregulation and downregulation of a respective protein means that the function is conducted by different proteins of which some were upregulated and downregulated during the analysis, respectively. A gene was considered to be regulated with a Benjamini–Hochberg false discovery rate BHQ < 0.05 and a fold change (FC) > 1.2 and FC < 1/1.2, respectively. The figure was modified from Kyoto Encyclopedia of Genes and Genomes (KEGG) Database with permission (Kanehisa & Goto, 2000; Kanehisa, Sato, Furumichi, Morishima, & Tanabe, 2017; 2019). A full list of proteins and FC is available in Table S2. Same analyses were performed for four additional mAb2 producing cell lines (Figures S10–S13). ER, endoplasmic reticulum; mAb, monoclonal antibody

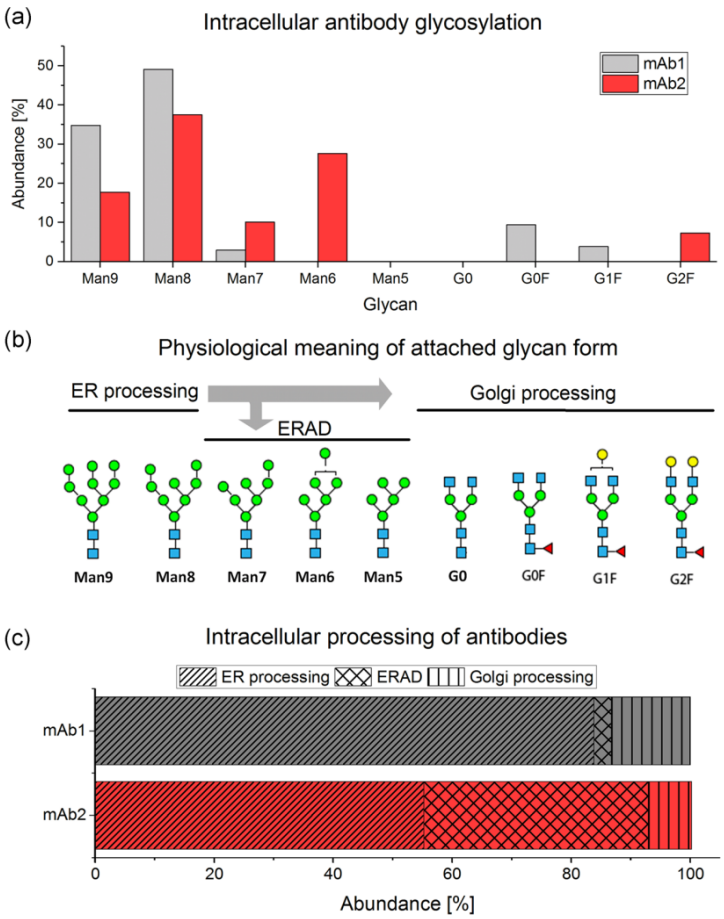

FIGURE 7 Glycan profile analysis of the intracellular accumulated antibody mAb2 validated massive degradation via ER-associated degradation (ERAD). (a) Abundance of different glycan forms were analyzed using mass spectrometry (MS). The antibody was purified as described and subsequently subjected to MS under reducing conditions. (b) Overview of different glycan forms and physiological meaning. (c) Summary of identified glycan forms and their physiological significance [Color figure can be viewed at wileyonlinelibrary.com]

4 | DISCUSSION

Since mammalian expression systems can show low performance in the production of the sustainably emerging complex protein formats and DTE antibodies, there is an urgent need to identify any rate limiting processing step. Even though the DTE protein mAb2 producing cell line showed significantly reduced mRNA levels in comparison to the mAb1 producing cell line, it is highly likely that the detected amount of transcripts enables high protein production. While there is a significant correlation between the protein abundance and mRNA levels, it was also shown that only part of the regulation of a protein's abundance can be explained by varying transcript levels, which is further complemented by mechanisms as degradation and translation rates (de Sousa Abreua, Penalvaa, Marcotte, & Vogel, 2009; Vogel & Marcotte, 2012). Therefore the reduced mRNA levels did not sufficiently explain the particular low production of mAb2 in CHO cells. However, immunofluorescence based microscopic analyses of the production cell lines revealed an aberrant ER morphology, in which the normally observed interconnected network of sacs and tubules collapsed to become large and distinct round-shaped structures (Schwarz & Blower, 2016). In other reports such an aberrant ER morphology has also been referred to as Russell Bodies (RBs), where IgGs aggregate in the lumen of the ER or derived vesicles thereof and can neither be degraded nor secreted (Kopito & Sitia, 2000). Similar structures can be found in plasma cells undergoing excessive synthesis of IgGs, especially as a manifestation of physiological abnormalities like multiple myeloma, inflammatory diseases, and autoimmune disorders (Decourt, Galea, Sirac, & Cogné, 2004; Jiang et al., 1997). Nevertheless, RBs have also been identified in recombinant IgG producing cell lines such as CHO and HEK293 (Hasegawa et al., 2017; Hasegawa, Woods, Kinderman, He, & Lim, 2014; Stoops, Byrd, & Hasegawa, 2012) as well as during over-expression of bispecific antibody formats in CHO cells (Mathias et al., 2018). Interestingly, this vesicularized phenotypic appearance of the ER has also been described independently in the context of several different and very diverse conditions including oxidative stress (Hendershot et al., 1995; Wei et al., 2012), downregulation of chaperones (Lee, Chu, Iwakoshi, & Glimcher, 2005; Li et al., 2008), and parts of the ERAD machinery (Sun et al., 2014). In contrast to these reports, we observed no evidence for oxidative stress (Figure S7) or downregulation of chaperones while analyzing CHO cells expressing the DTE antibody mAb2. In addition, it was clarified that

mAb2 did not form intracellular aggregates. The described aberrant ER morphology was detected in all investigated mAb2 producing cell lines (total number of five) even under different culture conditions as well as time points in cultivation and therefore did neither represent a clone-specific phenomenon nor was it exclusively induced by exogenous stress conditions (Figure S4).

However, when analyzing folding of the antibody, it became apparent that the disulfide bridge within the free mAb2 LC was not formed. As both antibodies share the same LC κ constant sequence (Figure S1), we speculated that it might be the variable domain of the mAb2 LC that hampers mAb2 from efficient transport and secretion. It may rapidly adopt an atypical folding state during translation and therefore is not readily recognized by ER resident chaperones catalyzing the formation of the respective disulfide bridge. Indeed, we showed that the incompletely folded mAb2 LC was less bound by the chaperone PDI, which may lead to a deficient catalysis of disulfide bridges. By expressing several noncognate antibody HC/LC pairs, Stoops et al. (2012) showed that a LC's manufacturability was sufficient to promote RB formation, which finally resulted in low secretion of the respective antibody. But contrary to this, an LC's manufacturability alone was not sufficient to ensure high secretion levels. The generation of noncognate mAb1 LC/mAb2 HC pairs and vice versa might further elucidate the detrimental properties of mAb2 LC.

Despite the heavily disrupted ER morphology, which was identified by microscopy, mAb2 production cells grew well and stayed viable under fed-batch cultivation pointing toward an at least partially functional ER. In addition, mAb2 producing CHO cells were still able to secrete approximately 10 pg/(cell·day) representing appreciable amounts of recombinant protein. Therefore, secretion might either be facilitated by not detectable but remaining amounts of functional ER or by secretion of residual mAb2 from affected RB-shaped ER structures. However, within these structures, we were able to show that also fully assembled entities of mAb2 were retained (Figure 4), which might be caused by the accidental assembly of some HCs with only partially folded LCs. It remains unknown whether those antibodies with partially folded LC and free LC can also be secreted into the production medium since proteins assigned for secretion displaying free cysteines are actively retained (Alberini, Bet, Milstein, & Sitia, 1990). However, it was shown that antibodies can escape cellular protein quality control mechanisms as some HCs possess constant HC domain 1 (CH1), which are inherently folded and thus secretion might occur without LC assembly (Stoyle et al., 2017).

As overproduction of mAb2 caused a massive aberrant ER phenotype, we analyzed effects on cellular pathways by transcriptome analysis to elucidate possible escape routes or survival mechanisms. The observed cellular reaction included a general downregulation of genes involved in processes such as protein synthesis and translocation as well as an upregulation of genes involved in protein degradation processes as ERAD (Figure 6). Again, it did not represent a clonal phenomenon as the ERAD pathway was upregulated in four additional and independently analyzed mAb2 producing cell lines (Figure S10–S13). Since misfolded proteins are tagged for ERAD by clipping of mannose residues (Ferris et al., 2014; Slominska-Wojewodzka & Sandvig, 2015), we subsequently determined the glycan profile of purified intracellular mAb2 and found increased number of glycan species which tag the protein for proteasomal degradation (Figure 7). Since intracellular mAb2 was purified using an Fc directed antibody, only fully assembled mAb2 and free HC were analyzed suggesting that also fully assembled antibody might be designated for degradation, possibly due to assembly with only partially folded LC. These amounts of proteins assigned for degradation via ERAD possibly overloaded the respective machinery and the resulting massive accumulation of proteins may in consequence represent the reason for the observed aberrant ER morphology in mAb2 producing CHO cells.

The UPR is a cellular stress response mechanism to an accumulation of unfolded proteins within the lumen of the ER (Hetz, 2012). It is enabled by the stress sensors activating transcription factor 6 (ATF6), protein kinase RNA-like ER kinase (PERK), and inositol-requiring protein 1α (IRE1α) by releasing BIP (Hetz, 2012; Hussain, Maldonado-Agurto, & Dickson, 2014; Ma & Hendershot, 2002). BIP is one of the central chaperones recognizing and interacting with exposed hydrophobic sequences of newly synthesized proteins actively maintaining its clients in a folding competent state (Behnke, Mann, Scruggs, Feige, & Hendershot, 2016; Pobre, Poet, & Hendershot, 2019). Interestingly, the UPR was not explicitly triggered in mAb2 producing CHO cells since ATF6, PERK, IRE1α downstream target genes were not upregulated (Figure S9), even though we clearly showed that mAb2 accumulated within the lumen of the ER and ER morphology was heavily disrupted. In addition, even if BIP was not upregulated in its expression, still no expected stronger interaction between BIP and the incompletely folded mAb2 LC in comparison to mAb1 was detected (Figure S8) and thus UPR not triggered. However, Hellman, Vanhove, Lejeune, Stevens, and Hendershot (1999) showed that the association with the chaperone BIP is not simply determined by the presence of sequences but also the folding state and protein stability. This again indicated that the mAb2 LC may adapt some kind of folded or stable state, which might impede terminal folding through PDIs. Subsequent investigations will show whether overexpression of PDI can rescue the respective phenotype.

It was demonstrated that mAb2 may be hampered from efficient secretion due to an only partially folded LC, which did not form all necessary intradomain disulfide bridges. Thus, this study revealed that with the continuous emergence of artificially designed and DTE therapeutic protein candidates more attention needs to be drawn to molecule design as well as detailed sequence investigations. Especially, LC sequences are of importance as the LC significantly contributes to the folding rate of the respective HC and thus the overall assembly and secretion of mAbs (Feige et al., 2009; Lee, Brewer, Hellman, & Hendershot, 1999).

ACKNOWLEDGMENTS

The authors are especially grateful to Tobias Kiechle, Jennifer Schütt and Corinna Keller for excellent technical assistance on confocal

microscopy. Further, they also thank Karin Rechtsteiner for supporting cell culture experiments, Melanie Luz and Jens Pösl for recombinant protein concentration measurements, and Dagmar Rädel, Anja Krämer and Martin Dass for electron microscopy. The research was further supported by Harald Bradl, Jürgen Fieder, Annika Held, and Kerstin Aßfalg.

CONFLICT OF INTERESTS

The authors declare that there are no conflict of interests. S. Mathias, A. Wippermann, I. Gorr, P. Schulz, S. Fischer, and M. Gamer are employees of Boehringer Ingelheim, which sells pharmaceuticals.

ORCID

Sven Mathias http://orcid.org/0000-0002-2842-8549
Nikolas Zeh http://orcid.org/0000-0003-4889-7761
Ingo Gorr http://orcid.org/0000-0003-0046-6452
Simon Fischer http://orcid.org/0000-0002-5188-7620

REFERENCES

Aebi, M., Bernasconi, R., Clerc, S., & Molinari, M. (2010). N-glycan structures: Recognition and processing in the ER. *Trends in Biochemical Sciences*, *35*(2), 74–82. https://doi.org/10.1016/j.tibs.2009.10.001

Alberini, C. M., Bet, P., Milstein, C., & Sitia, R. (1990). Secretion of immunoglobulin M assembly intermediates in the presence of reducing agents. *Nature*, *374*(18), 485–487. https://doi.org/10.1016/0021-9797(80)90501-9

Alberts, B., Johnson, A., Lewis, J., Raff, M., Roberts, K., & Walter, P. (2002). *The Molecular Biology of the Cell*. NY: Garland Pub.

Appenzeller-Herzog, C. (2011). Glutathione- and non-glutathione-based oxidant control in the endoplasmic reticulum. *Journal of Cell Science*, *124*(6), 847–855. https://doi.org/10.1242/jcs.080895

Behnke, J., Mann, M. J., Scruggs, F., Feige, M. J., & Hendershot, M. (2016). Members of the Hsp70 family recognize distinct types of sequences to execute ER quality control. *Molecular Cell*, *63*(5), 739–752. https://doi.org/10.1016/j.molcel.2016.07.012.Members

Bolger, A. M., Lohse, M., & Usadel, B. (2014). Trimmomatic: A flexible trimmer for Illumina sequence data. *Bioinformatics*, *30*(15), 2114–2120. https://doi.org/10.1093/bioinformatics/btu170

Braakman, I., & Hebert, D. (2013). Protein folding in the endoplasmic reticulum. *Cold Spring Harbor Prespectives in Biology*, *5*(5), a013201. https://doi.org/10.1016/B978-0-08-088504-9.00029-5

Decourt, C., Galea, H. R., Sirac, C., & Cogné, M. (2004). Immunologic basis for the rare occurrence of true nonsecretory plasma cell dyscrasias. *Journal of Leukocyte Biology*, *76*(3), 528–536. https://doi.org/10.1189/jlb.0803382

Dobin, A., Davis, C. A., Schlesinger, F., Drenkow, J., Zaleski, C., Jha, S., … Gingeras, T. R. (2013). STAR: Ultrafast universal RNA-seq aligner. *Bioinformatics*, *29*(1), 15–21. https://doi.org/10.1093/bioinformatics/bts635

Ellgaard, L., & Helenius, A. (2003). Quality control in the endoplasmic reticulum. *Nature Reviews Molecular Cell Biology*, *4*(3), 181–191. https://doi.org/10.1038/nrm1052

Feige, M. J., Groscurth, S., Marcinowski, M., Shimizu, Y., Kessler, H., Hendershot, L. M., & Buchner, J. (2009). An unfolded CH1 domain controls the assembly and secretion of IgG antibodies. *Molecular Cell*, *34*(5), 569–579. https://doi.org/10.1016/j.freeradbiomed.2008.10.025

Ferris, S. P., Kodali, V. K., & Kaufman, R. J. (2014). Glycoprotein folding and quality-control mechanisms in protein-folding diseases. *Disease Models & Mechanisms*, *7*(3), 331–341. https://doi.org/10.1242/dmm.014589

Hasegawa, H., Hsu, A., Tinberg, C. E., Siegler, K. E., Aaron, A., & Tsai, M. (2017). Single amino acid substitution in LC-CDR1 induces Russell body phenotype that attenuates cellular protein synthesis through eIF2 α phosphorylation and thereby downregulates IgG secretion despite operational secretory pathway traffic. *mAbs*, *9*(5), 854–873. https://doi.org/10.1080/19420862.2017.1314875

Hasegawa, H., Woods, C. E., Kinderman, F., He, F., & Lim, A. C. (2014). Russell body phenotype is preferentially induced by IgG mAb clones with high intrinsic condensation propensity: Relations between the biosynthetic events in the ER and solution behaviors in vitro. *mAbs*, *6*(6), 1518–1532. https://doi.org/10.4161/mabs.36242

Hebert, D. N., Garman, S. C., & Molinari, M. (2005). The glycan code of the endoplasmic reticulum: Asparagine-linked carbohydrates as protein maturation and quality-control tags. *Trends in Cell Biology*, *15*(7), 364–370. https://doi.org/10.1016/j.tcb.2005.05.007

Helenius, A., & Aebi, M. (2004). Roles of N-Linked glycans in the endoplasmic reticulum. *Annual Review of Biochemistry*, *73*(1), 1019–1049. https://doi.org/10.1146/annurev.biochem.73.011303.073752

Hellman, R., Vanhove, M., Lejeune, A., Stevens, F. J., & Hendershot, L. M. (1999). The in vivo association of BiP with newly synthesized proteins is dependent on the rate and stability of folding and not simply on the presence of sequences that can bind to BiP. *The Journal of Cell Biology*, *144*(1), 21–30. http://jcb.rupress.org/content/144/1/21.full.pdf+html

Hendershot, L. M., Wei, J. Y., Gaut, J. R., Lawson, B., Freiden, P. J., & Murti, K. G. (1995). In vivo expression of mammalian BiP ATPase mutants causes disruption of the endoplasmic reticulum. *Molecular Biology of the Cell*, *6*(3), 283–296. https://doi.org/10.1091/mbc.6.3.283

Hetz, C. (2012). The unfolded protein response: Controlling cell fate decisions under ER stress and beyond. *Nature Reviews Molecular Cell Biology*, *13*(2), 89–102. https://doi.org/10.1038/nrm3270

Huang, D. W., Sherman, B. T., & Lempicki, R. A. (2009a). Bioinformatics enrichment tools: Paths toward the comprehensive functional analysis of large gene lists. *Nucleic Acids Research*, *37*(1), 1–13. https://doi.org/10.1093/nar/gkn923

Huang, D. W., Sherman, B. T., & Lempicki, R. A. (2009b). Systematic and integrative analysis of large gene lists using DAVID bioinformatics resources. *Nature Protocols*, *4*(1), 44–57. https://doi.org/10.1038/nprot.2008.211

Hussain, H., Maldonado-Agurto, R., & Dickson, A. J. (2014). The endoplasmic reticulum and unfolded protein response in the control of mammalian recombinant protein production. *Biotechnology Letters*, *36*(8), 1581–1593. https://doi.org/10.1007/s10529-014-1537-y

Jiang, Y., Hirose, S., Hamano, Y., Kodera, S., Tsurui, H., Abe, M., … Shirai, T. (1997). Mapping of a gene for the increased susceptibility of B1 cells to Mott cell formation in murine autoimmune disease. *Journal of Immunology*, *158*(2), 992–997. http://www.ncbi.nlm.nih.gov/pubmed/8993021

Johari, Y. B., Estes, S. D., Alves, C. S., Sinacore, M. S., & James, D. C. (2015). Integrated cell and process engineering for improved transient production of a "difficult-to-express" fusion protein by CHO cells. *Biotechnology and Bioengineering*, *112*(12), 2527–2542. https://doi.org/10.1002/bit.25687

Jost, C., & Plückthun, A. (2014). Engineered proteins with desired specificity: DARPins, other alternative scaffolds and bispecific IgGs. *Current Opinion in Structural Biology*, *27*(1), 102–112. https://doi.org/10.1016/j.sbi.2014.05.011

Kanehisa, M., Furumichi, M., Tanabe, M., Sato, Y., & Morishima, K. (2017). KEGG: New perspectives on genomes, pathways, diseases and drugs. *Nucleic Acids Research*, *45*(D1), D353–D361. https://doi.org/10.1093/nar/gkw1092

Kanehisa, M., & Goto, S. (2000). KEGG: Kyoto Encyclopedia of Genes and Genomes. *Nucleic Acid Research*, *28*(1), 27–30.

Kanehisa, M., Sato, Y., Furumichi, M., Morishima, K., & Tanabe, M. (2019). New approach for understanding genome variations in KEGG. *Nucleic Acids Research*, *47*(D1), D590–D595. https://doi.org/10.1093/nar/gky962

Kopito, R. R., & Sitia, R. (2000). Aggresomes and Russell bodies. *EMBO Reports*, *1*(3), 225–231. https://doi.org/10.1093/embo-reports/kvd052

Kunert, R., & Reinhart, D. (2016). Advances in recombinant antibody manufacturing. *Applied Microbiology and Biotechnology*, *100*(8), 3451–3461. https://doi.org/10.1007/s00253-016-7388-9

Lee, A. H., Chu, G. C., Iwakoshi, N. N., & Glimcher, L. H. (2005). XBP-1 is required for biogenesis of cellular secretory machinery of exocrine glands. *EMBO Journal*, *24*(24), 4368–4380. https://doi.org/10.1038/sj.emboj.7600903

Lee, G. W., Fecko, J. K., Yen, A., Donaldson, D., Wood, C., Tobler, S., … Leonard, M. (2007). Improving the expression of a soluble receptor:Fc fusion protein in CHO cells by coexpression with the receptor ligand. *Cell Technology for Cell Products*, 29–39. https://doi.org/10.1007/978-1-4020-5476-1_4

Lee, Y. K., Brewer, J. W., Hellman, R., & Hendershot, L. M. (1999). BiP and immunoglobulin light chain cooperate to control the folding of heavy chain and ensure the fidelity of immunoglobulin assembly. *Molecular Biology of the Cell*, *10*(7), 2209–2219. https://doi.org/10.1091/mbc.10.7.2209

Li, J., Ni, M., Lee, B., Barron, E., Hinto, D. R., & Lee, A. S. (2008). The unfolded protein response regulator GRP78/BiP is required for endoplasmic reticulum integrity and stress-induced autophagy in mammalian cells. *Cell Death & Differentiation*, *15*(9), 1460–1471. https://doi.org/10.1016/j.cgh.2008.07.016.Cytokeratin

Lodish, H., Berk, A., Zipursky, S. L., Matsudaira, P., Baltimore, D., & Darnell, J. (2000). *Molecular Cell Biology* (4th.). New York: W.H. Freeman. https://doi.org/10.1002/bmb.8

Ma, Y., & Hendershot, L. M. (2002). The mammalian endoplasmic reticulum as a sensor for cellular stress. *Cell Stress & Chaperones*, *7*(2), 222–229.

Mathias, S., Fischer, S., Handrick, R., Fieder, J., Schulz, P., Bradl, H., … Otte, K. (2018). Visualisation of intracellular production bottlenecks in suspension-adapted CHO cells producing complex biopharmaceuticals using fluorescence microscopy. *Journal of Biotechnology*, *271*(Feb-February), 47–55. https://doi.org/10.1016/j.jbiotec.2018.02.009

Olzmann, J. A., Kopito, R. R., & Christianson, J. C. (2013). The mammalian endoplasmic reticulum-associated degradation system. *Cold Spring Harbor Perspectives in Biology*, *5*(9), 1–16. https://doi.org/10.1101/cshperspect.a013185

Pobre, K. F. R., Poet, G. J., & Hendershot, L. M. (2019). The endoplasmic reticulum (ER) chaperone BiP is a master regulator of ER functions: Getting by with a little help from ERdj friends. *Journal of Biological Chemistry*, *294*(6), 2098–2108. https://doi.org/10.1074/jbc.REV118.002804

Pybus, L. P., James, D. C., Dean, G., Slidel, T., Hardman, C., Smith, A., … Field, R. (2014). Predicting the expression of recombinant monoclonal antibodies in Chinese hamster ovary cells based on sequence features of the CDR3 domain. *Biotechnology Progress*, *30*(1), 188–197. https://doi.org/10.1002/btpr.1839

Ruggiano, A., Foresti, O., & Carvalho, P. (2014). ER-associated degradation: Protein quality control and beyond. *Journal of Cell Biology*, *204*(6), 869–879. https://doi.org/10.1083/jcb.201312042

Schwarz, D. S., & Blower, M. D. (2016). The endoplasmic reticulum: Structure, function and response to cellular signaling. *Cellular and Molecular Life Sciences*, *73*(1), 79–94. https://doi.org/10.1007/s00018-015-2052-6

Slominska-Wojewodzka, M., & Sandvig, K. (2015). The role of lectin-carbohydrate interactions in the regulation of ER-associated protein degradation. *Molecules*, *20*(6), 9816–9846. https://doi.org/10.3390/molecules20069816

de Sousa Abreua, R., Penalvaa, L. O., Marcotte, E. M., & Vogel, C. (2009). Global signatures of protein and mRNA expression levels. *Molecular BioSystems*, *5*(12), 1512–1526. https://doi.org/10.1039/b908315d.Global

Spiess, C., Zhai, Q., & Carter, P. J. (2015). Alternative molecular formats and therapeutic applications for bispecific antibodies. *Molecular Immunology*, *67*(2), 95–106. https://doi.org/10.1016/j.molimm.2015.01.003

Stoops, J., Byrd, S., & Hasegawa, H. (2012). Russell body inducing threshold depends on the variable domain sequences of individual human IgG clones and the cellular protein homeostasis. *Biochimica et Biophysica Acta*, *1823*(10), 1643–1657. https://doi.org/10.1016/j.bbamcr.2012.06.015

Stoyle, C. L., Stephens, P. E., Humphreys, D. P., Heywood, S., Cain, K., & Bulleid, N. J. (2017). IgG light chain-independent secretion of heavy chain dimers: Consequence for therapeutic antibody production and design. *Biochemical Journal*, *474*(18), 3179–3188. https://doi.org/10.1042/BCJ20170342

Sun, S., Shi, G., Han, X., Francisco, A. B., Ji, Y., Mendonça, N., … Qi, L. (2014). Sel1L is indispensable for mammalian endoplasmic reticulum-associated degradation, endoplasmic reticulum homeostasis, and survival. *Proceedings of the National Academy of Sciences*, *111*(5), E582–E591. https://doi.org/10.1073/pnas.1318114111

Trapnell, C., Williams, B. a, Pertea, G., Mortazavi, A., Kwan, G., van Baren, M. J., … Pachter, L. (2010). Transcript assembly and abundance estimation from RNA-Seq reveals thousands of new transcripts and switching among isoforms. *Nature Biotechnology*, *28*(5), 511–515. https://doi.org/10.1038/nbt.1621.Transcript

Vogel, C., & Marcotte, E. M. (2012). Insights into the regulation of protein abundance from proteomics and transcriptomis analyses. *Nature Reviews Genetics*, *13*(4), 227–232. https://doi.org/10.1038/nrg3185.Insights

Walsh, G. (2018). Biopharmaceutical benchmarks 18. *Nature Biotechnology*, *36*(12), 1136–1145. https://doi.org/10.1038/nbt0706-769

Wei, P. C., Hsieh, Y. H., Su, M. I., Jiang, X. J., Hsu, P. H., Lo, W. T., … Lee, W. H. (2012). Loss of the oxidative stress sensor NPGPx compromises GRP78 chaperone activity and induces systemic disease. *Molecular Cell*, *48*(5), 747–759.

Wu, X., & Rapoport, T. A. (2018). Mechanistic insights into ER-associated protein degradation. *Current Opinion in Cell Biology*, *53*, 22–28. https://doi.org/10.1016/j.ceb.2018.04.004

Xu, C., Bailly-Maitre, B., & Reed, J. C. (2005). Endoplasmic reticulum stress: Cell life and death decisions. *Journal of Clinical Investigation*, *115*(10), 2656–2664. https://doi.org/10.1172/JCI26373.2656

SUPPORTING INFORMATION

Additional supporting information may be found online in the Supporting Information section.

How to cite this article: Mathias S, Wippermann A, Raab N, et al. Unraveling what makes a monoclonal antibody difficult-to-express: From intracellular accumulation to incomplete folding and degradation via ERAD. *Biotechnology and Bioengineering*. 2019;1–12. https://doi.org/10.1002/bit.27196

Mathias et al. 2019, Biotechnology and Bioengineering Supplementary Material

Biotechnol Bioeng. 2020 Jan;117(1):5-16

doi: 10.1002/bit.27196

Epub 2019 Nov 15

Licensed under Creative Commons Attribution - NonCommercial 4.0 International, https://creativecommons.org/licenses/by-nc/4.0/

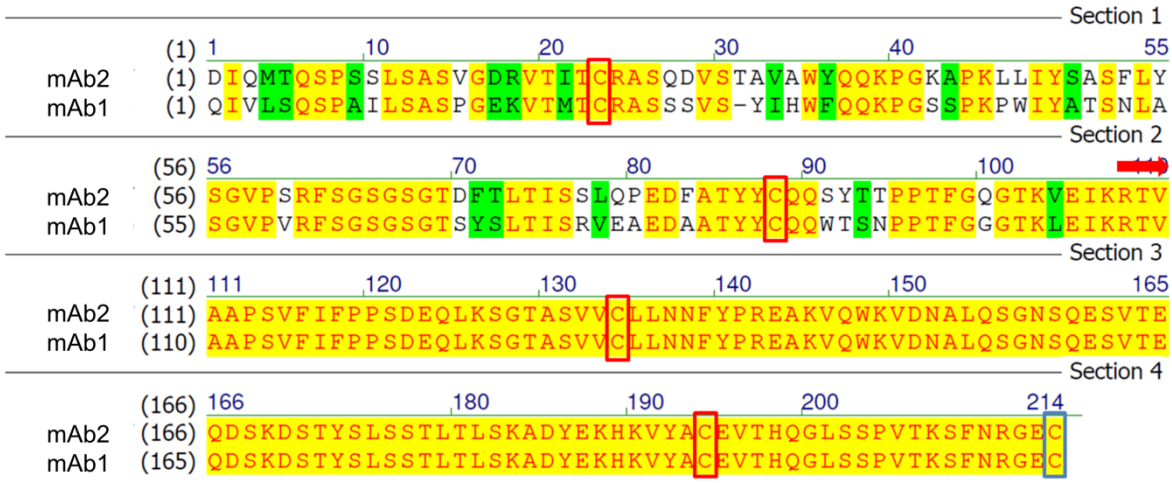

Supplementary Fig. S1. Sequence alignment of mAb1 and mAb2 light chain (LC) protein sequences. Yellow and green background at a certain position indicates identical amino acids and amino acids with same properties, respectively. The start of the constant domain is indicated by a red arrow. Cysteines forming the intra domain disulfide bridges are highlighted with red squares. The cysteine establishing the pairing with the heavy chain (HC) is highlighted with a blue square. The sequences are also available as FASTA file (Supplementary Data D1). The investigated antibodies bind CD20 (mAb1) and VEGF (mAb2). mAb1 was generated in animal immunization studies (Reff et al., 1994) and mAb2 was generated using phage display techniques (Lee et al., 2004).

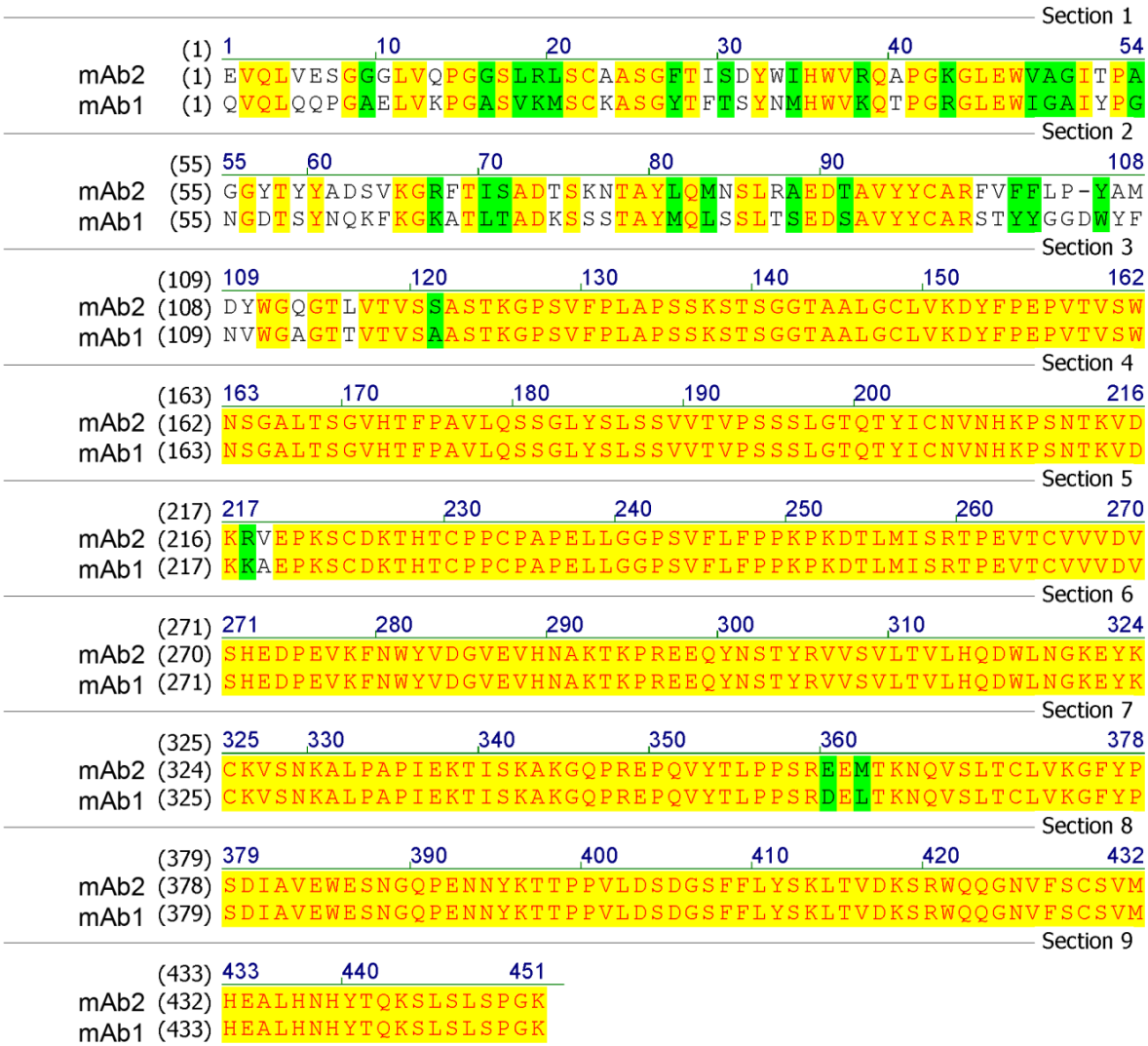

Supplementary Fig. S2. Sequence alignment of mAb1 and mAb2 heavy chain (HC) protein sequences. Yellow and green background at a certain position indicates identical amino acids and amino acids with same properties, respectively. The sequences are also available as FASTA file (Supplementary Data D1). The investigated antibodies bind CD20 (mAb1) and VEGF (mAb2). mAb1 was generated in animal immunization studies (Reff et al., 1994) and mAb2 was generated using phage display techniques (Lee et al., 2004).

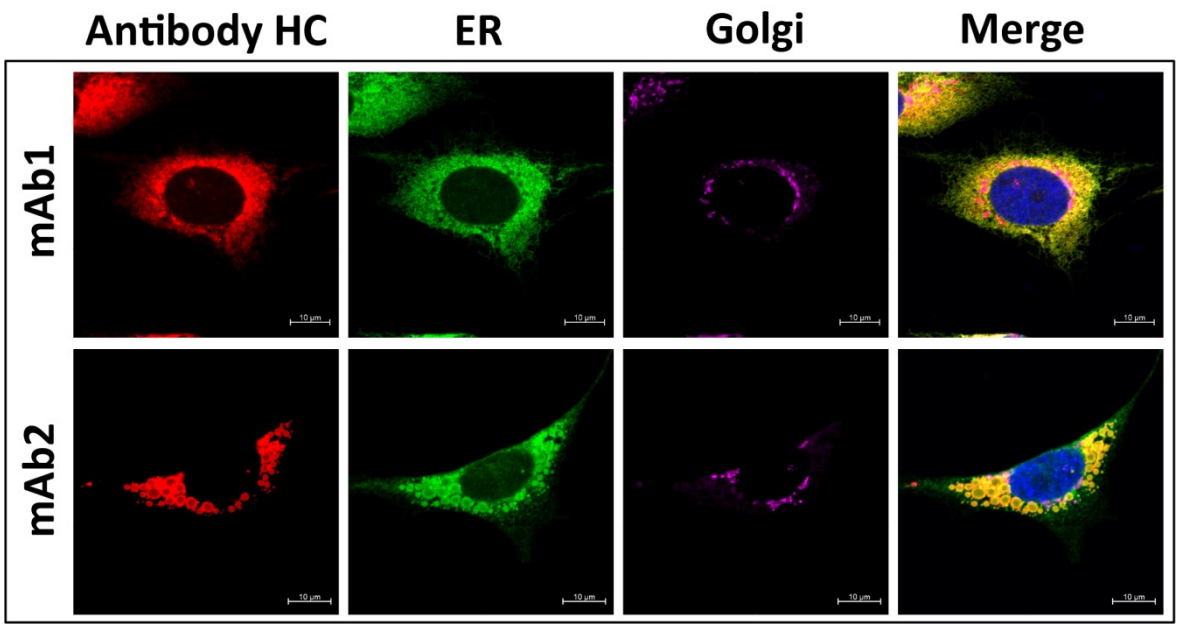

Supplementary Fig. S3. Immunofluorescence based cellular distribution analyses of the produced monoclonal antibodies showed impaired ER structures in the mAb2 producing cell line. Confocal images of the investigated cell line visualizing the distribution of the produced recombinant protein (HC) within the secretory organelles Endoplasmic reticulum (ER) and Golgi apparatus. For superior visualization of the distinct organelles cells have been cultures adherently for this analysis only. Investigated cell lines were fixed and the produced recombinant proteins, the ER as well as the Golgi apparatus were visualized with immunofluorescent antibodies and are shown in red, green and magenta, respectively. Nuclei were counterstained with DAPI (blue). Pictures were acquired at 63x primary magnification. The scale bars represent 10µm.

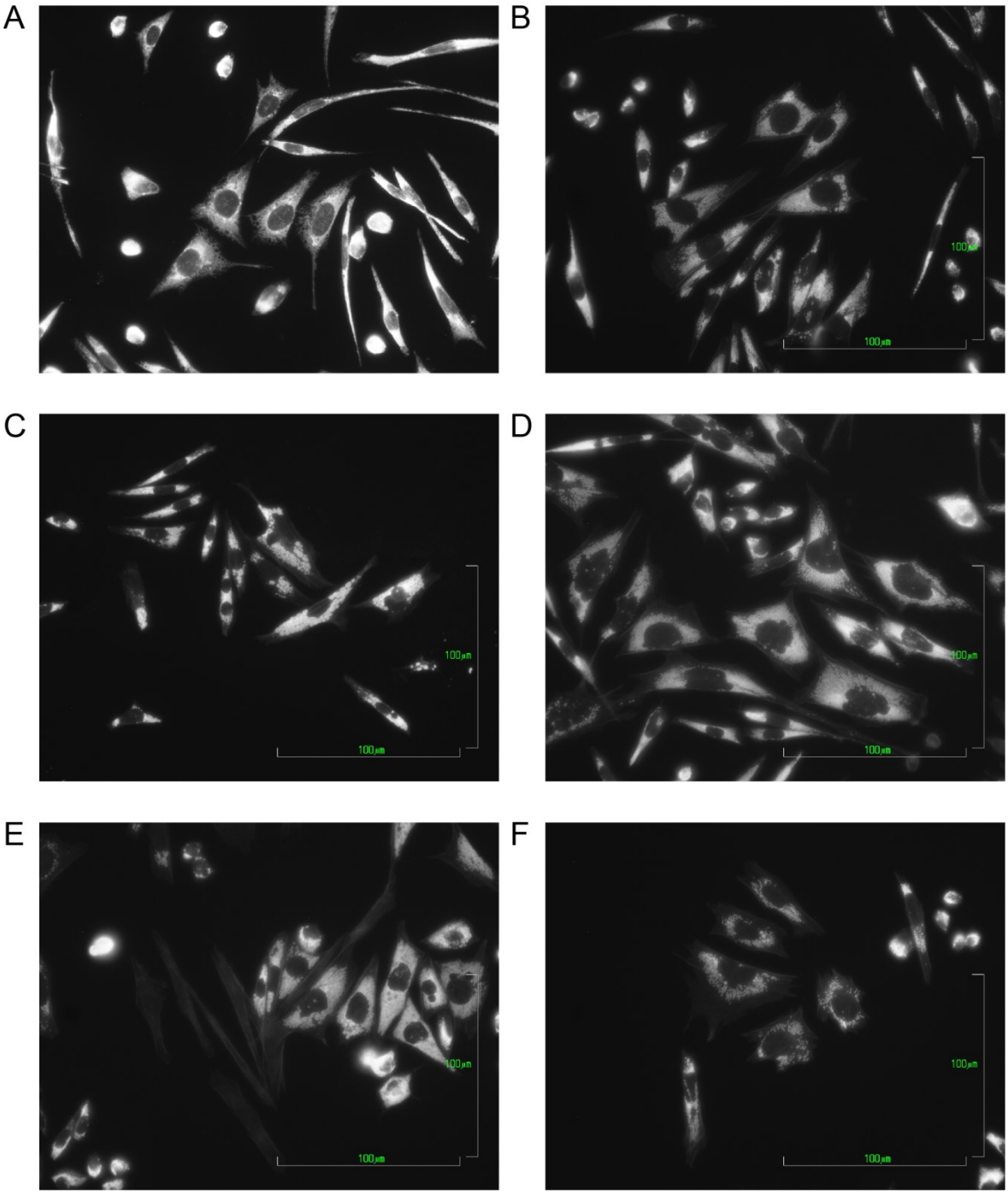

Supplementary Fig. S4. Immunofluorescence based cellular distribution analyses of the produced recombinant protein in several clonal mAb2 producing cell lines and the reference cell line (mAb1). For superior visualization of the distinct organelles cells have been cultures adherently for this analysis only. The investigated cell lines were fixed and the produced recombinant protein (HC) was visualized with an immunofluorescent antibody. Pictures were acquired at 40x primary magnification with an ECLIPSE TE2000-S with light source Intensilight C-HGFI (Nikon, Tokyo, Japan). The scale bars represent 100 µm. (A) mAb1 producing cell line. (B) mAb2 producing cell line investigated in this study. (C) mAb2 producing cell line clone 2. (D) mAb2 producing cell line clone 3. (E) mAb2 producing cell line clone 4. (F) mAb2 producing cell line clone 5.

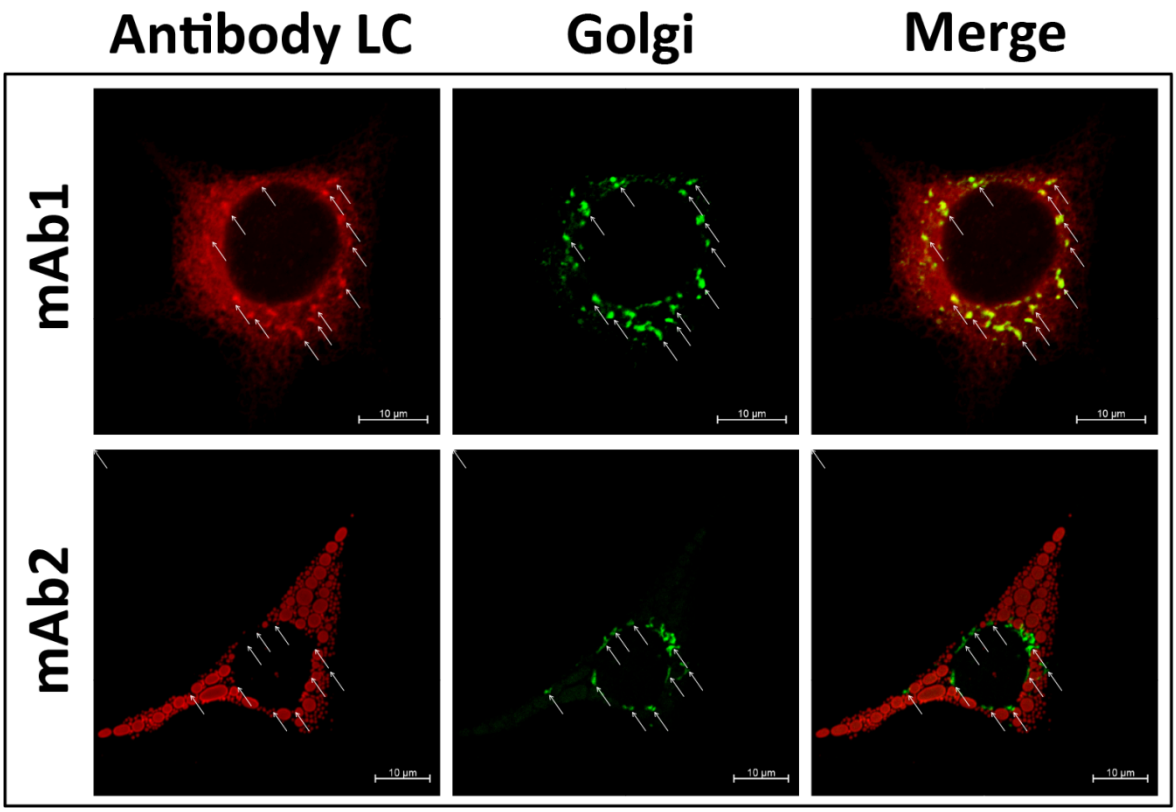

Supplementary Fig. S5. Immunofluorescence based cellular distribution analyses of the produced monoclonal antibodies. Confocal images of the investigated cell line visualizing the distribution of the produced recombinant protein (LC) within the Golgi apparatus. For superior visualization of the distinct organelles cells have been cultures adherently for this analysis only. Investigated cell lines were fixed and the produced recombinant proteins and the Golgi apparatus were visualized with immunofluorescent antibodies and are shown in red and green, respectively. Pictures were acquired at 63x primary magnification. The scale bars represent 10 µm. An overlay of only antibody staining and Golgi staining is shown. White arrows highlight individual centers of the Golgi apparatus.

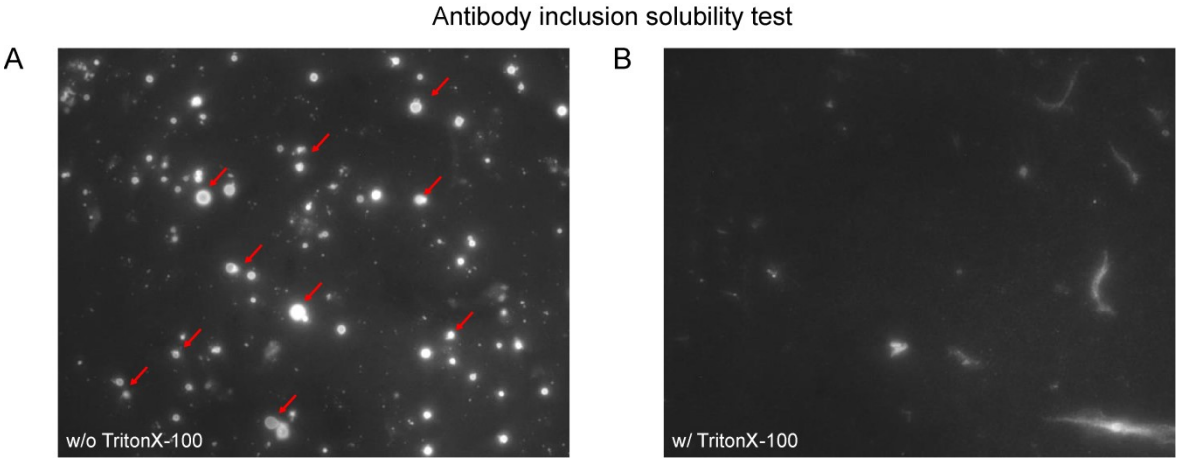

Supplementary Fig. S6. Testing whether purified inflated vesicles from mAb2 producing cell lines were dissolved completely with the milder detergent TritonX-100. Cells were treated using the Endoplasmic Reticulum Isolation Kit (Sigma Aldrich) according to the manufacturer´s instructions. Instead of 10 strokes cells were lysed with 40 strokes of a Dounce homogenizer and additionally passed 20 times through a 25-gauge needle (Henke-Sass Wolf, Tuttlingen, Germany). Afterwards lysates were passed through a 10 µm filter (Pall, Port Washington, NY, USA) and centrifuged for 3 min at 1000 g. Pellets were resuspended in extraction puffer (A) with or (B) without 0.1 % TritonX-100 (v/v), incubated on ice for 30 min and subsequently subjected to immunocytochemistry analyses staining the antibody heavy chain (HC). Isolated inflated ER vesicles are marked with red arrows and are dissolved after TritonX-100 treatment. It was not possible to purify appropriate vesicular structures from the mAb1 producing cell line.

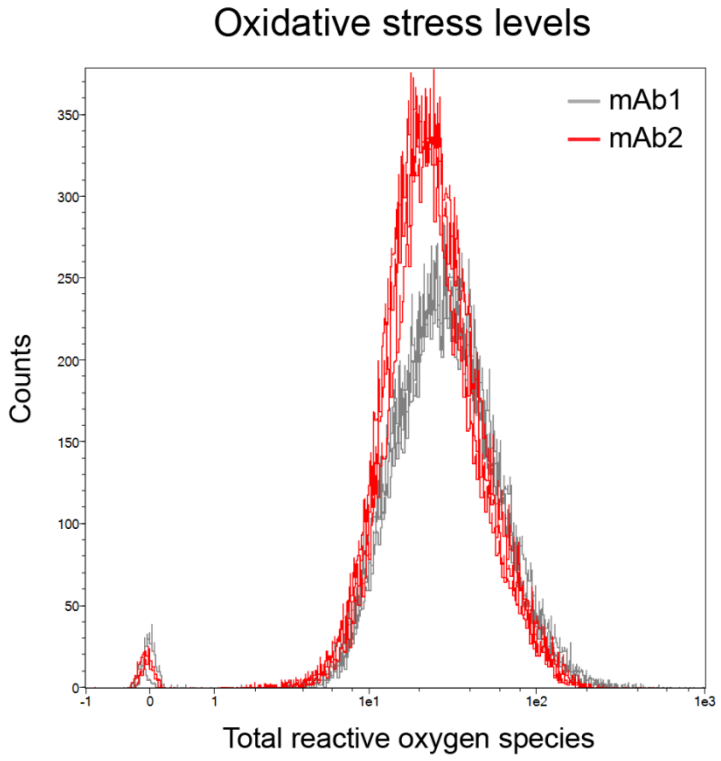

Supplementary Fig. S7. Oxidative stress is putatively not the reason for aberrant ER morphology. CellROX™ Green Flow Cytometry Assay Kit (Thermo Fisher Scientific) was used according to the manufacturer´s instructions for relatively quantification of reactive oxygen species in mAb1 and mAb2 producing cell lines. Cells were analyzed using a MACSQuant® Analyzer flow cytometer (Miltenyi Biotec, Bergisch Gladbach, Germany).

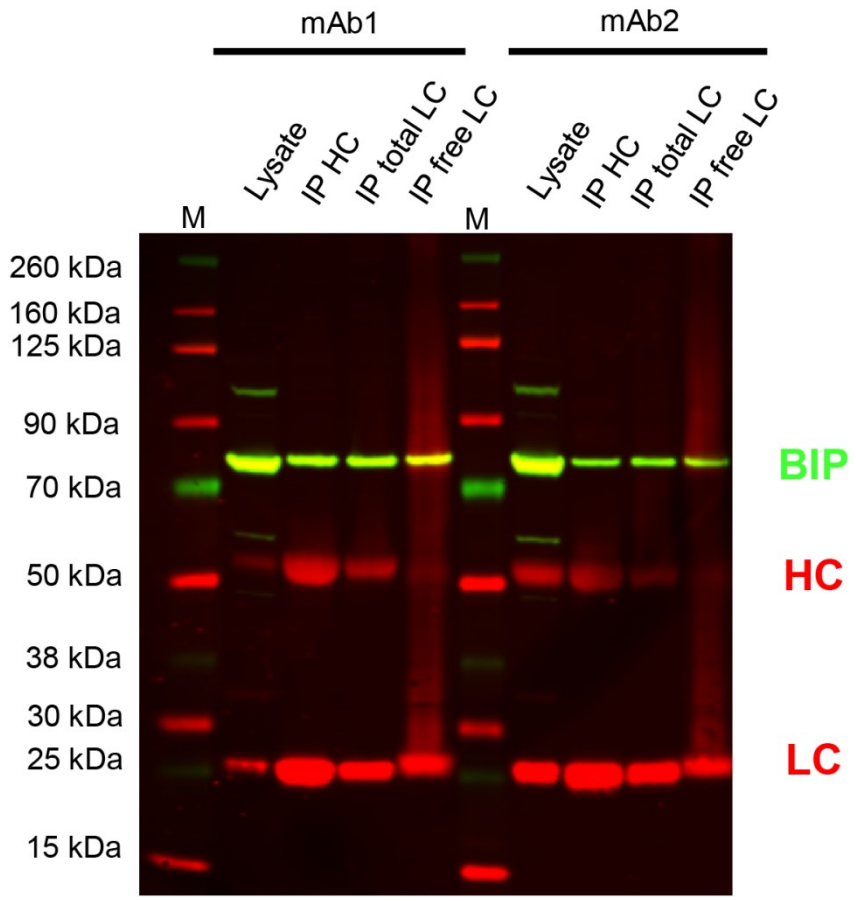

Supplementary Fig. S8. The only partially folded light chain (LC) of mAb2 is not more (in comparison to mAb1) recognized by the molecular chaperon binding immunoglobulin protein (BIP). For BIP detection the antibody ab21685 (abcam, Cambridge, UK) was used. IP, immunoprecipitation; HC, heavy chain

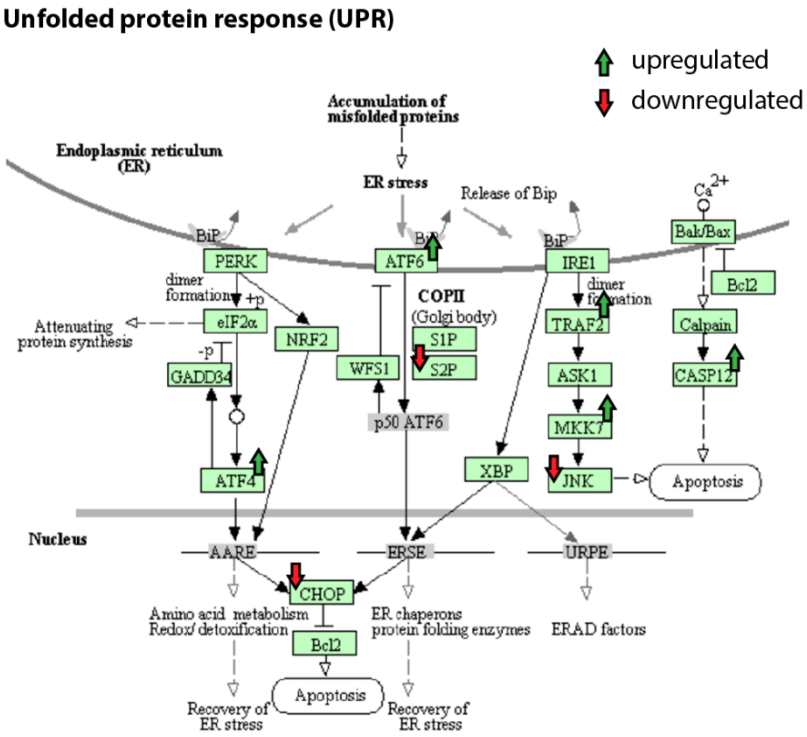

Supplementary Fig. S9. The unfolded protein response (UPR) is not explicitly triggered in mAb2 producing cell lines as revealed by gene expression analysis. Detailed pathway map of the UPR network where upregulated and downregulated genes are indicated by green and red arrows, respectively. A gene was considered to be regulated with a Benjamini-Hochberg false discovery rate BHQ < 0.05 and a fold change FC > 1.2 and FC < 1/1.2, respectively. The figure was modified from Kyoto Encyclopedia of Genes and Genomes (KEGG) Database with permission (Kanehisa and Goto, 2000; Kanehisa et al., 2017; 2019). A full list of proteins and FC is available in Supplementary Table S2.

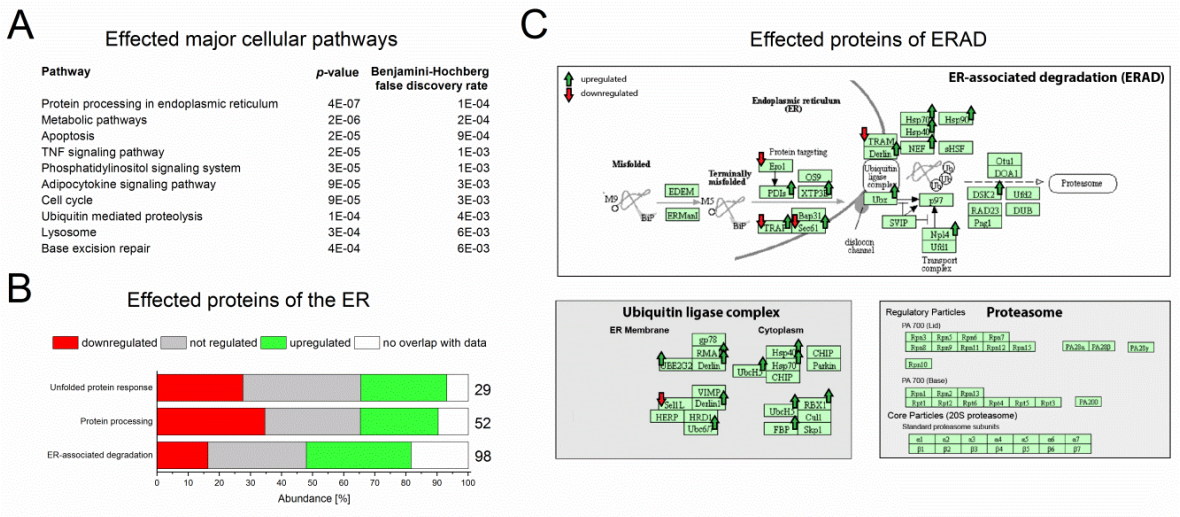

Supplementary Fig. S10. Gene expression analyses putatively indicated degradation of mAb2 via ER-associated degradation (ERAD) in a clonal production cell line (clone 2). (A) Canonical pathways which are affected by the production of the difficult-to-express antibody mAb2 in comparison to mAb1. (B) Transcriptionally upregulated and downregulated proteins in respect to mAb2 production belonging to major biochemical pathways within the Endoplasmic reticulum (ER): unfolded protein response (UPR), general protein processing and ERAD. (C) Detailed pathway map of the ERAD process and components of the respective ubiquitin ligase complex and proteasome where upregulated and downregulated genes are indicated by green and red arrows, respectively. The indication of an upregulation and downregulation of a respective protein means that the function is conducted by different proteins of which some were upregulated and downregulated during the analysis, respectively. A gene was considered to be regulated with a Benjamini-Hochberg false discovery rate BHQ < 0.05 and a fold change FC > 1.2 and FC < 1/1.2, respectively. The figure was modified from Kyoto Encyclopedia of Genes and Genomes (KEGG) Database with permission (Kanehisa and Goto, 2000; Kanehisa et al., 2017; 2019). A full list of proteins and FC is available in Supplementary Table S2.

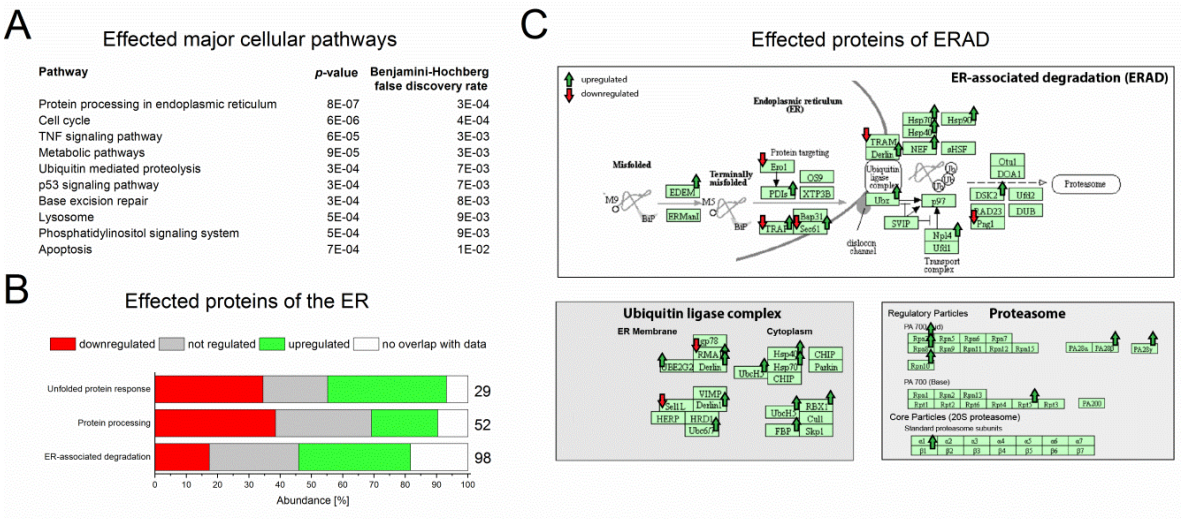

Supplementary Fig. S11. Gene expression analyses putatively indicated degradation of mAb2 via ER-associated degradation (ERAD) in a clonal production cell line (clone 3). (A) Canonical pathways which are affected by the production of the difficult-to-express antibody mAb2 in comparison to mAb1. (B) Transcriptionally upregulated and downregulated proteins in respect to mAb2 production belonging to major biochemical pathways within the Endoplasmic reticulum (ER): unfolded protein response (UPR), general protein processing and ERAD. (C) Detailed pathway map of the ERAD process and components of the respective ubiquitin ligase complex and proteasome where upregulated and downregulated genes are indicated by green and red arrows, respectively. The indication of an upregulation and downregulation of a respective protein means that the function is conducted by different proteins of which some were upregulated and downregulated during the analysis, respectively. A gene was considered to be regulated with a Benjamini-Hochberg false discovery rate BHQ < 0.05 and a fold change FC > 1.2 and FC < 1/1.2, respectively. The figure was modified from Kyoto Encyclopedia of Genes and Genomes (KEGG) Database with permission (Kanehisa and Goto, 2000; Kanehisa et al., 2017; 2019). A full list of proteins and FC is available in Supplementary Table S2.

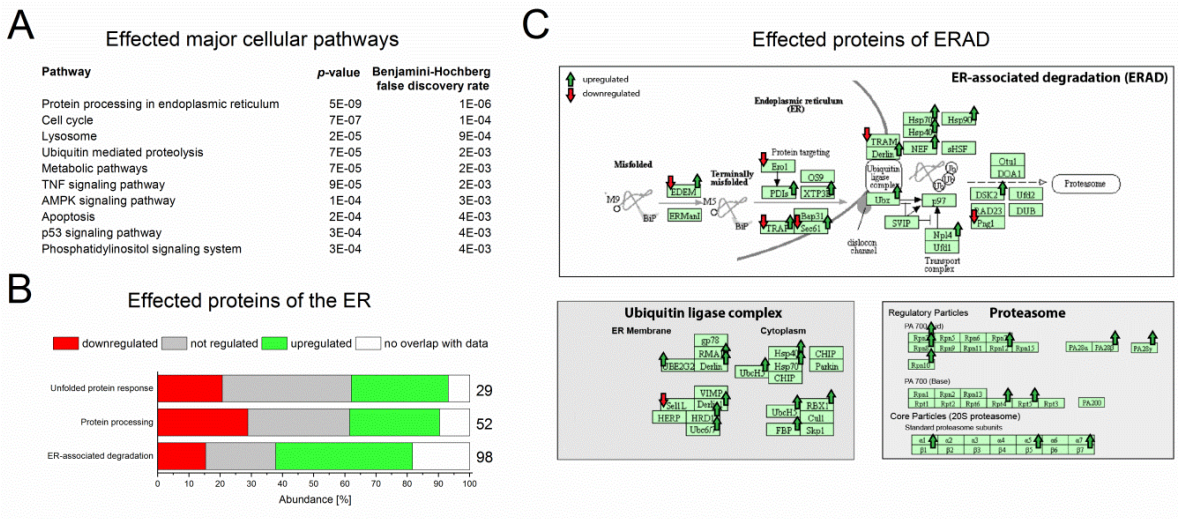

Supplementary Fig. S12. Gene expression analyses putatively indicated degradation of mAb2 via ER-associated degradation (ERAD) in a clonal production cell line (clone 4). (A) Canonical pathways which are affected by the production of the difficult-to-express antibody mAb2 in comparison to mAb1. (B) Transcriptionally upregulated and downregulated proteins in respect to mAb2 production belonging to major biochemical pathways within the Endoplasmic reticulum (ER): unfolded protein response (UPR), general protein processing and ERAD. (C) Detailed pathway map of the ERAD process and components of the respective ubiquitin ligase complex and proteasome where upregulated and downregulated genes are indicated by green and red arrows, respectively. The indication of an upregulation and downregulation of a respective protein means that the function is conducted by different proteins of which some were upregulated and downregulated during the analysis, respectively. A gene was considered to be regulated with a Benjamini-Hochberg false discovery rate BHQ < 0.05 and a fold change FC > 1.2 and FC < 1/1.2, respectively. The figure was modified from Kyoto Encyclopedia of Genes and Genomes (KEGG) Database with permission (Kanehisa and Goto, 2000; Kanehisa et al., 2017; 2019). A full list of proteins and FC is available in Supplementary Table S2.

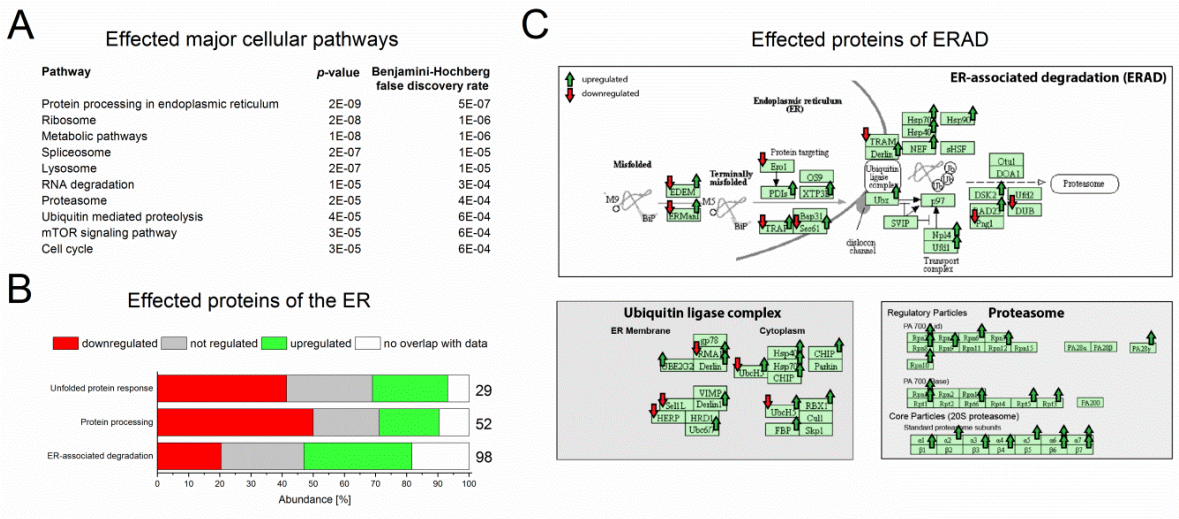

Supplementary Fig. S13. Gene expression analyses putatively indicated degradation of mAb2 via ER-associated degradation (ERAD) in a clonal production cell line (clone 5). (A) Canonical pathways which are affected by the production of the difficult-to-express antibody mAb2 in comparison to mAb1. (B) Transcriptionally upregulated and downregulated proteins in respect to mAb2 production belonging to major biochemical pathways within the Endoplasmic reticulum (ER): unfolded protein response (UPR), general protein processing and ERAD. (C) Detailed pathway map of the ERAD process and components of the respective ubiquitin ligase complex and proteasome where upregulated and downregulated genes are indicated by green and red arrows, respectively. The indication of an upregulation and downregulation of a respective protein means that the function is conducted by different proteins of which some were upregulated and downregulated during the analysis, respectively. A gene was considered to be regulated with a Benjamini-Hochberg false discovery rate BHQ < 0.05 and a fold change FC > 1.2 and FC < 1/1.2, respectively. The figure was modified from Kyoto Encyclopedia of Genes and Genomes (KEGG) Database with permission (Kanehisa and Goto, 2000; Kanehisa et al., 2017; 2019). A full list of proteins and FC is available in Supplementary Table S2.

Supplementary Table S1. Abbreviation list of identified proteins after co-immunoprecipitation of mAb1 and mAb2 from cell lysates, respectively.

Symbol	Name	Alternative name
PDIA4	Protein disulfide-isomerase A4	Endoplasmic reticulum resident protein 72 (Erp-72)
PDI	Protein disulfide-isomerase (A1)	
HSP105	Heat shock protein 105 kDa	
BAG-3	BAG family molecular chaperone regulator 3	
SEC61B	Protein transport protein Sec61 subunit beta	
HSP90b	Heat shock protein 90kDa beta (HSP90B)	
BIP	Endoplasmic reticulum chaperone BIP	Glucose-regulated protein 78 kDa (GRP78); Heat shock protein family A member 5 (HSPA5)
PDIA6	Protein disulfide-isomerase A6	Endoplasmic reticulum protein 5 (ERp5)
HSP60	60 kDa heat shock protein	
HSC71	Heat shock cognate 71 kDa protein	
SEC23B	Protein transport protein Sec23B	
COPA	Coatomer subunit alpha	
Erlin-2	Erlin-2	
COPE	Coatomer subunit epsilon	
PPIase B	Peptidyl-prolyl cis-trans isomerase B	Cyclophilin B
PPIase A	Peptidyl-prolyl cis-trans isomerase A	Cyclophilin A
PCGR	Parkin coregulated gene protein	
COPB	Coatomer subunit epsilon	

Supplementary Table S2. List of proteins of the major canonical pathways protein processing, unfolded protein response (UPR) and endoplasmic reticulum (ER) associated-degradation (ERAD) in the Endoplasmic reticulum (ER).

Official gene symbol	Pathway	Fold change Clone 1	Fold change Clone 2	Fold change Clone 3	Fold change Clone 4	Fold change Clone 5
Amfr	ERAD	0,91	0,98	0,92	0,94	1,10
Atf4	UPR	5,69	4,85	4,06	3,30	4,05
Atf6	UPR	0,73	0,82	0,72	0,68	0,50
Atf6b	UPR	1,64	1,76	1,52	1,74	1,76
Atxn3	ERAD	0,93	0,82	1,00	0,84	0,79
Bag1	ERAD	1,24	1,07	1,30	1,41	1,50
Bag2	ERAD	1,45	1,51	1,39	1,39	1,70
Bak1	UPR	no overlap with data	no overlap with data	no overlap with data	no overlap with data	no overlap with data
Bax	UPR	1,12	1,09	0,92	1,06	1,25
Bcap31	ERAD	0,79	0,77	0,89	1,02	1,00
Bcl2	UPR	0,74	0,88	0,69	0,71	0,79
Calr	Processing	no overlap with data	no overlap with data	no overlap with data	no overlap with data	no overlap with data
Canx	Processing	0,70	0,78	0,81	0,75	0,72
Capn1	UPR	1,13	1,07	1,23	1,36	1,07
Capn2	UPR	0,91	0,98	0,93	1,00	0,85
Casp12	UPR	1,58	1,38	1,58	1,89	1,30
Ckap4	Processing	1,21	1,23	1,37	1,67	1,23
Cryaa	ERAD	not detected	not detected	not detected	1,78	not detected
Cryab	ERAD	0,74	0,82	0,44	0,79	0,83
Cul1	ERAD	1,02	1,03	0,88	0,99	0,89
Dad1	Processing	1,06	1,00	1,20	1,31	0,74
Ddit3	UPR	0,34	0,30	0,27	0,28	0,27
Ddost	Processing	1,22	1,42	1,05	1,40	1,36
Derl1	ERAD	8,58	10,34	11,67	8,82	13,01
Derl2	ERAD	0,82	0,80	0,84	0,97	0,88
Derl3	ERAD	no overlap with data	no overlap with data	no overlap with data	no overlap with data	no overlap with data
Dnaja1	ERAD	1,12	1,12	1,27	1,42	1,46
Dnaja2	ERAD	1,11	1,13	1,10	1,20	1,16
Dnajb1	ERAD	1,77	1,78	1,87	2,00	2,31
Dnajb11	Processing	0,73	0,83	0,88	0,96	0,94
Dnajb12	ERAD	1,07	1,15	1,00	1,22	0,99
Dnajb2	ERAD	1,65	1,50	1,41	1,59	2,07
Dnajc1	Processing	0,78	0,70	0,67	0,90	0,62
Dnajc10	Processing	0,79	0,81	0,82	0,96	0,69
Dnajc3	Processing	0,74	0,74	0,66	1,00	0,43

Dnajc5	ERAD	1,23	1,06	1,23	1,24	1,14
Dnajc5b	ERAD	no overlap with data	no overlap with data	no overlap with data	no overlap with data	no overlap with data
Dnajc5g	ERAD	no overlap with data	no overlap with data	no overlap with data	no overlap with data	no overlap with data
EDEM1	ERAD	0,60	0,55	0,37	0,38	0,61
Edem2	ERAD	1,45	1,29	1,36	1,43	1,50
Edem3	ERAD	0,65	0,66	0,66	0,66	0,50
Eif2ak1	UPR	0,85	0,79	0,78	0,84	0,82
Eif2ak2	UPR	1,25	1,17	1,22	1,57	0,90
Eif2ak3	UPR	0,88	0,97	0,64	0,75	0,53
Eif2ak4	UPR	1,02	0,98	1,12	0,96	0,86
Eif2s1	UPR	0,87	0,85	0,89	0,91	0,99
Erlec1	ERAD	1,94	2,02	0,87	2,17	1,34
Ern1	UPR	0,55	0,54	0,48	0,44	0,33
Ero1l	ERAD	0,54	0,62	0,83	0,72	0,35
Ero1lb	ERAD	0,60	0,61	0,79	0,76	0,56
Erp29	ERAD	1,87	1,92	1,89	2,35	1,35
Fbxo2	ERAD	not detected	not detected	not detected	not detected	not detected
Fbxo6	ERAD	2,14	2,10	1,73	1,92	1,94
Ganab	Processing	0,87	0,86	0,87	0,96	0,90
Gm15266	Processing	no overlap with data	no overlap with data	no overlap with data	no overlap with data	no overlap with data
Gm9840	ERAD	no overlap with data	no overlap with data	no overlap with data	no overlap with data	no overlap with data
Herpud1	ERAD	1,12	1,03	1,13	1,15	0,83
HSP90a	ERAD	1,06	0,98	1,20	1,07	1,07
Hsp90ab1	ERAD	1,42	1,42	1,39	1,40	1,47
Hsp90b1	Processing	0,66	0,79	0,85	0,95	0,69
Hspa1a	ERAD	no overlap with data	no overlap with data	no overlap with data	no overlap with data	no overlap with data
Hspa1b	ERAD	no overlap with data	no overlap with data	no overlap with data	no overlap with data	no overlap with data
Hspa1l	ERAD	no overlap with data	no overlap with data	no overlap with data	no overlap with data	no overlap with data
Hspa2	ERAD	2,41	2,40	2,86	2,81	2,58
Hspa4l	ERAD	5,07	4,62	6,37	3,83	5,07
Hspa5	Processing, ERAD, UPR	0,74	1,02	0,94	1,21	0,63
Hspa8	ERAD	1,72	1,79	1,73	1,93	1,90
Hspbp1	ERAD	no overlap with data	no overlap with data	no overlap with data	no overlap with data	no overlap with data

Hsph1	ERAD	no overlap with data	no overlap with data	no overlap with data	no overlap with data	no overlap with data
Hyou1	Processing	0,82	0,88	0,87	1,01	0,67
Lman1	Processing	0,74	0,73	0,73	0,82	0,65
Lman1l	Processing	no overlap with data	no overlap with data	no overlap with data	no overlap with data	no overlap with data
Lman2	Processing	2,65	2,68	2,74	3,27	3,57
MAN1A1	Processing, ERAD	0,56	0,57	0,54	0,73	0,47
Man1a2	Processing, ERAD	0,91	0,95	0,77	0,90	0,88
Man1b1	Processing, ERAD	1,04	0,98	0,99	1,00	1,23
Man1c1	Processing, ERAD	0,95	0,73	0,66	0,77	0,35
Map2k7	UPR	1,82	1,72	1,39	1,68	1,43
Map3k5	UPR	no overlap with data	no overlap with data	no overlap with data	no overlap with data	no overlap with data
Mapk10	UPR	0,84	0,47	1,51	0,98	0,62
Mapk8	UPR	1,00	0,47	0,96	1,03	0,49
Mapk9	UPR	0,78	0,79	0,77	0,84	0,86
March6	ERAD	0,63	0,61	0,59	0,62	0,56
Mbtps1	UPR	1,13	1,12	0,87	1,20	1,03
MBTPS2	UPR	0,66	0,64	0,54	0,54	0,48
Mogs	Processing	1,65	2,37	1,34	1,55	1,14
Nfe2l2	UPR	1,04	1,12	1,33	1,20	1,17
Ngly1	ERAD	0,86	1,02	0,66	0,78	0,35
Nploc4	ERAD	1,33	1,26	1,42	1,28	1,61
Nsfl1c	ERAD	1,44	1,38	1,35	1,59	1,75
Os9	ERAD	1,23	1,20	1,15	1,38	1,09
P4hb	Processing, ERAD	1,00	1,04	0,91	1,28	1,03
Park2	ERAD	1,61	1,58	0,68	0,72	0,70
Pdia3	Processing	0,78	0,92	0,81	1,02	0,74
Pdia4	ERAD	1,13	1,81	0,86	1,38	0,89
Pdia6	ERAD	0,95	1,07	1,04	1,24	1,04
Plaa	ERAD	0,92	0,98	0,98	1,01	0,89
Ppp1r15a	UPR	1,86	1,80	1,27	1,39	1,58
Preb	Processing	1,35	1,28	1,30	1,27	1,11
Prkcsh	Processing	1,51	1,57	1,82	1,96	1,75
Rad23a	ERAD	no overlap with data	no overlap with data	no overlap with data	no overlap with data	no overlap with data
Rad23b	ERAD	1,16	1,20	1,02	1,14	1,28
Rbx1	ERAD	1,36	1,34	1,35	1,59	1,40
Rnf185	ERAD	1,16	1,05	0,49	1,02	0,59
Rnf5	ERAD	3,66	3,35	3,79	4,49	5,41

Rpn1	Processing	0,80	0,94	1,61	0,63	0,94
Rpn2	Processing	1,09	1,23	1,12	1,37	1,19
Rrbp1	Processing	0,71	0,68	0,71	0,81	0,57
Sar1a	Processing	1,08	1,01	1,09	1,28	1,27
Sar1b	Processing	0,99	0,90	0,99	0,94	0,99
Sec13	Processing	0,97	1,39	0,62	0,87	1,36
Sec23a	Processing	1,18	1,11	0,99	0,99	0,71
Sec23b	Processing	0,90	0,89	0,90	0,95	0,81
Sec24a	Processing	0,68	0,72	0,68	0,60	0,53
Sec24b	Processing	0,64	0,58	0,61	0,63	0,62
Sec24c	Processing	1,01	0,93	0,87	0,95	0,40
Sec24d	Processing	1,18	1,21	0,87	1,18	0,80
Sec31a	Processing	0,75	0,81	0,66	0,74	0,44
Sec31b	Processing	3,15	1,47	3,17	2,89	3,53
Sec61a1	Processing, ERAD	0,82	0,86	1,44	0,60	0,94
Sec61a2	Processing, ERAD	0,61	0,56	0,55	0,59	0,60
Sec61b	Processing, ERAD	1,98	1,83	1,75	2,30	2,31
Sec61g	Processing, ERAD	1,63	1,48	0,71	1,66	1,03
Sec62	Processing	0,69	0,66	0,69	0,75	0,66
Sec63	Processing	0,56	0,53	0,54	0,61	0,50
Sel1l	ERAD	0,54	0,62	0,58	0,64	0,44
Sel1l2	ERAD	no overlap with data	no overlap with data	no overlap with data	no overlap with data	no overlap with data
Sil1	Processing	no overlap with data	no overlap with data	no overlap with data	no overlap with data	no overlap with data
Skp1	ERAD	1,06	0,97	1,05	1,21	1,33
Ssr1	ERAD	1,45	1,46	1,50	1,66	1,42
Ssr2	ERAD	1,35	1,28	1,20	1,73	1,40
Ssr3	ERAD	0,80	0,69	0,60	0,76	0,65
Ssr4	ERAD	1,38	1,37	1,27	1,68	1,39
Stt3a	Processing	0,71	0,69	0,54	0,73	0,54
Stt3b	Processing	0,71	0,76	0,64	0,76	0,69
Stub1	ERAD	1,49	1,40	1,30	1,63	2,11
Svip	ERAD	not detected	not detected	not detected	not detected	not detected
Syvn1	ERAD	1,48	1,35	1,23	1,52	1,10
Traf2	UPR	1,66	1,45	1,83	1,88	2,34
Tram1	ERAD	0,70	0,73	0,64	0,74	0,71
Tusc3	Processing	1,84	2,03	2,04	2,26	1,78
Txndc5	ERAD	1,83	1,87	1,53	1,93	2,12
Ube2d1	ERAD	1,02	1,09	1,24	1,25	1,17

Ube2d2a	ERAD	no overlap with data	no overlap with data	no overlap with data	no overlap with data	no overlap with data
Ube2d2b	ERAD	no overlap with data	no overlap with data	no overlap with data	no overlap with data	no overlap with data
Ube2d3	ERAD	1,13	1,09	1,32	1,25	1,49
Ube2e1	ERAD	no overlap with data	no overlap with data	no overlap with data	no overlap with data	no overlap with data
Ube2e2	ERAD	1,12	1,26	0,86	1,14	0,53
Ube2e3	ERAD	1,27	1,27	1,13	1,33	1,36
Ube2g1	ERAD	0,98	1,10	1,08	1,02	1,04
Ube2g2	ERAD	1,49	1,46	1,49	1,62	1,87
Ube2j1	ERAD	0,98	0,95	0,95	1,01	1,03
Ube2j2	ERAD	1,35	1,38	1,45	1,42	1,12
Ube4b	ERAD	no overlap with data	no overlap with data	no overlap with data	no overlap with data	no overlap with data
Ubqln1	ERAD	no overlap with data	no overlap with data	no overlap with data	no overlap with data	no overlap with data
Ubqln2	ERAD	1,47	1,35	1,39	1,40	1,19
Ubqln3	ERAD	no overlap with data	no overlap with data	no overlap with data	no overlap with data	no overlap with data
Ubqln4	ERAD	1,21	1,20	0,98	1,04	1,24
Ubqlnl	ERAD	2,43	0,70	3,06	not detected	4,35
Ubxn6	ERAD	2,64	2,50	2,32	2,68	2,60
Ufd1l	ERAD	1,20	1,04	1,25	1,36	1,41
Uggt1	Processing	0,90	1,00	0,91	1,07	0,80
Uggt2	Processing	no overlap with data	no overlap with data	no overlap with data	no overlap with data	no overlap with data
Vcp	ERAD	1,06	1,01	0,98	1,10	1,18
Vimp	ERAD	no overlap with data	no overlap with data	no overlap with data	no overlap with data	no overlap with data
Wfs1	UPR	1,01	0,87	0,70	1,13	0,48
Xbp-1	UPR	1,57	1,59	0,62	1,46	0,66
Yod1	ERAD	1,06	1,17	1,08	0,95	0,82

Bauer and Mathias et al. 2020, monoclonal antibodies (mAbs)

MAbs. Jan-Dec 2020;12(1):1787121

doi: 10.1080/19420862.2020.1787121

Licensed under Creative Commons Attribution - NonCommercial 4.0 International,
https://creativecommons.org/licenses/by-nc/4.0/

Note: The in this thesis described mAb1 is annotated GTE mAb in the following publication.

MABS
2020, VOL. 12, NO. 1, e1787121 (14 pages)
https://doi.org/10.1080/19420862.2020.1787121

Taylor & Francis
Taylor & Francis Group

REPORT

OPEN ACCESS Check for updates

Rational optimization of a monoclonal antibody improves the aggregation propensity and enhances the CMC properties along the entire pharmaceutical process chain

Joschka Bauer[a*], Sven Mathias[b,c*], Sebastian Kube[a], Kerstin Otte[b], Patrick Garidel[a], Martin Gamer[c], Michaela Blech[a], Simon Fischer[d], and Anne R Karow-Zwick[a]

[a]Early Stage Pharmaceutical Development, Pharmaceutical Development Biologicals, Boehringer Ingelheim Pharma GmbH & Co. KG, Biberach/Riss, Germany; [b]Institute of Applied Biotechnology, University of Applied Sciences Biberach, Biberach/Riss, Germany; [c]Early Stage Bioprocess Development, Bioprocess Development Biologicals, Boehringer Ingelheim Pharma GmbH & Co. KG, Biberach/Riss, Germany; [d]Cell Line Development, Bioprocess Development Biologicals, Boehringer Ingelheim Pharma GmbH & Co. KG, Boehringer Ingelheim Pharma GmbH & Co. KG, Biberach/Riss, Germany

ABSTRACT

The discovery of therapeutic monoclonal antibodies (mAbs) primarily focuses on their biological activity favoring the selection of highly potent drug candidates. These candidates, however, may have physical or chemical attributes that lead to unfavorable chemistry, manufacturing, and control (CMC) properties, such as low product titers, conformational and colloidal instabilities, or poor solubility, which can hamper or even prevent development and manufacturing. Hence, there is an urgent need to consider the developability of mAb candidates during lead identification and optimization. This work provides a comprehensive proof of concept study for the significantly improved developability of a mAb variant that was optimized with the help of sophisticated *in silico* tools relative to its difficult-to-develop parental counterpart. Interestingly, a single amino acid substitution in the variable domain of the light chain resulted in a three-fold increased product titer after stable expression in Chinese hamster ovary cells. Microscopic investigations revealed that wild type mAb-producing cells displayed potential antibody inclusions, while the *in silico* optimized variant-producing cells showed a rescued phenotype. Notably, the drug substance of the *in silico* optimized variant contained substantially reduced levels of aggregates and fragments after downstream process purification. Finally, formulation studies unraveled a significantly enhanced colloidal stability of the *in silico* optimized variant while its folding stability and potency were maintained. This study emphasizes that implementation of bioinformatics early in lead generation and optimization of biotherapeutics reduces failures during subsequent development activities and supports the reduction of project timelines and resources.

ARTICLE HISTORY
Received 20 December 2019
Revised 16 June 2020
Accepted 18 June 2020

KEYWORDS
In silico; bioinformatic; antibody engineering; biotherapeutic development; CMC properties; pharmaceutical industry

Introduction

Therapeutic proteins including monoclonal antibodies (mAbs) are capable of addressing a wide variety of unmet medical needs.[1] Despite becoming a cornerstone in drug development, the soaring cost of developing new biological entities (NBEs) has put substantial pressure on biopharmaceutical organizations.[2,3] At the discovery stage, biological activity is one of the most important selection criteria. A lead molecule is then progressed into the early stage development phase to assess its developability, which describes chemistry, manufacturing, and control (CMC) properties such as expression titer, purity, conformational (i.e., protein folding) and colloidal stability (i.e., protein aggregation), solubility, and viscosity. The competitive biopharmaceutical environment has increased the demand for prediction and optimization of the developability of the lead candidate to accelerate the development timeline and raise approval success rates. One of the most frequently encountered development issues at each step of the process are product-related impurities, of which protein particle formation/aggregation is the primary impurity compromising efficacy, quality, and patient safety.[4]

In the first step of the bioprocess development, the proteinaceous active pharmaceutical ingredient (API) is recombinantly produced using mammalian cell culture systems. Interestingly, the efficient production of DS remains a continuing challenge even though high-yielding cell line development approaches have substantially advanced in the past several decades.[5] In particular, mammalian systems expressing aggregation-prone mAbs often underperform, showing low product titer and specific productivity.[6]

The downstream process is developed to achieve maximum yield in combination with an acceptable purity level. Preparative modes of chromatography involving Protein A affinity, anion and cation exchange chromatography are commonly used.[7,8] Substantial efforts, however, may be required to separate the product from product-related impurities, such as aggregates and fragments, which are monitored as high molecular weight (HMW) and low molecular weight

CONTACT Anne Karow-Zwick anne.karow-zwick@boehringer-ingelheim.com Boehringer Ingelheim Pharma GmbH & Co. KG, Biberach/Riss 88400, Germany
*Both authors contributed equally to this manuscript
Supplemental data for this article can be accessed here.

© 2020 The Author(s). Published with license by Taylor & Francis Group, LLC.
This is an Open Access article distributed under the terms of the Creative Commons Attribution-NonCommercial License (http://creativecommons.org/licenses/by-nc/4.0/), which permits unrestricted non-commercial use, distribution, and reproduction in any medium, provided the original work is properly cited.

(LMW) species during analytical size-exclusion chromatography (SEC) experiments.

Finally, a formulation is developed for the purified protein to ensure long-term storage stability and optimal routes of administration.[9] This step of the process can be challenging because the diversity and inherent structural complexity of biologicals and their individual interplay with excipients necessitate an individual evaluation and "trial-and-error"-based stabilization for the molecule of choice.[10] There is an increasing need for subcutaneous and intravitreal formulations, which often require high drug concentrations, preferably as liquid presentations. Among the various challenges in preparing stable, robust formulations for such routes of administration are concentration-dependent aggregation and high viscosity.[11] Possible challenges associated with aggregation of the drug product (DP), i.e., the formulated DS, are most commonly addressed by time-consuming and labor-intensive formulation development.

Recent advances in biopharmaceutical informatics have provided efficient computational tools for the assessment and optimization of sequences and structures, paving the way for engineering a candidate´s developability, in addition to its biological activity, already at the early discovery stage. An early prediction of development issues guides rational sequence optimization approaches, thereby minimizing the risk of costly delays and failures of biotherapeutic development programs.[6,12,13] Some biopharmaceutical companies along with some contract development and manufacturing organizations have started to perform sequence optimization via proprietary algorithms,[14,15] but there is currently relatively little knowledge about the benefits of *in silico* optimization performed at an early discovery stage on the performance of the DS and DP at each step of the bioprocess.[16] Published studies have used calculated structural descriptors to predict individual CMC properties such as viscosity,[17,18] chemical degradation,[18] and, in particular, aggregation.[6,19] Notably, a variety of *in silico* tools identifying aggregation-prone regions (APRs) were developed, emphasizing the strong demand for the prediction and prevention of protein particle formation.[20-31] Particular attention was paid to the Solubis method,[32] which was used in a previous study[6] to predict sequence variants of a therapeutic mAb (called mAb2) with reduced intrinsic aggregation propensity (TANGO)[33] under consideration of the thermodynamic stability of the native structure (FoldX).[34] A single amino acid exchange (S52R) in complementarity determining region 2 (CDR2) of the light chain (LC) was shown to diminish an APR that triggered aggregation of transiently expressed mAb2.[6]

Here, we developed the wild type and *in silico* optimized mAb2 in accordance with a bioprocess widely established in the pharmaceutical industry, providing detailed insights into the beneficial developability of a computationally optimized mAb. Predicted good- (variant) and difficult-to-develop (mAb2) antibodies were established in state-of-the-art platform processes along the value chain of the pharmaceutical development consisting of 1) generation of stable single clone-derived Chinese hamster ovary (CHO) production cell lines; 2) production in a representative 3 L scale bioreactor; 3) downstream purification; 4) physicochemical characterization; and 5) stability studies of respective DP formulations with functional investigations.

Results

In silico optimization enhanced mAb expression titer in stable CHO cells

The effect of an *in silico*-guided exchange of a single amino acid (SL52R) on the developability of the therapeutic antibody mAb2 was unraveled by performing a complete biopharmaceutical development program comprising establishment of stable cell lines and upstream and downstream processes, as well as development of a suitable formulation buffer for both the wild type and *in silico* optimized variant. The first obstacle was to establish stable CHO cell lines and to compare the upstream process performance of the best eight single clone-derived cell lines producing either mAb2 or its *in silico* optimized variant in controlled fed-batch cultivations with regard to differences in cell growth, viability, and mAb productivity. Observed peak viable cell densities (VCDs) ranged from ~8.0×10^6 to 14.0×10^6 cells/mL regardless of the identity of the mAb candidate (Figure 1a). Cell lines expressing the *in silico* optimized variant showed considerable differences in growth characteristics that indicated clonal variances.[35,36] The cell viability was slightly higher in the case of stable CHO cell lines expressing the *in silico* optimized variant. Final antibody titers and specific productivity of the *in silico* optimized variant were substantially improved compared to the parental antibody (Figure 1(b,c)). More specifically, mean mAb titer of mAb2 achieved ~0.6 g/L, while the *in silico* optimized variant expressing clones yielded a mean titer of ~2.3 g/L. The mean specific productivity of investigated mAb2 clones was ~6.5 pg/(cell·day), while the mean specific productivity of the *in silico* optimized variant was ~23.5 pg/(cell·day).

To further test the enhanced performance of the *in silico* optimized variant in a microscale cultivation process, the top performing cell lines for both mAb candidates were cultivated in a fed-batch process using a 3 L benchtop bioreactor system. While growth characteristics and cell viability profiles were highly comparable (Figure 1(d)), final mAb titers and specific productivity differed substantially between the two cell lines either producing mAb2 (~1.0 g/L with 5 pg/(cell·day)) or the *in silico* optimized variant (~3.3 g/L with 17 pg/(cell·day)), accounting for a three-fold increase in both product titer and specific productivity (Figure 1(e,f)). Clonal stability was confirmed not to be the major causative for different performances (supplementary figure S1). Three of the five stable cell lines were identified to be phenotypically stable for at least 90 days regardless of the identity of the expressed mAb (data not shown).

Analysis of intracellular inclusions in mAb2-producing CHO cells via immunocytochemistry

The difficult-to-develop mAb2 was previously reported to accumulate in the lumen of an aberrant endoplasmic reticulum (ER) of stable CHO cell lines.[37] To test whether the sequence optimization of the *in silico* optimized variant affects the cell

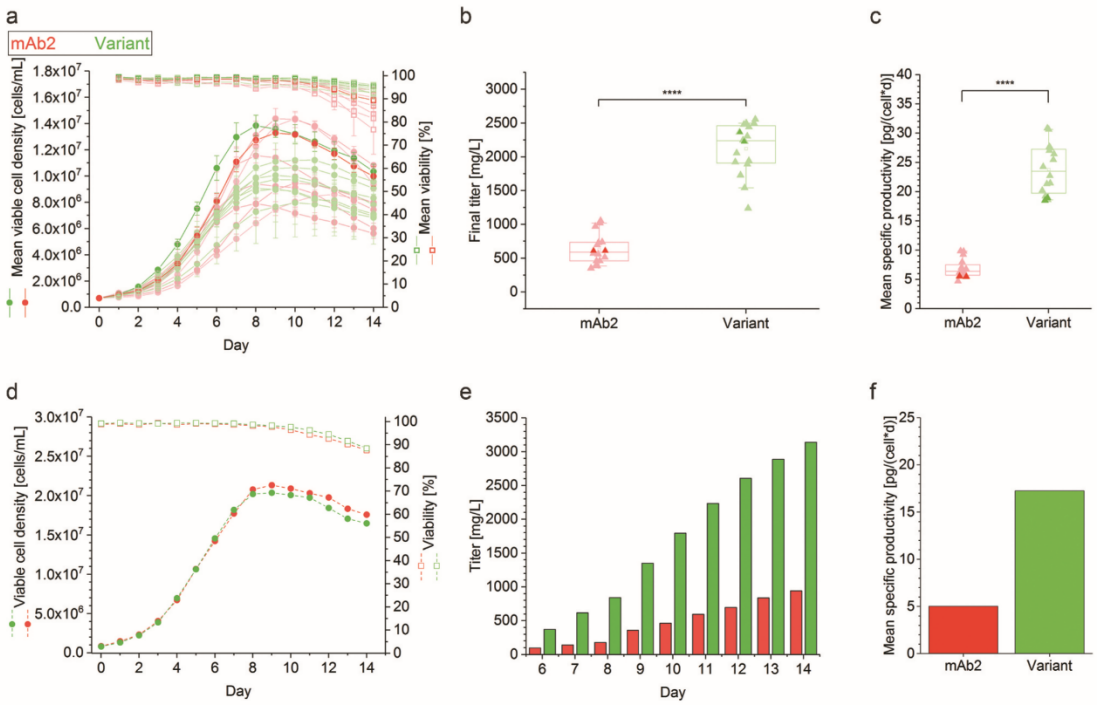

Figure 1. Cell culture performance of clonal cell lines producing either the mAb2 or its *in silico* optimized variant in controlled fed-batch production processes. (a) Viable cell density (VCD, filled circles) and viability (open square), and (b) final antibody titer and (c) mean specific productivity (filled triangle) of the top eight clonal cell lines are shown for a controlled 14-day micro-bioreactor fed-batch cultivation process (ambr^{TM} 15). In case of VCD and viability the mean and standard deviation of biological duplicates (n = 2) are displayed. Each replicate was used as single data point in the boxplot, and whiskers represent the 10th and the 90th percentile. The highlighted clones (thicker line and more intense color) were further investigated in 3 L benchtop bioreactors. An unpaired t-test confirmed statistical significance (****: $p < .0001$). (d) VCD (filled circles) and viability (open square), (e) cumulative antibody titer, and (f) calculated mean specific productivity of the best performing clonal cell lines in a controlled 14-day fed-batch cultivation process was performed in 3L bioreactors. The runs were performed without biological replicates, and antibody titer was determined starting from day 6. Clonal stability data can be found in Supplementary Figure S1.

morphology and intracellular mAb accumulation during expression, stable CHO cell lines were investigated using immunofluorescence microscopy. As expected, the good-to-express (GTE) reference mAb (producing >4.5 g/L under comparable conditions, supplementary Figure S2) was equally distributed in the cytoplasm of a highly productive reference cell line (Figure 2(a), supplementary Figure S3). In comparison, the mAb2-producing CHO cells were characterized by antibodies that accumulated in circular vesicles with a maximum diameter of ~2 µm. Interestingly, less pronounced vesicles were displayed in CHO cells that produced the *in silico* optimized variant. This was confirmed for five individually generated, single-clone-derived cell lines expressing either mAb2 or its *in silico* optimized variant (data not shown). To categorize and quantify CHO cells according to their morphologic appearance, a broad microscopic analysis of the respective cell populations was performed (Figure 2(b), supplementary Figure S4). The reference cells showed no accumulation of the GTE mAb, while more than 80% of the mAb2-expressing cells showed putative protein inclusions. Notably, the *in silico* optimized variant-expressing cells displayed a relieved phenotype in half of all stained cells.

The retention and intracellular accumulation of mAb2 are thought to be driven by a broken intramolecular disulfide bridge in the LC.[37] Therefore, the folding of mAb2 and its *in silico* optimized variant in CHO cells was investigated comparatively by coupling-free cysteines to PEG_{5000}-maleimide, followed by electrophoretic separation by western blotting-gel mobility shift assay. Interestingly, the *in silico* optimized variant was expressed in the cell with a significantly increased proportion of partly and completely folded antibody compared to mAb2 (Figure 2(c), supplementary figure S5), indicating that the *in silico* optimization supported the intracellular folding of the *in silico* optimized variant. mAb2 was not only particularly prone to accumulation in the lumen of the ER but also intracellular unfolding, creating a secretion bottleneck in mAb2-expressing CHO cells that was successfully alleviated by the introduction of the single amino acid substitution SL52R.

Antibody purification and product quality analysis

Progressing to the next step in the bioprocess value chain, increased antibody titer achieved in cell line and upstream development needs to fit with the constraints of the downstream processes.[38] Therefore, the purification of mAb2 and its *in silico* optimized variant was performed identically, in

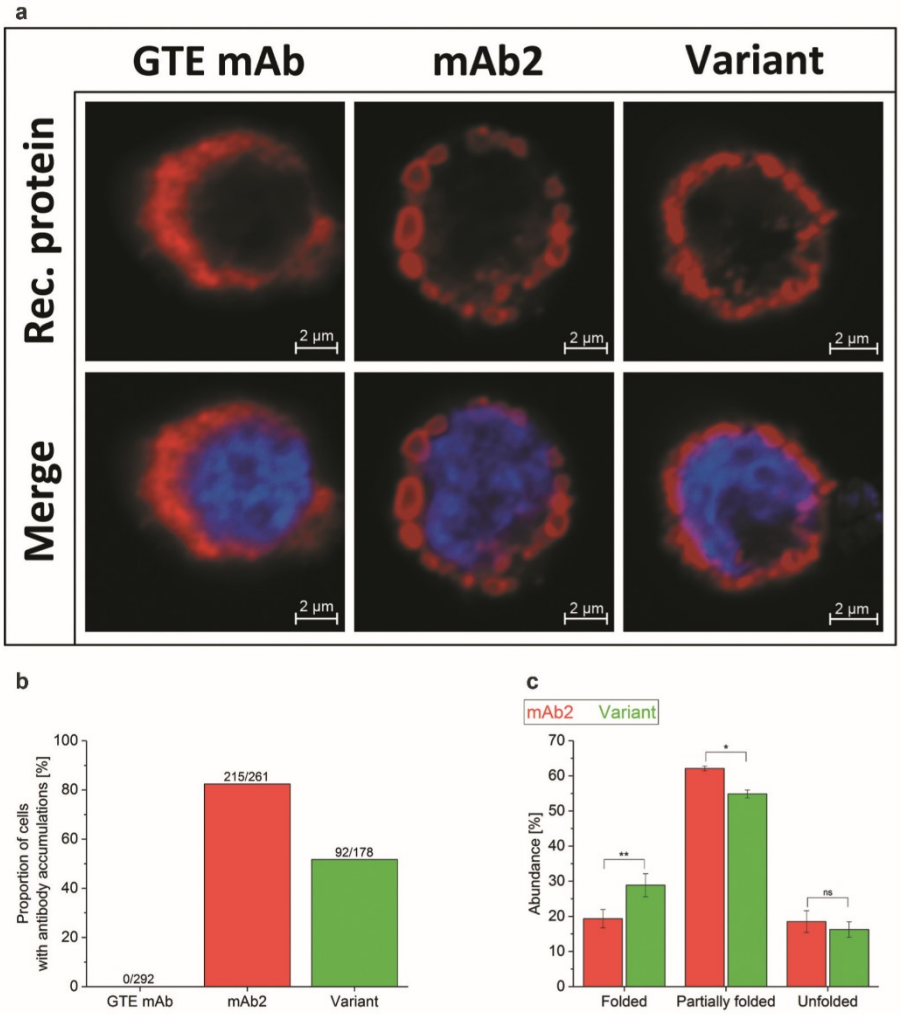

Figure 2. Investigation of CHO cells producing a good-to-express monoclonal antibody (GTE mAb) as reference, mAb2 and its *in silico* optimized variant. (a) Confocal images of cell lines producing the GTE mAb, mAb2 and the *in silico* optimized variant were acquired at a 63 x primary magnification. Additional information on productivity of the GTE mAb can be found in supplementary Figure S2. Nuclei and recombinant protein were stained using DAPI (blue) and a fluorescent secondary antibody (red). An overview can be found in supplementary Figure S3. (b) Ratio of single cells with intracellular antibody inclusions are shown for the total cell count. For visualization, cells have been cultured adherently for this analysis only. (c) The folding of free LC molecules (not bound to heavy chain) within the cell was analyzed densitometrically in three independent western blotting-electrophoretic mobility shift assays (supplementary Figure S5). An analysis of variance (ANOVA) determined statistical significance (*: $p < .05$; **: $p < .01$). M, Marker; ns, not significant.

accordance with a purification strategy widely applied in the pharmaceutical industry. Protein A affinity chromatography (AC) was conducted as a first purification step to capture the IgG and to remove process-related impurities such as host cell proteins and DNA. This was followed by an acidic treatment (AT) and depth filtration (DF) of the eluate to inactivate and remove any viruses. Next, anion exchange chromatography (AEX) was used to further remove DNA, host cell proteins, and leached Protein A. As expected, the content of HMW species was successfully reduced by DF and AEX (Figure 3(a–c)). Interestingly, the DS of wild type mAb2 contained higher levels of HMW species at each of the purification steps relative to the *in silico* optimized variant (Figure 3(a–c)). The HMW formation indicates strong aggregation of the product species, which reduced the product yield after separation. Furthermore, the *in silico* optimized variant exhibited a higher purity after elution from AEX (Figure 3(d)). The variant could be concentrated to 33 mg/mL via ultrafiltration/diafiltration (UF/DF), while visual investigation indicated mAb2 precipitation at concentrations above 15 mg/mL that correlated with a strong increase in HMW species (Figure 3(c)), as well as pressure and time required for ultrafiltration (data not shown). After UF/DF of both DSs into the formulation buffer and dilution to an anticipated mAb concentration of 10 mg/mL, the DS of the *in silico* optimized variant had a drastically reduced HMW content compared to mAb2 ($\Delta = -33.8\%$, Figure 3(c)). In

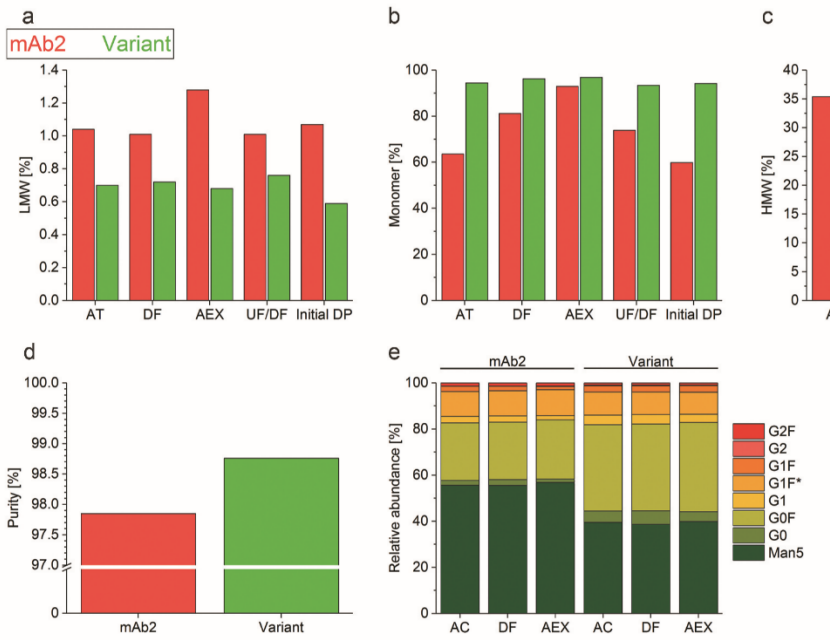

Figure 3. Characterization of the product quality after individual purification steps. (a–c) Low molecular weight – (LMW, A), high-molecular-weight species (HMW, C), and monomer (b) content of the drug substances of mAb2 and the *in silico* optimized variant were examined after individual purification steps by high-performance size-exclusion chromatography (HP-SEC). Acidic treatment, AT; depth filtration, DF; anion exchange chromatography, AEX; ultrafiltration/diafiltration, UF/DF; and initial drug product, initial DP. (d) The purity of the AEX-polished drug substance was determined by employing capillary electrophoresis on a Caliper. (e) The glycosylation profile of the drug substances was analyzed after protein A affinity chromatography (AC), DF and AEX by Caliper glycosylation analysis. G1 F* represents the second naturally existing glycan isomer of G1F. Man5, mannose-5; G, galactose; F, fucose.

summary, the *in silico* optimized variant was purified with an acceptable level of purity (98.8%) and a lower HMW content (5.2%) by applying a typical platform purification process, while the same process required significantly more development effort in the case of mAb2 (purity 97.9%, HMW 39.0%) to achieve an acceptable product quality and economically profitable yield.

Despite sharing identical glycosylation sites in their sequences, both mAbs were characterized via lab chip (caliper) analysis to test whether the heterogeneous N-glycosylation pattern was affected by differences seen in the CHO cell morphology, as well as upstream and downstream development processes (Figure 3(e)). We found that the basic core structure of mAb2 bore predominantly mannose-5 (~55%), while the *in silico* optimized variant was slightly more galactosylated and fucosylated into more complex oligosaccharides ($\Delta_{\text{relative abundance}}$ variant – mAb2: −17% Man5; +3% G0; +2% G1; +12% G0 F). Additionally, the glycosylation profile of mAb2 expressed by three cell clones was more variable when compared to the *in silico* optimized variant-producing clones (supplementary Figure S6). Notably, the N-glycosylation profiles of both mAb candidates were not altered during the downstream purification process (Figure 3(e)).

Biophysical characterization of the formulated protein

Physical and chemical instabilities of biopharmaceuticals can be an obstacle to development.[39,40] The above described *in silico* optimization of mAb2 was designed to diminish the APR to increase the colloidal stability, but it also applied the empirical force field FoldX to maintain the conformational stability. Differential scanning calorimetry (DSC) measurements of the multi-domain IgG indicated that the amino acid exchange SL52 R did not affect the heat-induced unfolding of the antigen-binding (Fab) domain, resulting in a consistent Fab T_m (Figure 4(a)). Moreover, the mutation did slightly alter the additional heat absorption peaks corresponding to the denaturation of further domains such as C_H2 and C_H3.

$$\Delta T_m Fab = T_m Fab(variant) - T_m Fab(mAb2) = 87.8\ ^\circ C \pm 0.1 - 88.1\ ^\circ C \pm\ 0.1 = -0.3\ ^\circ C \quad (1)$$

The relative conformational stability of both mAbs was additionally tested by intrinsic fluorescence (IF) measurements. Again, the *in silico* optimized variant exhibited a relatively similar Fab melting temperature (Fab T_m = 86.6°C ± 0.0) to mAb2 (Fab T_m = 87.2°C ± 0.0) (Figure 4(b)). The differences in the temperature-dependent fluorescence signal pointed toward an altered accessibility of aromatic residues between both mAbs. To summarize, the folding stability of the antibody was maintained after a computationally guided exchange of a single amino acid (SL52R) in the variable region of the LC. Therefore, this bioinformatic approach supports the identification of conformationally stable sequence variants with an improved probability of success for stabilizing the protein in a formulation buffer.

To further investigate the interplay of denaturation and aggregation, i.e., breakage of intramolecular and formation of

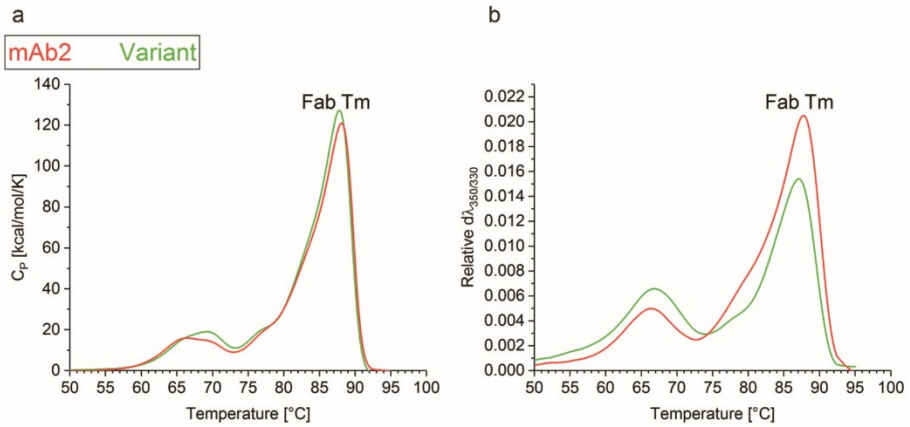

Figure 4. Thermal stability of the drug products. (a) Differential scanning calorimetry (DSC) and (b) Intrinsic fluorescence (IF) measurements indicated the thermal unfolding of mAb2 (red) and the *in silico* optimized variant (green). The change in (a) heat capacity and (b) first derivate of the fluorescence ratio indicate the T_m of the Fab.

intermolecular interaction, the aggregation temperature T_{agg} was assessed via light scattering simultaneous to IF measurement.[41] Strikingly, the T_{agg} of the *in silico* optimized variant (T_{agg} = 67.6°C ± 0.0) clearly exceeded that of mAb2 (64.7°C ± 0.2) (Figure 5(a)), underlining the variant's increased resistance to heat-induced aggregation. The increased T_{agg} of the *in silico* optimized variant expressed in stable CHO cell lines confirmed a similar trend reported for the analogs *in silico* optimized variant expressed transiently.[6] The computationally predicted strong self-association/-aggregation tendency of mAb2 was experimentally confirmed by an exponentially increasing diameter between 2 and 10 mg/mL, while that of the *in silico* optimized variant increased linearly (Figure 5(b)).

Long-term stability study of the formulated DP

Pharmaceutical stability testing is a routine procedure performed on DPs at various stages of the development process to assure an acceptable level of quality throughout a period covering the production, supply, storage, and utilization of the last unit of the product by the patient.[42] Here, mAb2 and its *in silico* optimized variant were investigated in real-time and in accelerated stability studies. In the case of the real-time stability study, the DPs are exposed to environmental conditions that cover the normal life cycle of the pharmaceutical by refrigeration (2–8°C) for a defined time period. In contrast, the accelerated stability study stresses the DPs by incubation at room temperature (25°C) or 40°C to accelerate aggregation/degradation processes and predict shelf lives.[43] Samples were taken initially and at analytical time points (ATP) after storage of one month, three months, and six months, and preservation of pH, osmolality, and protein concentration was controlled. The target parameters of the DP (pH 6.0, range of osmolality, c(API) = 10 mg/ml) were met after final formulation of both mAb candidates, and pH and osmolality were stable during the test period (data not shown).

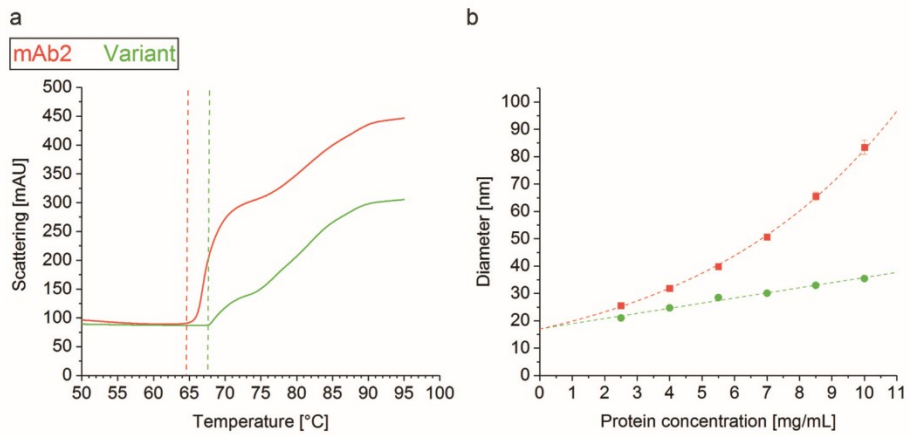

Figure 5. Colloidal stability of the drug products. (a) The aggregation temperature T_{agg} was determined simultaneously with the intrinsic fluorescence (IF) measurement by detection of dynamic light scattering (DLS). (b) DLS analysis unraveled an exponential increase of the mAb2 diameter within a protein concentration of 2–10 mg/ml, but a linear correlation in case of the *in silico* optimized variant.

The product quality, and in particular the particle formation, was monitored throughout the real-time and accelerated stability studies via a broad panel of diverse techniques comprising nephelometry, micro-flow imaging (MFI), high-performance size-exclusion chromatography (HP-SEC), and visual inspection (VI). The relative opalescence of proteins at a given concentration and formulation correlates with the nature of solute-solute and, associated therewith, solid-light interactions.[44] The opalescence of mAb2 was significantly higher than that of the *in silico* optimized variant at every ATP in both, real-time and accelerated stability studies, confirming the enhanced self-association/-aggregation tendency of mAb2 (Figure 6(a)). The striking decrease of opalescence with storage time indicates, inter alia, changes of the particle sizes over time. During storage of the DP of mAb2, subvisible particles were formed in various size ranges (≥ 25 µm < 1000 µm, Figure 6(b); ≥ 2 µm < 1000 µm, ≥ 10 µm < 1000 µm, supplementary Figure S7), presumably affecting the sedimentation tendency of the particles.

We found that the initial DP of mAb2 formed a significantly increased proportion of HMW species (12%) relative to the *in silico* optimized variant (2%). The HMW content of both mAbs was reduced after the initial time point and did slightly decrease further after storage for six months (Figure 6(c)). It is worth mentioning that this method predominantly detects oligomers ≤2 µm since the progressively formed particles with sizes of tens to hundreds of micrometers (Figure 6(b), supplementary Figure S7) are pre-filtered prior the SEC column. Moreover, the LMW species of mAb2 (12%) clearly exceeded that of the *in silico* optimized variant (1%) at the initial ATP, and increased stronger during six-month storage at elevated temperature (mAb2: Δ 4%, variant: Δ −1%) (supplementary Figure S7). Increasing HMW and LMW species resulted in a significant decrease in mAb2 monomers over time (Δ – 2%) relative to an unchanged monomer content of the *in silico* optimized variant (Δ 0%) (supplementary Figure S7). Visual inspection (VI) of the liquid formulations filled in glass vials confirmed this trend. The DP of mAb2 contained visible particles at the initial ATP, and particle formation was substantially triggered during storage at 25°C and 40°C. In contrast, the DP of the *in silico* optimized variant showed no visible particles after filling, and particles were only detected after storage for three months at 40°C. Additionally, the DP of the *in silico* optimized variant was characterized by a dramatically reduced color intensity and opalescence relative to the DP of mAb2 (Figure 6(d,e)).

Another challenge encountered in drug development is high viscosity of the concentrated DP, which often results from higher-order intermolecular interactions and non-native aggregation.[45] In this study, the rheological properties of the DPs could only be tested up to a protein concentration of 10 mg/ml due to the remarkably strong precipitation of mAb2 upon further concentration in UF/DF, an effect that was not observed for the *in silico* optimized variant. At this

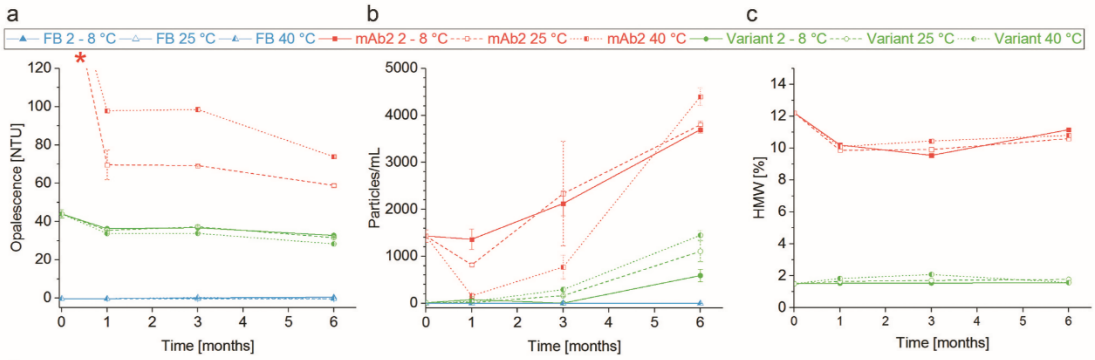

d

		Opalescence	Color	Visible particles			
				initial	1 mo	3 mos	6 mos
2-8°C	FB	-	-	no	no	no	no
	mAb2	+++	+	many	many	few	many
	Variant	+	++	no	no	no	few
25°C	FB	-	-	no	no	no	no
	mAb2	+++	+	many	many	many	many*
	Variant	+	++	no	no	few	few
40°C	FB	-	-	no	no	no	no
	mAb2	+++	+	many	many	many	many*
	Variant	+	++	no	no	few	many

e

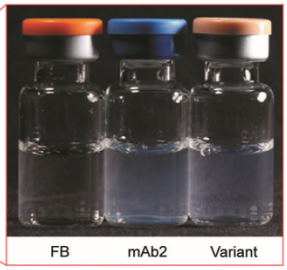

Figure 6. Product quality and colloidal stability of the drug products (DPs) during storage study. (a) Opalescence of the DPs and the formulation buffer was determined nephelometrically at a wavelength of 633 nm. * Initial mAb2 samples and samples stored at 2°C exceeded the calibrated range of the nephelometer (120 NTU). FB, Formulation buffer (25 mM Na-citrate, 125 mM NaCl, pH 6.0). (b) Particles with a size between ≥25 µm and <1000 µm of DPs and formulation buffer were quantified per ml using micro-flow imaging (MFI). (c) The proportion of high-molecular-weight (HMW) species in the DPs was examined by running high-performance size-exclusion chromatography (HP-SEC). (d) Samples were visually inspected concerning opalescence, color intensity and presence of particles. *Filamentous particles. (e) Example image of DPs and formulation buffer stored in glass vials for three month at 25°C.

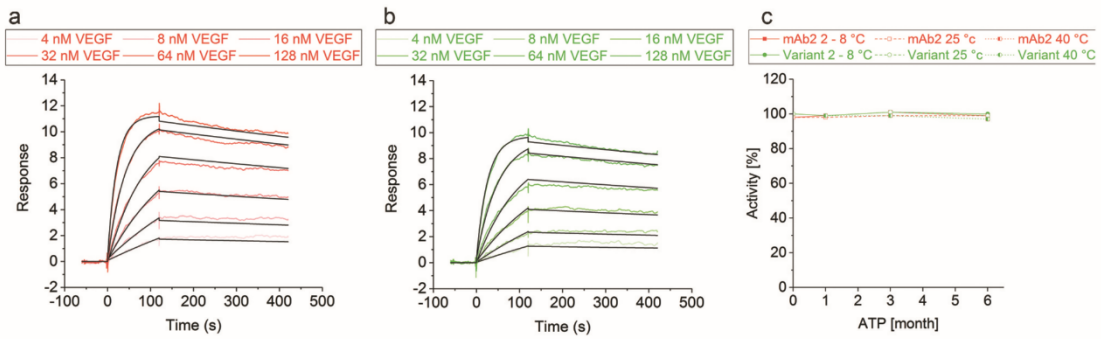

Figure 7. Vascular endothelial growth factor binding activity of mAb2 and its *in silico* optimized variant. Binding kinetics of a concentration series of vascular endothelial growth factor (4, 8, 16, 32, 64 and 128 nM) to immobilized (a) mAb2 and (b) the *in silico* optimized variant was measured. Double-referenced curves were fitted to a 1:1 binding model (black line). (c) Binding of the initial drug product (DP) of mAb2 to vascular endothelial growth factor was measured by SPR, and the response was set to 100%. The activity of all other samples was compared in percentage difference to that of the initial mAb2 DP. SEC indicated that aggregates of mAb2 are resolved in SPR buffer (data not shown).

Table 1. Antibody-antigen binding kinetics: association and dissociation rate constants and equilibrium dissociation constant (K_D).

	k_a [M^{-1} s^{-1}]	k_d [s^{-1}]	K_D [M]
mAb2	$3.66 \cdot 10^{-5}$	$4.05 \cdot 10^{-4}$	$1.11 \cdot 10^{-9}$
Variant	$3.03 \cdot 10^{-5}$	$3.75 \cdot 10^{-4}$	$1.24 \cdot 10^{-9}$

moderate mAb concentration of the DPs, a comparable viscosity (mAb2: 1.75 mPas s ± 0.08; variant: 1.51 mPas s ± 0.08 at 20°C) was detected at the initial ATP, which increased slightly during storage at elevated temperatures (supplementary Figure S8).

Functional characterization of the formulated DP

During sequence optimization, it can be challenging to replace critical amino acid residues to improve the CMC properties while also maintaining the mAb's target affinity. *In silico* analysis of the mAb2-vascular endothelial growth factor (VEGF) co-structure (PDB ID: 2FJF)[46] recommended the exchange of a single amino acid in LCDR2 that did not contribute to target binding. Preservation of the *in silico* optimized variants affinity to VEGF was verified by determining the binding kinetics via surface plasmon resonance (SPR) spectroscopy. The equilibrium dissociation constant (K_D) of both DPs was in the low nanomolar range qualifying the *in silico* optimized variant to bind VEGF with a similar high affinity as seen for mAb2 molecule (Figure 7(a,b); Table 1).

Storage of both DPs for up to six months at 2–8°C, 25°C and even at 40°C did not alter the activity that was assessed via SPR binding experiments (Figure 7(c)). This finding confirmed that the *in silico* optimized variant maintained its expected biological activity, which is fundamentally important for the product's shelf life.

Discussion

MAbs of the same subtype differ greatly in their biophysical and CMC properties even though they share a high sequence identity, except in the affinity-mediating variable domain.[12,16,45,47] In particular, physical and chemical instability of biopharmaceuticals in aqueous solutions is a major obstacle that must be overcome during the development of a formulation to avoid significant delay or even termination of programs.[10,16] The promising approach of bioinformatics has greatly advanced over the past decade, and can now predict biophysical characteristics of a mAb candidate based on its primary sequence early on, without the need for material. The extremely high speed, low costs, and versatile and automatable performance of computational tools enable characterization of a large set of sequence variants, and selection of the most promising candidates predicted to have superior overall CMC properties early in the discovery phase.[6,16,48] However, there is currently still little knowledge of how the *in silico* optimization of a biotherapeutic performed at the discovery stage will translate into bioprocess development comprising cell line, upstream, downstream, and development of a formulation.

In this study, a difficult-to-develop antibody (mAb2) and the *in* silico optimized variant thereof, which only differs in one (SL52R) of ~650 amino acids per heavy-light chain pair, were developed in accordance with an industrial antibody manufacturing process. Remarkably, stable mammalian CHO cell lines produced the *in silico* optimized variant with a three-fold increased antibody titer without impairing cell growth or viability. Enhanced performance of mammalian cell lines producing antibody variants with improved biophysical properties was similarly reported for different mAbs.[6,16,49] Obviously, improved biophysical properties of an antibody candidate are not only beneficial extracellularly but also support antibody biosynthesis, modification, folding and secretion, causing significantly different expression rates.[50] The intracellular accumulation of mAb2 represented a bottleneck[37] that was mitigated in cells producing the *in silico* optimized variant. Similarly, the formation of intracellular aggregates of another antibody within the ER of HEK293 cells was affected by an amino acid substitution in the LC CDR1.[51] We were further able to show that the recovered cell morphology was accompanied by a more complex N-linked glycosylation pattern of the *in silico* optimized variant that potentially affects the biological activity, protein folding, conformation, stability,

solubility, secretion, pharmacokinetics, and antigenicity.[52] However, both mAbs shared a relatively high level of immature mannose structures potentially causing undesirable elevated clearance from blood[53-55] while improving potency by enhanced antibody-dependent cell-mediated cytotoxicity.[55-57]

After each step of the downstream purification process, the *in silico* optimized variant consistently contained less HMW species, i.e., more monomeric product, which supports the hypothesis that antibody candidates with reduced aggregation tendency can be purified with a higher monomer content.[12,16] It was previously shown that subtle changes in the amino acid sequence of the mAb largely affect the clearance of interacting host cell proteins such as enzymes,[58] capable of causing particle formation in the DP via self-assembly of host cell proteins or degradation products of enzymatically digested excipients such as polysorbates.[59] The simultaneously reported reduction of viscosity[12,16] was confirmed by successful ultrafiltration of the *in silico* optimized variant, while mAb2 was non-processable into highly concentrated liquid formulations (HCLF) without additional development efforts.[60] It can be reasonably assumed that viscosity differences between mAb2 and the variant would be even more pronounced if the DP could be concentrated to the range of 100–200 mg/mL, further strengthening protein–protein interactions, and therefore the associated opalescence, protein aggregation, and viscosity.[45] Notably, the viscosity of a concentrated protein solution represents a major challenge in attaining feasible manufacturing processes such as UF/DF, sterile filtration, as well as during fill and finish, which necessitates a closer link between formulation studies and manufacturing.[61,62] Additionally, current trends lean toward HCLFs to enable subcutaneous and intravitreal administration via thin needles that require low viscosity DPs.[45,61]

Our bioinformatic approach guided the modification of another difficult-to-develop mAb, and successfully reduced the viscosity of the HCLF (supplementary Figure S9). The final product titers of this mAb were also enhanced (from 1.5 g/L to >5.5 g/L) by expression in stable CHO cell lines cultivated in a standard fed-batch process (supplementary Figure S9). Remarkably, the single amino acid exchange did not affect the biological activity but increased the aggregation onset temperature (T_{agg}), which translated into a reduced aggregation tendency.[6]

The early research stage of biotherapeutics development typically involves the study of a large number of potential candidates, although limited samples of each are needed.[16] Once the antibody lead passes through the discovery phase, the sequence is virtually "locked", precluding subsequent changes that might help to overcome later occurring development issues.[16,63] This study emphasizes the substantial and not yet fully exploited potential of *in silico* tools to identify and optimize developable/manufacturable therapeutic mAb candidates based on sequence-structural properties.[16] Attractively, bioinformatics investigations are cheap to implement, fast to conduct and applicable to all stages of biological drug discovery, reducing the risk of failure at later stages due to, for example, formulation issues.[13,16] We evaluated the molecular properties of an aggregation-prone mAb by using a simple aqueous formulation buffer (25 mM Na-citrate, 150 mM NaCl, pH 6.0) that lacked additive agents often required to stabilize liquid protein formulation of mAbs.[10] Moderately aggregation-prone antibodies can alternatively be formulated using a more sophisticated buffer to meet safety and efficacy requirements.[6] However, a universal strategy for the DP stabilization is excluded by the diversity of antibody drug candidates, which is characterized by a complex and individual interplay between CDR and framework regions,[64] making the identification of the most appropriate additive(s) a time-consuming, resource-intensive, trial and error process.[10] The limitations of a classical wet-lab approach increase the attractiveness of an *in silico* based complement for the selection and design of molecules that combine biological activity with developability to reduce the costs and time to market.

The superior developability of the *in silico* optimized variant produced by stable cell lines fit well with previous findings on the transiently expressed analog.[6] Particularly striking for the consistent trend observed for transiently and stably produced material, the colloidal stability of the *in silico* optimized variant was likewise increased as indicated by a higher initial monomer content and decelerated monomer loss over time.[6] Furthermore, the herein determined biological activity confirmed previously conducted microscale thermophoresis and SPR binding experiments.[6] The good interplay between both studies qualifies transient material for an early screening of *in silico*-designed antibody variants concerning biological activity combined with manufacturability, paving the way for routine testing of *in silico* optimized sequences using transient expression systems early in the process chain.[12,36,49] Subsequently, only the most promising candidates move into full cell line development campaigns. As a consequence, the successful combination of *in silico* tools with robust bioprocess development platforms will be key for future advancement within the inherently complex field of biopharmaceutical development, helping to bring innovative therapeutics to patients more quickly.

To estimate the benefit and success of bioinformatics on the development of biologicals in even higher detail, several limitations and aspects need to be addressed in future studies. These key aspects include: 1) the need for larger and more heterogeneous sets of experimental data that can be fed-back to train the computational counterpart; 2) the expansion from standard IgG to structural diverse formats, such as non-IgG-derivatives, nanoparticles, viruses; 3) the consideration of post-translational modifications such as glycosylation; 4) the extension of computational predictions, for example, on charged and hydrophobic patches that are associated with viscosity;[12] and 5) *in vivo* studies and safety investigations of in silico optimized candidates.

In conclusion, this study showed that an exemplarily in silico optimized variant of the difficult-to-develop antibody mAb2 possessed enhanced biophysical properties, such as an improved colloidal stability. Further, long-term storage of the investigated DP formulations confirmed reduced opalescence and particle formation. In silico prediction and optimization of mAb2 substantially enhanced its manufacturability throughout the entire production process from cell line development and cell culture-based production, downstream purification, to final formulation and storage, without negatively affecting product quality or binding capacity. This study emphasizes the great and not yet fully exploited potential of bioinformatics

to facilitate the lead generation, optimization, development, and manufacturing of biotherapeutics. Complementary approaches combining high-throughput computational tools and automated experimental studies hold great potential for a more successful but less burdensome discovery of promising drug candidates. A valuable side effect of this hybrid strategy is the mutual generation of a multidimensional database combining computational and experimental data that can be used to further train bioinformatic predictions of the candidate's developability, manufacturability, and fit to platform processes. This approach will thereby help to reduce failures during development activities and support the reduction of project timelines and resources.

Materials and methods

Mutant design

The *in silico* analysis of the therapeutic mAb was previously described in detail.[6] APRs were identified using TANGO,[33] the crystal structure of mAb2 (PDB ID: 2FJF)[46] was prepared for analysis using YASARA Structure,[65] and finally prepared and analyzed using FoldX force field.[34] The *in silico* optimized variant distinguishes from mAb2 in a single amino acid (SL52R) that was predicted by a computational analysis called mutant aggregation and stability spectrum (MASS).[66]

Generation of stable antibody-producing CHO cell lines

For the generation of stable CHO production cell lines expressing the investigated mAbs, the Boehringer Ingelheim (BI) glutamine synthetase (GS) deficient BI-HEX® CHO-K1GS cell platform was used. In brief, suspension-adapted CHO-K1GS host cells were transfected with a plasmid comprising both the respective antibody heavy chain (HC) and LC genes and the GS gene. Stable cell pools selected in glutamine-free medium were subjected to single cell cloning (SCC) into 384-well plates using fluorescent-activated cell sorting on a FACSAria™ Fusion cell sorter (BD Biosciences). Automated high-throughput microscopy was routinely performed on days 0, 7, and 14 post SCC using a Cellavista™ imaging system (Synentec bio Services) to ensure monoclonality. Based on cell growth and mAb productivity, the best performing monoclonal cell lines were further expanded from 384-well plate to 96-well plate to 6-well plate (cultivated statically), thereby gradually reducing the number to eight clones per investigated mAb. After upscaling, cell lines were routinely cultured in BI proprietary glutamine-free and chemically defined media. Unless otherwise stated, the cultivation was performed in shake flasks (Corning) in an orbital, non-humidified incubator shaker (Infors) at 36.5°C, 5% CO_2 and agitation at 120 rpm (50 mm orbit). Cell cultures were seeded at 4.0×10^5 viable cells per mL and passaged every 2–3 days. Viable cell concentration was assessed using a Cedex HiRes Analyzer™ (Roche Diagnostics) by means of trypan blue exclusion.

Fed-batch cultivation

To investigate bioprocess performance, the eight best stable clones of each investigated mAb were subjected to controlled fed-batch cultivation using an advanced micro bioreactor system ambr™ 15 (Sartorius Stedim). Further, the most representative clones producing either mAb2 or the *in silico* optimized variant were additionally evaluated in a 3 L benchtop scale bioreactor. Briefly, cells were seeded at 7.0×10^5 cells/mL in production medium and fed daily with 30 mL/L of culture start volume starting from day one using BI proprietary feed medium. Glucose levels were adjusted to 5 g/L if determined <3 g/L via glucose bolus addition. Cell concentration and viability were analyzed each day using a Cedex HiRes Analyzer™ (Roche Diagnostics) by means of trypan blue exclusion. Glucose and lactate concentrations were determined daily using a Biosen C-Line System (EKF Diagnostics), and pH and pO_2 were analyzed daily using a RAPIDLab®248 system (Siemens Healthcare). Determination of mAb concentration was started on day 6 by biolayer interferometry (BLI) on an Octet® HTX system (Pall Life Science). For BLI analytics, respective Protein A labeled sensors were equilibrated in cell culture medium before measurement. Sensor regeneration was performed in 10 mM glycine at pH 1.5 between each measurement. A standard curve of the respective antibody was used to calculate the product concentration in the culture supernatant.

Immunocytochemistry

Investigated single clone-derived CHO cell lines were cultivated in suspension using BI proprietary chemically defined media until day 4, and either directly fixed or additionally cultivated adherently in Nunc™ Lab-Tek™ II Chamber Slides™ using Ham´s F-12 Nutrient Mixture supplemented with 1% of fetal calf serum (Sigma Aldrich) for 48 h. Cells were fixed with 4% paraformaldehyde. Following a permeabilization step using 0.1% TritonX-100, samples were blocked and incubated with an appropriate dilution of antibodies for 1 h. The directly Dylight® 550-labeled antibody (#ab98620, abcam) used for HC detection of the recombinantly produced proteins was diluted 1:50. Isotype controls were diluted accordingly. Nuclei were counterstained with 4′,6-Diamidin-2´-phenylindol (DAPI, Sigma-Aldrich). After staining, samples were mounted with Prolong® Diamond Antifade Mountant medium (Invitrogen) and analyzed. Pictures were acquired with a Zeiss LSM 710 confocal microscope equipped with a 405 nm, and 561 nm laser (Carl Zeiss). A GTE antibody-producing cell line was used as reference.

Intracellular recombinant protein folding analysis

The intracellular formation of intra-domain disulfide bridges of the antibodies LC was quantified as previously described.[37] Respective CHO cells were lysed for 30 min on ice by addition of lysis buffer (1% TritonX 100 (v/v), 50 mM Tris(hydroxymethyl)-aminomethane (Tris), 150 mM NaCl, pH 7.5) supplemented with either 20 mM PEG_{5000}-maleimide (Sigma Aldrich) or N-ethylmaleimide (Alfa Aesar). After centrifugation, free kappa LC was immunoprecipitated from the supernatant by a previously desthiobiotinylated (DSB-X Biotin Protein Labeling Kit, D20655, Thermo Fisher Scientific) murine antibody (MAB8461, Abnova). Samples were incubated overnight at 4°C on a rotary shaker.

Equilibrated Pierce™ Streptavidin Plus Ultralink™ Resin (Thermo Fisher Scientific) was added, and samples were further incubated for 1 h at 4°C. The beads were washed three times with ice-cold lysis buffer. Subsequently, the beads were separated via SDS-PAGE using NuPAGE® 4–12% or 10% Bis-Tris Gels (Invitrogen) and transferred to a nitrocellulose membrane using the iBlot® 2 dry blotting system (Invitrogen). The antibody used for LC detection (#K3502, Sigma Aldrich) and the secondary IRDye®800CW-labeled donkey anti-mouse antibody (#925-32212, LI-COR) were added to the membrane and detected by conducting the Odyssey Infrared Scanning System (LI-COR). Three independent western blots were analyzed densitometrically based on pixel intensity using Image Studio Software Version 5.2.5 (LI-COR).

Antibody purification

The mAbs were purified similarly in accordance with a state-of-the-art strategy commonly used in the pharmaceutical industry.[67,68] The mAbs were isolated using a Protein A capture chromatography, separated from viruses by employing a low-pH virus inactivation and filtration step, and further purified by conducting a sequential AEX. Subsequently, tangential flow filtration was applied to concentrate the bulk DS to a mAb concentration of >15 mg/mL and diafilter (Sartorius)[69] using a 30 kDa nominal molecular weight cut off polyethersulfone membrane (Sartocon Slice 200, Sartorius) into the formulation buffer (25 mM sodium citrate, 125 mM sodium chloride, pH 6.0).[70]

Product quality assessment

The purity and glycosylation profile of the DSs were analyzed by capillary electrophoresis (Caliper Life Sciences, PerkinElmer). Sample preparation was performed according to the instructions of the manual using the Protein Express Kit and Sample Buffers (PerkinElmer). Relative fluorescence of each sample was measured for 45 sec. and evaluated using the LabChip GX software (PerkinElmer). LMW, HMW, and monomer species were separated by SEC (TSK-Gel G3000SWXL, TOSOH Bioscience). An HP chromatography system (Waters) running buffer (50 mM Tris HCl, pH 7.4, 150 mM NaCl) at a flow rate of 1 mL min^{-1} was used. A KrudKatcher Classic (Phenomenex) in-line filter with a pore size of 2 µm was installed before the column. Samples were diluted to a protein concentration of 5 mg/mL by addition of running buffer, and 6 µL of the prepared sample was injected. The UV absorption was detected at a wavelength of 280 nm using the UV/VIS-detector 2489 (Waters), and relative areas of LMW, monomer, and HMW peaks were quantified using Empower Pro 2.0.

Stability studies of formulated DP

The mAb solutions were filtered using a 0.22 µm sterile filter membrane (Rotilabo, Carl Roth GmbH & Co. KG), diluted to a mAb concentration of 10 mg/mL by addition of formulation buffer, and 2 mL were filled into 2 R clear glass type I vials. The samples were characterized initially and rubber stopper sealed vials were placed upright in stability chambers that were temperature-/humidity-controlled at 2–8°C/unspecified relative humidity (RH), 25°C/60% RH and 40°C/75% RH. Samples were analyzed at ATP after storage for one, three, and six months.

UV-vis absorption spectroscopy

Protein concentration was determined via the SoloVPE spectrophotometer (C Technologies), which measures the absorbance at a wavelength of 280 nm and applies a scattering correction at 320 nm. The theoretical molar extinction coefficient of the mAb2 wild type coincides with that of its *in silico* optimized variant (215,380 M^{-1} cm^{-1}).

Osmolality and pH assessment according to pharmacopeia

The osmolality and pH of the samples were examined by running the Osmomat 3000 (Gonotec) and Seven2Go pH meter (Mettler Toledo), respectively, previously equilibrated with buffers of pH 4.0 and pH 7.0 (Mettler Toledo).

Visual inspection of formulated DP

The DPs were visually investigated for particles by a trained personal at an illuminance level of 2000–3750 lx. The presence of particles was then categorized. Moreover, the opalescence of the DP was characterized quantitatively and qualitatively (none, -; weak, +; medium, ++; strong, +++), and the color intensity was assessed by visual comparison to BY color standards. Photographic images of each sample were taken with an EOS 700D (Canon).[71]

Nephelometry

Opalescence was measured nephelometrically at a wavelength of 633 nm via a BI-internal custom-built photospectrometer equipped with a right-angle laser light scatter setup analyzing the scattered light. The instrument was calibrated with StablCal Standard of 20 NTU and 100 NTU stabilized formazin opalescence solutions (Hach Lange).

Micro-flow imaging

Protein solutions were tested for the presence of sub-visible particles that were quantitatively characterized by the MFI system DPA4200 (Brightwell Technologies). The system was flushed with particle-free water before each sample analysis to provide a clean baseline. Samples of 0.6 mL with a pre-run of 0.2 mL were analyzed at a flow rate of 0.17 mL/min and a fixed camera rate.[71] Images were processed by the MVAS software (Version 1.4.0, Brightwell Technologies) to extract each particle and its characteristics, including size, shape, transparency, and an individual image.[72]

Rheology

The viscosity of 200 µL samples was rheologically determined by the HAAKE MARS III rheometer (Thermo Fisher Scientific) equipped with 35 mm titanium cone with an angle of 1°. The protein solutions were sheared at 20°C for 100 s at a constant rate of 1000 s^1, with measurements averaged over 1-s intervals. Similarly, the temperature-dependence was investigated in the interval between 4°C and 40°C.

Dynamic light scattering

Samples were filtered (0.8 µm) and diluted to a final protein concentration of 10.0, 8.5, 7.0, 5.5, 4.0, and 2.0 mg/mL by addition of formulation buffer. DLS measurements were performed in triplicates using the DynaPro Platereader II (Wyatt). Ten acquisitions were taken per sample using a laser at a wavelength of 830 nm and detecting the scattered light at an angle of 158°. The apparent hydrodynamic radius of diluted spherical particles was calculated using the Stoke-Einstein-Equation and plotted versus the protein concentration.

In vitro functional characterization of the DP

SPR spectroscopy was used to investigate the binding activity of mAb2 and its *in silico* optimized variant to their antigen (VEGF). All experiments were conducted using a Biacore T200 System equipped with a Protein A sensor chip (GE Healthcare). The Protein A Chip was conditioned for 30 s running a 10 mM Glycine buffer (pH 1.5) at a flow rate of 50 µl/min. For the SPR binding experiments, a 1 µg/ml antibody solution was injected for 120 s at a flow rate of 10 µl/min, followed by loading of a 10 µg/ml antigen solution for 120 s. Binding kinetics were determined by injection of 0.5 µg/ml antibody for 12 s at a flow rate of 10 µl/min, followed by a 120 s injection of an antigen concentration series at a flowrate of 50 µl/min. The resulting double-referenced curves were fitted to a 1:1 binding model. After each measurement, the chip surface was regenerated by injection of 10 mM Glycine (pH 1.5) for 30 s at 50 µl/min.

Nano scanning fluorimetry

Intrinsic fluorescence (IF) and light scattering measurements were performed using the Prometheus NT.48 fluorimeter (Nano Temper Technologies GmbH) equipped with standard capillaries. The onset (T_{on}), melting temperature (T_m) of unfolding, and the onset temperature (T_{agg}) of aggregation were determined in triplicates by applying a heating rate of 1° C/min between 20°C and 95°C.[41] Protein unfolding was obtained from the ratio of the intrinsic fluorescence signal at wavelengths 350 and 330 nm as a function of temperature. The T_m was calculated as local maxima of the first derivative curves using the ThermControl software (version 2.1.1). Aggregation was simultaneously recorded via light scattering at 385 nm. The T_{agg} was determined as the onset point of a two-state fit via the ThermControl software (version 2.1.1).

Differential scanning calorimetry

The MicroCal PEAQ-DSC automated calorimeter (Malvern) was used to characterize the unfolding of proteins in solutions that were diluted to 2 mg/mL by addition of formulation buffer. Thermograms were recorded in duplicates between 10°C and 95°C at a heating rate of 1°C/min using the MicroCal PEAQ-DSC software (version 1.30). Subsequently, the baseline was subtracted and the melting temperatures (T_m) of denaturation evaluated as the maxima and the integral of the specific heat capacity Cp plotted against the temperature.

Acknowledgments

This research was supported by Christian Heinz, Torben Langer, Joey Studts, Annika Held, Patrick Schulz, Ingo Gorr, Harald Bradl, Angela Koller and Kerstin Walke from Boehringer Ingelheim Pharma GmbH & Co KG.

Disclosure statement

This research is sponsored by Boehringer Ingelheim and may lead to the development of products, in which I have a business interest. I have disclosed those interests fully to Taylor & Francis, and have in place an approved plan for managing any potential conflicts arising from this arrangement.

References

1. Strohl WR, Knight DM. Discovery and development of biopharmaceuticals: current issues. Curr Opin Biotechnol. 2009;20:668–72. doi:10.1016/j.copbio.2009.10.012.
2. DiMasi JA. Innovating by developing new uses of already-approved drugs: trends in the marketing approval of supplemental indications. Clin Ther. 2013;35:808–18. doi:10.1016/j.clinthera.2013.04.004.
3. Evens RP. Pharma success in product development-does biotechnology change the paradigm in product development and attrition. AAPS J. 2016;18:281–85. doi:10.1208/s12248-015-9833-6.
4. Obrezanova O, Arnell A, de la Cuesta RG, Berthelot ME, Gallagher TR, Zurdo J, Stallwood Y. Aggregation risk prediction for antibodies and its application to biotherapeutic development. MAbs. 2015;7:352–63. doi:10.1080/19420862.2015.1007828.
5. Kunert R, Reinhart D. Advances in recombinant antibody manufacturing. Appl Microbiol Biotechnol. 2016;100:3451–61. doi:10.1007/s00253-016-7388-9.
6. van der Kant R, Karow-Zwick AR, Van Durme J, Blech M, Gallardo R, Seeliger D, Aßfalg K, Baatsen P, Compernolle G, Gils A, et al. Prediction and reduction of the aggregation of monoclonal antibodies. J Mol Biol. 2017;429:1244–61. doi:10.1016/j.jmb.2017.03.014.
7. Shukla AA, Hubbard B, Tressel T, Guhan S, Low D. Downstream processing of monoclonal antibodies–application of platform approaches. J Chromatogr B Analyt Technol Biomed Life Sci. 2007;848:28–39. doi:10.1016/j.jchromb.2006.09.026.
8. Gagnon P. Technology trends in antibody purification. J Chromatogr A. 2012;1221:57–70. doi:10.1016/j.chroma.2011.10.034.
9. Shire SJ. Formulation and manufacturability of biologics. Curr Opin Biotechnol. 2009;20:708–14. doi:10.1016/j.copbio.2009.10.006.
10. Wang W. Instability, stabilization, and formulation of liquid protein pharmaceuticals. Int J Pharm. 1999;185:129–88. doi:10.1016/S0378-5173(99)00152-0.
11. Shire SJ, Shahrokh Z, Liu J. Challenges in the development of high protein concentration formulations. J Pharm Sci. 2004;93:1390–402. doi:10.1002/jps.20079.
12. Nichols P, Li L, Kumar S, Buck PM, Singh SK, Goswami S, Balthazor B, Conley TR, Sek D, Allen MJ, et al. Rational design of viscosity reducing mutants of a monoclonal antibody: hydrophobic

versus electrostatic inter-molecular interactions. MAbs. 2015;7:212–30. doi:10.4161/19420862.2014.985504.
13. Kumar S, Plotnikov NV, Rouse JC, Singh SK. Biopharmaceutical Informatics: supporting biologic drug development via molecular modelling and informatics. J Pharm Pharmacol. 2018;70:595–608. doi:10.1111/jphp.12700.
14. Popovic B, Gibson S, Senussi T, Carmen S, Kidd S, Slidel T, Strickland I, Jianqing X, Spooner J, Lewis A, et al. Engineering the expression of an anti-interleukin-13 antibody through rational design and mutagenesis.. Protein Eng Des Sel. 2017;30(4):303–11. doi:10.1093/protein/gzx001.
15. Shan L, Mody N, Sormani P, Rosenthal KL, Damschroder MM, Esfandiary R. Developability assessment of engineered monoclonal antibody variants with a complex self-association behavior using complementary analytical and in silico tools. Mol Pharm. 2018;15:5697–710. doi:10.1021/acs.molpharmaceut.8b00867.
16. Kumar S, Roffi K, Tomar DS, Cirelli D, Luksha N, Meyer D, Mitchell J, Allen MJ, Li L. Rational optimization of a monoclonal antibody for simultaneous improvements in its solution properties and biological activity. Protein Eng Des Sel. 2018;31(7–8):313–25. doi:10.1093/protein/gzy020.
17. Tomar DS, Li L, Broulidakis MP, Luksha NG, Burns CT, Singh SK, Kumar S. In-silico prediction of concentration-dependent viscosity curves for monoclonal antibody solutions. MAbs. 2017;9 (3):476–89. doi:10.1080/19420862.2017.1285479.
18. Sharma VK, Patapoff TW, Kabakoff B, Pai S, Hilario E, Zhang B, Li C, Borisov O, Kelley RF, Chorny I. In silico selection of therapeutic antibodies for development: viscosity, clearance, and chemical stability. Proc Natl Acad Sci U S A. 2014;111(52):18601–06. doi:10.1073/pnas.1421779112.
19. Dobson CL, Devine PW, Phillips JJ, Higazi DR, Lloyd C, Popovic B, Arnold J, Buchanan A, Lewis A, Goodman J, et al. Engineering the surface properties of a human monoclonal antibody prevents self-association and rapid clearance in vivo. Sci Rep. 2016;6(1):38644. doi:10.1038/srep38644.
20. Tartaglia GG, Vendruscolo M. The Zyggregator method for predicting protein aggregation propensities. Chem Soc Rev. 2008;37:1395–401. doi:10.1039/b706784b.
21. Louros N, Konstantoulea K, De Vleeschouwer M, Ramakers M, Schymkowitz J, Rousseau F. WALTZ-DB 2.0: an updated database containing structural information of experimentally determined amyloid-forming peptides. Nucleic Acids Res. 2019;48(D1): D389–393.
22. Maurer-Stroh S, Debulpaep M, Kuemmerer N, Lopez de la Paz M, Martins IC, Reumers J, Morris KL, Copland A, Serpell L, Serrano L, et al. Exploring the sequence determinants of amyloid structure using position-specific scoring matrices. Nat Methods. 2010;7 (3):237–42. doi:10.1038/nmeth.1432.
23. Thompson MJ, Sievers SA, Karanicolas J, Ivanova MI, Baker D, Eisenberg D. The 3D profile method for identifying fibril-forming segments of proteins. Proc Natl Acad Sci U S A. 2006;103:4074–78. doi:10.1073/pnas.0511295103.
24. Rawat P, Kumar S, Michael Gromiha M. An in-silico method for identifying aggregation rate enhancer and mitigator mutations in proteins. Int J Biol Macromol. 2018;118:1157–67. doi:10.1016/j.ijbiomac.2018.06.102.
25. Sanchez de Groot N, Pallares I, Aviles FX, Vendrell J, Ventura S. Prediction of "hot spots" of aggregation in disease-linked polypeptides. BMC Struct Biol. 2005;5:18. doi:10.1186/1472-6807-5-18.
26. Trovato A, Seno F, Tosatto SC. The PASTA server for protein aggregation prediction. Protein Eng Des Sel. 2007;20:521–23. doi:10.1093/protein/gzm042.
27. Zibaee S, Makin OS, Goedert M, Serpell LC. A simple algorithm locates beta-strands in the amyloid fibril core of alpha-synuclein, Abeta, and tau using the amino acid sequence alone. Protein Sci. 2007;16:906–18. doi:10.1110/ps.062624507.
28. Frousios KK, Iconomidou VA, Karletidi CM, Hamodrakas SJ. Amyloidogenic determinants are usually not buried. BMC Struct Biol. 2009;9:44. doi:10.1186/1472-6807-9-44.
29. Tian J, Wu N, Guo J, Fan Y. Prediction of amyloid fibril-forming segments based on a support vector machine. BMC Bioinformatics. 2009;10(Suppl 1):S45. doi:10.1186/1471-2105-10-S1-S45.
30. Galzitskaya OV, Garbuzynskiy SO, Lobanov MY. Prediction of amyloidogenic and disordered regions in protein chains. PLoS Comput Biol. 2006;2:e177. doi:10.1371/journal.pcbi.0020177.
31. Chennamsetty N, Voynov V, Kayser V, Helk B, Trout BL. Design of therapeutic proteins with enhanced stability. Proc Natl Acad Sci U S A. 2009;106:11937–42. doi:10.1073/pnas.0904191106.
32. Van Durme J, De Baets G, Van Der Kant R, Ramakers M, Ganesan A, Wilkinson H, Gallardo R, Rousseau F, Schymkowitz J. Solubis: a webserver to reduce protein aggregation through mutation. Protein Eng Des Sel. 2016;29:285–89. doi:10.1093/protein/gzw019.
33. Fernandez-Escamilla AM, Rousseau F, Schymkowitz J, Serrano L. Prediction of sequence-dependent and mutational effects on the aggregation of peptides and proteins. Nat Biotechnol. 2004;22:1302–06. doi:10.1038/nbt1012.
34. Schymkowitz J, Borg J, Stricher F, Nys R, Rousseau F, Serrano L. The FoldX web server: an online force field. Nucleic Acids Res. 2005;33:W382–8. doi:10.1093/nar/gki387.
35. Davies SL, Lovelady CS, Grainger RK, Racher AJ, Young RJ, James DC. Functional heterogeneity and heritability in CHO cell populations. Biotechnol Bioeng. 2013;110:260–74. doi:10.1002/bit.24621.
36. Mason M, Sweeney B, Cain K, Stephens P, Sharfstein ST. Identifying bottlenecks in transient and stable production of recombinant monoclonal-antibody sequence variants in Chinese hamster ovary cells. Biotechnol Prog. 2012;28:846–55. doi:10.1002/btpr.1542.
37. Mathias S, Wippermann A, Raab N, Zeh N, Handrick R, Gorr I, Schulz P, Fischer S, Gamer M, Otte K. Unravelling what makes a monoclonal antibody difficult-to-express: from intracellular accumulation to incomplete folding and degradation via ERAD. Biotechnol Bioeng. 2019;117:5–16. doi:10.1002/bit.27196.
38. Gronemeyer P, Ditz R, Strube J. Trends in upstream and downstream process development for antibody manufacturing. Bioeng (Basel). 2014;1:188–212. doi:10.3390/bioengineering1040188.
39. Paborji M, Pochopin NL, Coppola WP, Bogardus JB. Chemical and physical stability of chimeric L6, a mouse-human monoclonal antibody. Pharm Res. 1994;11:764–71. doi:10.1023/A:1018948901599.
40. Zheng JY, Janis LJ. Influence of pH, buffer species, and storage temperature on physicochemical stability of a humanized monoclonal antibody LA298. Int J Pharm. 2006;308(1–2):46–51. doi:10.1016/j.ijpharm.2005.10.024.
41. Garidel P, Karow AR, Blech M. Orthogonal spectroscopic techniques for the early developability assessment of therapeutic protein candidates. Spectrosc Eur. 2014;26:9–13.
42. Kommanaboyina B, Rhodes CT. Trends in stability testing, with emphasis on stability during distribution and storage. Drug Dev Ind Pharm. 1999;25:857–68. doi:10.1081/DDC-100102246.
43. Pokharana M, Vaishnav R, Goyal AAS. Stability testing guidelines of pharmaceutical products. J Drug Delivery Ther. 2018;8:169–75. doi:10.22270/jddt.v8i2.1564.
44. Sukumar M, Doyle BL, Combs JL, Pekar AH. Opalescent appearance of an IgG1 antibody at high concentrations and its relationship to noncovalent association. Pharm Res. 2004;21:1087–93. doi:10.1023/B:PHAM.0000032993.98705.73.
45. Tomar DS, Kumar S, Singh SK, Goswami S, Li L. Molecular basis of high viscosity in concentrated antibody solutions: strategies for high concentration drug product development. MAbs. 2016;8:216–28. doi:10.1080/19420862.2015.1128606.
46. Fuh G, Wu P, Liang WC, Ultsch M, Lee CV, Moffat B, Wiesmann C. Structure-function studies of two synthetic anti-vascular endothelial growth factor Fabs and comparison with the Avastin Fab. J Biol Chem. 2006;281:6625–31. doi:10.1074/jbc.M507783200.
47. Yadav S, Laue TM, Kalonia DS, Singh SN, Shire SJ. The influence of charge distribution on self-association and viscosity behavior of

monoclonal antibody solutions. Mol Pharm. 2012;9:791–802. doi:10.1021/mp200566k.
48. Sormanni P, Aprile FA, Vendruscolo M. Third generation antibody discovery methods: in silico rational design. Chem Soc Rev. 2018;47:9137–57. doi:10.1039/C8CS00523K.
49. Pybus LP, James DC, Dean G, Slidel T, Hardman C, Smith A, Daramola O, Field R. Predicting the expression of recombinant monoclonal antibodies in Chinese hamster ovary cells based on sequence features of the CDR3 domain. Biotechnol Prog. 2014;30:188–97. doi:10.1002/btpr.1839.
50. Bentley KJ, Gewert R, Harris WJ. Differential efficiency of expression of humanized antibodies in transient transfected mammalian cells. Hybridoma. 1998;17:559–67. doi:10.1089/hyb.1998.17.559.
51. Hasegawa H, Hsu A, Tinberg CE, Siegler KE, Nazarian AA, Tsai MM. Single amino acid substitution in LC-CDR1 induces Russell body phenotype that attenuates cellular protein synthesis through eIF2alpha phosphorylation and thereby downregulates IgG secretion despite operational secretory pathway traffic. MAbs. 2017;9:854–73. doi:10.1080/19420862.2017.1314875.
52. Dwek RA. Biological importance of glycosylation. Dev Biol Stand. 1998;96:43–47.
53. Reusch D, Tejada ML. Fc glycans of therapeutic antibodies as critical quality attributes. Glycobiology. 2015;25:1325–34. doi:10.1093/glycob/cwv065.
54. Goetze AM, Liu YD, Zhang Z, Shah B, Lee E, Bondarenko PV, Flynn GC. High-mannose glycans on the Fc region of therapeutic IgG antibodies increase serum clearance in humans. Glycobiology. 2011;21:949–59. doi:10.1093/glycob/cwr027.
55. Yu M, Brown D, Reed C, Chung S, Lutman J, Stefanich E, Wong A, Stephan J-P, Bayer R. Production, characterization and pharmacokinetic properties of antibodies with N-linked Mannose-5 glycans. MAbs. 2012;4(4):475–87. doi:10.4161/mabs.20737.
56. Shields RL, Namenuk AK, Hong K, Meng YG, Rae J, Briggs J, Xie D, Lai J, Stadlen A, Li B, et al. High resolution mapping of the binding site on human IgG1 for Fc gamma RI, Fc gamma RII, Fc gamma RIII, and FcRn and design of IgG1 variants with improved binding to the Fc gamma R. J Biol Chem. 2001;276:6591–604. doi:10.1074/jbc.M009483200.
57. Nimmerjahn F, Ravetch JV. Fcgamma receptors as regulators of immune responses. Nat Rev Immunol. 2008;8:34–47. doi:10.1038/nri2206.
58. Levy NE, Valente KN, Choe LH, Lee KH, Lenhoff AM. Identification and characterization of host cell protein product-associated impurities in monoclonal antibody bioprocessing. Biotechnol Bioeng. 2014;111:904–12. doi:10.1002/bit.25158.
59. Dwivedi M, Blech M, Presser I, Garidel P. Polysorbate degradation in biotherapeutic formulations: identification and discussion of current root causes. Int J Pharm. 2018;552:422–36. doi:10.1016/j.ijpharm.2018.10.008.
60. Goswami S, Wang W, Arakawa T, Ohtake S. Developments and Challenges for mAb-Based Therapeutics. Antibodies. 2013;2:452–500. doi:10.3390/antib2030452.
61. Garidel P, Kuhn AB, Schafer LV, Karow-Zwick AR, Blech M. High-concentration protein formulations: how high is high? Eur J Pharm Biopharm. 2017;119:353–60. doi:10.1016/j.ejpb.2017.06.029.
62. Yang Y, Velayudhan A, Thornhill NF, Farid SS. Multi-criteria manufacturability indices for ranking high-concentration monoclonal antibody formulations. Biotechnol Bioeng. 2017;114:2043–56. doi:10.1002/bit.26329.
63. Zurdo J. Developability assessment as an early de-risking tool for biopharmaceutical development. Pharm Bioprocess. 2013;1:29–50. doi:10.4155/pbp.13.3.
64. van der Kant R, Bauer J, Karow-Zwick AR, Kube S, Garidel P, Blech M, Rousseau F, Schymkowitz J Adaption of human antibody λ and κ light chain architectures to CDR repertoires. PEDS. 2019;32:109–127. doi:10.1093/protein/gzz012.
65. Krieger E, Vriend G. Models@Home: distributed computing in bioinformatics using a screensaver based approach. Bioinformatics. 2002;18:315–18.
66. Siekierska A, De Baets G, Reumers J, Gallardo R, Rudyak S, Broersen K, Couceiro J, Van Durme J, Schymkowitz J, Rousseau F. alpha-Galactosidase aggregation is a determinant of pharmacological chaperone efficacy on Fabry disease mutants. J Biol Chem. 2012;287:28386–97. doi:10.1074/jbc.M112.351056.
67. Bergemann K, Eckermann C, Garidel P, Grammatikos S, Jacobi A, Kaufmann H, Kempken R, Pisch-Heberle S. Production and downstream processing. In: Dübel S, editor. Handbook of therapeutic antibodies. Wiley-VCH. 2008. p. 199–237.
68. Jacobi A, Enenkel B, Garidel P, Eckermann C, Knappenberger M, Presser I, Kaufmann H. Process development and manufacturing of therapeutic antibodies. In: Dübel S, editor. Handbook of therapeutic antibodies. Wiley-VCH. 2014. p. 601–64.
69. Karow AR, Bahrenburg S, Garidel P. Buffer capacity of biologics–from buffer salts to buffering by antibodies. Biotechnol Prog. 2013;29:480–92. doi:10.1002/btpr.1682.
70. Zydney AL, Kurlyel R. Protein concentration and buffer exchange using ultrafiltration. In: Desai MA editor. Downstream processing of proteins. Methods in biotechnology. Totowa (NJ): Humana Press; 2000. p. 9.
71. Garidel P, Herre A, Kliche W. Microscopic methods for particle characterization in protein pharmaceuticals. In: Mahler HC, Jiskoot W, editors. Analysis of aggregates and particles in protein pharmaceuticals. New Jersey: John Wiley & Sons; 2012. p. 269–302. doi:10.1002/9781118150573.ch12
72. Weinbuch D, Zolls S, Wiggenhorn M, Friess W, Winter G, Jiskoot W, Hawe A. Micro-flow imaging and resonant mass measurement (Archimedes)–complementary methods to quantitatively differentiate protein particles and silicone oil droplets. J Pharm Sci. 2013;102:2152–65. doi:10.1002/jps.23552.

Bauer and Mathias et al. 2020, monoclonal antibodies (mAbs)

Supplementary material

MAbs. Jan-Dec 2020;12(1):1787121

doi: 10.1080/19420862.2020.1787121

Licensed under Creative Commons Attribution - NonCommercial 4.0 International,
https://creativecommons.org/licenses/by-nc/4.0/

Note: The in this thesis described mAb1 is annotated GTE mAb in the following publication.

Supplementary Figure S1

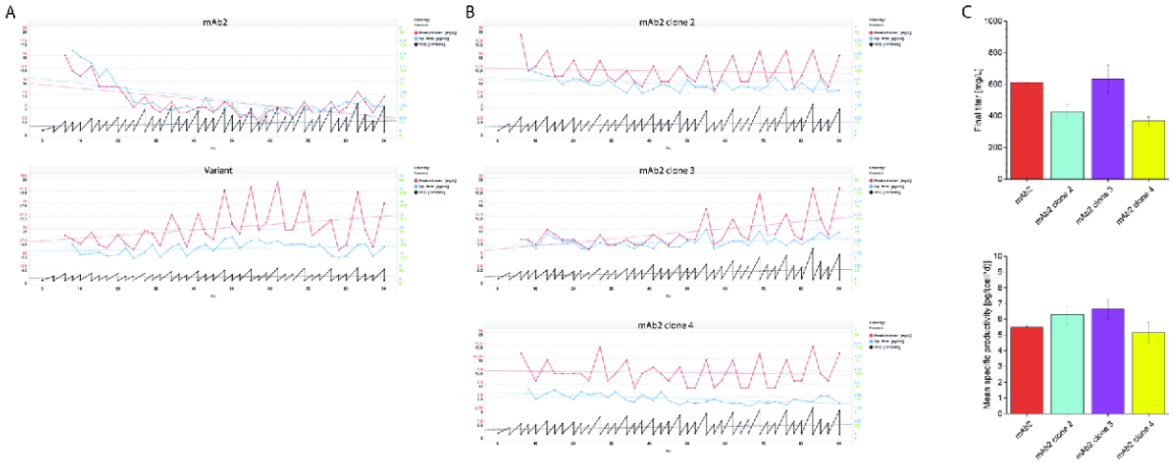

Supplementary Figure S2

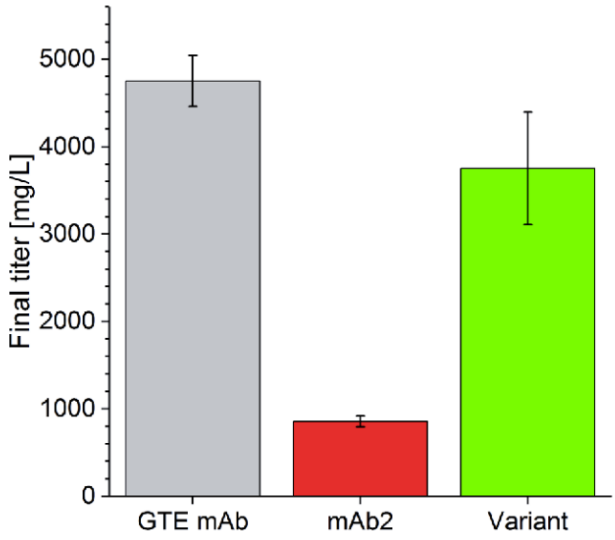

Supplementary Figure S3

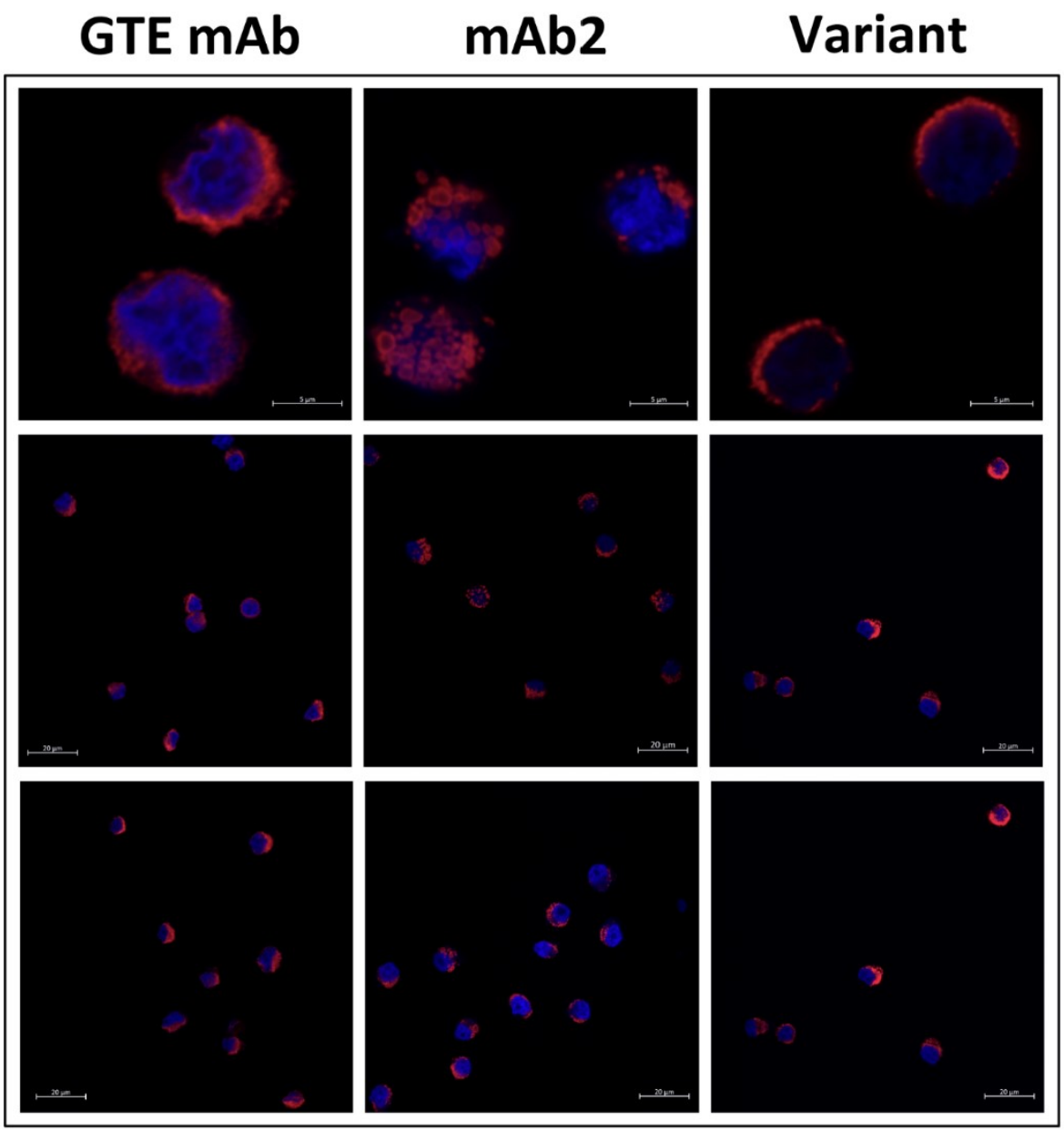

Supplementary Figure S4

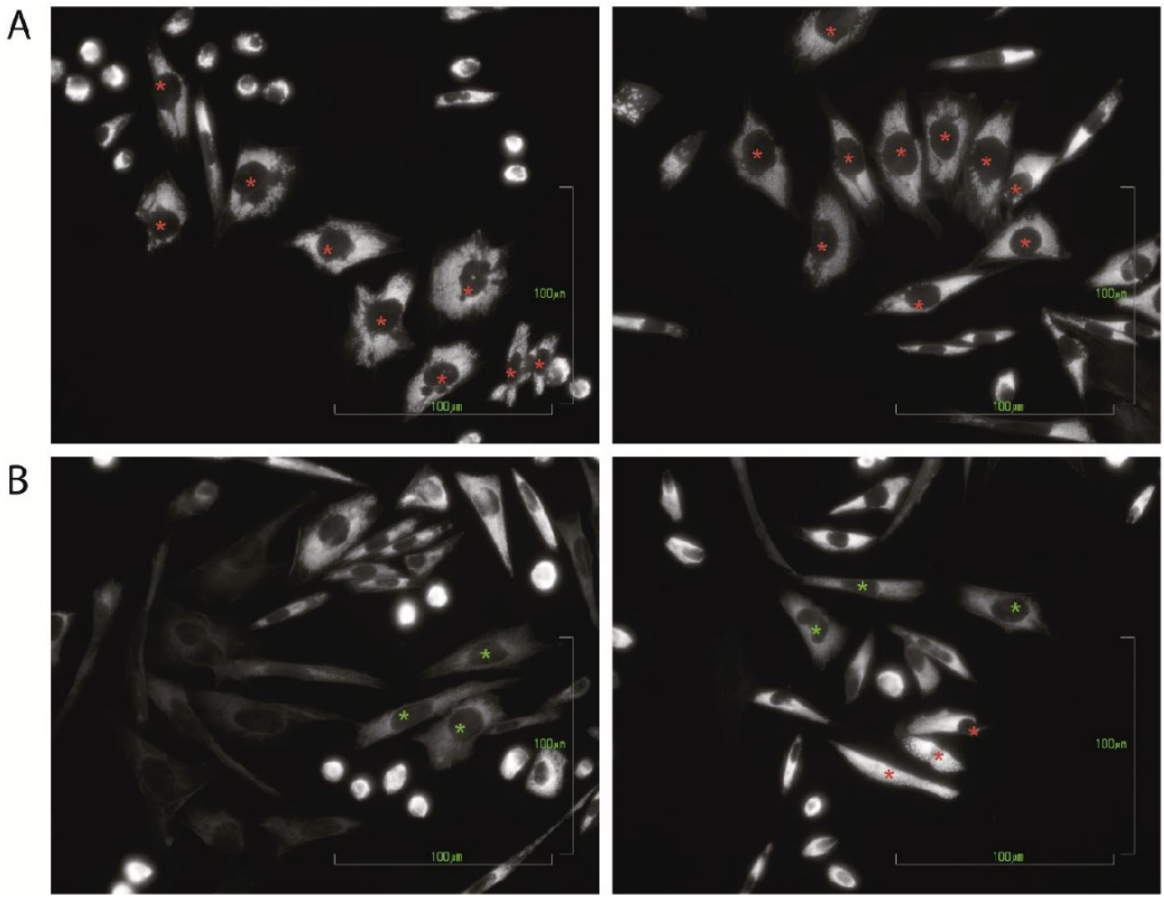

Supplementary Figure S5

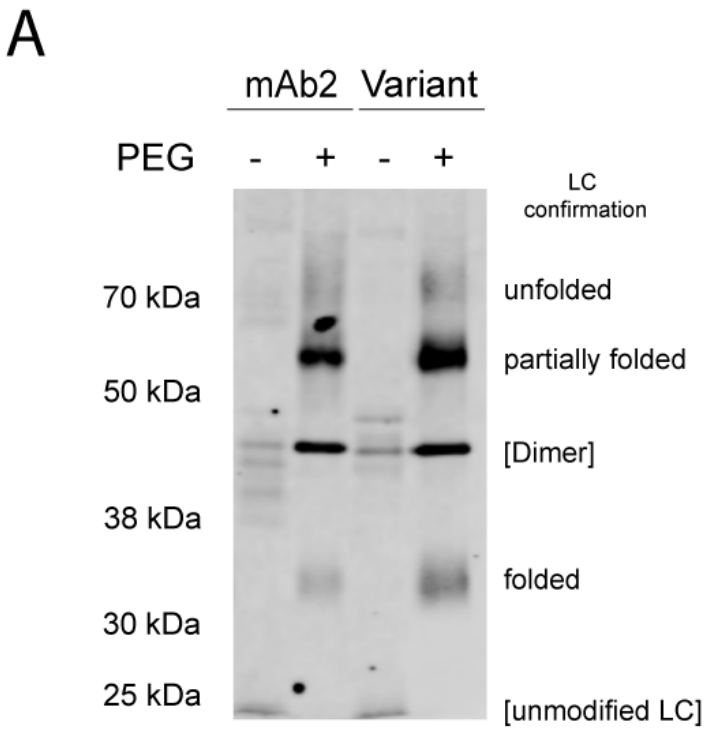

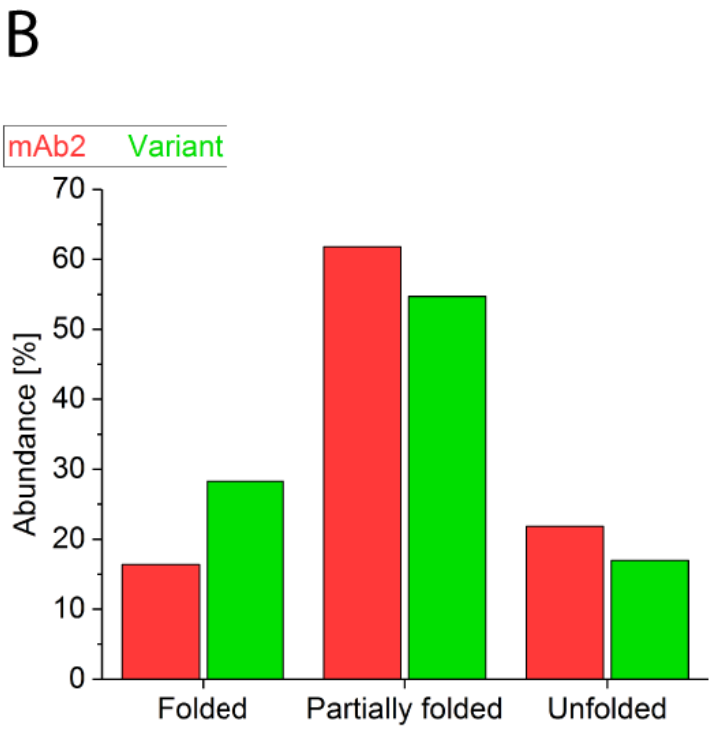

Supplementary Figure S6

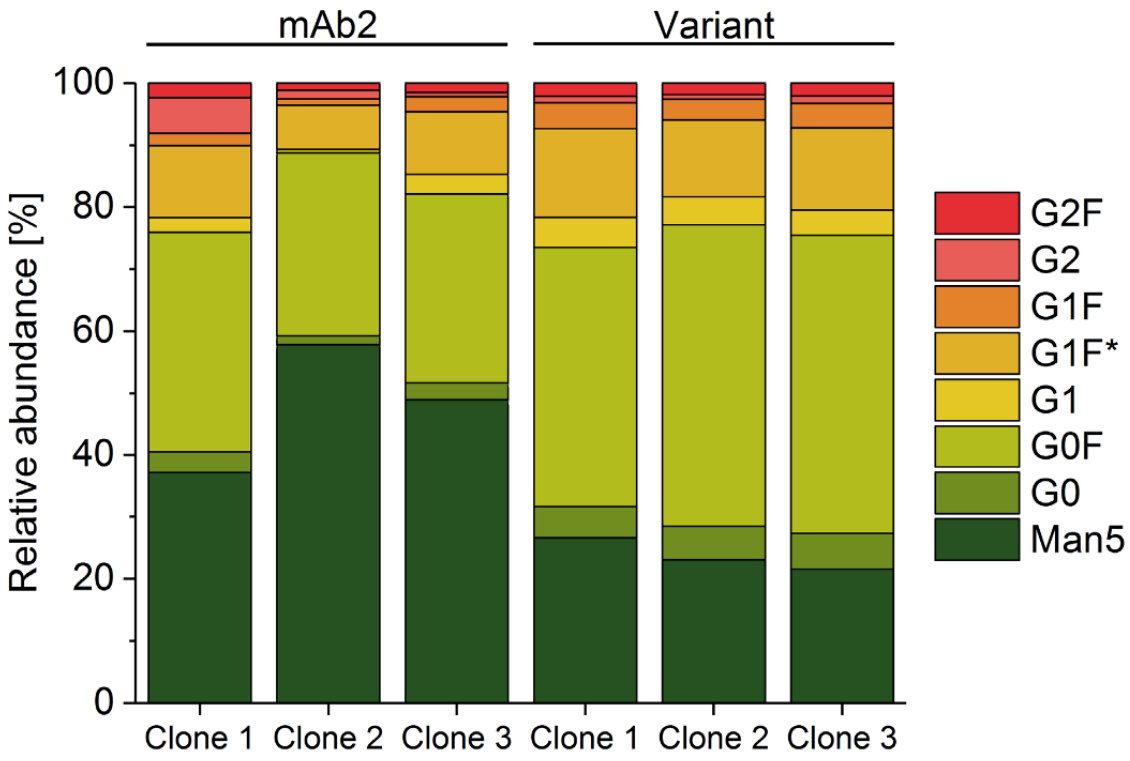

Supplementary Figure S7

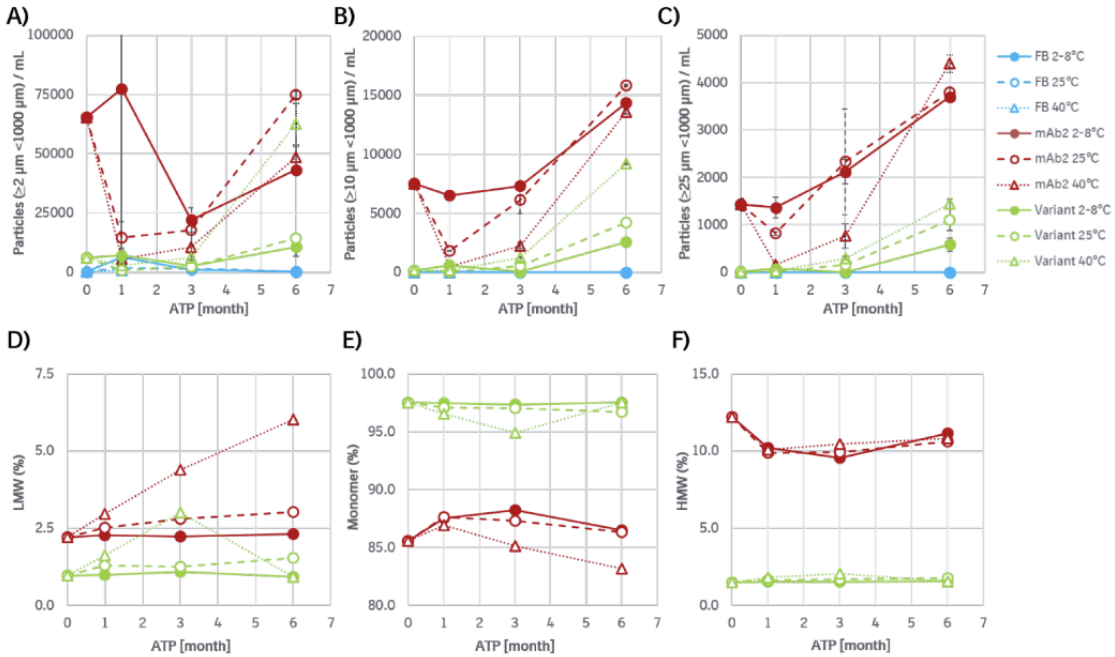

Supplementary Figure S8

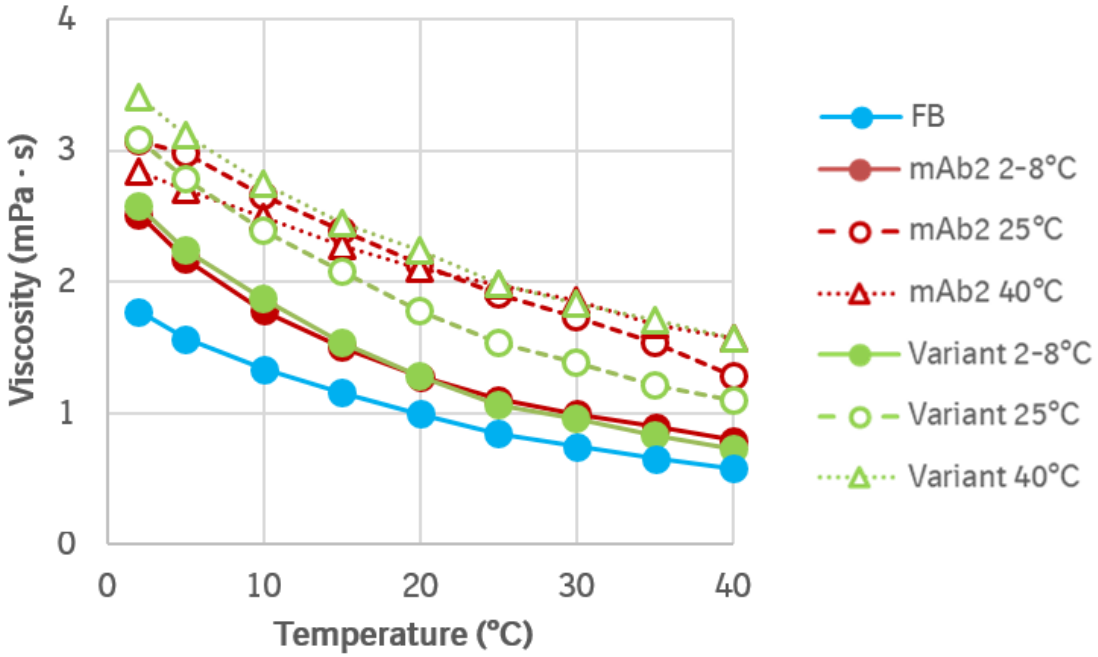

Supplementary Figure S9

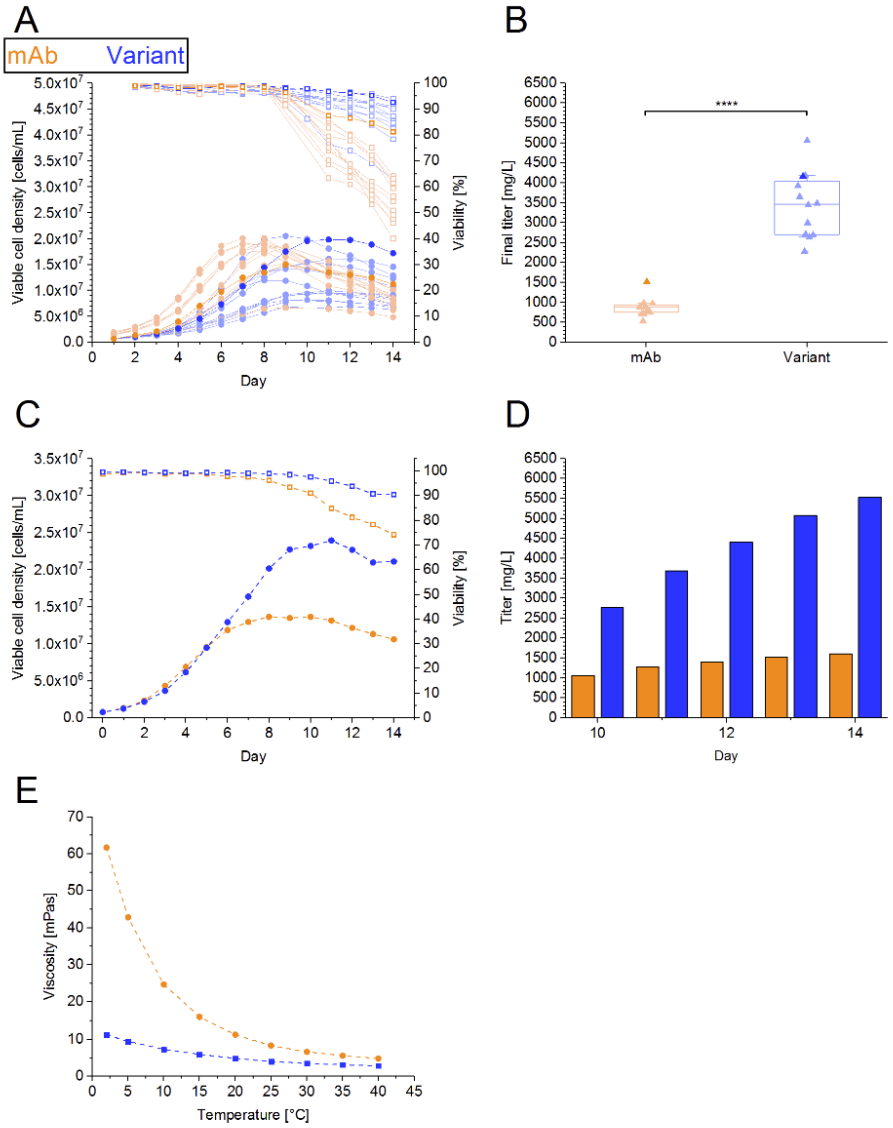

Supplementary Figure S1: (A) Cell lines producing mAb2 and its *in silico* optimized variant of choice were cultivated in parallel to (B) additional cell lines producing mAb2. Titer and specific productivity were used to estimate phenotypic stability. (C) Titer and mean specific productivity of additional mAb2 producing cell lines. The cell line of choice showed a significant reduction of mAb2 production over time, while other mAb2 producing clones performed equally over 90 days. However, final titer and mean specific productivity of the small-scale production run showed comparable productivity regardless of clonal stability data.

Supplementary Figure S2: Cell culture performance of clonal cell lines producing either mAb2 or its *in silico* optimized variant relative to a good-to-express (GTE) mAb. In a fed-batch production processes in shake flasks, the *in silico* optimized variant showed with a final titer of ~ 3.8 g/L an increase of more than four-fold in comparison its parental counterpart mAb2 (~ 0.8 g/L), while the GTE mAb-producing cell line achieved a final titer of ~ 4.8 g/L.

Supplementary Figure S3: Microscopic investigation of CHO cells producing a good-to-express monoclonal antibody (GTE mAb) as reference, mAb2 and its *in silico* optimized variant. Confocal images of cell lines producing GTE mAb, mAb2 and the *in silico* optimized variant were acquired at a 63x primary magnification. Nuclei and recombinant protein were stained using DAPI (blue) and a fluorescent secondary antibody (red). Scale bar in first line represents 5 µm. Scale bar in second and third line represents 20 µm.

Supplementary Figure S4: Example images of the microscopic investigation of CHO cells producing (A) mAb2 and its (B) in silico optimized variant . Red asterisks label cells with antibody inclusions, while green asterisks label cells without antibody inclusions.

Images were acquired at a 40 x primary magnification. Recombinant proteins were stained using a fluorescent antibody (red). Scale bar represents 100 µm.

Supplementary Figure S5: Intracellular light chain (LC) folding indicated enhanced folding of the *in silico* optimized variant of mAb2. (A) Gel mobility shift assay detecting not formed intradomain disulfide bridges in the antibody LC. In brief, available cysteines of the free LC were coupled to PEG_{5000}-maleimide and the respective molecule subsequently purified and subjected to western blot analyses. (B) Densitometric analysis of the respective western blot using Image Studio Software Version 5.2.5 (LI-COR).

Supplementary Figure S6: Characterization of the glycosylation profile of three cell clones expressing mAb2 and, respectively, the in silico optimized variant SL52R. The glycosylation profile of the antibodies was analyzed by Caliper glycosylation analysis. G1F* represents the second naturally existing glycan isomer of G1F. Man5, mannose-5; G, galactose; F, fucose.

Supplementary Figure S7: Product quality and colloidal stability of the drug products was evaluated in a storage study. A-C) Particles with a size between (A) ≥2 µm and <1000, (B) ≥10 µm and <1000, and (C) ≥25 µm and <1000 µm per ml drug product (10 mg/ml API) and formulation buffer (25 mM sodium citrate, 125 mM sodium chloride, pH 6.0) were quantified by MFI. **D-F)** The proportion of (D) low- and (F) high-molecular weight species (HMW) as well as (E) monomer content in the drug products was examined by HP-SEC.

Supplementary Figure S8: Rheological evaluation of the drug product. The viscosity of the drug product of mAb2 and the *in silico* optimized variant (API: 10 mg/ml) as well as formulation buffer (25 mM sodium citrate, 125 mM sodium chloride, pH 6.0) stored for six month at 2-8 °C, 25 °C and 40 °C was determined temperature-dependently within a gradient of 2-40°C.

Supplementary Figure S9: Cell culture performance of clonal cell lines producing either a wildtype mAb showing high viscosity in final formulation buffer or its in silico optimized variant in controlled fed-batch production processes. (A) Viable cell density (VCD) and viability as well as (B) final antibody titer of the top twelve clonal cell lines are shown for a controlled 14-day micro bioreactor fed-batch cultivation process (ambr^{TM} 15). Production process was performed without biological replicates. Shown whiskers represent the 10th and the 90th percentile. The highlighted clones were further investigated in 3L benchtop bioreactors. An unpaired Students t-test was used to determine statistical significance (****: $p < 0.0001$). (C) VCD (filled circles and boxes), viability (open circles and boxes) and (D) cumulative antibody titer of the best performing clonal cell lines in a controlled 14-day fed batch cultivation process performed in 3 L benchtop bioreactors. 3 L bioreactor runs were performed without biological replicates. Antibody titer was determined starting from day 10. (E) Rheologically determined viscosity of wildtype mAb and the in silico optimized variant containing formulations.

Curriculum Vitae

Personal information

Name	Sven Mathias

Academic career

10/2009 - 08/2013	**Biberach University of Applied Sciences**
Bachelor program	Subject: Pharmaceutical Biotechnology Graduation: Bachelor of Science
08/2011 - 01/2012	**University of Copenhagen**
Semester abroad	Subject: Pharmaceutical Science Focus: Pharmacology, Design of Experiments, Drug Design
03/2013 - 05/2013	**University of Freiburg**
Bachelor thesis	Chair Plant Biotechnology
Grade: 1.0	Head of Group: PD Dr. Eva Decker Topic: Characterization of a cold-inducible promoter for the production of heterologous proteins in *Physcomitrella patens*
10/2013 - 09/2015	**Biberach University of Applied Sciences and University of Ulm**
Master program	Subject: Pharmaceutical Biotechnology Graduation: Master of Science
01/2015 - 06/2015	**Boehringer Ingelheim Pharma GmbH & Co. KG**
Master thesis	Department: Molecular Biological Development
Grade: 1.0	Head of Group: Dr. Markus Michael Müller, Dr. Patrick Schulz Topic: Molecular biological characterization of a hot spot genomic location in CHO cell lines using the sequence-specific endonuclease Cas9
02/2016 - 07/2019	**Biberach University of Applied Sciences and**
Doctoral program	**Boehringer Ingelheim Pharma GmbH & Co. KG** Institute of Applied Biotechnology Head of Group: Prof. Dr. Kerstin Otte Topic: Identification, Characterization and Removal of Intracellular Secretion Bottlenecks in Industrial CHO Production Cell Lines

Working experience

07/2015 - 11/2015	**Boehringer Ingelheim Pharma GmbH & Co. KG**
Temporary employee	Department: Molecular Biological Development
09/2019 - today	**Boehringer Ingelheim Pharma GmbH & Co. KG**
Post-Doc	Department: Bioprocess Development Biologicals

Qualifications

Software	Microsoft Office (very good), Origin (good), R (basics), VectorNTI (good), Pymol (good), ImageJ (basics), IPA (basics)

Awards

11/2013	**Preis der Boehringer Ingelheim Pharma GmbH & Co. KG** Award for Bachelor thesis
11/2015	**Preis der Boehringer Ingelheim Pharma GmbH & Co. KG** Award for Master thesis

Conferences

10/2016	**1. European Society for Animal Cell Technology (ESACT) Frontiers Retreat**, Lyon (FR), Participation: Poster Production and transport of a recombinantly expressed antibody in a stable CHO production cell line
05/2017	**25. European Society for Animal Cell Technology (ESACT) Meeting**, Lausanne (CH), Participation: Poster Identification of bottlenecks in suspension-adapted CHO cells producing complex biopharmaceuticals using fluorescence microscopy
01/2019	**1. Gordon Research Conference (GRC) on Biotherapeutics and Vaccines Development**, Galveston (USA), Participation: Poster Identification and characterisation of antibody production bottlenecks in current CHO production cell lines
05/2019	**26. European Society for Animal Cell Technology (ESACT) Meeting, Copenhagen (DK),** Participation: Oral presentation Intracellular bottlenecks in monoclonal antibody production

Publications

07/2014	**Biotechnology Journal (2014): Fischer, S., Buck, T., Wagner, A., Ehrhart, C., Giancaterino, J., Mang, S., Schad, M., Mathias, S. et al.** A functional high-content miRNA screen identifies miR-30 family to boost recombinant protein production in CHO cells
10/2015	**Journal of Biotechnology (2015): Fischer, S., Mathias, S. et al.** Enhanced protein production by microRNA-30 family in CHO cells is mediated by the modulation of the ubiquitin pathway
10/2015	**Biotechnology & Bioengineering (2015): Fischer, S., Paul, A.J., Wagner, A., Mathias, S. et al.** miR-2861 as novel HDAC5 inhibitor in CHO cells enhances productivity while maintaining product quality
04/2018	**Journal of Biotechnology (2018): Mathias, S. et al.** Visualisation of intracellular production bottlenecks in suspension-adapted CHO cells producing complex biopharmaceuticals using fluorescence microscopy
05/2019	**Biotechnology Journal (2019): Raab, N., Mathias, S. et al.** CRISPR/Cas9-mediated knockout of microRNA-744 improves antibody titer of CHO production cell lines
08/2019	**PLos One (2019): Zeh, N., Schneider, H., Mathias, S. et al.** Human CAP cells represent a novel source for functional, miRNA-Loaded exosome production
10/2019	**Biotechnology and Bioengineering (2019): Mathias, S. et al.** Unraveling what makes a monoclonal antibody difficult-to-express: From intracellular accumulation to incomplete folding and degradation via ERAD
07/2020	**mAbs (2020): Bauer, J. and Mathias, S. et al.** Rational Optimization of a Monoclonal Antibody Improves the Aggregation Propensity and Enhances the CMC Properties Along the Entire Pharmaceutical Process Chain

Declaration

I hereby declare that I wrote the present dissertation with the topic

“Identification, Characterization and Removal of Intracellular Secretion Bottlenecks in Industrial CHO Production Cell Lines”

independently and used no other aids that those cited. In each individual case, I have clearly identified the source of the passages that are taken word for word or paraphrased from other works.

I also hereby declare that I have carried out my scientific work according to the principles of good scientific practice in accordance with the current „Satzung der Universität Ulm zur Sicherung guter wissenschaftlicher Praxis“ (Rules of the University of Ulm for Assuring Good Scientific Practice). I further declare that the dissertation has not previously been submitted in this or similar form in another doctoral procedure at home or abroad.

Ulm, 28 July 2021